

UNIVERSITY OF CALIFORNIA,  
IRVINE

Optical Properties, Chemical Composition, and Aqueous Photochemistry of Secondary Organic  
Aerosol

DISSERTATION

submitted in partial satisfaction of the requirements  
for the degree of

DOCTOR OF PHILOSOPHY

in Chemistry

by

Dian Elizabeth Romonosky

Ph.D. Dissertation Committee:  
Professor Sergey A. Nizkorodov, Chair  
Professor Donald R. Blake  
Assistant Professor Craig Murray

2016

ProQuest Number: 10168497

All rights reserved

INFORMATION TO ALL USERS

The quality of this reproduction is dependent upon the quality of the copy submitted.

In the unlikely event that the author did not send a complete manuscript and there are missing pages, these will be noted. Also, if material had to be removed, a note will indicate the deletion.



ProQuest 10168497

Published by ProQuest LLC (2016). Copyright of the Dissertation is held by the Author.

All rights reserved.

This work is protected against unauthorized copying under Title 17, United States Code  
Microform Edition © ProQuest LLC.

ProQuest LLC.  
789 East Eisenhower Parkway  
P.O. Box 1346  
Ann Arbor, MI 48106 - 1346

Chapter 2 © 2016 Elsevier Ltd.  
Chapter 3 © 2015 American Chemical Society  
Chapter 5 © 2015 Taylor & Francis  
All other materials © 2016 Dian Elizabeth Romonosky

## **Dedication**

*To my Grandparents: Peter, Helen, Paul, and Vivian*

*“I get up every morning determined to both change the world and have one hell of a good time.  
Sometimes this makes planning my day difficult.”  
- E.B. White*

*“The woman who follows the crowd will usually go no further than the crowd. The woman who  
walks alone is likely to find herself in places no one has ever been before.”  
- Alan Ashley-Pitt*



# TABLE OF CONTENTS

<b>List of Figures</b> .....	<b>vi</b>
<b>List of Tables</b> .....	<b>xiv</b>
<b>Acknowledgments</b> .....	<b>xvii</b>
<b>Curriculum Vitae</b> .....	<b>xx</b>
<b>Abstract of the Dissertation</b> .....	<b>xxxii</b>
<b>Chapter 1: Introduction</b> .....	<b>1</b>
1.1. Background and Motivation.....	2
1.1.1. Secondary Organic Aerosol (SOA) .....	2
1.1.2. VOC Serving as Precursors of SOA .....	3
1.1.3. Photochemical Aging of Organic Aerosols .....	4
1.1.4. Nitrogen-Containing Compounds in SOA.....	6
1.2. Goals of the Dissertation.....	8
1.3. General Methods .....	11
1.3.1. SOA Generation and Collection in Chamber.....	11
1.3.2. SOA Generation and Collection in Flow Tube.....	13
1.3.3. High-Resolution Composition Analysis with LTQ-Orbitrap .....	13
1.3.4. Data Processing and Accurate-Mass Assignments.....	15
1.3.5. Data Analysis .....	15
<b>Chapter 2: Effective Absorption Cross Sections and Photolysis Rates of Anthropogenic and Biogenic Secondary Organic Aerosols</b> .....	<b>17</b>
2.1. Abstract .....	18
2.2. Introduction .....	19

2.3. Experimental .....	21
2.3.1. SOA Generation and Collection .....	21
2.3.2. UV-Vis Absorption Measurements.....	24
2.4. Results and Discussion.....	27
2.5. Conclusion.....	51
<b>Chapter 3: Chemical Composition and Aqueous Photochemistry Products of Secondary Organic Aerosol .....</b>	<b>52</b>
3.1. Abstract .....	53
3.2. Introduction.....	55
3.3. Experimental .....	59
3.3.1. SOA Generation and Collection .....	59
3.3.2. Aqueous Photolysis and Flux Calculation .....	60
3.3.3. High-Resolution Mass Spectrometry .....	63
3.4. Results and Discussion.....	64
3.4.1. Comparison of High-Resolution Mass Spectra of Unphotolyzed SOA Samples .....	64
3.4.2. Effect of Photolysis on SOA Composition .....	73
3.5. Conclusion.....	86
<b>Chapter 4: Aqueous Photochemistry of Secondary Organic Aerosol of <math>\alpha</math>-Pinene and <math>\alpha</math>-Humulene Oxidized with Ozone, Hydroxyl Radical, and Nitrate Radical.....</b>	<b>88</b>
4.1. Abstract .....	89
4.2. Introduction .....	90
4.3. Experimental .....	92

4.3.1. Secondary Organic Aerosol Generation .....	92
4.3.2. High-Resolution Electrospray Ionization Mass Spectrometry (HR-ESI-MS) of Aqueous Photolysis and Control Samples.....	94
4.4. Results and Discussion .....	96
4.4.1. Composition of SOA Before Photolysis.....	96
4.4.2. Photolysis Induced Changes in Molecular Composition .....	102
4.5. Conclusion .....	107
<b>Chapter 5: Absorption Spectra and Aqueous Photochemistry of <math>\beta</math>-Hydroxyalkyl Nitrates</b>	
.....	<b>109</b>
5.1. Abstract .....	110
5.2. Introduction .....	111
5.3. Methods.....	115
5.3.1. Experimental Methods .....	115
5.3.2. Theoretical Methods .....	118
5.4. Results and Discussion.....	119
5.4.1. Absorption Spectra.....	119
5.4.2. Computed Structures and Absorption Spectra.....	125
5.5. Photochemical Fates of $\beta$ -Hydroxyalkyl Nitrates.....	134
5.6. Conclusions .....	140
<b>References .....</b>	<b>142</b>

## List of Figures

Figure 1.1	Chamber diagram.....	11
Figure 1.2	Diagram of flow tube reactor for ozonolysis reactions.....	13
Figure 2.1	A comparison of MAC values for 1MPYR/O <sub>3</sub> SOA, extracted in either water or methanol.....	26
Figure 2.2	Absorbance of GUA/OH SOA vs. solution mass concentration. ....	27
Figure 2.3	Mass absorption coefficient of $\alpha$ -pinene (APIN) SOA.....	28
Figure 2.4	Mass absorption coefficient of $\alpha$ -pinene (APIN) SOA. ....	28
Figure 2.5	Mass absorption coefficient of $\beta$ -pinene (BPIN) SOA.....	29
Figure 2.6	Mass absorption coefficient of $\beta$ -myrcene (MYR) SOA.....	29
Figure 2.7	Mass absorption coefficient of farnesene (FAR) SOA.....	30
Figure 2.8	Mass absorption coefficient of farnesene (FAR) SOA.....	30
Figure 2.9	Mass absorption coefficient of guaiacol (GUA) SOA.....	31
Figure 2.10	Mass absorption coefficient of farnesene (FAR) SOA.....	31
Figure 2.11	Mass absorption coefficient of imidazole (IMID) SOA. ....	32
Figure 2.12	Mass absorption coefficient of isoprene (ISO) SOA. ....	32
Figure 2.13	Mass absorption coefficient of isoprene (ISO) SOA.....	33
Figure 2.14	Mass absorption coefficient of limonene (LIM) SOA.....	33
Figure 2.15	Mass absorption coefficient of linalool (LIN) SOA. ....	34
Figure 2.16	Mass absorption coefficient of linalool (LIN) SOA. ....	34
Figure 2.17	Mass absorption coefficient of ocimene (OCI) SOA.....	35
Figure 2.18	Mass absorption coefficient of ocimene (OCI) SOA.....	35
Figure 2.19	Mass absorption coefficient of para-xylene (XYL) SOA. ....	36

Figure 2.20	Mass absorption coefficient of para-xylene (XYL) SOA.....	36
Figure 2.21	Mass absorption coefficient of 1-methylpyrrole (1MPYR) SOA.....	37
Figure 2.22	Mass absorption coefficient of 2-methylpyrrole (2MPYR) SOA.....	37
Figure 2.23	Mass absorption coefficient of 2-methylpyrrole (2MPYR) SOA.....	38
Figure 2.24	Mass absorption coefficient of 2-methylpyrrole (2MPYR) SOA.....	38
Figure 2.25	Mass absorption coefficient of naphthalene (NAP) SOA.....	39
Figure 2.26	Mass absorption coefficient of naphthalene (NAP) SOA.....	39
Figure 2.27	Mass absorption coefficient of toluene (TOL) SOA.....	40
Figure 2.28	Mass absorption coefficient of toluene (TOL) SOA.....	40
Figure 2.29	A comparison of MAC values for XYL, APIN, and ISO SOA, as well as all other SOA samples. The higher MAC values observed for the XYL samples are representative of the SOA derived from aromatic precursors .....	42
Figure 2.30	Two models for the wavelength dependence of quantum yield used in this work: unity quantum yield (as in H <sub>2</sub> O <sub>2</sub> ) with the threshold set at 400 nm and quantum yield for the photolysis of acetone at 1 atm. These quantum yields were convoluted with the effective absorption cross sections (an example for 2MPYR/O <sub>3</sub> is shown) and solar spectral flux to obtain the effective photochemical rate constants.....	44
Figure 2.31	Photochemical rate constant, <i>J</i> , of the most-absorbing (2MPYR/O <sub>3</sub> ) and the least-absorbing (ISO/OH) SOA sample in our set as a function of SZA calculated using Eq. (2.5) and assuming the H <sub>2</sub> O <sub>2</sub> model for the quantum yields.....	46

Figure 2.32	Photochemical rate constant, $J$ , for the same SOA samples as used in Fig. 2.31 plotted as a function of time over a 24 hour period in Los Angeles (34° latitude) on June 22, 2014. The 24-hour average values of $\langle J \rangle$ are listed in Table 2.3 for all the SOA types probed in this work. ....	46
Figure 3.1	The spectral flux density in the photolysis cuvette compared to the solar spectral flux density at SZA=0. The right axis shows the effective absorption cross sections of GUA/NO <sub>x</sub> . ....	63
Figure 3.2	Reconstructed mass spectra for all the unphotolyzed O <sub>3</sub> SOA samples (before photolysis) recorded in this work. The x-axis corresponds to the molecular weight of the neutral SOA compounds. The x-axis of the left panel corresponds to the molecular weight of the neutral SOA compounds. The y-axis of the right panel is on a log scale to make the weaker peaks of oligomeric compounds easier to see. ....	65
Figure 3.3	Reconstructed mass spectra for all OH/NO <sub>x</sub> SOA samples (before photolysis) recorded in this work. The x-axis corresponds to the molecular weight of the neutral SOA compounds. The y-axis of the left panel corresponds to the molecular weight of the neutral SOA compounds. The y-axis of the right panel is on a log scale to make the weaker peaks of oligomeric compounds easier to see. Peaks in orange denote nitrogen-containing compounds. ....	66
Figure 3.4	Mass spectra of APIN/O <sub>3</sub> and APIN/NO <sub>x</sub> SOA solutions before (black) and after (green) 1 h of photolysis. The mass spectra after photolysis are inverted for clarity. The difference (red, after - before) is representative of the change that occurred during photolysis the time. ....	74

Figure 3.5	Mass spectra of BPIN/O <sub>3</sub> and BPIN/NO <sub>x</sub> SOA solutions before (black) and after (green) 1 h of photolysis. The mass spectra after photolysis are inverted for clarity. The difference (red, after - before) is representative of the change that occurred during photolysis the time. ....74
Figure 3.6	Mass spectra of HUM/O <sub>3</sub> and HUM/NO <sub>x</sub> SOA solutions before (black) and after (green) 1 h of photolysis. The mass spectra after photolysis are inverted for clarity. The difference (red, after - before) is representative of the change that occurred during photolysis the time. ....75
Figure 3.7	Mass spectra of MYR/O <sub>3</sub> and MYR/NO <sub>x</sub> SOA solutions before (black) and after (green) 1 h of photolysis. The mass spectra after photolysis are inverted for clarity. The difference (red, after - before) is representative of the change that occurred during photolysis the time. ....75
Figure 3.8	Mass spectra of GUA/NO <sub>x</sub> SOA solutions before (black) and after (green) 1 h of photolysis. The mass spectra after photolysis are inverted for clarity. The difference (red, after - before) is representative of the change that occurred during photolysis the time. ....76
Figure 3.9	Mass spectra of LIM/O <sub>3</sub> SOA solutions before (black) and after (green) 1 h of photolysis. The mass spectra after photolysis are inverted for clarity. The difference (red, after - before) is representative of the change that occurred during photolysis the time. ....76
Figure 3.10	Mass spectra TMB/NO <sub>x</sub> SOA solutions before (black) and after (green) 1 h of photolysis. The mass spectra after photolysis are inverted for clarity. The

difference (red, after - before) is representative of the change that occurred during photolysis the time. ....77

Figure 3.11 Panel A shows the average number of carbon atoms per molecule before (dark grey bars) and after (light grey bars) 1 h of photolysis. Panel B shows the percent change,  $(\text{after}-\text{before})/\text{before} \times 100$ , in the average number of C (purple), H (blue), and O (yellow) atoms following the 1 h of photolysis. ....79

Figure 4.1 Mass spectra for the  $\alpha$ -pinene (APIN) SOA samples formed from three oxidation conditions (ozonolysis, OH/NO<sub>x</sub> photooxidation, and reaction with NO<sub>3</sub>). The x-axis corresponds to the molecular weight of the neutral SOA compounds. Peaks in red denote nitrogen-containing organic compounds (NOC).....98

Figure 4.2 Mass spectra for the  $\alpha$ -humulene SOA samples formed from three oxidation (ozonolysis, NO<sub>x</sub> photooxidation, and reaction with NO<sub>3</sub>) before photolysis. The x-axis corresponds to the molecular weight of the neutral SOA compounds. Peaks in red denote NOC. .... 101

Figure 4.3 High-resolution mass spectra of the APIN/O<sub>3</sub> [A], APIN/NO<sub>x</sub> [B], APIN/NO<sub>3</sub> [C], HUM/O<sub>3</sub> [D], HUM/NO<sub>x</sub> [E], and HUM/NO<sub>3</sub> [F] aqueous SOA extracts at  $t = 0$  h, the dark control after 4 hours, and the photolysis sample after 4 hours ( $t = 4$ ). The X-axis corresponds to the molecular weight of the neutral compounds and the Y-axis corresponds to the intensity in the positive ion mode ESI mass spectrum. Peaks are normalized with respect to the largest peak in the sample. Peaks in red denote NOC. ....104



Figure 4.4	The time-dependent average number of carbon atoms and elemental ratios in the photolysis (open circles) and dark control samples (closed circles) for each of the $\alpha$ -pinene oxidation conditions.....	106
Figure 4.5	The time-dependent average number of carbon atoms and elemental ratios in the photolysis (open circles) and dark control samples (closed circles) for each of the $\alpha$ -humulene oxidation conditions.....	107
Figure 5.1	Sample FTIR spectrum of compound F (4-hydroxytetrahydrofuran-3-yl nitrate) with bands attributable to the $-\text{ONO}_2$ and $-\text{OH}$ groups labeled.....	117
Figure 5.2	Representative UV-VIS spectra of 2-hydroxycyclohexyl nitrate (compound A) at different solution concentrations. The inset shows an example of calculating the molar extinction coefficient from Beer's law at 325 nm; such calculations have been done at every wavelength for every nitrate investigated in this work...	119
Figure 5.3	Panel (a): wavelength dependent molar extinction coefficients for $\beta$ -hydroxyalkyl nitrates A, B, C, D (in various shades of red with markers) and alkyl nitrates J, K (in shades of blue without markers) measured in methanol. Gas-phase data (in black and green) for isopropyl nitrate (K), <sup>1</sup> ethyl nitrate (EN), <sup>1</sup> hydroxyethyl nitrate (HEN), <sup>2</sup> trans-2-hydroxycyclopentyl-1-nitrate (HCPN) <sup>3</sup> are provided for comparison (only a limited number of points were reported for HCPN). Panel (b) contains the measured molar extinction coefficients for compound L measured in various solvents.....	123

Figure 5.4	Molecular orbitals (obtained by MP2) involved in electronic transitions of conformer 1 (right panel) and conformer 3 (left panel) of ethyl nitrate listed in Table 5.4. and Table 5.5.....	128
Figure 5.5	Structures of the conformers of $\beta$ -hydroxyethyl nitrate as calculated by MP2 listed in Table 5.6. Same colors around the frame correspond to different rotamers around one bond.....	129
Figure 5.6	Molecular orbitals as obtained by MP2 involved in electronic transitions of the lowest energy conformer of $\beta$ -hydroxyethyl nitrate listed in Table 5.7. ....	130
Figure 5.7	Comparison of theoretically predicted absorption cross sections of ethyl nitrate (red noisy trace) and $\beta$ -hydroxyethyl nitrate (blue noisy trace). The absorption cross sections for ethyl nitrate (red solid line) and hydroxyethyl nitrate (blue solid line) are shown for comparison. The two theoretical results have been arbitrarily scaled by the same factor. Note that the experiments and simulations predict spectral shifts in the opposite direction for the two compounds. ....	132
Figure 5.8	Decomposition of the predicted absorption spectra of ethyl nitrate (a) and $\beta$ -hydroxyethyl nitrate (b) into contribution from the four lowest electronic states. ....	133
Figure 5.9	Predicted absorption spectrum of ethyl nitrate calculated by inclusion of one (red trace – labeled nitrate-1) and four (blue trace – labeled nitrate-4) states in the MD simulations. The one-state calculation was scaled down by 50 (to account for the difference in sampling). The shape of the low-energy tail of the spectrum is nearly identical in both cases. ....	134

Figure 5.10 Likely photoinduced atmospheric sinks of studied compounds at a solar zenith angle of  $65^\circ$ .  $Q$  is defined as the ratio of the aqueous oxidation by OH rate and the aqueous photolysis rate.  $Z$  is defined as the ratio of the gas photolysis rate and aqueous photolysis rate. The lack of points with  $Q < 1$  and  $Z < 1$  indicates that liquid phase photolysis of nitrate compounds considered in this work is too slow relative other sink processes under typical atmospheric conditions. ....139

## List of Tables

Table 2.1	Names and abbreviations for the VOC used to generate SOA samples in a smog chamber. The SOA samples are referred to using the code VOC/oxidation conditions; specifically, VOC/OH and VOC/OH/NO <sub>x</sub> refer to samples prepared under low-NO <sub>x</sub> and high-NO <sub>x</sub> conditions, respectively. The reaction time in the chamber is equivalent to the irradiation time. ....23
Table 2.2	Names and abbreviations for the VOC used to generate flow tube ozonolysis SOA samples. The initial VOC concentration in flow tube experiments is the steady-state mixing ratio the VOC would have in the absence of ozone. Ozone was added in small excess with respect to the VOC. The flow tube residence time is on the order of minutes. ....24
Table 2.3	Effective SOA lifetimes with respect to photochemistry for Los Angeles....47
Table 3.1	The structures of VOC precursors used for the generation for SOA samples, abbreviations by which they are referred to in this paper, and their commercial sources and purities. ....58
Table 3.2	Experimental conditions and code names for the SOA samples examined in this chapter.....60
Table 3.3	Major peaks observed in the mass spectra for all samples analyzed in this chapter. ....69
Table 3.4	Overlap of peaks between NO <sub>x</sub> samples and O <sub>3</sub> samples. ....72
Table 3.5	The average molecular formulas and double bond equivalents (DBE) before and after 1 h of photolysis of SOA solutions.....80

Table 3.6	The average atomic ratios X/C, where X is O, H, or N, before and after 1 h of photolysis of SOA solutions. ....	81
Table 4.1	Experimental conditions for the SOA samples prepared from $\alpha$ -pinene (APIN) and $\alpha$ -humulene (HUM).....	93
Table 4.2	Major peaks for $\alpha$ -pinene SOA from each set of oxidation conditions.....	99
Table 4.3	Percentage of 0N ( $C_xH_yO_z$ ), 1N ( $C_xH_yO_zN$ ), 2N ( $C_xH_yO_zN_2$ ), and 3N ( $C_xH_yO_zN_3$ ) compounds for APIN SOA samples. ....	100
Table 4.4	Major peaks for Humulene SOA in each oxidation condition.....	102
Table 4.5	Percentage of 0N ( $C_xH_yO_z$ ), 1N ( $C_xH_yO_zN$ ), 2N ( $C_xH_yO_zN_2$ ), and 3N ( $C_xH_yO_zN_3$ ) compounds for HUM samples. ....	102
Table 5.1	Summary of synthesized (A-I) and purchased (J-L) organic nitrates studied in this work. The first column contains letter abbreviations by which different nitrates are referred to in other tables and figures. ....	115
Table 5.2	Molar extinction coefficients (in $L mol^{-1} cm^{-1}$ ) for the investigated nitrates. The solvent is methanol, except for compound L, which was additionally investigated in water (w), acetonitrile (acn), octanol (oct), and tetrahydrofuran (thf). Each molar extinction coefficient is obtained from a fit of the available absorbance vs. concentration data as shown in Figure 5.2.....	121
Table 5.3	Optimized geometries, relative energies, and dipole moments of ethyl nitrate conformers as calculated with MP2/cc-pVDZ.....	126
Table 5.4	The lowest electronic excited states of conformer 1 of ethyl nitrate. All parameters are calculated at CC2 level, but the OM2 energies are also provided for comparison. ....	127

Table 5.5	The lowest electronic excited states of conformer 3 of ethyl nitrate. All parameters are calculated at CC2 level, but the OM2 energies are also provided for comparison. ....	127
Table 5.6	Relative energies (as calculated with MP2) and relative Boltzmann populations of $\beta$ -hydroxyethyl nitrate conformers at 300 K. ....	130
Table 5.7	The electronic excited states of the lowest energy conformer of $\beta$ -hydroxyethyl nitrate as calculated by CC2. All parameters are calculated at CC2 level, but the OM2 energies are also provided for comparison. ....	131
Table 5.8	Cross-comparison of orbitals of ethyl nitrate and $\beta$ -hydroxyethyl nitrate.....	131
Table 5.9	Henry's constants used for predicting aqueous partitioning of nitrates examined in this work.....	136

## Acknowledgments

Sergey was the first person I heard from at UCI when he called me and left me a voicemail, congratulating me on being accepted to UCI and how he hoped to see me at one of the visitation weekends. After one more voicemail, I made the last minute decision to visit UCI. After my visitation, I was pretty much sold on attending, and well, now I'm graduating from UCI with a PhD. From the first time I stepped into Sergey's lab, it has always felt like a second home to me, which is especially important considering I could spend 18 hours in lab some days before PNNL trips. Sergey has let me work independently, at my own pace, for the 5 years I've been here. Although this has meant lengths of time where I'm drowning in data analysis and go radio-silent until I'm complete, I don't think he has worried about my progress once (or if he has, I haven't noticed). Sergey, thanks for leaving those initial voicemails, and I am honored to be graduating from your aerosol photochemistry group.

For my PhD., I spent a lot of time in Richland, Washington, at Pacific Northwest National Laboratory using their facilities. Without this time on the high-resolution mass spectrometer, this dissertation would not exist. With that being said, I need to thank Dr. Alex Laskin and Dr. Julia Laskin, as well as Dr. Bingbing Wang and Dr. Peng Lin for all their help, guidance, and patience over the years.

To all the faculty and staff here at UCI, especially my committee members Dr. Donald Blake and Dr. Craig Murrari, as well as the rest of the AirUCI family and the ladies of Iota Sigma Pi, thank you.

To all group members, both former and current, thanks for all the memorable times. There's no way I'm going to forget our group BBQs, Dave and Buster outings, group movie nights, and my personal favorite, bowling and food trucks!

Lastly, I need to thank the funding sources I have had over the years, most notably the NSF Graduate Research Fellowship. This fellowship allowed me to pursue my research interests full time. I also need to thank NSF and NOAA as additional funding sources during my first year in the lab.

My love and appreciation of chemistry, especially as a career, had to start somewhere and for that I have to thank my high school chemistry teacher, Mrs. Linae Hahn. I can still remember things she taught me as if it were yesterday (such as the mole song) that have stuck with me for the last 12 years and have now been incorporated into my own teaching.

When I decided to go to Millikin University, a school known for their musical theatre program and not science, many were skeptical of my choice. However, from the first time I walked in to Leighty-Tabor Science Center, I have never felt more comfortable. This is largely due to the amazing chemistry faculty: Dr. Ed Acheson, Dr. Paris Barnes, Dr. George Bennett, and Dr. Clarence Josefson. Each one of you has inspired me and pushed me in some way that has laid the groundwork for the scientist I have become. Paris took me on as an undergraduate chemistry researcher in his group and let me design my own project. Dr. Ed always answered my questions with another question and although this annoyed me as a student, his way of teaching exponentially helped my critical thinking skills and turned me the extremely inquisitive person I am today. Without Dr. Bennett and Dr. J., who seriously cornered me one day and asked why I was not applying to REU programs, I can honestly say I would not be at UCI today.

My first experience with atmospheric chemistry came through an NSF Research Experience for Undergraduates (REU) at Washington State University in the Laboratory for Atmospheric Research. It was through this experience that solidified the idea that I wanted to go to graduate school and pursue atmospheric chemistry. Many thanks to Shelley Pressley, who was



in charge of the REU program and who helped me tremendously with advice when I ran in to some problems. Also, many thanks to George Mount and Elena Spinei, who let me work in their lab for those 10 weeks. Now that I have mentored my own summer students, I can truly appreciate the time and patience they shared with me, while also trusting me in using and monitoring their field instrument after such a short training time. I also need to acknowledge all other faculty members in the Department of Civil and Environmental Engineering at WSU who exposed me to programming and software such as IgorPro, which I now use all the time, for the first time.

None of this would have been possible if I did not have the close friendships that I do. From random packages arriving at my door, to a text message or phone call when I needed it, and everything in between, I have many friends I need to thank, both here at UCI and across the US, whom have provided much encouragement and support over the last five years. There are too many of you to name, and for fear of leaving someone out, let's just say you know who you are, and leave it as that.

Saving the best for last, I need to thank my Mom, Dad, and sister, Kara, for their support over the years. Since I began research at Millikin University, you had absolutely no idea what I was doing; yet you always supported me in what I wanted to do, even if it was just smiling and nodding while pretending to understand my presentation, or driving me halfway across the country so I could visit Los Alamos National Laboratory for a day. From my original work in making a smokeless combustible (aka, fireworks) to atmospheric chemistry and having to hear my rants on climate change, air pollution, and the politics that goes with it, you have stood my by side on the good days as well as the bad ones where all I wanted to do was quit. Thanks again for always being there. I can finally say, "I did it!"

## Curriculum Vitae

### Education and Research:

- 2016** Ph.D. in Chemistry, University of California, Irvine
- 2011-2015** Visiting Scholar, to the Environmental Molecular Sciences Laboratory, Pacific Northwest National Laboratory
- 2011-2016** Graduate Research Assistant, in the Sergey A. Nizkorodov Research Group, University of California, Irvine
- 2011** B.S. in Chemistry, Millikin University
- 2010** Visiting Undergraduate Research Assistant, in the George Mount Group, Washington State University
- 2009-2011** Undergraduate Research Assistant, in the Paris Barnes Group, Millikin University

### Awards and Honors:

- 2016** Jackie Smitrovich Prize
- 2013** National Science Foundation, Graduate Research Fellowship
- 2011** American Institute of Chemists Award
- 2011** Carl and Lucile Weatherbee Chemistry Award
- 2011** ACS Undergraduate Inorganic Chemistry Award
- 2010** National Science Foundation, Research Experience for Undergraduates
- 2010** Illinois Chemical Education Foundation Scholarship
- 2010** ACS Undergraduate Analytical Chemistry Award
- 2009, 2010** Dr. And Mrs. William Henderson Prize
- 2009-2011** James Millikin Scholar
- 2009-2011** Leighty Science Scholar
- 2008** Chemical Rubber Company Award

### Publications:

3. **Romonosky, D.E.**, Ali, N.N., Saiduddin, M.N., Wu, M., Lee, H.J., Aiona, P.K., and Nizkorodov, S.A. Effective Absorption Cross Sections and Photolysis Rates of Model Anthropogenic and Biogenic Secondary Organic Aerosol. *Atmos. Environ.* **130** (2016) 172-179. DOI:10.1016/j.atmosenv.2015.10.019
2. **Romonosky, D.E.**, Nguyen, L.Q., Shemesh, D., Nguyen, T.B., Epstein, S.A., Martin, D.B.C., Vanderwal, C.D., Gerber R.B. and Nizkorodov, S.A. Absorption Spectra and Aqueous Photochemistry of  $\beta$ -hydroxyalkyl Nitrates of Atmospheric Interest. *Mol. Phys.* **113** (2015) 2179-2190. DOI: 10.1080/00268976.2015.1017020
1. **Romonosky, D.E.**, Laskin, A., Laskin, J. and Nizkorodov, S.A. High-Resolution Mass Spectrometry and Molecular Characterization of Aqueous Photochemistry Products of Common Types of Secondary Organic Aerosols. *J. Phys. Chem. A* **119** (2015) 2594-2606. DOI: 10.1021/jp509476r

### Publications in Preparation:

1. **Romonosky, D.E.**, Li, Y., Shiraiwa, M., Laskin, A., Laskin, J. and Nizkorodov, S.A. Aqueous Photochemistry of Secondary Organic Aerosol of  $\alpha$ -Pinene and  $\alpha$ -Humulene Oxidized with Ozone, Hydroxyl Radical, and Nitrate Radical.

## **Abstract**

Optical Properties, Chemical Composition, and Aqueous Photolysis of Secondary Organic Aerosol

By

Dian Elizabeth Romonosky

Doctor of Philosophy in Chemistry

University of California, Irvine, 2016

Professor Sergey A. Nizkorodov, Chair

A large fraction of organic aerosol particles are formed as secondary organic aerosol (SOA) resulting from the condensation of partially oxidized biogenic and anthropogenic volatile organic compounds (VOCs) with gas phase oxidants such as  $O_3$ , OH,  $NO_x$ , and  $NO_3$ . An additional pathway for SOA formation is by the photochemical aqueous processing of VOC occurring inside cloud and fog droplets, followed by droplet evaporation. Once formed, SOA can age through heterogeneous oxidation and fog photochemical processes involving the hydroxyl radical (OH) as well as various other oxidants in the atmosphere. In addition to condensed phase oxidation, SOA can also age in the atmosphere upon exposure to radiation, for many of these organic compounds are photolabile and can degrade through direct photolysis, wherein the compounds absorb radiation and break into products, and indirect photolysis, wherein absorption of solar radiation initiates chemistry through the production of non-selective oxidants such as OH. These photochemical aging processes have the potential to be on time scales that are comparable to the typical lifetimes of droplets (hours) and particles (days), making them relevant to study further for both climate and health reasons. This dissertation presents a systematic investigation of the optical properties, molecular composition, and the extent of photochemical

processing in different types of SOA from various biogenic and anthropogenic VOC precursors. Chamber- or flowtube-generated SOA is made and then analyzed using high-resolution mass spectrometry (HR-MS) to observe the extent of change in the molecular level composition of the material before and after aqueous photolysis. Significant differences in the molecular composition between biogenic and anthropogenic SOA were observed, while the composition further evolved during photolysis. To study the optical properties and lifetimes of organic aerosol, spectroscopy tools such as UV-Vis is utilized. Results of this study suggest that the condensed phase photolysis of SOA can occur with effective lifetimes ranging from minutes to hours, and therefore represents a potentially important aging mechanism for SOA. The outcome of this dissertation will be improved understanding of the role of condensed-phase photochemistry in chemical aging of aerosol particles and cloud droplets.

# Chapter 1: Introduction

## 1.1. Background and Motivation

### 1.1.1. Secondary Organic Aerosol (SOA)

Understanding the formation and fate of atmospheric organic aerosols has been an important area of research since Went reported that the oxidation of volatile organic compounds (VOCs) emitted by plants and vegetation could lead to the formation of an organic “blue haze”.<sup>4</sup> There are two types of organic aerosol in the atmosphere: primary organic aerosol and secondary organic aerosol. Primary organic aerosol (POA) are directly emitted into the atmosphere by sources such as fossil fuel combustion, biomass burning, and vegetation.<sup>5</sup> Secondary organic aerosol (SOA) are created when VOCs undergo atmospheric oxidation to form condensable products. The oxidation can happen in one of the following ways: (1) gas-phase oxidation of VOCs followed by condensation of the products into new particles or onto pre-existing particles; (2) heterogeneous uptake reactions of VOCs on particle surfaces; and (3) aqueous processing of VOCs, such as photochemical processes occurring inside cloud and fog droplets, followed by droplet evaporation.<sup>6</sup> Until recently, the first pathway was thought to be the main mechanism of SOA formation, resulting in a comprehensive compilation of reference tables of photochemical and kinetic data for hundreds of compounds<sup>7</sup> and in tabulation of SOA yields from oxidation of different VOC precursors by the hydroxyl radical (OH), ozone (O<sub>3</sub>), and the nitrate radical (NO<sub>3</sub>). However, in the last several years, it has been realized that a very significant fraction of SOA is produced through cloud and fog photochemical processes.<sup>8,9</sup>

SOA often constitutes a sizable fraction of fine particulate matter known as PM<sub>2.5</sub>, and can have significant effects on both the physical and chemical characteristics of atmospheric aerosols. PM<sub>2.5</sub> negatively affects air quality on a local, regional, and global scale, most notably through the decline in visibility,<sup>10</sup> but can also have an effect on climate via direct and indirect

radiative forcing.<sup>11,12</sup> Exposure to PM<sub>2.5</sub> has also been associated with increases in human mortality and morbidity levels, while decreases of PM<sub>2.5</sub> have been associated with an increase in life expectancy.<sup>13</sup>

### **1.1.2. VOC Serving as Precursors of SOA**

This dissertation focuses on the optical properties and chemical composition of a variety of SOA created from the oxidation of biogenic and anthropogenic VOCs. Studies of plant signaling and defense, as well as food and flavor chemistry, have led to the detection of thousands of individual VOCs, yet only a small fraction of these have been studied by the atmospheric science community.<sup>14</sup> Biogenic VOCs include isoprene (C<sub>5</sub>H<sub>8</sub>), the most abundant non-methane hydrocarbon in the atmosphere,<sup>15</sup> as well as  $\alpha$ -pinene,  $\beta$ -pinene, myrcene, and limonene, which are among the top six most abundant monoterpenes.<sup>16</sup> A monoterpene, or a VOC that has the chemical formula of C<sub>10</sub>H<sub>16</sub>, are major components of VOCs emitted from forested environments, with emissions of monoterpenes having been observed from a variety of plants including pines, spruce, and some deciduous trees, such as oaks.<sup>17-20</sup> On a global scale, monoterpenes contribute ~10% of the total biogenic hydrocarbon emissions and are approximately equal to emissions from all anthropogenic sources combined.<sup>21,22</sup>

In addition to monoterpenes, sesquiterpenes, VOCs that have the chemical formula C<sub>15</sub>H<sub>24</sub>, were studied throughout this dissertation. Chosen sesquiterpenes include  $\alpha$ -humulene and farnesene, compounds found to be emitted not only from pine trees, but also thale cress, orange orchards, marsh elders, tobacco, sunflowers, and hops.<sup>23-30</sup> Relative to monoterpenes, sesquiterpenes contribute ~2.5% to total biogenic hydrocarbon emissions.<sup>31</sup> Sesquiterpenes have a much higher potential to form SOA than monoterpenes, and the presence of multiple double



bonds allows for fast reactions with oxidants, such as O<sub>3</sub>, making them an important component to study in regards to aerosol formation.<sup>32–35</sup>

In urban areas, major sources of VOCs are from fossil fuel combustion, resulting in a number of products including aromatic compounds as well as various other hydrocarbons found in gasoline and diesel fuels. In this work, 1,3,5-trimethylbenzene, a product of diesel combustion,<sup>36</sup> and also a well studied system,<sup>37–41</sup> was chosen to represent the aromatic constituents of anthropogenic VOC emissions. Likewise, biomass burning has gained the attention of the atmospheric community, largely due to brown carbon (BrC) and its light-absorbing properties.<sup>42</sup> Guaiacol, a product of biomass-burning,<sup>43</sup> as well as 1-methylpyrrole<sup>44</sup> and 2-methylpyrrole,<sup>45</sup> are included as biomass-burning precursors. This aerosol is also a model system for Humic-Like Substances (HULIS), which contain an aromatic and/or olefinic chemical structure and highly oxidized functional groups with high chemical diversity in addition to having a small particle size, relatively low molecular weight and typical optical features in the UV-Vis range.<sup>46</sup>

### **1.1.3. Photochemical Aging of Organic Aerosols**

Once in the atmosphere, organic aerosol (OA) is known to undergo both physical and chemical aging processes from reactions with sunlight and atmospheric oxidants.<sup>47,48</sup> It is important to understand the nature of these changes in order to predict the health and climate impacts of atmospheric aerosols that travel long distances from the point of their initial formation. Prevalent chemical mechanisms for OA aging involve multiphase oxidation of OA constituents by atmospheric oxidants. The most dominant oxidant involved in the multiphase oxidation of OA, as well as aqueous-phase oxidation of water-soluble atmospheric organics, is the OH radical.<sup>8,47</sup> NO<sub>3</sub>, O<sub>3</sub>, and other oxidants also contribute to these aging processes.<sup>49</sup> OA

compounds can additionally be aged by condensed-phase photochemical reactions occurring in the bulk of the SOA material upon exposure to solar actinic radiation.<sup>47</sup>

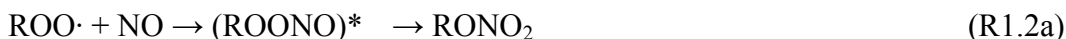
Aqueous photochemical processes involve organic compounds in cloud and fog water that undergo direct photolysis, wherein the compounds absorb radiation and break into products, and indirect photolysis, wherein absorption of solar radiation initiates chemistry through the production of non-selective oxidants such as hydroxyl radical (OH) and superoxide ( $O_2^-$ ). Direct photolysis processes are well-known to control lifetimes of many gas-phase species;<sup>17</sup> they are likely to be just as important for compounds found in biogenic and anthropogenic SOA, and in cloud droplets. Oxidation by OH is the primary competitive channel for photolysis, but in cloud and fog water affected by urban emissions, as well as inside organic aerosol particles, the oxidative capacity of OH may be too low to oxidize the high concentrations of the dissolved SOA.<sup>50,51</sup> Furthermore, select compounds, such as pyruvic acid, photolyze faster than they react with OH under representative cloud and fog water conditions.<sup>52,53</sup> Additionally, the higher dissolved SOA concentrations have been shown to suppress photochemical OH production enough to shut down the OH-initiated loss pathway chemistry while not affecting the direct photochemical pathways.<sup>8</sup>

Direct and indirect photolysis processes occur simultaneously but their relative importance can be predicted only for the simplest organic compounds, which are not representative of SOA composition.<sup>54</sup> While much attention has been given to the oxidation of organic compounds with the OH radical,<sup>8</sup> there are critical gaps in our knowledge about the direct photolysis of atmospherically relevant organics in water, especially for processes involving multifunctional organic compounds. Furthermore, it is important to study the response of complex aqueous mixtures to irradiation (as opposed to solutions of isolated compounds)

since they are more representative of cloud and fog chemistry. Finally, little is known about the photochemistry of SOA-relevant multifunctional organic compounds such as highly-substituted carbonyls and organonitrates (esters of nitric acid).

#### 1.1.4. Nitrogen-Containing Compounds (NOC) in SOA

Esters of nitric acid, better known as organic nitrates, represent an important group of atmospheric organic compounds.<sup>17</sup> Oxidation of saturated hydrocarbons in air by OH in the presence of NO<sub>x</sub> (NO + NO<sub>2</sub>) is a common pathway to unsubstituted alkyl nitrates:



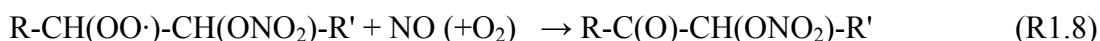
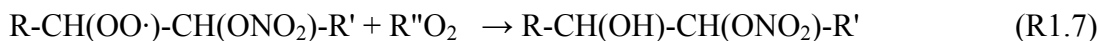
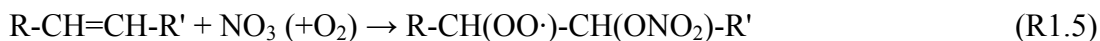
The yield of reaction (R1.2a) increases with the size of the alkyl group R and approaches ~30% for larger peroxy radicals ROO<sup>•</sup>.<sup>17</sup> Oxidation of unsaturated hydrocarbons under the same conditions commonly produces nitrates with a hydroxyl (–OH) group in the β position relative to the nitroxy (–ONO<sub>2</sub>) group.<sup>55–58</sup>



Reactions (R1.3) and (R1.4) are especially important in oxidation of biogenically emitted isoprene, monoterpenes, and other unsaturated volatile organic compounds in air masses affected by urban emissions. The resulting β-hydroxyalkyl nitrates have been observed in significant concentrations in both urban and remote environments in a number of field studies.<sup>59–62</sup>

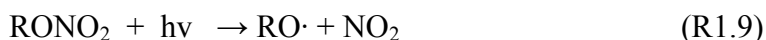
Reactions of nitrate radicals with alkenes also serve as an important source of nitrates<sup>63–69</sup>

substituted by a hydroxyl, hydroperoxyl (–OOH) or carbonyl group (=O) in the  $\beta$ -position, for example through the following sequence of reactions:



Other pathways to  $\beta$ -substituted alkyl nitrates also exist; a comprehensive review of these mechanisms is beyond the scope of this dissertation.

For unsaturated nitrates, such as the ones derived from isoprene, the reaction with OH serves as the most important daytime sink, while the reaction with  $\text{NO}_3$  dominates at night.<sup>70</sup> For saturated nitrates, other sink mechanisms may become competitive. One of the known degradation pathways for alkyl nitrates is gas-phase photolysis by means of the weak  $n \rightarrow \pi^*$  transition:<sup>71,72</sup>



The absorption cross sections<sup>2,71–75</sup> and photolysis quantum yields<sup>76,77</sup> of gas-phase alkyl nitrates have been studied extensively making it possible to reliably predict the rate of reaction (R1.9) under all relevant atmospheric conditions. In contrast to the simple alkyl nitrates, photochemistry of  $\beta$ -substituted nitrates is less well understood. Investigation of the neighboring group effects on photochemistry of atmospheric organic compounds is important; for example, the synergetic interaction between the carbonyl and nitroxy groups on the neighboring carbon atoms has been shown to lead to an efficient photolysis of  $\beta$ -carbonyl nitrates that occurs at faster rates than reaction with OH.<sup>78</sup>

Depending on their solubility and volatility, organic nitrates can remain in the gas-phase, partition into cloud and fog droplets, or partition in aerosol particles. The presence of a hydroxyl group decreases the vapor pressure and increases the solubility of small  $\beta$ -hydroxyalkyl nitrates enough to make their wet and dry deposition a significant sink. The magnitudes of the measured Henry's solubility constants suggest that  $\beta$ -hydroxyalkyl nitrates partition into aqueous phase to a significant extent whenever cloud and fog droplets are present.<sup>79,80</sup> Larger  $\beta$ -hydroxyalkyl nitrates, such as the ones derived from oxidation of monoterpenes, may have sufficiently low vapor pressures to efficiently partition into aerosols and onto environmental surfaces, especially if they are decorated with additional functional groups. Indeed, there have been a number of observations of  $\beta$ -hydroxyalkyl nitrates in particle-phase products of oxidation of isoprene,<sup>81,82</sup> alpha-pinene,<sup>56,67,83</sup> and other terpenes.

## 1.2. Goals of the Dissertation

The first goal of this dissertation is to determine the optical properties and chemical composition of a number of SOA, made from a variety of biogenic and anthropogenic VOC precursors. The second goal is to show how the molecular composition of different types of SOA changes due to aqueous photolysis.

Chapter 2 first discusses the optical properties of SOA representative of biogenic and anthropogenic environments. After creating the samples, mass absorption coefficients, or MAC values, were measured. Wavelength-dependent MAC (measured in units of  $\text{cm}^2 \text{g}^{-1}$ ) can be used to quantitatively predict how much solar radiation a given SOA would absorb. Specifically, the imaginary refractive index, which is used as an input to radiative transfer models, can be calculated from MAC.<sup>42</sup>

$$k(\lambda) = \frac{MAC_{material}(\lambda) \times \rho_{material} \times \lambda}{4\pi} \quad (1.1)$$

The higher the MAC values are in the visible range of the spectrum, the more absorbing the SOA is and the more it affects climate. High MAC values in the near-UV range affect the actinic flux available for photochemistry in the particles as well as in the surrounding gaseous phase. The MAC spectra measured in this dissertation were used to estimate effective absorption cross sections and lifetimes of the SOA with respect to photodegradation. The resulting lifetimes suggest that condensed-phase photochemistry has the ability to compete with other known aerosol aging processes.

Recognizing that all aerosols absorb near-UV radiation to some extent, Chapter 3 explores the chemical composition of a variety of biogenic and anthropogenic SOA, and the effect of solar radiation on the composition. A comparison of the mass spectra taken before and after irradiation showed that SOA compounds, especially the oligomeric ones, photodegrade in solution on atmospherically relevant time scales. Peroxides, carbonyls, organonitrates, and nitroaromatic compounds likely contributed to the observed SOA photodegradation. The extent of the photodegradation is not correlated with the absorption coefficient; the SOA prepared from aromatic precursors appear to be more resilient to photodegradation despite being more absorbing than SOA prepared from monoterpenes. The irradiation tends to reduce the average size (carbon number) of SOA compounds. However, the average atomic ratios O/C and H/C do not change significantly suggesting that this type of photochemical aging would be missed by methods relying on measurements of the average composition instead of detailed molecular characterization. These findings have important implications for understanding the aging chemistry of atmospheric aerosols during their cloud processing cycles.

Chapter 4 continues this work, exploring how different oxidation pathways effect the chemical composition of SOA, and how the composition evolves over photolysis in an aqueous environment. The analysis revealed significant differences in the molecular composition between monoterpene and sesquiterpene SOA formed by the different oxidation pathways. Our  $\alpha$ -pinene (APIN) /O<sub>3</sub> and APIN/NO<sub>x</sub> mass spectra agreed with our previously published data, while the APIN/NO<sub>3</sub> mass spectrum was reported for the first time. The most striking difference between the APIN/NO<sub>3</sub> SOA and APIN/NO<sub>x</sub> SOA was a much higher fraction of nitrogen-containing compounds (NOC) in the former, most likely due to NO<sub>3</sub> reacting with  $\alpha$ -pinene directly by addition to the double bond, resulting in NOC at the first generation of products. Similarly, the importance of NOC in the SOA compounds increases in the series:  $\alpha$ -humulene (HUM)/O<sub>3</sub> (where NOC are present at the small level of impurities), HUM/NO<sub>x</sub>, HUM/NO<sub>3</sub>. We also examined the effect of photolysis on the molecular composition of SOA produced by NO<sub>3</sub> oxidation. The composition of the SOA further evolved during photolysis, most notably in the depletion of nitrogen-containing compounds. Hydrolysis of nitrogen-containing compounds also occurred, but it was considerably slower than photolysis. This study highlights the potential importance of aqueous photochemistry in the aging of biogenic SOA.

Chapter 5 then concludes this dissertation with a study on a specific type of compound found in SOA, organonitrates. Results of this work suggest that the  $\beta$ -hydroxyl group appears to have a relatively minor effect on the absorption coefficients of organic nitrates in methanol, and by extension, in an aqueous solution. Therefore, it is unlikely that the photochemical loss of  $\beta$ -hydroxyalkyl nitrates will accelerate once they partition in cloud droplets or aerosol particles. A more quantitative analysis of the relative rates of loss of nitrates by gas-phase and aqueous-phase oxidation confirms that direct aqueous photolysis is not likely to compete with gas-phase

oxidation and photolysis, and with aqueous-phase oxidation by OH. The absorption coefficients of organic nitrates appear to increase slightly in solutions relative to the gas phase. However, the effect is not dramatic. Therefore, it should be reasonable to approximate gas-phase absorption coefficients by solution-based measurements, and vice versa. This should simplify measurements for nitrates that have low volatility (and hence cannot be studied by gas-phase techniques) or low solubility (cannot be studied by solution-based methods).

### 1.3. General Methods

#### 1.3.1. SOA Generation and Collection in Chamber

This section of the dissertation describes the method for generating SOA in the UCI environmental chamber. Any deviations from this method will be mentioned in the individual chapters. The oxidation of biogenic and anthropogenic VOC precursors was performed in a 5 m<sup>3</sup> Teflon chamber under dry conditions (RH < 2%) in the absence of seed particles. For all experiments, the chamber was flushed overnight with dried air from an FTIR purge gas generator (Parker Balston, Model 75-62), until particle concentrations were below 0.01 µg/m<sup>3</sup>. Figure 1.1 shows the chamber set up.

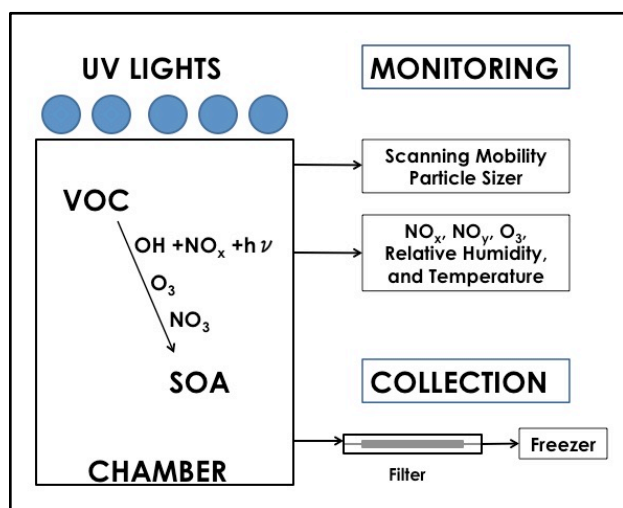
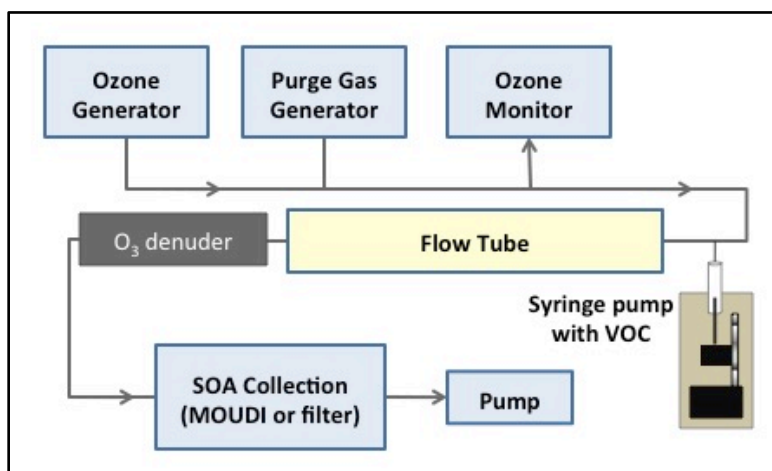


Figure 1.1. Chamber diagram.



VOCs serving as SOA precursors were added to the chamber by evaporation with a stream of air. For experiments in which OH was added, a measured volume of hydrogen peroxide ( $\text{H}_2\text{O}_2$ , Aldrich, 30% by volume in water) was used as the OH precursor and added in the same manner. For high-NO<sub>x</sub> experiments, NO was introduced by adding a calibrated volume of a primary standard (Parxair, 5000 ppm NO in N<sub>2</sub>) into the chamber. For O<sub>3</sub> reactions, a 1 SLM (standard liters per minute) flow of oxygen (99.994% purity) was sent through an UV O<sub>3</sub> generator into the chamber. The reagents were mixed in the chamber for several minutes using a fan, which was then shut off to minimize wall losses. UV-B lamps (FS40T12/UVB, Solarc System Inc.) with emission centered at 310 nm, were turned on to initiate the photochemistry when needed. SOA particles formed in the chamber were monitored by a TSI model 3936 scanning mobility particle sizer (SMPS), while a Thermo Scientific model 49i ozone monitor and a Thermo Scientific model 42i-Y NO<sub>y</sub> monitor recorded O<sub>3</sub> and NO/NO<sub>y</sub> data, respectively. The SOA was collected through an activated carbon denuder using poly(tetrafluoroethylene) (PTFE) filters (Millipore 0.2 μm pore size), which were then sealed and frozen for further offline analysis.

### 1.3.2. SOA Generation and Collection in Flow Tube



**Figure 1.2.** Diagram of flow tube reactor for ozonolysis reactions.

Alternatively, SOA can be made from O<sub>3</sub>-initiated reactions that were carried out in a 17 L flow tube reactor as seen in Figure 1.2. The reactor was maintained at <2% relative humidity, ambient atmospheric pressure, and ambient room temperature. Liquid VOC was injected into a 5-7 SLM air flow using a syringe pump at a rate of 25  $\mu\text{L/hr}$ . A pure oxygen (Airgas; 99.994% purity) flow of  $\sim 0.6$  SLM passed through an ozone generator and a photometric ozone detector. The two flows were mixed at the entrance of the flow tube resulting in the initial VOC and ozone mixing ratios of  $\sim 5$  ppm and 50-100 ppm, respectively. The residence time in the flow tube was less than 5 minutes, but sufficient for oxidizing all of the injected VOC and forming SOA. A 1-m long charcoal denuder removed residual O<sub>3</sub> and gaseous organic compounds from the flow exiting the reactor, while letting most of the particles go through. The SOA was collected on PTFE filters which were weighed before and after collection with a Sartorius ME-5F filter balance (1  $\mu\text{g}$  precision), then sealed and frozen for later analysis.

### 1.3.3. High-Resolution Composition Analysis with LTQ-Orbitrap

The SOA samples collected on filters and extracted in solvent were analyzed using a high-resolution linear ion trap (LTQ) Orbitrap™ (Thermo Corp.) mass spectrometer available at

the Wiley Environmental Molecular Sciences Laboratory (EMSL) user facility at Pacific Northwest National Laboratory (PNNL). All high-resolution mass spectrometry (HR-MS) analyses presented in this work were performed in collaboration with PNNL scientists Drs. Alexander Laskin and Julia Laskin. Mass spectra were acquired in the positive ion mode for all samples, and the instrument was operated at the resolving power ( $m/\Delta m$ ) of  $10^5$  at  $m/z$  400. A typical set of HR-MS measurements included a series of SOA aqueous extracts photolyzed for different time and a control (non photolyzed) sample. Blank samples included a solvent/water mixture. The photolysis of samples at UCI will be described in detail in Chapter 3 and the photolysis of samples at PNNL will be described in detail in Chapter 4.

The mass spectrometer used in this work was equipped with a direct-infusion electrospray ionization (ESI) source. ESI is a soft ionization method that converts molecules in the sample into positive or negative ions without fragmentation, allowing for the organic molecule to be assigned a molecular formula in later analysis.<sup>84</sup> This soft ionization method has great benefits over traditional electron impact ionization, which fragments organic compounds rather extensively. In ESI, the analyte solution is dispersed into a mist of highly charged droplets produced at the end of a capillary to which a high voltage is applied. The droplets are transferred into the inlet of the mass spectrometer, where they undergo desolvation resulting in the formation of analyte ions. Positive mode ESI spectra typically contain protonated  $[M + H^+]$  molecules, or molecules cationized on sodium  $[M + Na^+]$ . Polar organic solvents such as water, typically also mixed with acetonitrile or methanol, are used. Acetonitrile or methanol is added to decrease surface tension and improve the stability of the electrospray ionization (ESI) source.<sup>85</sup>

#### 1.3.4. Data Processing and Accurate-Mass Assignments

To process the large number of mass spectra recorded during this work, data analysis was performed in the following manner. For each spectrum, a list of peak position and intensities was generated using the Decon2LS program developed at PNNL. Peaks with a signal-to-noise ratio of 3 and higher were selected for analysis. The resulting peak lists for all the files in the same experimental batch, including blank samples, were then processed with a Labview 7.0 code that assigned peaks based on their measured  $m/z$  values within a specified tolerance ( $m/z \pm 0.001$ ) and constraints imposed on the elemental ratios ( $0 \leq \text{O:C} \leq 3.0$ ,  $0.8 \leq \text{H:C} \leq 2.5$ ). The molecules containing C, H, and O atoms generally result in peaks with odd nominal masses in ESI, however, no even/odd constraints were imposed because N-containing compounds can appear at even nominal masses in the mass spectra. The double bond equivalent (DBE, see Equation 4 below) was constrained to integer values for the neutral species. Peaks that corresponded to molecules containing one  $^{13}\text{C}$  atom or impurities were excluded. The initial set of assigned peaks was used to verify the calibration of the  $m/z$  axis. If deviations were noticeable (greater than  $\pm 0.0005$   $m/z$  units), the axis was recalibrated with respect to the trusted peaks. The vast majority of peaks corresponded to sodiated molecules ( $\text{C}_x\text{H}_y\text{O}_z\text{Na}^+$ ). After the peak assignment for a given batch of SOA samples was completed, O:C, H:C, and DBE values were calculated for the neutral species.

#### 1.3.5. Data Analysis

The average atom numbers (C, H, O, N), average elemental ratios (H:C, O:C, and N:C), and average molecular size, represented by the number of C atoms per molecule, were extracted from the assigned molecular formulas, and given the formula  $\text{C}_c\text{H}_h\text{O}_o\text{N}_n$ . These average quantities were used to assess the extent in the photolysis-induced overall change in SOA

composition.  $\langle O:C \rangle$  traditionally describes the degree of oxidation, while  $\langle H:C \rangle$  is a good indicator of the degree of unsaturation in SOA molecules.<sup>17</sup> All averaged quantities were calculated with respect to the relative intensity (*Intensity*), for all assigned compounds, indexed with *i*.<sup>15</sup>

$$\langle X \rangle = \frac{\sum Intensity_i \frac{X_i}{c_i}}{\sum Intensity_i} \quad (X = c, o, h, n, DBE) \quad (1.2)$$

$$\langle X:C \rangle = \frac{\sum Intensity_i \frac{X_i}{c_i}}{\sum Intensity_i} \quad (X = o, h, n) \quad (1.3)$$

The average double bond equivalent (DBE) value,  $\langle DBE \rangle$ , also known as “degree of unsaturation” to organic chemists,<sup>21</sup> was calculated by,

$$DBE = 1 - \frac{h}{2} + \frac{n}{2} + c \quad (1.4)$$

which should be equal to the total number of C=C bonds, C=O bonds, and rings in a molecule. Since most of the N-containing compounds in SOA are expected to be either nitrocompounds (-NO<sub>2</sub>) or nitric acid esters (-ONO<sub>2</sub>), the true DBE is higher than that predicted by Eq. (5) by the average number of nitrogen atoms, *n*:

$$\langle DBE_{corrected} \rangle = 1 - \frac{\langle h \rangle}{2} + \frac{3\langle n \rangle}{2} + \langle c \rangle = \langle DBE_{corrected} \rangle + \langle n \rangle \quad (1.5)$$

## **Chapter 2: Effective Absorption Cross Sections and Photolysis Rates of Anthropogenic and Biogenic Secondary Organic Aerosols**

---

Portions of this chapter are reproduced with permission from: D.E. Romonosky, N.N. Ali, M.N. Saiduddin, M. Wu, H.J. Lee, P.K. Aiona and S.A. Nizkorodov, “Effective absorption cross sections and photolysis rates of anthropogenic and biogenic secondary organic aerosols” *Atmospheric Environment* 130 (2016) 172-179; DOI: 10.1016/j.atmosenv.2015.10.019. Copyright 2016 by Elsevier Ltd.

## 2.1. Abstract

Mass absorption coefficient (MAC) values were measured for secondary organic aerosol (SOA) samples produced by flow tube ozonolysis and smog chamber photooxidation of a wide range of volatile organic compounds (VOC), specifically:  $\alpha$ -pinene,  $\beta$ -pinene,  $\beta$ -myrcene, d-limonene, farnesene, guaiacol, imidazole, isoprene, linalool, ocimene, p-xylene, 1-methylpyrrole, and 2-methylpyrrole. Both low-NO<sub>x</sub> and high-NO<sub>x</sub> conditions were employed during the chamber photooxidation experiments. MAC values were converted into effective molecular absorption cross sections assuming an average molecular weight of 300 g/mol for SOA compounds. The upper limits for the effective photolysis rates of SOA compounds were calculated by assuming unity photolysis quantum yields and convoluting the absorption cross sections with a time-dependent solar spectral flux. A more realistic estimate for the photolysis rates relying on the quantum yield of acetone was also obtained. The results show that condensed-phase photolysis of SOA compounds can potentially occur with effective lifetimes ranging from minutes to days, suggesting that photolysis is an efficient and largely overlooked mechanism of SOA aging.

## 2.2. Introduction

Currently, experimental evidence to determine the relative importance of condensed-phase photochemistry occurring in OA relative to multi-phase oxidation processes is limited. Chamber studies have begun to examine this effect by studying the properties and composition of SOA before and after exposure to UV light. Presto et al.<sup>86</sup> found that the formation of  $\alpha$ -pinene ozonolysis SOA in a smog chamber was suppressed by 20-40% when exposed to UV light. Kroll et al.<sup>87</sup> observed that low-NO<sub>x</sub> isoprene SOA grew during the initial irradiation period, but that was followed by a decrease in particle size as the SOA mixture was further irradiated. However,  $\beta$ -pinene low-NO<sub>x</sub> SOA particles did not shrink upon irradiation, indicating that the photochemical effects of UV exposure are dependent on the chemical composition of the SOA. Surratt et al.<sup>88</sup> detected a similar decrease in the particle size of low-NO<sub>x</sub> isoprene SOA upon irradiation. In these experiments, it was difficult to separate the effects of gas-phase and condensed-phase photochemistry. To bypass this limitation, Epstein et al.<sup>89</sup> used a denuder to remove VOC from  $\alpha$ -pinene ozonolysis SOA before the irradiation. They observed that UV light slightly reduced both the particle mass concentration and the average particle size; the fraction of organic peroxides in the particles decreased upon irradiation. Epstein et al.<sup>89</sup> and Wong et al.<sup>90</sup> similarly observed a reduction in the particle size for  $\alpha$ -pinene ozonolysis SOA material that was collected on a filter and re-aerosolized back in a photolysis chamber; the effect was larger at elevated relative humidity (RH). In contrast, Kourtchev et al.<sup>91</sup> observed no significant change to molecular level composition of SOA prepared by ozonolysis of a mixture of four biogenic VOC ( $\alpha$ -pinene,  $\beta$ -pinene, D3-carene and isoprene) and exposed to actinic UV radiation. In summary, chamber experiments suggest that photochemical processes in SOA particles are possible, but the results are inconsistent.



Qualitative experiments with irradiation of bulk SOA samples were carried out by Walser et al.<sup>92</sup> and Mang et al.<sup>93</sup> Both studies showed that SOA particles formed from limonene ozonolysis absorbed radiation in the actinic region, most likely due to the carbonyl and peroxide functional groups present, and that the ensuing photochemistry generated a number of small VOC as detectable products. The carbonyl functional groups appeared to play a significant role in this aging, as evidenced by the production of measureable quantities of CO, CH<sub>4</sub>, acetaldehyde, acetone, and other VOC, many of which could be explained by standard Norrish type-I and Norrish type-II carbonyl photochemistry.<sup>93,94</sup>

Condensed-phase photochemistry is not limited to OA particles; it can also take place in cloud/fog droplets. The irradiation of aqueous extracts of limonene ozonolysis SOA resulted in a significant change in the molecular composition, in which oligomeric and carbonyl compounds were depleted.<sup>95</sup> The photolytic processing appeared to be more efficient when SOA was dissolved in an aqueous solution as compared to dry SOA particles. The direct aqueous photolysis of high-NO<sub>x</sub> isoprene SOA also produced major changes in the molecular composition.<sup>96</sup> On average, 30% of the SOA by mass was significantly modified, suggesting that the effects of direct aqueous photolysis should not be ignored. Aqueous solutions of light absorbing OA compounds, such as SOA formed by photooxidation of naphthalene under high-NO<sub>x</sub> conditions, SOA formed by limonene ozonolysis and aged with ammonia vapor, and products of aqueous reaction of glyoxal and methylglyoxal with ammonium sulfate were shown to efficiently photobleach and undergo a large change in composition upon exposure to irradiation.<sup>97-99</sup> Finally, a systematic study of photochemistry of different types of SOA by Romonosky et al.<sup>100</sup> showed that aqueous photolysis might be an effective aging mechanism for SOA derived from biogenic, anthropogenic, and biomass burning VOC precursors. The

experiments done so far have been qualitative in nature; the diversity in structure and reactivity of VOC complicate the scientific understanding of the photochemistry of atmospheric aerosols. To better estimate the time scales of these photochemical processes under realistic atmospheric conditions, this study focuses on the quantitative measurements of absorption coefficients of SOA formed through the oxidation of biogenic and anthropogenic VOC using common atmospheric oxidants, specifically OH (in presence or absence of NO<sub>x</sub>) and O<sub>3</sub>. From these data, the rates of photolysis for a variety of SOA were calculated, resulting in a better understanding of the lifetimes of SOA in the atmosphere with respect to condensed-phase photochemistry.

## **2.3. Experimental**

### **2.3.1. SOA Generation and Collection**

Both O<sub>3</sub>-initiated and OH-initiated oxidation conditions, with and without added NO<sub>x</sub>, were used to prepare model SOA from VOC as shown in Table 2.1 and Table 2.2. Chamber experiments were performed as described in Section 1.3.1. For flow tube experiments described in Section 1.3.2, multiple SOA collection methods were used. In most experiments, SOA was collected on the PTFE filters. Other methods of SOA collection included impaction on foil substrates using a multi-orifice uniform-deposit impactor (MOUDI, MSP model 110-R) sampling at 30 SLM (standard liters per minute). In other experiments, SOA was collected on stage D of a Sioutas impactor<sup>101</sup> modified to accept either a CaF<sub>2</sub> window or foil substrates. The specified cutoff point of this impactor stage was 0.25 μm at 9 SLM flow rate, but sampling was done at 15 SLM to drive the cut-off point to lower particle sizes. The foil substrates and CaF<sub>2</sub> windows were weighed before and after SOA collection to determine the mass of SOA collected. Absorption coefficients from SOA collected on foil substrates, CaF<sub>2</sub> windows, and PTFE filters were comparable in magnitude. Depending on the yield of SOA, collection time for the flow tube

was approximately 30 min to 2 h. The samples were either analyzed immediately or sealed and frozen for later analysis.

Chamber experiments, described in Section 1.3.1 were carried out under either “high- $\text{NO}_x$ ” oxidation conditions, with approximately 300 ppb (parts per billion by volume) of  $\text{NO}$  added to the chamber to simulate an urban atmospheric environment, or “low- $\text{NO}_x$ ” oxidation conditions, with no additional  $\text{NO}$  added to the chamber in order to simulate a remote atmospheric environment. For the OH precursor, 90  $\mu\text{L}$  of  $\text{H}_2\text{O}_2$  (Aldrich; 30% by volume) was injected in the chamber by evaporation under a stream of zero air resulting in  $\sim 4$  ppm of  $\text{H}_2\text{O}_2$  vapor in the chamber. Precursor VOC was added to the chamber using the same method as was used for the  $\text{H}_2\text{O}_2$  addition, with VOC concentrations in the chamber varying from 500 ppb to 1 ppm. One exception was isoprene; we had to increase its starting mixing ratio to 4 ppm in order to generate enough SOA for further analysis. The chamber content was mixed for several minutes using a fan, which was then turned off to minimize particle wall losses. The UV-B lamps were turned on for 1.5 to 4 hours to initiate photochemistry (see Table 2.1). SOA particles passed through an activated carbon denuder at approximately 15 SLM and were collected using PTFE filters. Collection times ranged from 2 to 3 hours, with approximately 100  $\mu\text{g}$  to 3500  $\mu\text{g}$  of SOA collected on the filter, depending on the sample. The amount of SOA on the filter was estimated from SMPS data, assuming an SOA particle density of  $1.2 \text{ g/cm}^3$  and 100% collection efficiency by the filters. This assumed value of particle density represents an average of densities of anthropogenic and biogenic SOA materials reported by Hallquist et al.<sup>102</sup>

**Table 2.1.** Names and abbreviations for the VOC used to generate SOA samples in a smog chamber. The SOA samples are referred to using the code VOC/oxidation conditions; specifically, VOC/OH and VOC/OH/NO<sub>x</sub> refer to samples prepared under low-NO<sub>x</sub> and high-NO<sub>x</sub> conditions, respectively. The reaction time in the chamber is equivalent to the irradiation time.

<b>Precursor (abbreviated name)</b>	<b>Oxidant</b>	<b>Initial VOC (ppm)</b>	<b>Initial NO (ppb)</b>	<b>Reaction time (h)</b>	<b>Collection time (h)</b>	<b>Amount typically collected (mg)</b>
2-Methylpyrrole (2MPYR)	OH	0.5	<1	3	2	1.3
2MPYR	OH/NO <sub>x</sub>	0.5	300	2	3	1.8
$\alpha$ -Pinene (APIN)	OH/NO <sub>x</sub>	0.5	300	2	3	2.3
Farnesene (FAR)	OH	0.5	<1	1.5	3	3.5
FAR	OH/NO <sub>x</sub>	0.5	300	1.5	3	3.0
Guaiacol (GUA)	OH	0.5	<1	2	3	0.95
GUA	OH/NO <sub>x</sub>	0.5	300	1	3	1.3
Isoprene (ISO)	OH	4.0	<1	4	2.5	0.10
Linalool (LIN)	OH	0.5	<1	2	3	1.5
LIN	OH/NO <sub>x</sub>	0.5	300	2	3	1.5
Naphthalene (NAP)	OH	0.4	<1	2	3	1.0
NAP	OH/NO <sub>x</sub>	0.4	400	2	3	1.0
Ocimene (OCI)	OH	0.5	<1	2	3	2.0
OCI	OH/NO <sub>x</sub>	0.5	300	2	3	1.2
Toluene (TOL)	OH	1.0	<1	3	3	1.3
TOL	OH/NO <sub>x</sub>	1.0	1000	3.5	4	0.70
p-Xylene (XYL)	OH	1.0	<1	3	3	0.60
XYL	OH/NO <sub>x</sub>	1.0	300	3	3	1.0

**Table 2.2.** Names and abbreviations for the VOC used to generate flow tube ozonolysis SOA samples. The initial VOC concentration in flow tube experiments is the steady-state mixing ratio the VOC would have in the absence of ozone. Ozone was added in small excess with respect to the VOC. The flow tube residence time is on the order of minutes.

Precursor	Initial VOC (ppm)	Amount typically collected (mg)
2MPYR	20	0.80
APIN	10	2.0
ISO	10	0.15
1-Methylpyrrole (1MPYR)	20	0.20
Imidazole (IMID)	30	0.20
$\beta$ -Myrcene (BMYR)	10	0.40
$\beta$ -Pinene (BPIN)	10	0.70
d-Limonene (LIM)	10	7.3

### 2.3.2. UV-Vis Absorption Measurements

All of the samples were dissolved by vigorous shaking of the substrates immersed in 5 mL of water or methanol for 10 to 15 minutes. Sonication was avoided to prevent formation of peroxides in the extract.<sup>103</sup> Water was used as the extracting solvent in initial experiments, but not all SOA were found to be fully soluble in water.<sup>100,104</sup> Therefore, methanol was used as the extracting solvent for the remaining experiments. To determine the extraction efficiency using methanol, filters were extracted twice in two separate aliquots of solvent, and absorption spectra were taken using a UV/Vis spectrometer, as described below. From comparison of the recorded absorbance values, it was concluded that extraction efficiency in the first extraction step was greater than 80% in all cases. We did not correct for the incompletely extracted material and assumed that the first step extracted everything; this assumption introduces up to 20% uncertainty in the resulting absorption coefficients. Typical concentrations of SOA in the extract were 20-900  $\mu\text{g/mL}$ , which translates into 70-3000  $\mu\text{M}$ , assuming an effective molecular weight of 300 g/mol for the SOA compounds.

The SOA extracts were placed in a 1 cm quartz cuvette for absorption measurements. A dual beam spectrometer (Shimadzu UV-2450), with pure solvent as the reference, was used to take the UV/Vis absorption spectra. Wavelength-dependent mass absorption coefficients (MAC), in units of  $\text{cm}^2 \text{g}^{-1}$ , were calculated from the base-10 absorbance,  $A_{10}$ , of an SOA extract with the solution mass concentration,  $C_{\text{mass}}$  ( $\text{g cm}^{-3}$ ), and path length,  $b$  (cm):

$$MAC_{\text{material}}(\lambda) = \frac{A_{10}^{\text{solution}}(\lambda) \times \ln(10)}{b \times C_{\text{mass}}} \quad (2.1)$$

The subscript “material” attached to MAC emphasizes the fact that we are reporting mass-normalized absorption coefficients of the bulk SOA material as opposed to mass-normalized absorption cross section of aerosol particles.<sup>42</sup> In order to calculate  $C_{\text{mass}}$  from the SMPS data we assumed an average density of  $1.2 \text{ g/cm}^3$  for all the SOA samples we generated. A number of other values for the SOA densities have been reported.<sup>102</sup> The following equation can be used to correct the MAC values reported in this work to the actual MAC values if a different SOA density is adopted:

$$MAC_{\text{corrected}}(\lambda) = \frac{MAC_{\text{reported}}(\lambda) \times 1.2 \text{ g/cm}^3}{\rho_{\text{actual}}} \quad (2.2)$$

where  $\rho_{\text{actual}}$  refers to any other assumed or determined density. If  $\rho_{\text{actual}} > 1.2 \text{ g/cm}^3$ , the resulting MAC value would be smaller than the ones reported here, while  $\rho_{\text{actual}} < 1.2 \text{ g/cm}^3$  would result in a larger MAC values. In either case we do not expect the adjustment to be larger than 20% based on the SOA densities listed in Hallquist et al.<sup>102</sup> In combination with the 20% uncertainty for the completeness of SOA extraction, the overall accuracy of the reported MAC values should be on the order of  $\pm 30\%$ . This is sufficient for the purpose of estimation of lifetimes done in this paper.

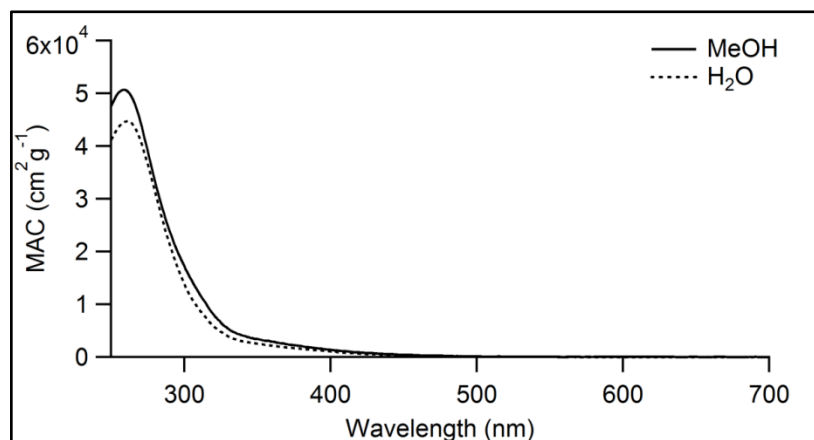


**Figure 2.1.** A comparison of MAC values for IMPYR/O<sub>3</sub> SOA, extracted in either water or methanol.

For water-soluble SOA investigated in this study, the MAC values from the absorption spectra of methanol extracts and the water extracts were found to be comparable in magnitude, as seen in Figure 2.1. For SOA that was poorly soluble in water, the shape of the absorption spectrum in water and in methanol were similar, but the methanol spectrum had higher absorbance because it contained more dissolved material. In view of the small sensitivity of the shape of the spectrum to the extracting solvent, it is expected that the absorption spectra of SOA compounds are not too sensitive to the environment, and MAC calculated from Eq. (2.1) approximated MAC of bulk SOA material reasonably well.

Equation (2.1) is only valid in the low concentration limit in which the Beer-Lambert law is obeyed. Figure 2.2 is an example of verification of linearity of the measure base-10 absorbance as a function of the mass concentration of SOA in the solution.

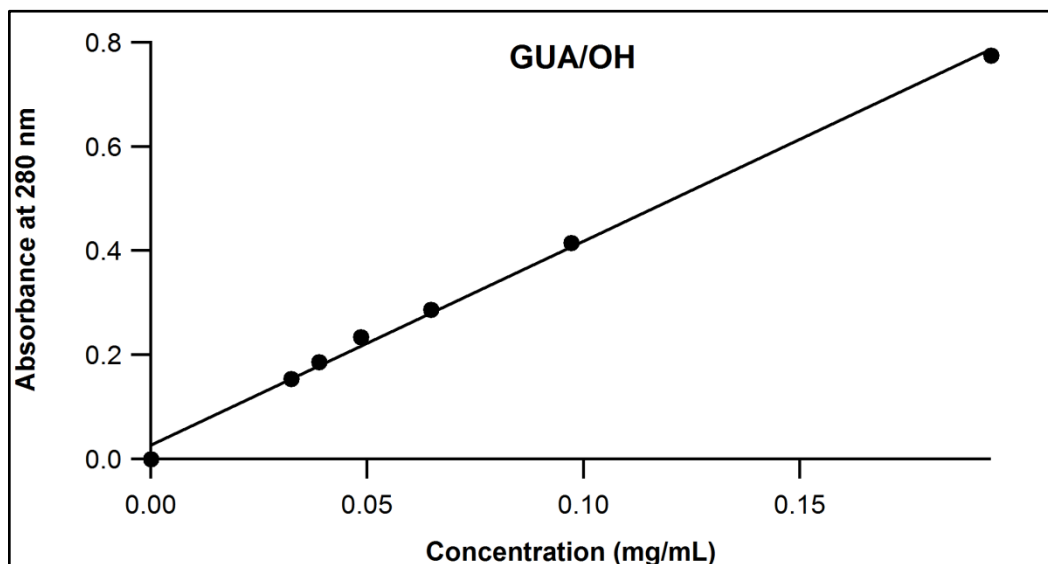


**Figure 2.2.** Absorbance of GUA/OH SOA vs. solution mass concentration.

Such absorbance linearity checks were carried out for all the SOA samples examined in this work, typically at 280 nm, where all SOA had easily detectable absorbance. Because absorbance values of the SOA solutions were recorded at different SOA concentration levels, the MAC spectra were built from the absorbance data in a piecewise fashion, wherein the solutions with higher concentrations were used to get MAC at longer wavelengths, and solutions with lower concentration were used to get MAC at shorter wavelengths. This helped improve the signal-to-noise ratio in MAC at longer wavelengths without having to violate the Beer-Lambert law at shorter wavelengths.

## 2.4. Results and Discussion

The MAC values for all the SOA samples prepared in this study are shown below in Figures 2.3-2.28. In all cases, the black lines correspond to MAC values obtained by averaging results of several independent trials, and shaded areas correspond to  $\pm$  one standard deviation. The MAC spectra have characteristic shapes for absorption spectra of common organic molecules, with the peak of absorption occurring in the UV range and a tail of absorption in the near-UV and visible ranges. The MAC values for some of the SOA samples, especially the ones



generated from ISO, appear noisy because of the low SOA mass yield resulting in low measured absorbance values for the SOA solutions.

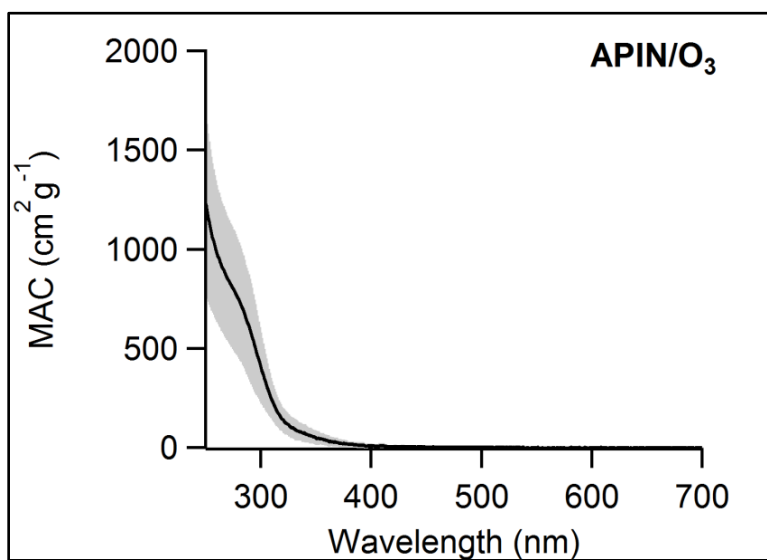


**Figure 2.3.** Mass absorption coefficient of  $\alpha$ -pinene (APIN) SOA.

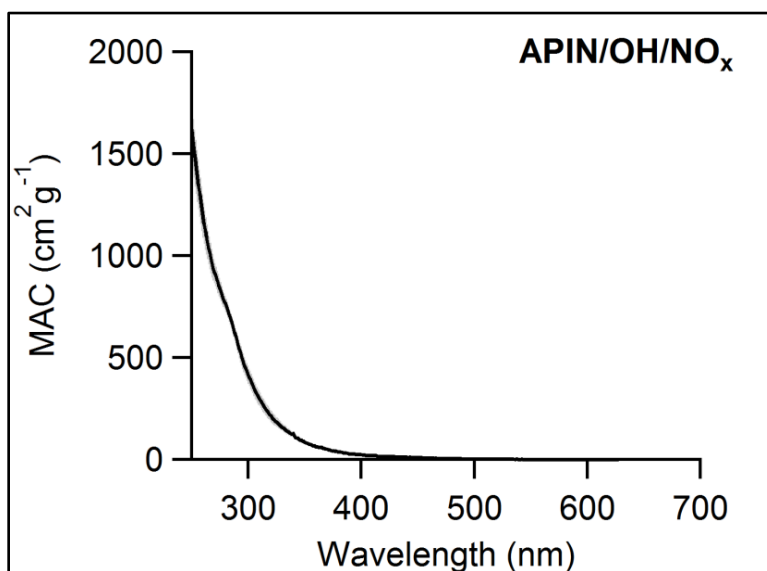


**Figure 2.4.** Mass absorption coefficient of  $\alpha$ -pinene (APIN) SOA.

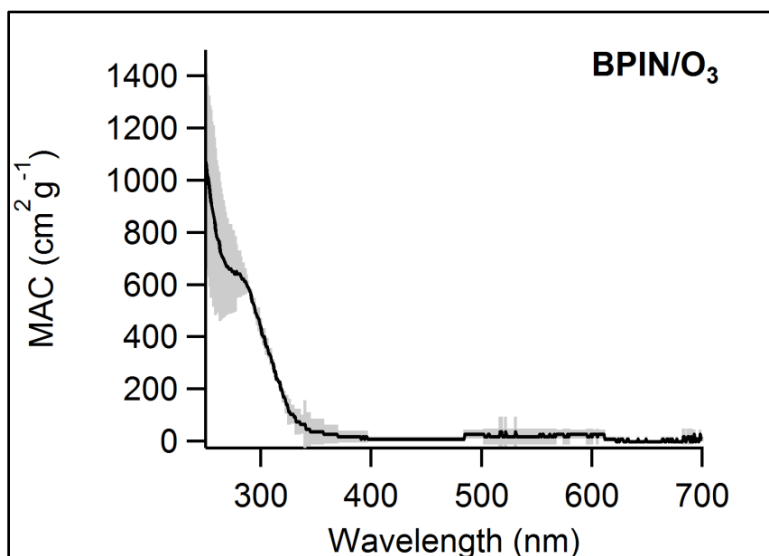


Figure 2.5. Mass absorption coefficient of  $\beta$ -pinene (BPIN) SOA.

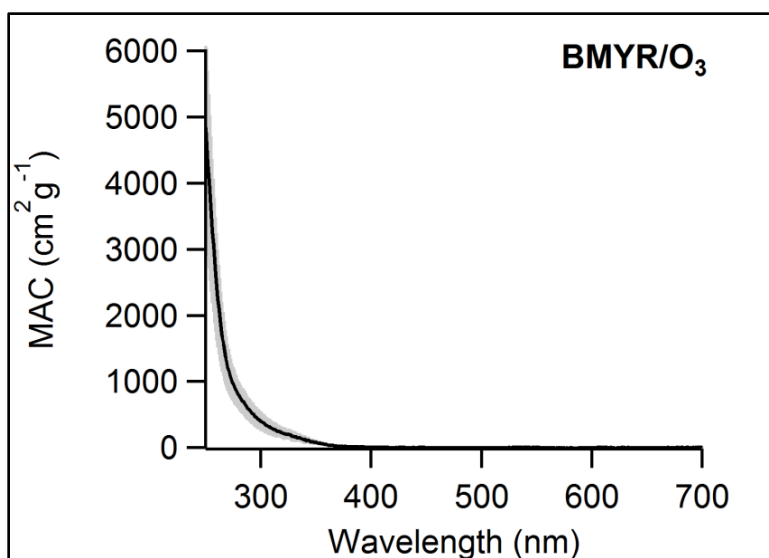
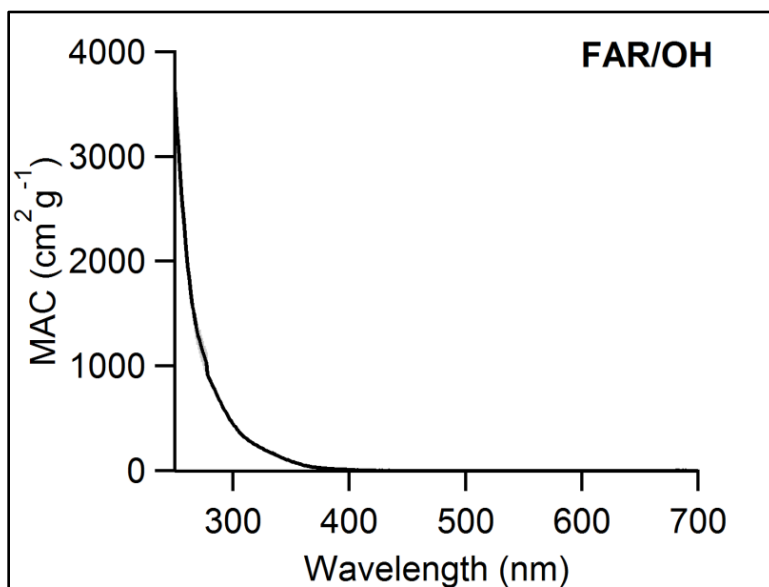
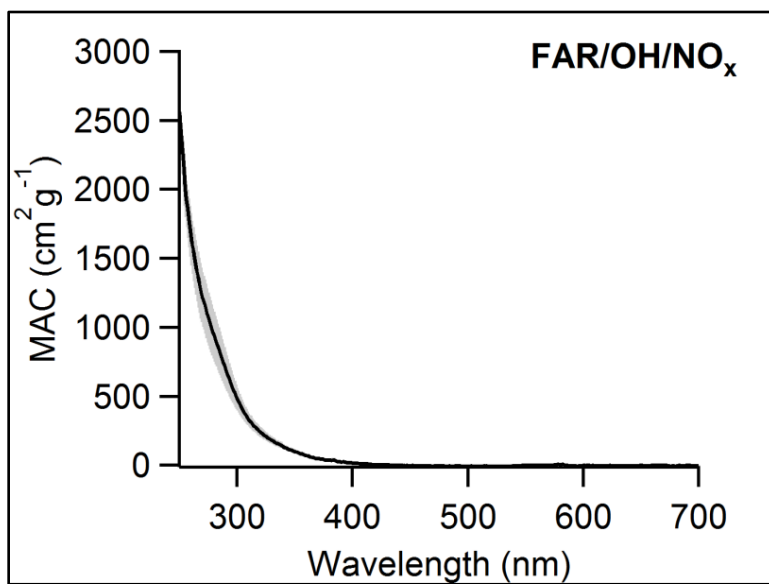


Figure 2.6. Mass absorption coefficient of  $\beta$ -myrcene (MYR) SOA.



**Figure 2.7.** Mass absorption coefficient of farnesene (FAR) SOA.



**Figure 2.8.** Mass absorption coefficient of farnesene (FAR) SOA.

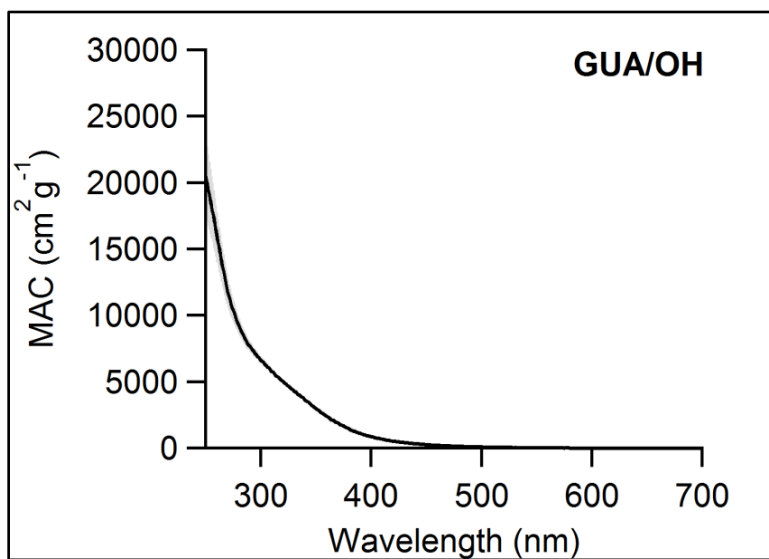


Figure 2.9. Mass absorption coefficient of guaiacol (GUA) SOA.

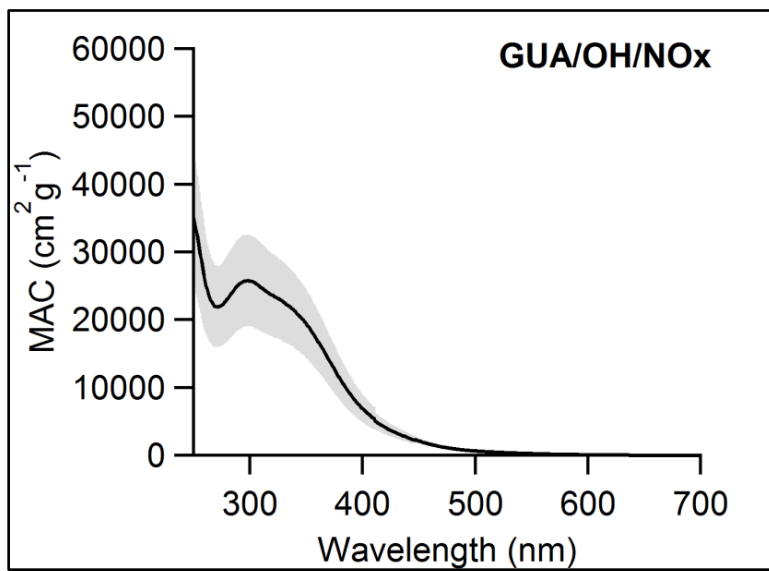


Figure 2.10. Mass absorption coefficient of farnesene (FAR) SOA.

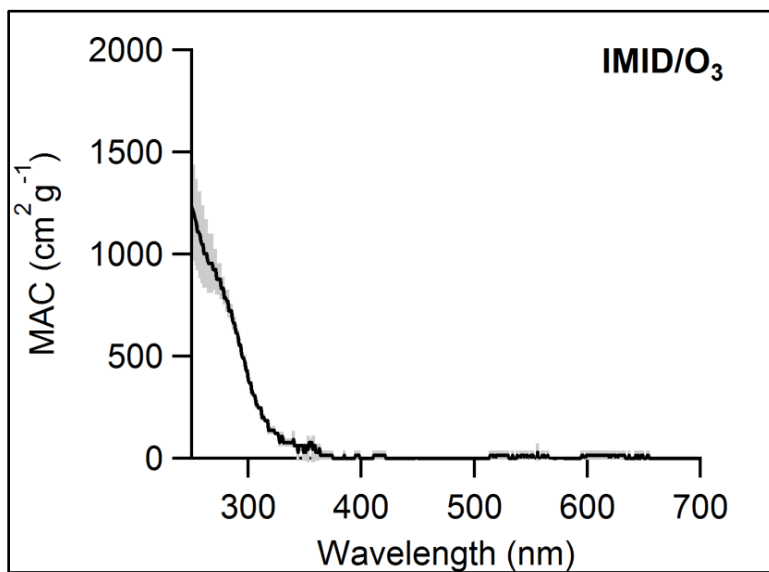


Figure 2.11. Mass absorption coefficient of imidazole (IMID) SOA.

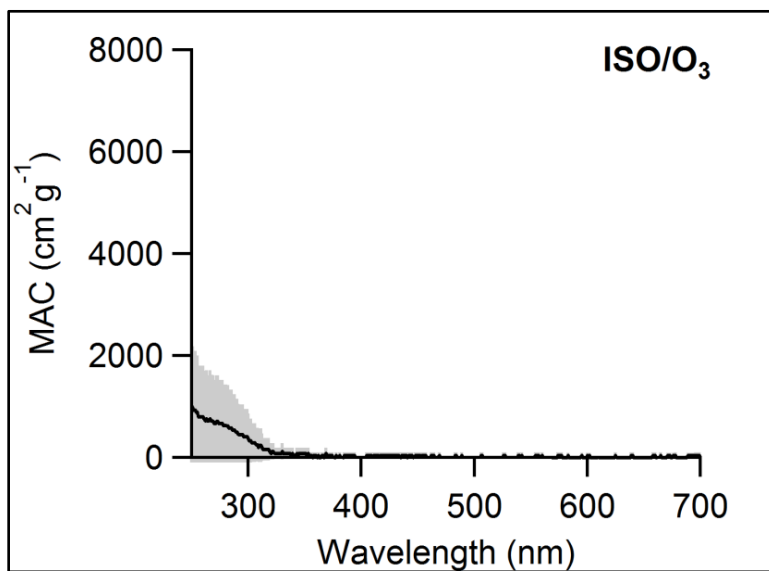


Figure 2.12. Mass absorption coefficient of isoprene (ISO) SOA.

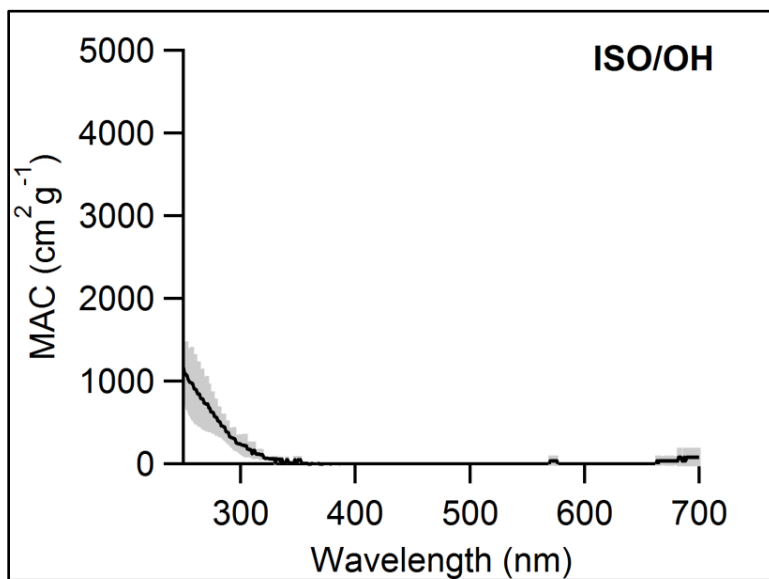


Figure 2.13. Mass absorption coefficient of isoprene (ISO) SOA.

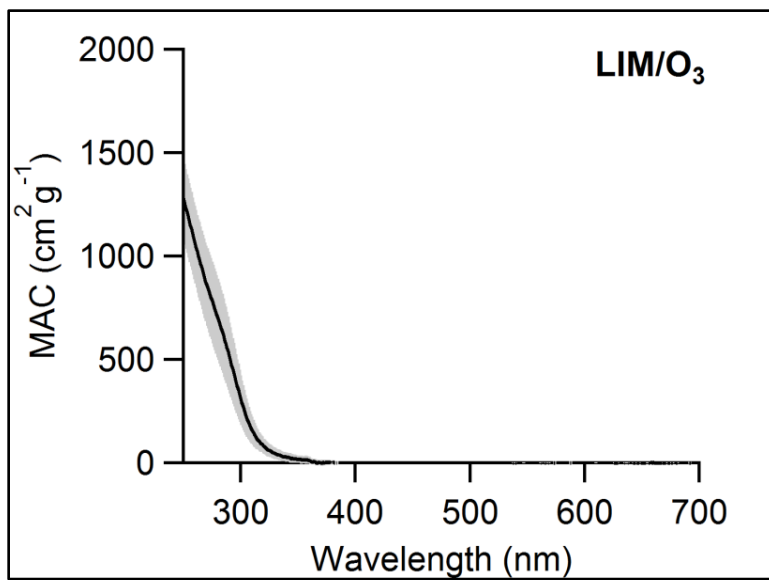


Figure 2.14. Mass absorption coefficient of limonene (LIM) SOA.

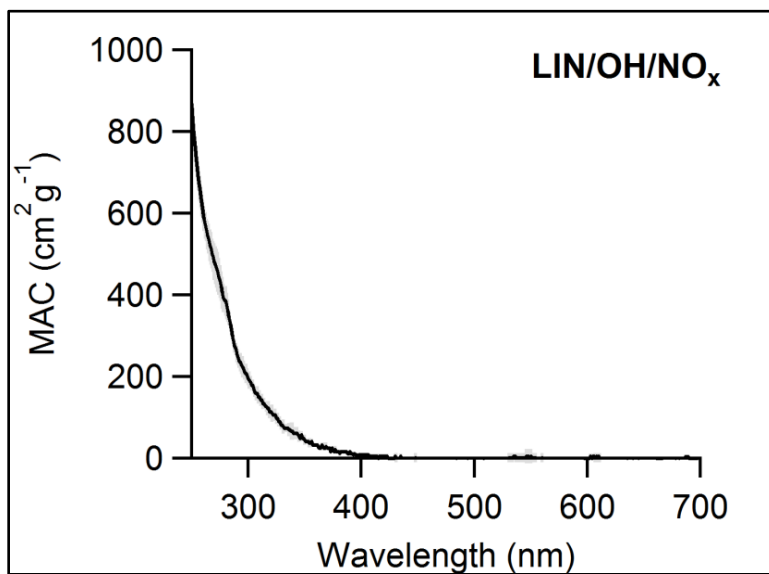


Figure 2.15. Mass absorption coefficient of linalool (LIN) SOA.

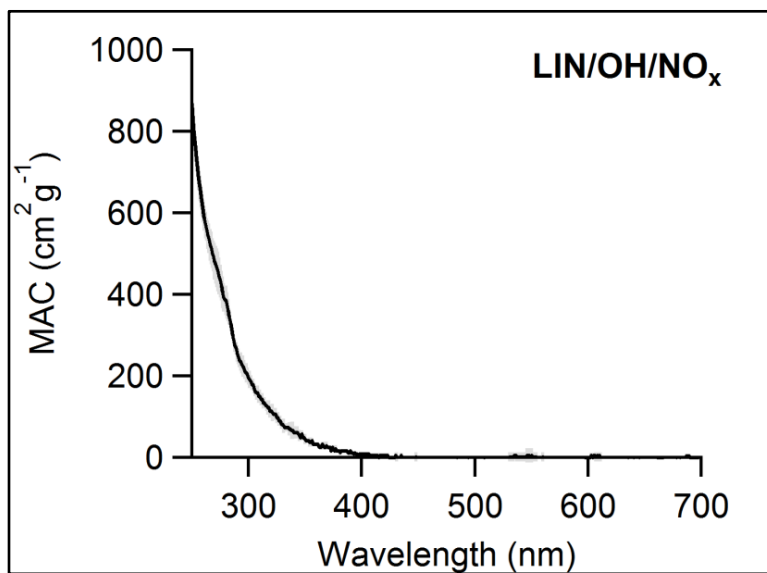
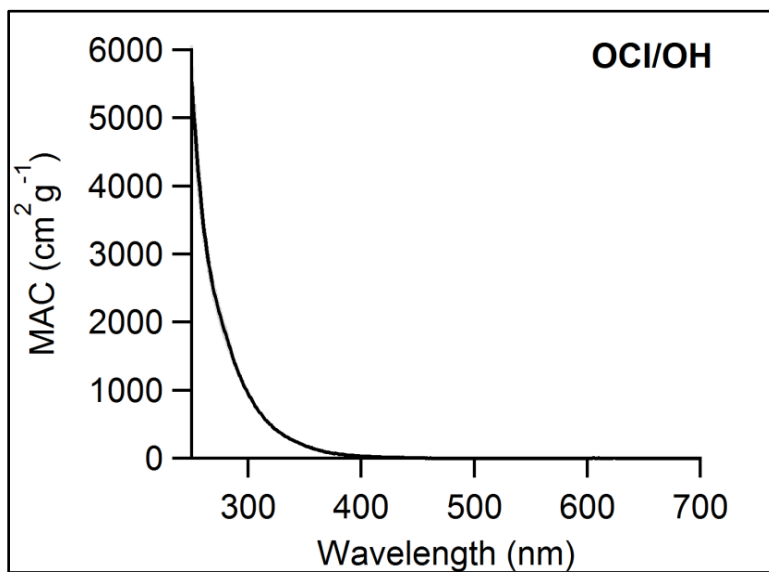
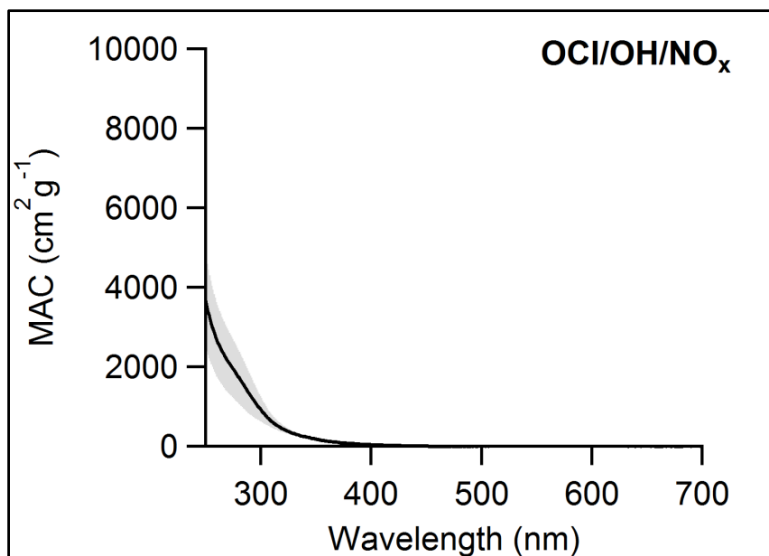


Figure 2.16. Mass absorption coefficient of linalool (LIN) SOA.



**Figure 2.17.** Mass absorption coefficient of ocimene (OCI) SOA.



**Figure 2.18.** Mass absorption coefficient of ocimene (OCI) SOA.



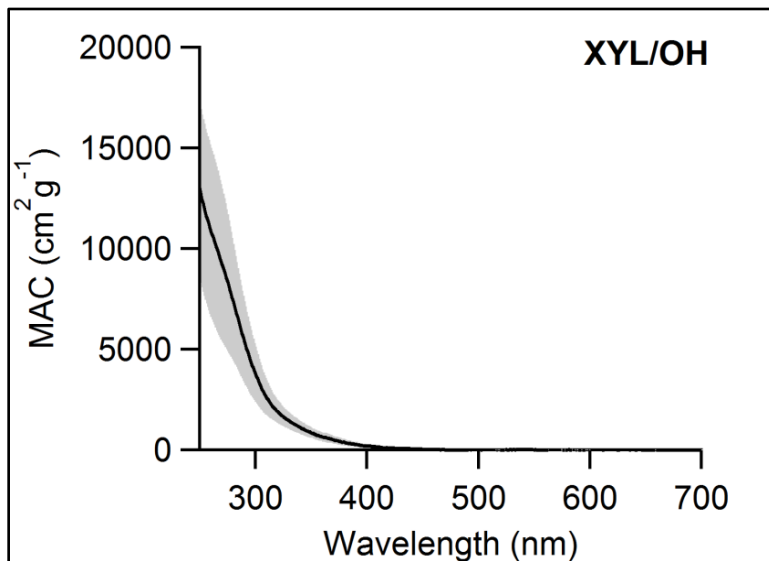


Figure 2.19. Mass absorption coefficient of para-xylene (XYL) SOA.

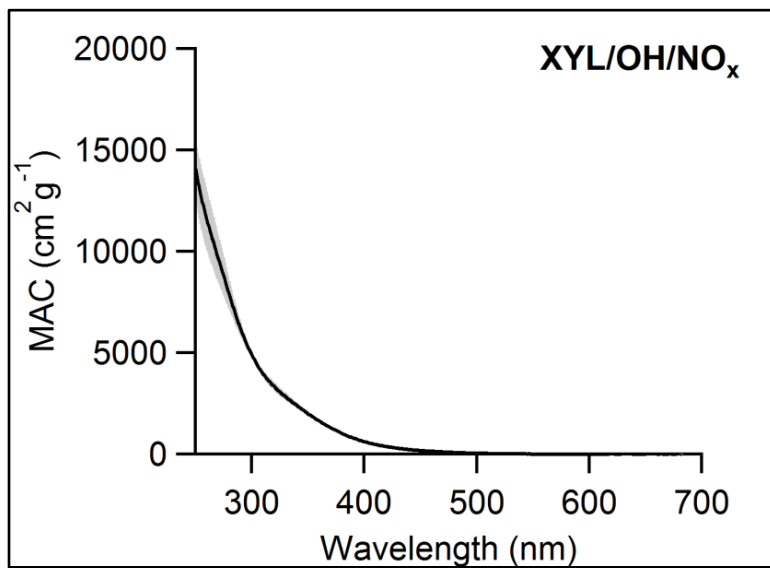
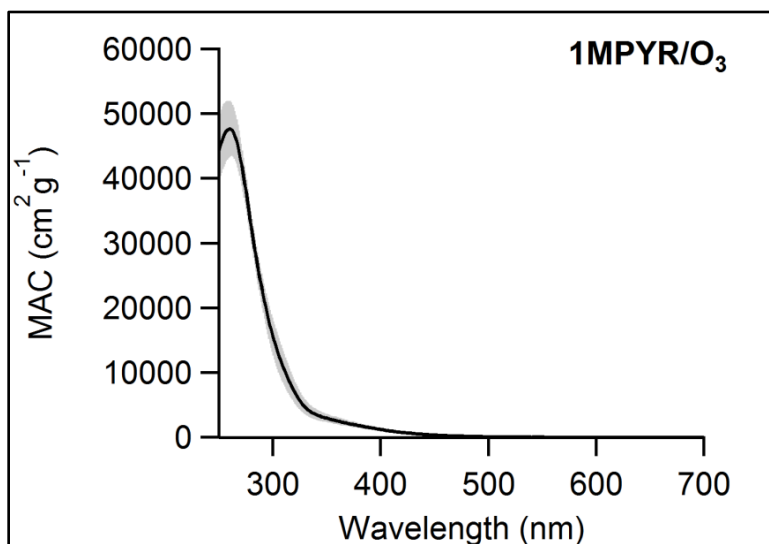
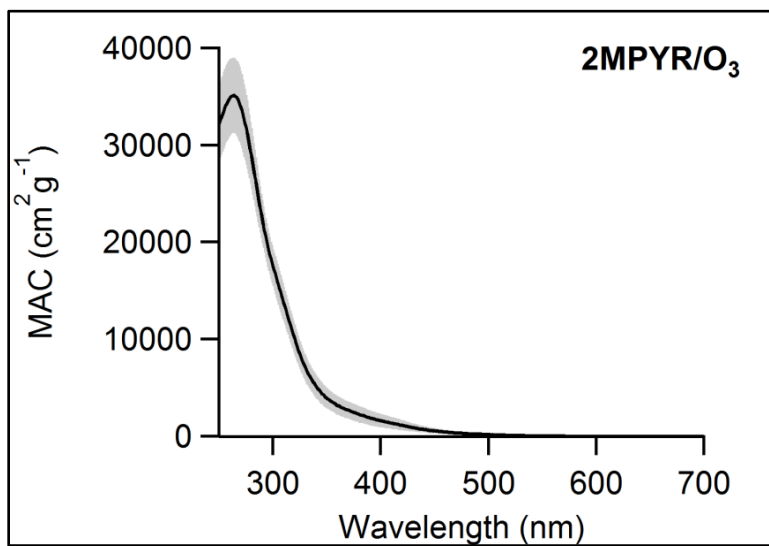


Figure 2.20. Mass absorption coefficient of para-xylene (XYL) SOA.



**Figure 2.21.** Mass absorption coefficient of 1-methylpyrrole (1MPYR) SOA.



**Figure 2.22.** Mass absorption coefficient of 2-methylpyrrole (2MPYR) SOA.

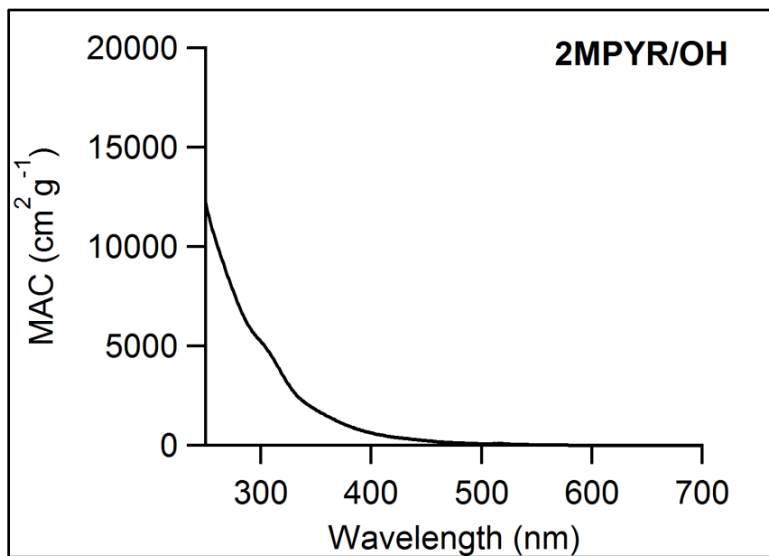


**Figure 2.23.** Mass absorption coefficient of 2-methylpyrrole (2MPYR) SOA.

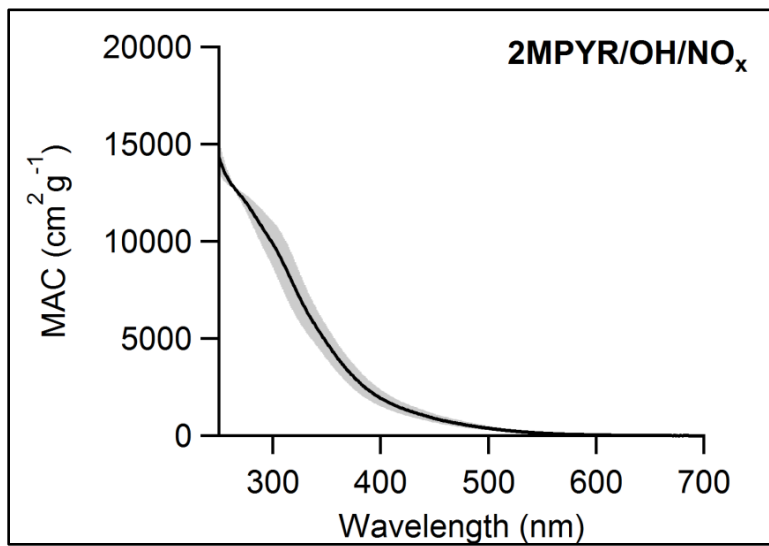


**Figure 2.24.** Mass absorption coefficient of 2-methylpyrrole (2MPYR) SOA.

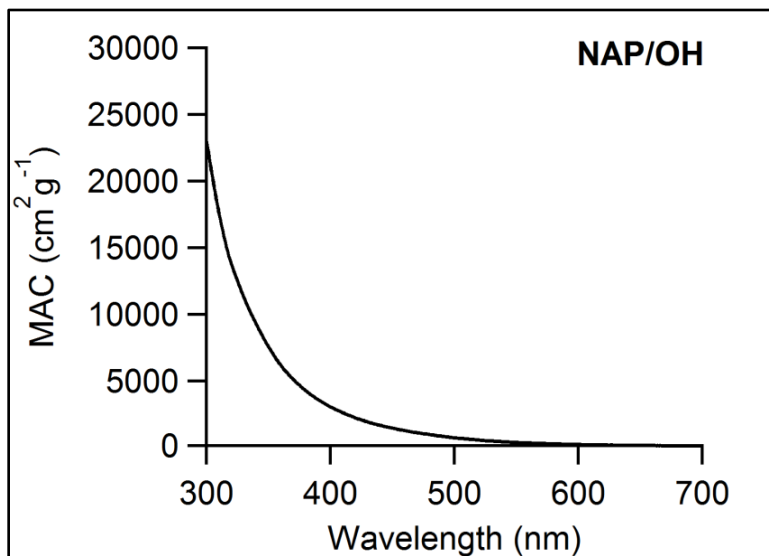


**Figure 2.25.** Mass absorption coefficient of naphthalene (NAP) SOA.

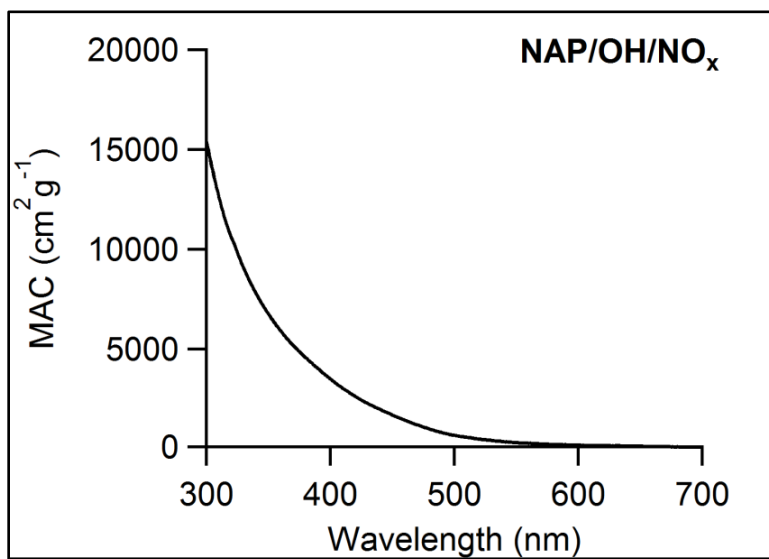


**Figure 2.26.** Mass absorption coefficient of naphthalene (NAP) SOA.

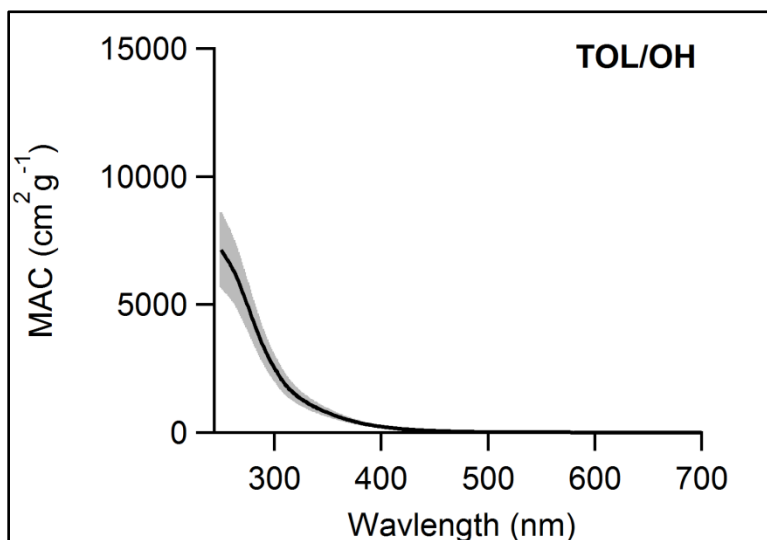


**Figure 2.27.** Mass absorption coefficient of toluene (TOL) SOA.

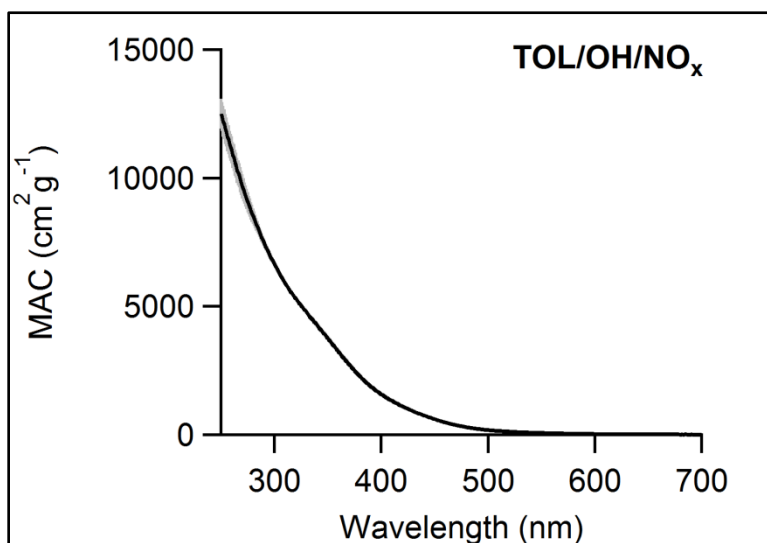


**Figure 2.28.** Mass absorption coefficient of toluene (TOL) SOA.

In agreement with the observations of Liu et al.<sup>105</sup> the MAC values for the SOA from aromatic precursors (TOL, XYL, GUA, NAP) are roughly an order of magnitude higher than MAC values for the SOA from isoprene and terpenes. Surprisingly, high MAC values were observed for SOA derived from heteroaromatic precursors 1MPYR (Fig. 2.21) and 2MPYR (Figs. 2.22-2.24). It was initially suspected that the presence of heterocyclic nitrogen atoms in these compounds

might contribute to the high absorption coefficients of their SOA; however, ozonolysis of IMID resulted in SOA with relatively low MAC values (Fig. 2.11). Clearly, the absorption spectra of SOA produced from nitrogen containing organics are highly sensitive to the structure of the VOC precursor.

The rate constant of a photochemical reaction,  $J$ , for any compound in SOA can be calculated from

$$J = \int \sigma(\lambda)\phi(\lambda)F(\lambda)d\lambda \quad (2.3)$$

where  $\sigma$  is the absorption cross-section [ $\text{cm}^2 \text{molec}^{-1}$ ],  $\phi$  is the quantum yield for the process of interest, and  $F$  is the spectral flux density [ $\text{photon cm}^{-2} \text{s}^{-1} \text{nm}^{-1}$ ]. Whereas the gas-phase absorption cross-sections and quantum yields are well known for a number of simple organic compounds,<sup>106</sup> there is only limited information available for the multifunctional molecules found in SOA. Furthermore, significant matrix effects on absorption spectra and quantum yields can be expected in the highly-viscous environment inside the particles.<sup>107</sup> Another complication is that a complex environmental mixture, such as an organic aerosol, contains a broad spectrum of compounds with different photophysical and photochemical processes. Some of them do not measurably absorb radiation in the wavelength of interest. Others absorb the radiation, but can dissipate the energy without undergoing a reaction, i.e., through internal conversion. Only a certain fraction of the components of aerosol can undergo photolysis, photoisomerization, photoassociation and other photochemical reactions leading to a change in the aerosol composition.

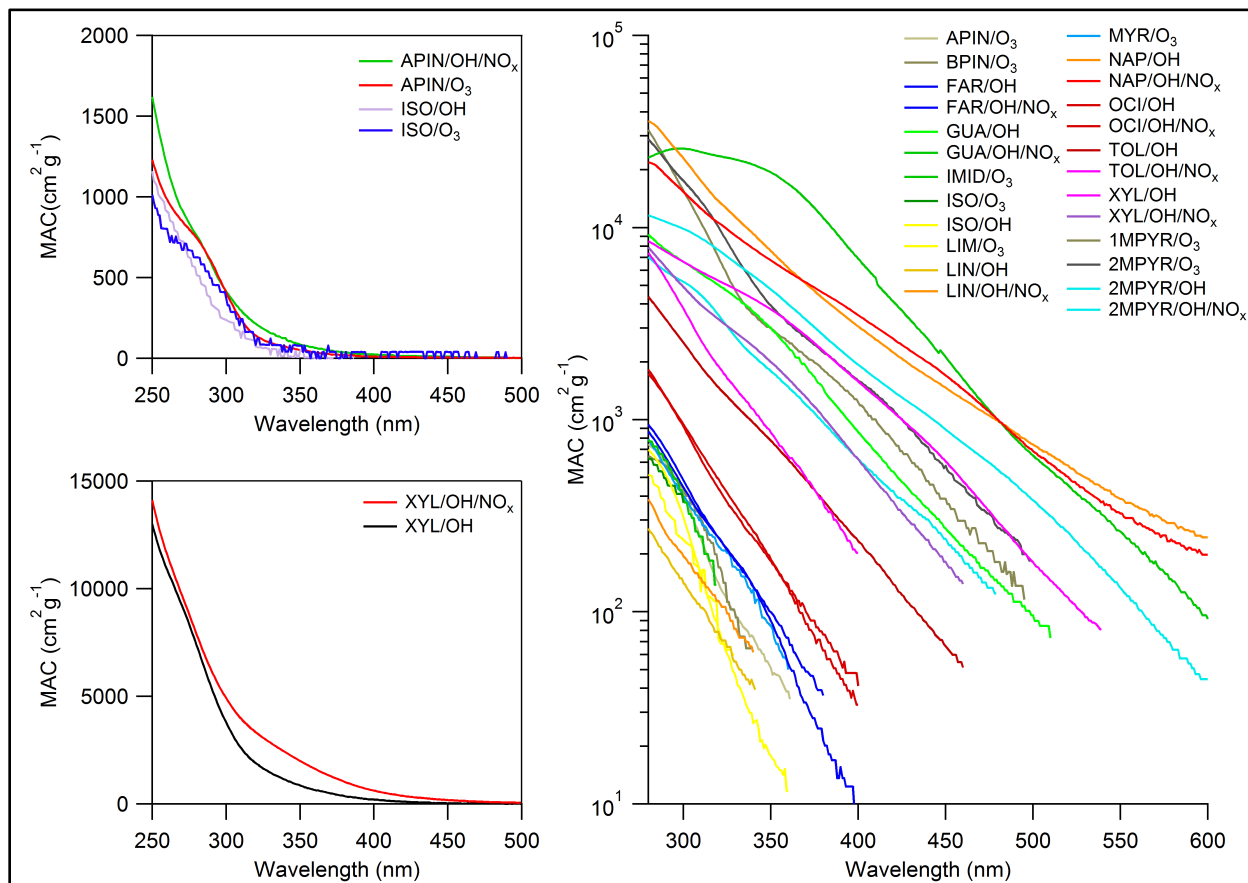


**Figure 2.29.** A comparison of MAC values for XYL, APIN, and ISO SOA, as well as all other SOA samples. The higher MAC values observed for the XYL samples are representative of the SOA derived from aromatic precursors.

In this work, a simplified approach was taken in which an effective photochemical rate constant is calculated from sample-averaged properties. This approach assumes that the composition of the SOA can be represented by an average formula with an effective molecular weight (MW), and that all of the SOA molecules have identical photophysical properties. The effective MW used for this study was 300 g/mol, as determined by averaging MWs from high-resolution mass spectra of a broad range of SOA reported by Romonosky et al.<sup>100</sup> The effective absorption cross section can then be estimated from MAC values (where  $N_A$  is the Avogadro's constant).

$$\sigma_{effective}(\lambda) = \frac{MAC_{material}(\lambda) \times MW}{N_A} \quad (2.4)$$

The quantum yields for the photochemical reactions of SOA compounds inside the particles are not known. As a limiting case, unity quantum yield is assumed, characteristic of the photolysis of hydrogen peroxide.<sup>106</sup> Specifically, a step-function wavelength dependence of the quantum yield is used, in which  $\phi = 1$  at all wavelengths below  $\lambda_0 = 400$  nm, and  $\phi = 0$  above  $\lambda_0$ . The upper wavelength limit is introduced because the quantum yield can be expected to drop sharply below the dissociation threshold. For example,  $\text{NO}_2$  photolysis occurs with  $\phi \sim 1$  below 398 nm, and quantum yield declines rapidly above this threshold wavelength.<sup>17</sup> Likewise,  $\text{O}_3$  has a high quantum yield below its dissociation threshold at 310 nm, and it drops sharply above 310 nm.

The assumption of the unity value may be unrealistic for condensed-phase photochemical processes; therefore, a model in which the quantum yield decreases with increasing wavelengths is also considered. The wavelength dependence of the quantum yield of acetone at 1 atm is adopted as a more realistic case. Specifically, acetone undergoes efficient photolysis only below



~300 nm, where the solar spectral flux is quite small, and is resilient to photolysis at longer wavelengths. Similar behavior is expected from condensed-phase carbonyl compounds as well as other types of organic species. Figure 2.30 shows the assumed quantum yields for both the H<sub>2</sub>O<sub>2</sub>-like model and the acetone-like model.

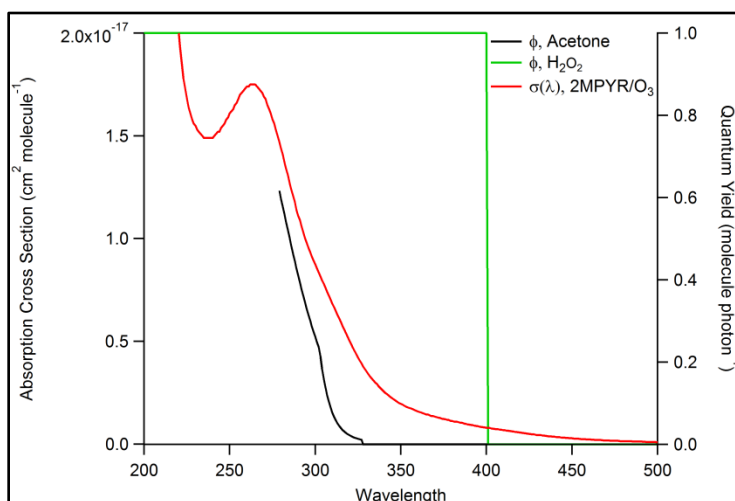


**Figure 2.30.** Two models for the wavelength dependence of quantum yield used in this work: unity quantum yield (as in H<sub>2</sub>O<sub>2</sub>) with the threshold set at 400 nm and quantum yield for the photolysis of acetone at 1 atm. These quantum yields were convoluted with the effective absorption cross sections (an example for 2MPYR/O<sub>3</sub> is shown) and solar spectral flux to obtain the effective photochemical rate constants.

With these assumptions, the effective photochemical rate constants can be calculated for the solar-zenith-angle (SZA) dependent values of solar spectral flux,  $F$ .

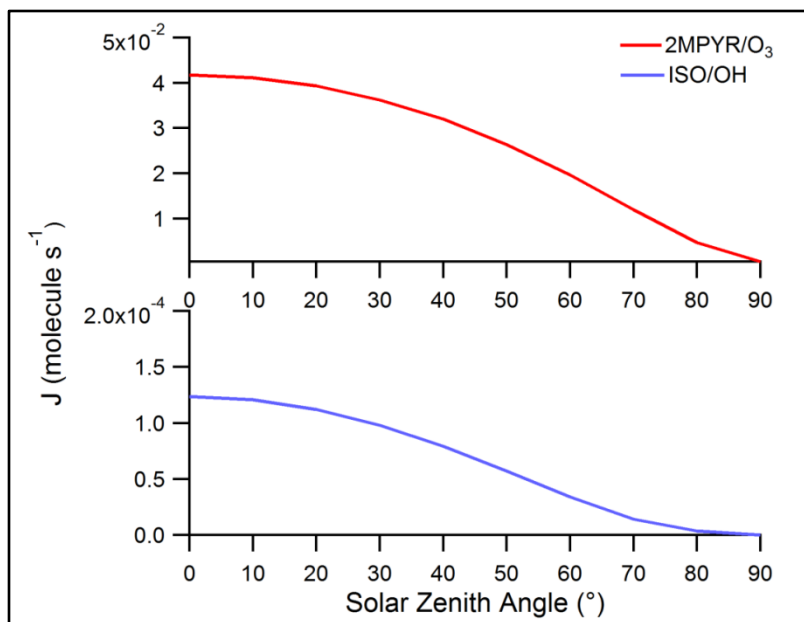
$$J_{effective} = \int \sigma_{effective}(\lambda) \phi(\lambda) F(\lambda, SZA) d\lambda \quad (2.5)$$

Figure 2.31 shows the resulting dependence of  $J$  on SZA for 2MPYR/O<sub>3</sub> (the most absorbing SOA in our data set) and ISO/OH (the least absorbing SOA). The peak values of  $J$  range from  $10^{-2}$  to  $10^{-4} \text{ s}^{-1}$  (when using the H<sub>2</sub>O<sub>2</sub> model for the quantum yields), which represent fast processes in comparison to typical atmospheric reactions. Figure 2.32 shows the dependence of  $J$  on the time of day for Los Angeles (34° latitude) on June 22, 2014.

The effective lifetime for the photochemical change in SOA can be calculated as an inverse of the 24-hour average rate

$$\tau = \left( \langle J_{effective} \rangle_{24hr} \right)^{-1} \quad (2.6)$$

The resulting values calculated from Eq. (2.6) for all the SOA types probed here for both the H<sub>2</sub>O<sub>2</sub> and acetone models of quantum yields are summarized in Table 2.3. This table also lists the lifetimes during the peak irradiation in Los Angeles at 13:00 hours, which is more meaningful for compounds with very short lifetimes.



**Figure 2.31.** Photochemical rate constant,  $J$ , of the most-absorbing (2MPYR/O<sub>3</sub>) and the least-absorbing (ISO/OH) SOA sample in our set as a function of SZA calculated using Eq. (2.5) and assuming the H<sub>2</sub>O<sub>2</sub> model for the quantum yields.

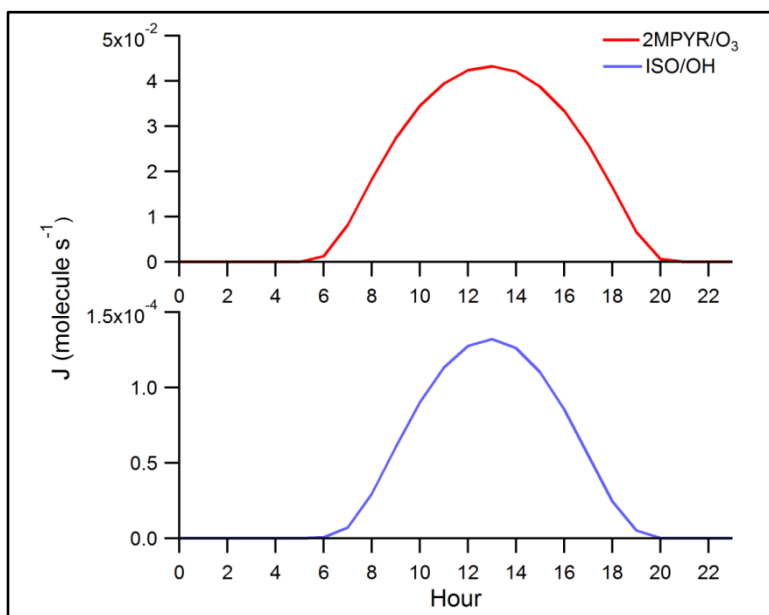


**Figure 2.32.** Photochemical rate constant,  $J$ , for the same SOA samples as used in Fig. 2.31 plotted as a function of time over a 24-hour period in Los Angeles (34° latitude) on June 22, 2014. The 24-hour average values of  $\langle J \rangle$  are listed in Table 2.3 for all the SOA types probed in this work.

**Table 2.3.** Effective SOA lifetimes with respect to photochemistry for Los Angeles.

Sample	Effective Lifetime using QY of H <sub>2</sub> O <sub>2</sub> (24 h average) (min)	Peak Effective Lifetime using QY of H <sub>2</sub> O <sub>2</sub> (min)	Effective Lifetime using QY of acetone (24 h average) (min)	Peak Effective Lifetime using QY of acetone (min)
1MPYR/O <sub>3</sub>	1.4	0.52	110	31
2MPYR/O <sub>3</sub>	1.0	0.39	85	24
2MPYR/OH	2.6	0.96	260	75
2MPYR/OH/NO <sub>x</sub>	1.0	0.38	130	37
APIN/O <sub>3</sub>	85	30	4800	1300
MYR/O <sub>3</sub>	58	21	3800	1100
BPIN/O <sub>3</sub>	90	31	4000	1100
FAR/OH	53	19	3500	1000
FAR/OH/NO <sub>x</sub>	47	17	3400	960
GUA/OH	1.7	0.63	190	56
IMID/O <sub>3</sub>	95	34	4800	1300
ISO/O <sub>3</sub>	88	32	5400	1500
ISO/OH	410	130	7600	2100
LIM/O <sub>3</sub>	230	77	7200	2000
LIN/OH/NO <sub>x</sub>	100	37	7700	2200
LIN/OH	160	56	11000	3100
OCI/OH	25	8.9	1700	480
OCI/OH/NO <sub>x</sub>	25	9.1	1800	520
XYL/OH	5.5	2.0	430	120
XYL/OH/NO <sub>x</sub>	2.5	0.9	280	81
Toluene/OH	6.2	2.3	590	170
Toluene/OH/NO <sub>x</sub>	1.3	0.50	190	58
Naphthalene/OH	0.62	0.23	64	18
Naphthalene/OH/NO <sub>x</sub>	0.68	0.25	89	26
Catechol/O <sub>3</sub> <sup>a</sup>	3.0	1.1	260	75
IEPOX/MgSO <sub>4</sub> seed particle/dry conditions <sup>b</sup>	6.4	2.3	540	154

<sup>a</sup> The MAC data were obtained from Liu et al. (2013) and used in lifetime calculations.

<sup>b</sup> The MAC data were obtained from Lin et al. (2014) and used in lifetime calculations.

The data in Table 2.3 reflect the high level of diversity in the optical properties of different types of biogenic and anthropogenic SOA. They also suggest that photochemical reactions in SOA can potentially occur on atmospherically meaningful time scales. Lifetime estimates for the SOA samples using the quantum yield of H<sub>2</sub>O<sub>2</sub> are on the order of minutes, with

the peak irradiation lifetimes being as short as a few seconds in some cases. These lifetimes are probably unrealistically short because it is unlikely that SOA compounds can photolyze with quantum yields approaching unity. The lifetime estimates relying on the quantum yield of acetone range from 60–11000 minutes (1-180 hours) and likely represent a more realistic estimate for the time scales of photochemical reactions occurring in aerosols. For example, the lifetime predicted for APIN/O<sub>3</sub> SOA with the acetone model for quantum yields (4800 min or 3.3 days) is of the same order of magnitude as the lifetime for the photolysis-induced loss of peroxides from APIN/O<sub>3</sub> SOA (~10 days) measured by Epstein et al.<sup>89</sup> It is noted that a direct comparison is complicated in this case by the possible photochemical recycling of peroxides in the particles. The predicted average lifetimes of 60-90 h for NAP SOA (with the acetone model for a quantum yield) are also in fair agreement with the observed lifetimes for photobleaching of NAP SOA solutions in water, which ranged from ~15 to 90 h depending on the observation wavelength.<sup>97</sup> Assuming that molecules in SOA can undergo photochemistry with photolysis quantum yields similar to that of acetone, condensed-phase photochemistry can become competitive with the more traditional mechanisms of SOA aging, such as multi-phase oxidation by OH. This is the most important conclusion of this work.

The SOA examined in this work was prepared under dry conditions and without using seed particles because we wanted to minimize contributions from the seed particle material to the measured absorption coefficients of SOA. While neutral seed particles, such as ammonium sulfate, are not expected to affect the optical absorption properties of the SOA material, highly-acidic seed particles may affect both the mechanism of SOA production<sup>108</sup> and the optical absorption properties<sup>109–111</sup> of SOA. For example, Lin et al.<sup>112</sup> found that SOA formed by uptake of isoprene epoxydiol (IEPOX) onto acidic particles was considerably more absorbing than that

SOA formed on neutralized seed particles. To test for the effect of the seed particle acidity, we have included the IEPOX/acidic seed data from Lin et al.<sup>112</sup> in Table 2.3. The estimated lifetime of the IEPOX/acidic seed SOA is more than an order of magnitude shorter than that for ISO/OH or ISO/O<sub>3</sub> SOA. Clearly, the effect of the aerosol seed acidity (and the coupled effect of the relative humidity) on the optical absorption properties of SOA is significant and deserves further study.

Tables 2.1 and 2.2 indicate that that amount of collected SOA material was typically between 0.2 and up to 3.5 mg. The large amount of SOA material was necessary for the accurate measurement of absorption coefficients. The high material requirements of these experiments necessitated using unrealistically high concentrations of VOC precursors, especially in the case of isoprene, and for all flow tube experiments. Future experiments should address the question whether the MAC values are strongly dependent on the VOC concentration used in the SOA preparation.

While our analysis predicts that condensed-phase photochemistry in SOA may be reasonably fast under typical atmospheric conditions, it does not say anything about the effect of these photochemical reactions on the climate- and health-related properties of aerosols, such as their mass concentration, average particle size, absorption coefficient, toxicity, etc. This effect will, of course, depend on the prevailing type of photochemistry occurring in SOA particles. For example, in the SOA derived from monoterpenes and isoprene, photolysis of peroxide and carbonyl functional groups can be expected to fragment SOA compounds into smaller molecules,<sup>100</sup> which may then evaporate from particles to gaseous phase as observed in several previous experiments with bulk SOA samples.<sup>92,93,113</sup> The evaporation will lead to SOA particle shrinking, as observed, for example in experiments by Epstein et al.<sup>89</sup> and Wong et al.<sup>90</sup> with

APIN/O<sub>3</sub> SOA. However, it should not be assumed that fragmentation is always going to be the dominant photochemical pathway. For example, cis-pinonic acid, a major product of ozonolysis of APIN, undergoes a reasonably efficient photoisomerization into limononic acid, a structural isomer of cis-pinonic acid.<sup>114</sup> For the cases when photoisomerization is the dominant photochemical process, there should not be any effect on the particle size or mass concentration. Photoassociation reactions, in which two SOA compounds dimerize after absorbing a photon, will produce larger products than the initial reactants. This will have an effect of reducing the volatility of SOA compounds making the aerosol less likely to evaporate upon dilution. An even more interesting scenario is conceivable in which a photoexcited species on the particle surface reacts with a nearby VOC producing less volatile products and leads to an increase in the particle mass, as observed in recent laboratory experiments with aerosols containing photosensitizers.<sup>115,116</sup> In summary, condensed-phase photochemistry can either decrease or increase the particle mass and size depending on the nature of the dominant photochemical processes.

The effect of condensed-phase photochemistry on the optical properties of SOA is also very important because it has direct consequences for the radiative forcing by aerosols.<sup>42</sup> Light-absorbing SOA can lose or gain their chromophoric species as a result of various photochemical reactions. For example, recent laboratory experiments demonstrated that the wavelength dependence of the absorption coefficient can be dramatically altered by UV irradiation of several types of model brown carbon compounds.<sup>97–99,117,118</sup> Such changes in the absorption coefficient of SOA are also important for gas-phase photochemistry because aerosols are capable of screening UV radiation and reducing ozone production in heavily polluted areas.<sup>17</sup> Clearly, more

work is needed to explore the rate and occurrence of such photochemical effects on the SOA absorption spectra before these effects can be incorporated in climate and air pollution models.

## **2.5. Conclusion**

The optical properties of SOA representative of biogenic and anthropogenic atmospheric environments were examined by making model SOA in a chamber or a flow tube and measuring their bulk mass absorption coefficients (MAC). This information was used to estimate the effective absorption cross sections of SOA and lifetimes of SOA compounds with respect to possible condensed-phase photochemical reactions. The calculated lifetimes suggest that condensed-phase photochemistry may potentially compete with other aerosol aging processes. These findings have important implications for understanding the aging of atmospheric aerosols, and the potential effect of this photochemical aging on climate- and health-related properties of SOA.



## **Chapter 3: Chemical Composition of Aqueous Photochemistry Products of Secondary Organic Aerosols**

---

Portions of this chapter are reproduced with permission from: D.E. Romonosky, A. Laskin, J. Laskin, and S.A. Nizkorodov, “High-resolution mass spectrometry and molecular characterization of aqueous photochemistry products of common types of secondary organic aerosols” *Journal of Physical Chemistry A* 119 (2015) 2594-2606; DOI: 10.1021/jp509476r. Copyright 2015 by American Chemical Society.

### 3.1. Abstract

This work presents a systematic investigation of the molecular level composition and the extent of aqueous photochemical processing in different types of secondary organic aerosol (SOA) from biogenic and anthropogenic precursors including  $\alpha$ -pinene,  $\beta$ -pinene,  $\beta$ -myrcene, d-limonene,  $\alpha$ -humulene, 1,3,5-trimethylbenzene, and guaiacol, oxidized by ozone (to simulate a remote atmosphere) or by OH in the presence of NO<sub>x</sub> (to simulate an urban atmosphere). Chamber- and flow-tube-generated SOA samples were collected, extracted in a methanol/water solution, and photolyzed for 1 h under identical irradiation conditions. In these experiments, the irradiation was equivalent to about 3–8 h of exposure to the sun in its zenith. The molecular level composition of the dissolved SOA was probed before and after photolysis with direct-infusion electrospray ionization high-resolution mass spectrometry (ESI-HR-MS). The mass spectra of unphotolyzed SOA generated by ozone oxidation of monoterpenes showed qualitatively similar features and contained largely overlapping subsets of identified compounds. The mass spectra of OH/NO<sub>x</sub>-generated SOA had more unique visual appearance and indicated a lower extent of product overlap. Furthermore, the fraction of nitrogen-containing species (organonitrates and nitroaromatics) was highly sensitive to the SOA precursor. These observations suggest that attribution of high-resolution mass spectra in field SOA samples to specific SOA precursors should be more straightforward under OH/NO<sub>x</sub> oxidation conditions compared to the ozone-driven oxidation. Comparison of the SOA constituents before and after photolysis showed the tendency to reduce the average number of atoms in the SOA compounds without a significant effect on the overall O/C and H/C ratios. SOA prepared by OH/NO<sub>x</sub> photooxidation of 1,3,5-trimethylbenzene and guaiacol were more resilient to photolysis despite being the most light absorbing. The composition of SOA prepared by ozonolysis of monoterpenes changed more

significantly as a result of the photolysis. The results indicate that aqueous photolysis of dissolved SOA compounds in cloud/fog water can occur in various types of SOA, and on atmospherically relevant time scales. However, the extent of the photolysis-driven change in molecular composition depends on the specific type of SOA.

### 3.2. Introduction

Primary and secondary organic aerosols (POA and SOA) influence the Earth's climate and contribute to air pollution in urban areas.<sup>17,119</sup> POA are directly emitted, whereas the more abundant SOA are produced in one of the following ways: (1) gas-phase oxidation of volatile organic compounds (VOCs) followed by condensation of the products into new particles or onto preexisting particles;<sup>120,121</sup> (2) heterogeneous reactive uptake of VOCs on particle surfaces;<sup>116</sup> (3) photochemical aqueous processing of VOCs occurring inside cloud and fog droplets, followed by droplet evaporation.<sup>6,8</sup> Until recently, the first pathway was thought to be the main mechanism of SOA formation and attracted significant attention from the scientific community. Numerous studies have contributed to a comprehensive compilation of reference tables of photochemical and kinetic data for hundreds of VOCs<sup>122</sup> and in tabulation of SOA yields<sup>32</sup> from oxidation of different VOC precursors by the hydroxyl radical (OH), ozone (O<sub>3</sub>), and the nitrate radical (NO<sub>3</sub>). In the past several years, it has been recognized that a significant fraction of SOA is produced and subsequently aged through cloud and fog photochemical processes.<sup>8</sup> This represents a significant shift in scientific knowledge of the SOA chemistry, and new data are required to assess the relative contribution of aqueous processes to SOA formation and aging.

Photochemical processes involving organic compounds in cloud and fog water include direct photolysis, wherein the compounds absorb radiation and break into products, and indirect photooxidation, wherein absorption of solar radiation drives chemistry through the production of oxidants such as OH, superoxide (O<sub>2</sub><sup>-</sup>), and electronically excited organic compounds. Direct photolysis processes are well-known to determine lifetimes of many gas-phase species,<sup>17</sup> and they are likely to be just as important for compounds found in the particle phase and in cloud/fog droplets. Oxidation by OH is the primary competitive channel for photolysis. However, in cloud

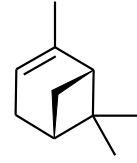
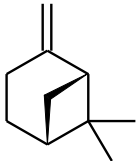
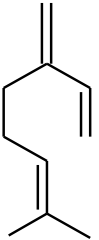
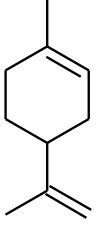
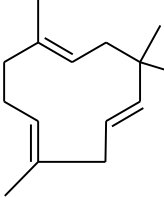
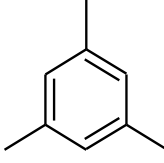
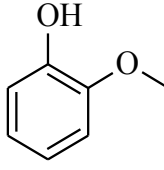
and fog water affected by urban emissions, as well as inside organic aerosol particles, the oxidative capacity of OH may be too low to oxidize the high concentrations of all dissolved SOA during the cloud/fog lifetime.<sup>8</sup> Additionally, the higher dissolved SOA concentrations may suppress photochemical OH production enough to shut down the OH-initiated loss pathway chemistry while not affecting the direct photochemical pathways. Dissolved organics may also serve as a source of OH through the photolysis of nitrates, H<sub>2</sub>O<sub>2</sub>, and organic chromophores.<sup>8,123,124</sup> Depending on the prevailing mechanisms, aqueous photochemistry can both degrade dissolved organic compounds into smaller volatile products or conversely generate larger, nonvolatile products. For example, previous studies demonstrated that OH-driven oxidation of small water-soluble organics often leads to a complex and concentration-dependent mixture of oligomeric compounds.<sup>53,95,125–127</sup> Formation of oligomeric products was also observed in the photolysis of aqueous pyruvic acid.<sup>117,128</sup> In contrast, the photolysis of aqueous solutions of model SOA prepared by the oxidation of isoprene, limonene, and naphthalene was found to lead to photodegradation of larger organics into smaller products.<sup>95–97</sup>

Direct and indirect photolysis processes occur simultaneously, but their relative importance can be predicted only for the simplest organic compounds, which are not representative of SOA composition.<sup>54</sup> While much attention has been given to the aqueous oxidation of organic compounds with the OH radical,<sup>8</sup> there is limited knowledge about the direct photolysis of atmospherically relevant organics in water, especially for processes involving multifunctional organic compounds. Furthermore, it is important to study the response of complex aqueous mixtures to irradiation (as opposed to solutions of isolated compounds which may behave differently from the mixtures) since they are more representative of cloud and fog chemistry. Finally, little is known about the photochemistry of SOA-relevant multifunctional

organic compounds such as highly substituted carbonyls, organonitrates (esters of nitric acid), and organosulfates (esters of sulfuric acid), etc., which are common in SOA but challenging to synthesize and study in pure form.

In this chapter, we investigate the effects of aqueous photolysis on the molecular level composition of different representative types of SOA of both biogenic and anthropogenic origin (Table 3.1). We use high-resolution mass spectrometry (HR-MS) methods<sup>129</sup> to analyze changes in SOA composition upon exposure to UV radiation. In addition, we compare high-resolution mass spectra of various types of SOA, something that has not been done systematically in previous literature. Biogenic SOA precursors include  $\alpha$ -pinene,  $\beta$ -pinene, myrcene, and D-limonene, which are among the top six most abundant monoterpenes in the atmosphere.<sup>16</sup> A product of diesel combustion, 1,3,5-trimethylbenzene,<sup>36</sup> and a product of biomass burning, guaiacol,<sup>43</sup> are included as model anthropogenic and biomass-burning precursors. The oxidants include ozone, which controls the oxidation of many unsaturated organics in clean air, and OH in the presence of NO<sub>x</sub> (= NO + NO<sub>2</sub>) concentration, which is representative of an urban environment. In combination with previous studies of aqueous photolysis of limonene, isoprene, and naphthalene SOA,<sup>95-97</sup> this study provides a database for making general conclusions about the role of aqueous photochemistry in the atmospheric processing of SOA.

**Table 3.1.** The structures of VOC precursors used for the generation for SOA samples, abbreviations by which they are referred to in this paper, and their commercial sources and purities.

Compound	Abbreviation	Manufacturer/Purity	Structure
$\alpha$ -Pinene	APIN	Sigma Aldrich, 98%	
$\beta$ -Pinene	BPIN	Sigma Aldrich, 98%	
$\beta$ -Myrcene	MYR	Fisher Scientific, 92.9%	
(+)-Limonene	LIM	Sigma Aldrich, 97%	
$\alpha$ -Humulene	HUM	Sigma Aldrich, >96%	
1,3,5-trimethylbenzene	TMB	Sigma Aldrich, 5000 $\mu\text{g/mL}$ in methanol	
Guaiacol	GUA	Sigma Aldrich, >98%	

### 3.3 Experimental

#### 3.3.1. SOA Generation and Collection

Both O<sub>3</sub>-initiated and OH/NO<sub>x</sub>-initiated oxidation experiments were performed to generate SOA from suitable biogenic and anthropogenic VOCs. All the OH/NO<sub>x</sub> photooxidation SOA are labeled as VOC/NO<sub>x</sub> and ozonolysis SOA are labeled as VOC/O<sub>3</sub> in the remainder of this chapter. Conditions for each experiment and code names for the SOA are summarized in Table 3.2. For the OH/NO<sub>x</sub>-initiated reactions, the photooxidation of VOC precursors was performed as described in Section 1.3.1 with approximately 300-400 ppb of NO added to the chamber. The SOA was collected through an activated carbon denuder at 30 SLM (standard liters per minute) onto PTFE filters (Millipore 0.2 μm pore size). Two hours of collection yielded 30-1900 μg of SOA on each filter (the amount was estimated from the SMPS data assuming a generic SOA particle density of 1.2 g cm<sup>-3</sup> and 100% collection efficiency by the filters) before it was sealed and frozen for further analysis.

The O<sub>3</sub>-initiated reactions were carried out in the flow tube reactor as described in Section 1.3.2. The liquid VOC precursor was injected in a 5-7 SLM flow of zero air at a rate of 25 μL/hr using a syringe pump. Pure oxygen (Airgas, 99.994% purity) flow of ~0.6 SLM passed through an ozone generator and a photometric ozone detector. The two flows were mixed at the entrance of the flow tube resulting in the initial VOC and ozone mixing ratios of ~5 ppm and 50-100 ppm respectively. The residence time in the flow tube was less than 5 min, but sufficient for oxidizing all of the injected VOC and forming SOA. A 1-m long charcoal denuder removed residual ozone and gaseous organic compounds from the flow exiting the reactor while letting most of the particles go through. The SOA was collected for approximately 2 h on PTFE filters, which were weighed before and after collection with a Sartorius ME-5F filter balance (1 μg precision), then sealed and frozen for later analysis.



**Table 3.2.** Experimental conditions and code names for the SOA samples examined in this chapter.

SOA code <sup>a</sup>	Oxidant	Initial VOC (ppm)	Initial NO (ppb)	Reaction time (h)	Collection time (h)	Amount collected ( $\mu\text{g}$ )
APIN/O <sub>3</sub>	O <sub>3</sub>	~5	0	< 0.1	1	930
APIN/NO <sub>x</sub>	OH	0.80	330	2	3	460
BPIN/O <sub>3</sub>	O <sub>3</sub>	~5	0	< 0.1	1	260
BPIN/NO <sub>x</sub>	OH	0.80	360	2	3	1900
LIM/O <sub>3</sub>	O <sub>3</sub>	~5	0	< 0.1	1	1300
MYR/O <sub>3</sub>	O <sub>3</sub>	~5	0	< 0.1	1	170
MYR/NO <sub>x</sub>	OH	0.50	370	3	3.5	1200
HUM/O <sub>3</sub>	O <sub>3</sub>	~5	0	< 0.1	1	470
HUM/NO <sub>x</sub>	OH	0.25	260	3	2.5	90
GUA/NO <sub>x</sub>	OH	0.50	360	1	3	2600
TMB/NO <sub>x</sub>	OH	0.090	440	6	4	30

<sup>a</sup> The OH/NO<sub>x</sub> photooxidation SOA are labeled as VOC/NO<sub>x</sub> and ozonolysis SOA are labeled as VOC/O<sub>3</sub>. All the OH/NO<sub>x</sub> samples were prepared in a smog chamber starting from the specified initial mixing ratios, and all the O<sub>3</sub> samples were prepared in a flow tube. Steady state mixing ratios that the VOC precursor would have had in the absence of ozone are listed (ozone was added to the flow in excess with respect to the VOC). The reaction time in the flow tube is estimated from the effective residence time; the reaction time in the chamber is equivalent to the irradiation duration.

### 3.3.2. Aqueous Photolysis and Flux Calculation

The sealed filter samples were allowed to equilibrate to room temperature, unsealed, and extracted by a 70/30 methanol/water v/v solution for about 10 minutes using sonication. The methanol/water extracts prepared in this manner had typical concentrations of organics in the range of 50-250  $\mu\text{g/mL}$ , which corresponds to 170  $\mu\text{M}$  – 800  $\mu\text{M}$ , assuming an effective molecular weight of 300 g/mol for SOA compounds. The concentrations used in this study are comparable to concentrations of organic compounds observed in cloud water.<sup>130,131</sup> Deliquesced atmospheric particles typically have higher concentrations of dissolved organics of the order of

0.1-10 M.<sup>132</sup> Therefore, the experimental conditions presented in this study are more relevant for cloud and fog droplets than for hygroscopically grown aerosols.

Methanol was added to ensure a more complete extraction of the SOA material from the filters, and to improve the stability of the electrospray ionization (ESI) source used in the composition analysis before and after photolysis. Our initial intention was to study photolysis in pure water, but this was not possible for example for HUM/O<sub>3</sub>, which (similarly to cedrene)<sup>104</sup> dissolved poorly in water but dissolved readily in methanol. Although methanol is known to react with SOA carbonyl compounds to form hemiacetals,<sup>133</sup> this reaction is expected to have a similar effect on photochemical properties of carbonyls (an elimination of the n→π\* transition associated with the carbonyl group) as the hydration reaction with water leading to gem-diols. Therefore, in first-order approximation, photochemistry of SOA in water and in methanol/water mixtures should be qualitatively similar.

The samples were photolyzed in a 1 cm uncapped quartz cuvette from the side. A Xenon UV lamp in a Newport model 66902 housing served as the radiation source. A 90-degree dichroic mirror (Newport model 60159) and a U-330 band-pass filter (Edmund optics #46-438) were used to reduce the visible and IR radiation. The spectrum of the resulting radiation was recorded using a portable UV-Vis spectrometer (Ocean Optics, USB4000) with most of the radiation falling in the 280-400 nm range. The samples were exposed to lab air during photolysis and therefore contained dissolved oxygen. After photolysis, the samples were placed into clean storage vials and frozen for later mass spectrometric analysis. An azoxybenzene actinometer was used under the same experimental conditions to determine the flux of the lamp as described by Lignell et al.<sup>114</sup>

The wavelength-dependent spectral flux density in the photolysis cuvette is shown in Fig. 3.1, where it is compared to the ground-level spectral flux density from the sun at solar zenith angle (SZA) of 0° (calculated with the “Quick TUV” calculator<sup>33</sup> using the following parameters: 300 Dobson overhead ozone, surface albedo of 0.1, ground elevation and altitude = 0 km). We also show the effective absorption cross sections of GUA/NO<sub>x</sub> SOA determined in this work from the following equation:

$$\sigma_{effective}(\lambda) = \frac{A_{10}(\lambda) \times \ln(10) \times MW}{C_{mass} \times N_A \times l} \quad (3.1)$$

where  $N_A$  is Avogadro’s number,  $A_{10}$  is base-10 absorbance of an SOA extract with mass concentration  $C_{mass}$  contained in a cuvette with pathlength  $l$ . We used  $MW = 300$  g/mol for the effective molecular weight of GUA/NO<sub>x</sub> SOA molecules (the average molecular weight of all the compounds detected by HR-MS in all the SOA types). GUA/NO<sub>x</sub> SOA was the most absorbing compared to the rest of SOA probed here (its samples were yellow in color; the rest of the SOA samples were colorless). The ratio of the relative rates of photolysis by the lamp under our experimental conditions and by the sun can be estimated from

$$\frac{J_{sun}}{J_{lamp}} = \frac{\int \sigma_{effective}(\lambda) \phi(\lambda) Flux_{sun}(\lambda) d\lambda}{\int \sigma_{effective}(\lambda) \phi(\lambda) Flux_{lamp}(\lambda) d\lambda} \quad (3.2)$$

assuming that only wavelengths below 400 nm contribute to photolysis, and assuming that the photolysis quantum yield  $\phi$  is wavelength-independent. The assumption of the constant  $\phi$  is certainly an approximation, but this is a practical approach based on the limited available information on photophysics of SOA compounds. With these assumptions, we estimate that 1 h of photolysis by the lamp is equivalent to ~4 h of photolysis with the overhead sun. Note that this ratio depends on the shape (but not the magnitude) of the absorption cross sections of SOA. For

example, for APIN/O<sub>3</sub> SOA, which is much less absorbing at  $\lambda > 300$  nm, the 1 h of lamp irradiation would be equivalent to  $\sim 8$  h of irradiation by the sun in its zenith. Note that our lamp has a measurable emission at  $\lambda < 290$  nm according to Fig. 3.1. With the integration wavelength limited to  $\lambda > 290$  nm, the expected lifetime for GUA/NO<sub>x</sub> SOA becomes  $\sim 3.5$  h, while that for APIN/O<sub>3</sub> SOA becomes  $\sim 5.5$  h. Therefore, the measured photolysis rates may be affected by the contribution of harder UV ( $\lambda < 290$  nm) to some extent.

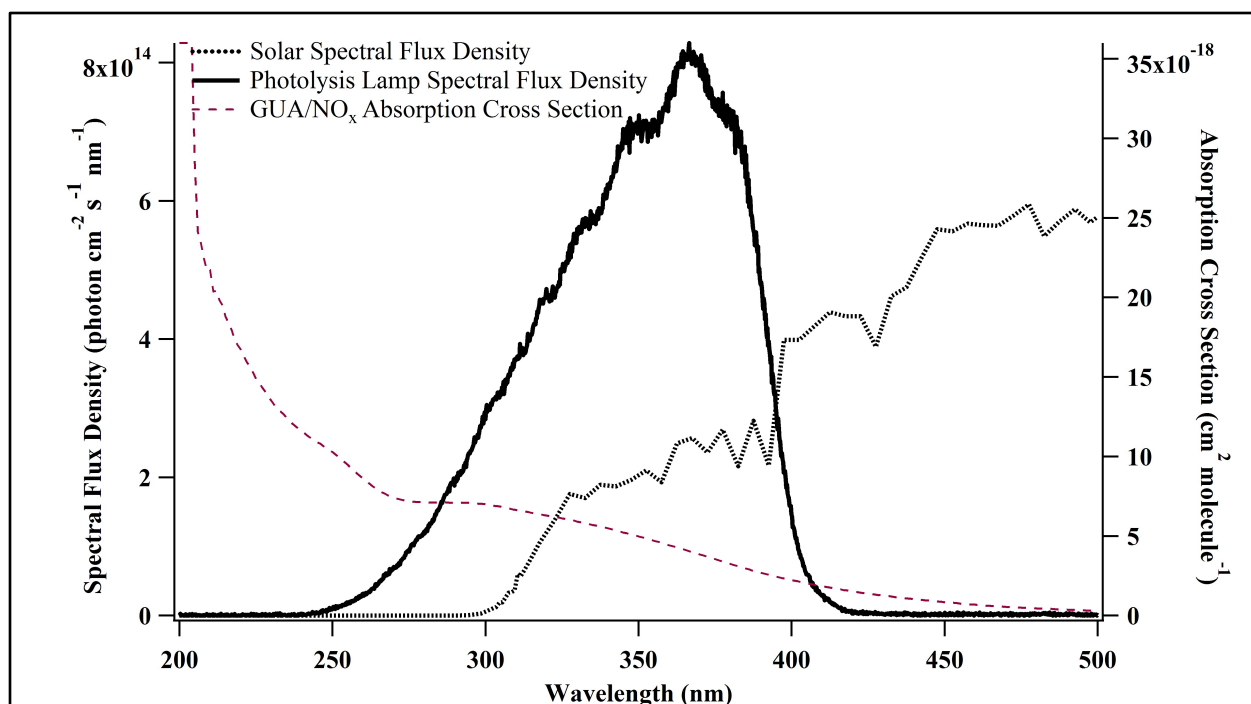


**Figure 3.1.** The spectral flux density in the photolysis cuvette compared to the solar spectral flux density at SZA=0. The right axis shows the effective absorption cross sections of GUA/NO<sub>x</sub> calculated from Eq. (3.1).

### 3.3.3. High-Resolution Mass Spectrometry

Extracted SOA samples were analyzed before and after photolysis using a high-resolution LTQ-Orbitrap™ mass spectrometer equipped with a modified ESI source.<sup>81,82,95,96,134–136</sup> Mass spectra of the solvent were also collected in order to subtract from the sample mass spectra

during the data analysis stage. Mass spectra were acquired in the positive ion mode for all samples. The instrument was operated at the resolving power of  $10^5 m/\Delta m$  at  $m/z$  400.

To process the large number of mass spectra recorded during this work, data analysis was performed similarly to our previous work.<sup>81,82,136</sup> For each spectrum, a list of peak positions and intensities was generated using Decon2LS (<http://omics.pnl.gov/software/decontools-decon2ls>). The resulting peak lists for all the files in the same experimental batch, including blank samples, were first assigned with a  $m/z$  tolerance of  $\pm 0.001$  to molecular formulas  $C_cH_hO_oN_nNa_x^+$  (small letters c, h, o, n refer to the number of corresponding atoms in the ion; the number of Na atoms x is restricted to 0 or 1). Constraints were imposed on the elemental ratios ( $0.05 \leq o/c \leq 1.3$ ,  $0.7 \leq h/c \leq 2.0$ ) and parities ( $(c-(h+x))/2+n/2+1$  must be half-integer for closed-shell protonated or sodiated molecules). Peaks that corresponded to molecules containing  $^{13}C$  atoms or obvious impurities with anomalous mass defects were excluded from further analysis. The initial set of assigned peaks was used to refine the calibration of the  $m/z$  axis. If deviations were noticeable (greater than  $\pm 0.0005 m/z$  units), the axis was internally recalibrated with respect to the confidently-assigned peaks, and the mass spectra were then reassigned with a lower tolerance of  $0.00075 m/z$ . The vast majority of peaks corresponded to sodiated molecules ( $C_cH_hO_oN_nNa^+$ ); protonated molecules ( $C_cH_hO_oN_nH^+$ ) generally had small abundance. For the remainder of this paper, we discuss formulas for the corresponding neutral species,  $C_cH_hO_oN_n$ .

### **3.4. Results and Discussion**

#### **3.4.1. Comparison of High-Resolution Mass Spectra of Unphotolyzed SOA Samples**

High-resolution mass spectrometry (HR-MS) is a powerful tool for molecular characterization of SOA.<sup>129</sup> However, most of the results published so far have been limited to

SOA made from a limited number of precursors (limonene,  $\alpha$ -pinene, isoprene, diesel fuel) and to filter extracts from a small number of field studies.<sup>137-156</sup> A database of HR mass spectra for laboratory-generated SOA is needed to help interpret HR-MS data for ambient aerosol samples. In this work, HR mass spectra of both natural and anthropogenic SOA are qualitatively compared to one another to identify the extent of similarity between them.

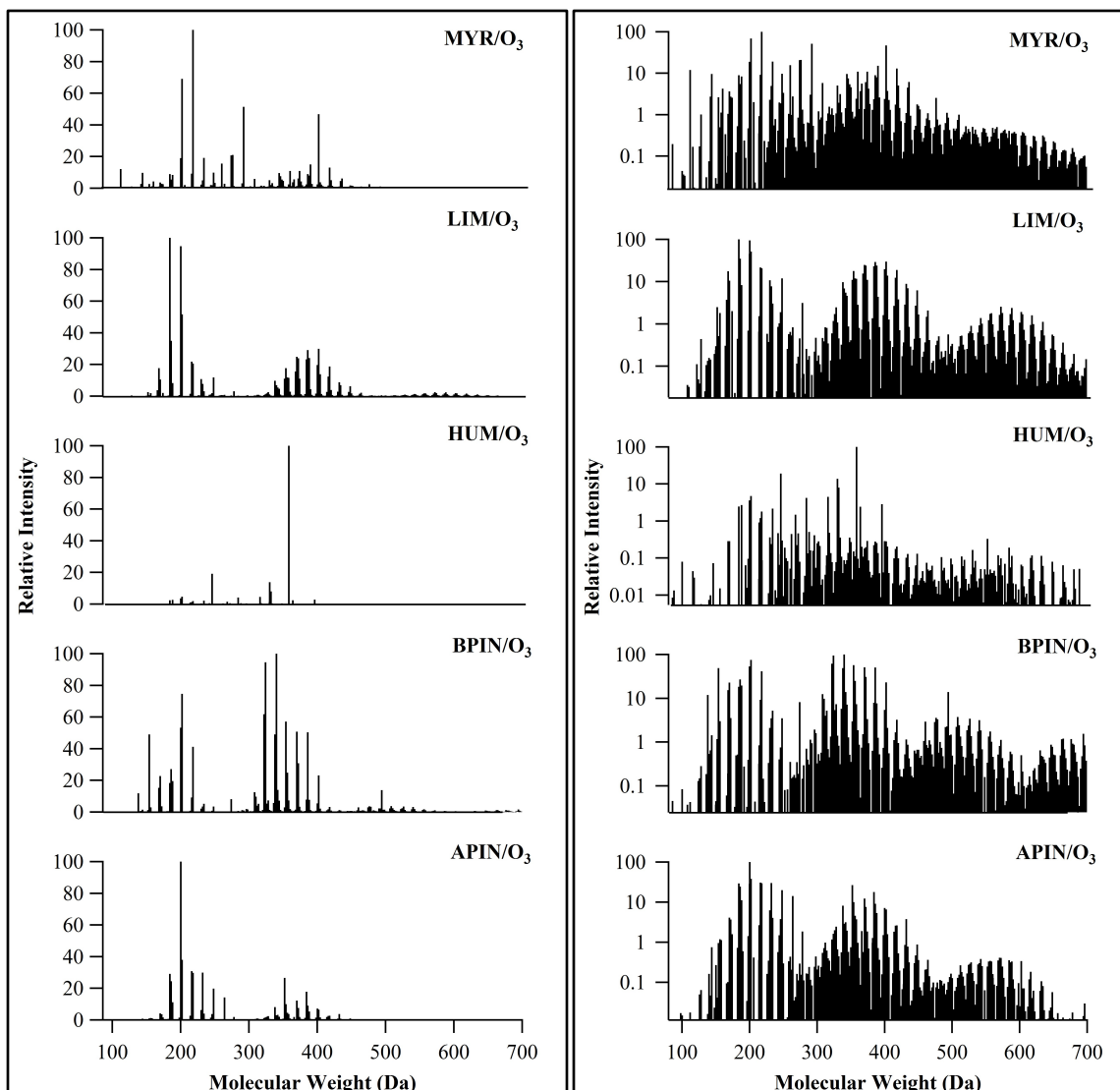


**Figure 3.2.** Reconstructed mass spectra for all the unphotolyzed O<sub>3</sub> SOA samples (before photolysis) recorded in this work. The x-axis corresponds to the molecular weight of the neutral SOA compounds. The x-axis of the left panel corresponds to the molecular weight of the neutral SOA compounds. The y-axis of the right panel is on a log scale to make the weaker peaks of oligomeric compounds easier to see.

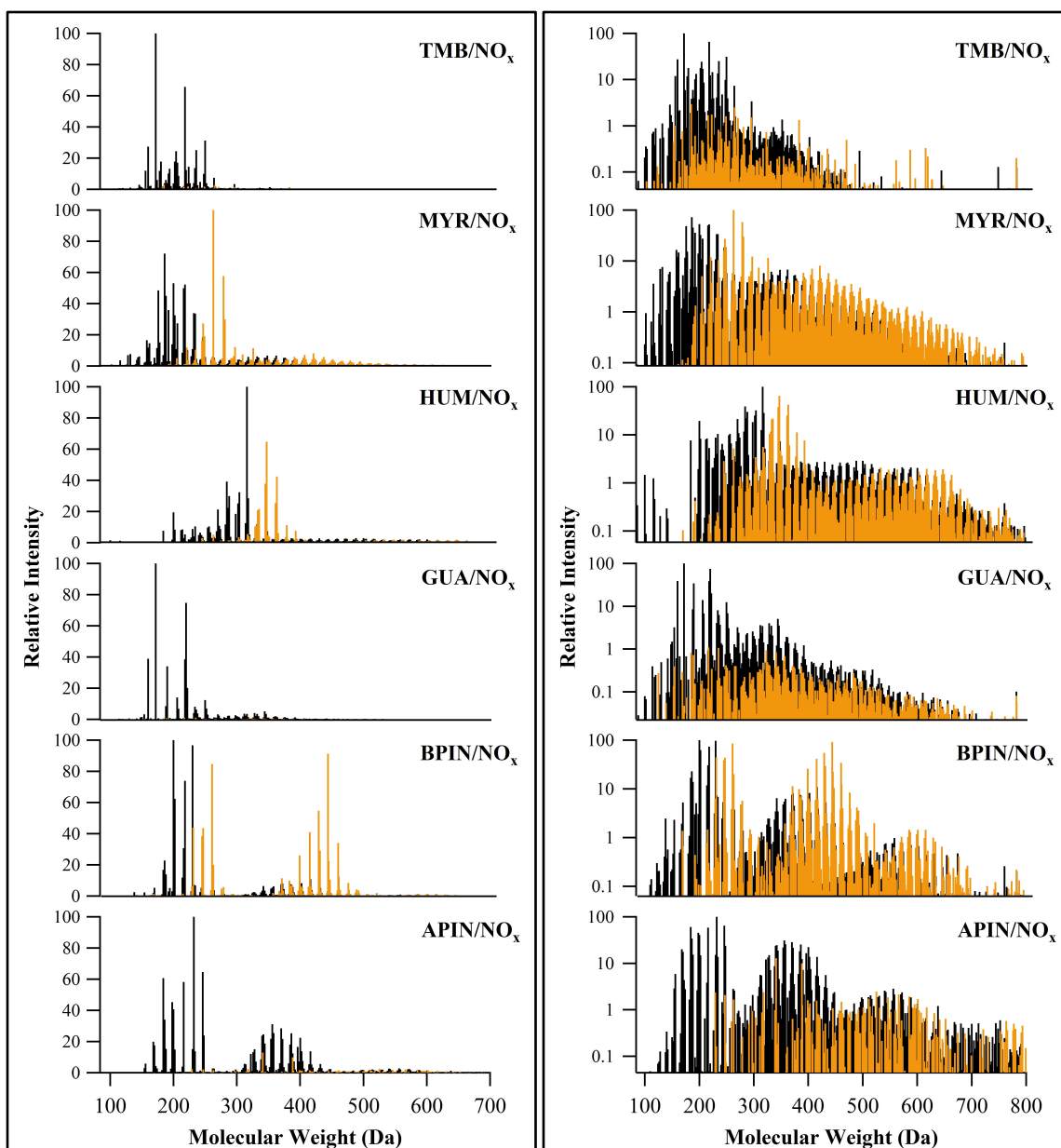


**Figure 3.3.** Reconstructed mass spectra for all OH/NO<sub>x</sub> SOA samples (before photolysis) recorded in this work. The x-axis corresponds to the molecular weight of the neutral SOA compounds. The y-axis of the left panel corresponds to the molecular weight of the neutral SOA compounds. The y-axis of the right panel is on a log scale to make the weaker peaks of oligomeric compounds easier to see. Peaks in orange denote nitrogen-containing compounds.

Figures 3.2 and 3.3 compare mass spectra of all the fresh (unphotolyzed) SOA samples. The peak abundances are shown on both linear and logarithmic scale; the latter is useful for emphasizing smaller peaks in the mass spectra. The SOA produced by ozonolysis of

monoterpenes APIN, BPIN, MYR, and LIM produce qualitatively similar mass spectra (Fig. 3.2) with a clear grouping of peaks into the monomeric (< 300 Da), dimeric (300-500 Da) and larger oligomer groups. We refer to the molecules containing two oxidized VOC molecules joined together as “dimers”, three molecules joined together as “trimers”, etc. The mass spectrum of HUM/O<sub>3</sub> SOA is qualitatively different, and appears to be dominated by a few monomeric products (this is especially obvious on the linear scale Fig. 3.2). The mass spectra from OH/NO<sub>x</sub> photooxidation SOA samples display a greater level of diversity (Fig. 3.3). The grouping of peaks into oligomeric species is still apparent for SOA from monoterpene precursors (e.g. APIN/NO<sub>x</sub>, BPIN/NO<sub>x</sub>, and MYR/NO<sub>x</sub> SOA) while mass spectra of SOA from sesquiterpene and aromatic precursors (e.g. HUM/NO<sub>x</sub>, GUA/NO<sub>x</sub>, and TMB/NO<sub>x</sub>) are dominated by monomeric products.

The fraction of nitrogen-containing compounds (shown in orange in Fig. 3.3) varies greatly between the SOA types; especially striking is the difference between the APIN/NO<sub>x</sub> and BPIN/NO<sub>x</sub> SOA. We note that organonitrates (ONs) produced under OH/NO<sub>x</sub> conditions may decompose by solvolysis reactions with water or methanol in the extracts before the HR-MS analysis. The SOA compounds remained in the methanol/water solutions for approximately one week prior to the HR-MS analysis, and although the solutions were frozen for most of that time, the solvolysis could potentially occur in ~2 h before freezing and after thawing. The solvolysis rates for most SOA compounds are not known, but primary ONs are known to be more stable with respect to the solvolysis than tertiary ONs, and therefore more likely to survive in solution.<sup>157,158</sup> The fraction of primary ONs formed in BPIN (exocyclic double bond) oxidation should be higher than that in APIN (endocyclic double bond) oxidation, which may explain the higher fraction of the remaining ONs in the BPIN/NO<sub>x</sub> SOA extract.



Table 3.3 lists the most dominant peaks observed in each mass spectrum. In general, the major products tend to retain the carbon number of the precursor VOC. The monoterpenes ( $C_{10}H_{16}$ ), humulene ( $C_{15}H_{24}$ ), guaiacol ( $C_7H_8O_2$ ), and trimethylbenzene ( $C_9H_{12}$ ) produce for the most part  $C_{10}$ ,  $C_{15}$ ,  $C_7$ , and  $C_9$  compounds, respectively. For example, a major peak appearing in the APIN/ $NO_x$  and LIM/ $O_3$  SOA is  $C_{10}H_{16}O_3$ , which can be assigned to pinonic acid, limonic acid and other isomers sharing this formula.<sup>92,135,136</sup> Compound  $C_{10}H_{16}O_4$ , presumably an isomer of hydroxy pinonic acid, is the most abundant peak in BPIN/ $NO_x$  SOA. The  $C_7H_8O_5$  compounds in GUA/ $NO_x$  SOA may correspond to guaiacol with three more hydroxyl groups added to the ring.

However, there are many interesting deviations from the general trend of conserving the starting VOC precursor carbon number. For example, while the strongest peaks in HUM/ $NO_x$  SOA have 15 or 14 C atoms ( $C_{15}H_{24}O_7$ ,  $C_{15}H_{25}O_8N$ ,  $C_{15}H_{25}O_9N$ ,  $C_{14}H_{24}O_7$  and  $C_{15}H_{24}O_5$ ), the largest peak in HUM/ $O_3$  SOA, namely  $C_{21}H_{42}O_4$ , appears to have little in common with the starting VOC precursor formula. It is likely a reaction product of a  $C_{15}$  and a  $C_6$  product of humulene ozonolysis. The major peaks in BPIN/ $NO_x$  SOA ( $C_{20}H_{32}O_9$ ) and in BPIN/ $O_3$  SOA ( $C_{19}H_{32}O_5$ ) correspond to dimeric compounds in contrast to other SOA, in which monomeric compounds prevail.

The occurrence of major  $C_{11}$  compounds in SOA from monoterpenes,  $C_8$  compounds in GUA/ $NO_x$  SOA, and  $C_{10}$  compounds in TMB/ $NO_x$  (Table 3.3) can be explained by hemiacetal (R3.1) and/or ester (R3.2) formation reactions between the SOA compounds and methanol as previously observed by Bateman et al.<sup>133</sup>



Bateman et al.<sup>30</sup> showed that reaction (R3.1) quickly reaches equilibrium in methanol solutions, and is more significant for aldehydes than for ketones, while reaction (R3.2) is kinetically constrained. The hemiacetals produced in the 70 v/v % methanol/water solution should contain one additional carbon atom compared to their SOA carbonyl precursors. For example, the C<sub>11</sub>H<sub>20</sub>O<sub>3</sub> compound, which appears as one of the major peaks in APIN/O<sub>3</sub> and LIM/O<sub>3</sub> SOA is a hemiacetal of C<sub>10</sub>H<sub>16</sub>O<sub>2</sub> (pinonaldehyde or limononaldehyde) and methanol.<sup>133</sup> The C<sub>11</sub>H<sub>18</sub>O<sub>5</sub> compound in BPIN/NO<sub>x</sub> is presumably a hemiacetal corresponding to C<sub>10</sub>H<sub>14</sub>O<sub>4</sub>. Likewise, the C<sub>11</sub>H<sub>18</sub>O<sub>4</sub> compound observed in the APIN/O<sub>3</sub>, BPIN/O<sub>3</sub>, LIM/O<sub>3</sub>, and MYR/O<sub>3</sub> samples must be a hemiacetal corresponding to C<sub>10</sub>H<sub>14</sub>O<sub>3</sub> (it would otherwise be challenging to explain why a major product of a monoterpene oxidation should have a formula C<sub>10</sub>H<sub>18</sub>O<sub>4</sub> corresponding to a decanedioic acid isomer). The TMB/NO<sub>x</sub> compound C<sub>10</sub>H<sub>18</sub>O<sub>7</sub> is conceivably a hemiacetal of C<sub>9</sub>H<sub>14</sub>O<sub>6</sub> (the latter is also observed as a major species in TMB/NO<sub>x</sub>). The compounds C<sub>8</sub>H<sub>10</sub>O<sub>7</sub> and C<sub>8</sub>H<sub>12</sub>O<sub>7</sub> in GUA/NO<sub>x</sub> SOA could also be products of reactions (R3.1) or (R3.2). As mentioned in the experimental section, the hemiacetal formation is not expected to drastically affect photochemical properties of SOA relative to pure water solutions.

**Table 3.3.** Major peaks observed in the mass spectra for all samples analyzed in this chapter.

Sample	Neutral Mass	Chemical Formula <sup>a</sup>	Relative Intensity (Before Photolysis)	Relative Intensity (After Photolysis)
APIN/NO <sub>x</sub>	232.0576	C <sub>9</sub> H <sub>12</sub> O <sub>7</sub>	100	100
	246.0892	C <sub>14</sub> H <sub>14</sub> O <sub>4</sub>	65	66
	184.1094	C <sub>10</sub> H <sub>16</sub> O <sub>3</sub>	61	78
BPIN/NO <sub>x</sub>	200.1042	C <sub>10</sub> H <sub>16</sub> O <sub>4</sub>	100	100
	230.1144	<b>C<sub>11</sub>H<sub>18</sub>O<sub>5</sub></b>	97	61
	444.2102	C <sub>20</sub> H <sub>32</sub> O <sub>9</sub>	91	11
	202.1198	<b>C<sub>10</sub>H<sub>18</sub>O<sub>4</sub></b>	62	92
GUA/NO <sub>x</sub>	172.0367	C <sub>7</sub> H <sub>8</sub> O <sub>5</sub>	100	100

	220.0577	<b>C<sub>8</sub>H<sub>12</sub>O<sub>7</sub></b>	75	54
	160.0367	C <sub>6</sub> H <sub>8</sub> O <sub>5</sub>	39	39
	218.0421	<b>C<sub>8</sub>H<sub>10</sub>O<sub>7</sub></b>	38	46
HUM/NO <sub>x</sub>	316.1517	C <sub>15</sub> H <sub>24</sub> O <sub>7</sub>	100	100
	347.1574	C <sub>15</sub> H <sub>25</sub> O <sub>8</sub> N	65	35
	363.1523	C <sub>15</sub> H <sub>25</sub> O <sub>9</sub> N	42	23
	304.1516	C <sub>14</sub> H <sub>24</sub> O <sub>7</sub>	32	56
	284.1617	C <sub>15</sub> H <sub>24</sub> O <sub>5</sub>	39	48
MYR/NO <sub>x</sub>	263.0998	C <sub>10</sub> H <sub>17</sub> O <sub>7</sub> N	100	64
	186.0886	C <sub>9</sub> H <sub>14</sub> O <sub>4</sub>	72	100
	279.0947	C <sub>10</sub> H <sub>17</sub> O <sub>8</sub> N	58	27
	188.0679	C <sub>8</sub> H <sub>12</sub> O <sub>5</sub>	45	82
	176.0679	C <sub>7</sub> H <sub>12</sub> O <sub>5</sub>	49	77
TMB/NO <sub>x</sub>	172.0367	C <sub>7</sub> H <sub>8</sub> O <sub>5</sub>	100	100
	218.0784	C <sub>9</sub> H <sub>14</sub> O <sub>6</sub>	66	93
	250.1044	<b>C<sub>10</sub>H<sub>18</sub>O<sub>7</sub></b>	31	60
APIN/O <sub>3</sub>	200.1407	<b>C<sub>11</sub>H<sub>20</sub>O<sub>3</sub></b>	100	100
	202.1199	<b>C<sub>10</sub>H<sub>18</sub>O<sub>4</sub></b>	38	46
	216.1355	<b>C<sub>11</sub>H<sub>20</sub>O<sub>4</sub></b>	31	23
	186.1251	<b>C<sub>10</sub>H<sub>18</sub>O<sub>3</sub></b>	24	41
BPIN/O <sub>3</sub>	340.2241	C <sub>19</sub> H <sub>32</sub> O <sub>5</sub>	100	100
	324.1928	C <sub>18</sub> H <sub>28</sub> O <sub>5</sub>	95	55
	202.1199	<b>C<sub>10</sub>H<sub>18</sub>O<sub>4</sub></b>	75	89
	154.0989	C <sub>9</sub> H <sub>14</sub> O <sub>2</sub>	49	64
HUM/O <sub>3</sub>	358.3075	C <sub>21</sub> H <sub>42</sub> O <sub>4</sub>	100	100
	246.146	C <sub>12</sub> H <sub>22</sub> O <sub>5</sub>	19	33
	330.2765	C <sub>19</sub> H <sub>38</sub> O <sub>4</sub>	14	13
LIM/O <sub>3</sub>	184.1094	C <sub>10</sub> H <sub>16</sub> O <sub>3</sub>	100	78
	200.1407	<b>C<sub>11</sub>H<sub>20</sub>O<sub>3</sub></b>	95	100
	202.1199	<b>C<sub>10</sub>H<sub>18</sub>O<sub>4</sub></b>	52	76

MYR/O <sub>3</sub>	218.1148	<b>C<sub>10</sub>H<sub>18</sub>O<sub>5</sub></b>	100	100
	202.1199	<b>C<sub>10</sub>H<sub>18</sub>O<sub>4</sub></b>	69	85
	292.1517	C <sub>13</sub> H <sub>24</sub> O <sub>7</sub>	51	40

<sup>a</sup> Formulas that are bolded likely correspond to hemiacetals formed through reaction R3.1 with methanol. The formulas of the original SOA compounds can be obtained from the hemiacetal formulas by subtracting CH<sub>4</sub>O.

We evaluated the extent of overlap between the exact *m/z* values reported between all the OH/NO<sub>x</sub> and O<sub>3</sub> SOA samples examined in this work (Table 3.4). For both sets of oxidation conditions, close to 50% of the assigned peaks are unique to the specific precursors. Furthermore, the fraction of peaks appearing in all samples produced under the same oxidation conditions is relatively low, especially for the subset of OH/NO<sub>x</sub> SOA. Since we used only terpenes in the O<sub>3</sub> experiments and both terpene and aromatic precursors in the OH/NO<sub>x</sub> experiments, we also calculated the extent of the peak overlap for a smaller subset of SOA made from four terpene precursors APIN, BPIN, HUM, and MYR. The fractions of unique peaks remained significant and the fraction of peaks appearing in all samples produced under the same oxidation conditions remained relatively low even for this subset of closely related precursors. These observations suggest that HR-MS could potentially be used to distinguish SOA made from different VOC precursors based on the distribution of peaks in the mass spectra.

**Table 3.4.** Overlap of peaks between NO<sub>x</sub> samples and O<sub>3</sub> samples.

SOA class <sup>a</sup>	All VOC/NO <sub>x</sub> SOA	Subset of APIN/NO <sub>x</sub> , BPIN/NO <sub>x</sub> , HUM/NO <sub>x</sub> , MYR/NO <sub>x</sub>	All VOC/O <sub>3</sub> SOA	Subset of APIN/O <sub>3</sub> , BPIN/O <sub>3</sub> , HUM/O <sub>3</sub> , MYR/O <sub>3</sub>
<b>Total Peaks Assigned</b>	4178	3005	1474	1379
<b>Peaks unique to a specific VOC precursor</b>	2427 (58.1%)	1722 (57.3%)	653 (44.3%)	755 (54.7%)
<b>Peaks observed from more than one precursor</b>	1741 (41.7%)	1150 (38.3%)	638 (43.3%)	436 (31.6%)
<b>Peaks that appear in all samples</b>	10 (0.2%)	133 (4.4%)	183 (12.4%)	188 (13.6%)

<sup>a</sup> The analysis is carried out for all the VOC/NO<sub>x</sub> SOA and VOC/O<sub>3</sub> SOA examined in this work. An analysis of a subset of data with four overlapping VOC precursors (APIN, BPIN, HUM, MYR) is also included for comparison.

However, it will not be possible to unambiguously attribute SOA to a specific set of precursors and oxidants using only the information on the major peaks appearing in the direct infusion ESI mass spectra (Table 3.3). Coupling to LC methods would be required to remove some of the ambiguity. For example, one of the molecular formulas appearing in all the O<sub>3</sub> samples is C<sub>10</sub>H<sub>16</sub>O<sub>3</sub>, which could correspond to pinonic acid, but could also be limononic acid or any of the keto-acids produced from monoterpenes.<sup>159</sup> Another molecular formula, C<sub>9</sub>H<sub>14</sub>O<sub>3</sub>, identified as ketolimononaldehyde in limonene SOA,<sup>160</sup> is also appearing in all the O<sub>3</sub> samples. Other common formulas observed in all O<sub>3</sub> and all OH/NO<sub>x</sub> samples include C<sub>10</sub>H<sub>14</sub>O<sub>5</sub>, possibly peroxy-pinonic acid or its isomer,<sup>161</sup> previously observed in  $\alpha$ -pinene ozonolysis as well as campholenic aldehyde ozonolysis,<sup>162</sup> and C<sub>10</sub>H<sub>16</sub>O<sub>6</sub>, which has been potentially identified as an ester of glutaric acid or 5-hydroxy-pentanoic acid as seen in the study of ozonolysis of

cyclohexene by Hamilton et al.<sup>163</sup> A study of the ozonolysis of  $\alpha$ -pinene and limonene by Warscheid and Hoffmann<sup>164</sup> also identified the molecular formula of  $C_{10}H_{16}O_6$  through an on-line MS<sup>n</sup> technique. Their analysis showed two structurally different carboxylic acid species - a hydroxyl-acidic ester as well as a peroxyacetyl carboxylic acid. It is also of interest that one recurring molecular formula in all OH/NO<sub>x</sub> samples is that of  $C_9H_{13}O_7N$ . Assuming that it is a nitric acid ester ( $ROH + HONO_2 \rightarrow RONO_2 + H_2O$ ), the unesterified compound would have the formula  $C_9H_{14}O_5$ , a compound observed in APIN, BPIN, HUM, MYR, and TMB OH/NO<sub>x</sub> samples in this study as well as in ozonolysis of alpha-pinene,<sup>165</sup> limonene,<sup>166,167</sup> campholenic aldehyde<sup>162</sup> in previous studies. It is not clear how the  $C_9H_{13}O_7N$  could be formed from the aromatic precursors; however, we cannot exclude the possibility that its occurrence in all samples is an experimental artifact from “carry-over” between SOA generated from different precursors on different days.

### **3.4.2. Effect of Photolysis on SOA Composition**

Figures 3.4-3.10 show representative high-resolution mass spectra before and after 1 h of photolysis for the SOA samples investigated here. In the case of APIN SOA (Figure 3.4), the mass spectra noticeably change after irradiation, especially in the dimeric (300-500  $m/z$ ) and trimeric (500-700  $m/z$ ) regions. The higher molecular weight (MW) compounds appear to be converted to lower molecular weight species by photolysis with an accompanying shift in the distribution of relative intensity toward lower-MW compounds. Similar trends are observed for other SOA.

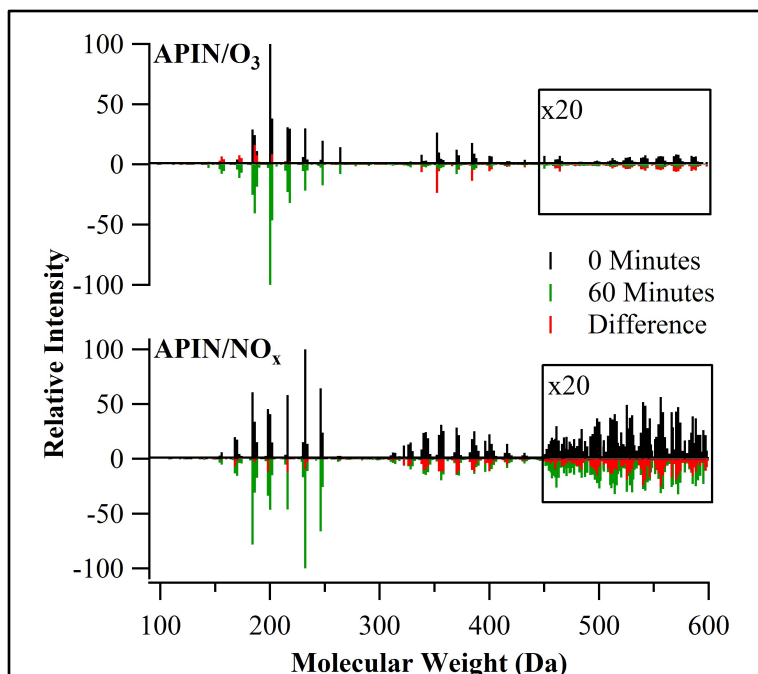


**Figure 3.4.** Mass spectra of APIN/O<sub>3</sub> and APIN/NO<sub>x</sub> SOA solutions before (black) and after (green) 1 h of photolysis. The mass spectra after photolysis are inverted for clarity. The difference (red, after - before) is representative of the change that occurred during photolysis the time.

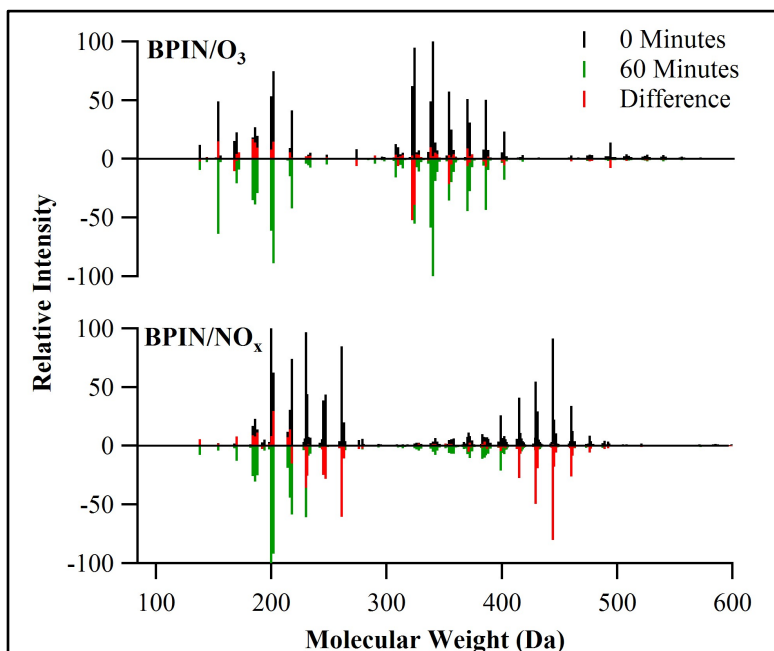


**Figure 3.5.** Mass spectra of BPIN/O<sub>3</sub> and BPIN/NO<sub>x</sub> SOA solutions before (black) and after (green) 1 h of photolysis. The mass spectra after photolysis are inverted for clarity. The difference (red, after - before) is representative of the change that occurred during photolysis the time.

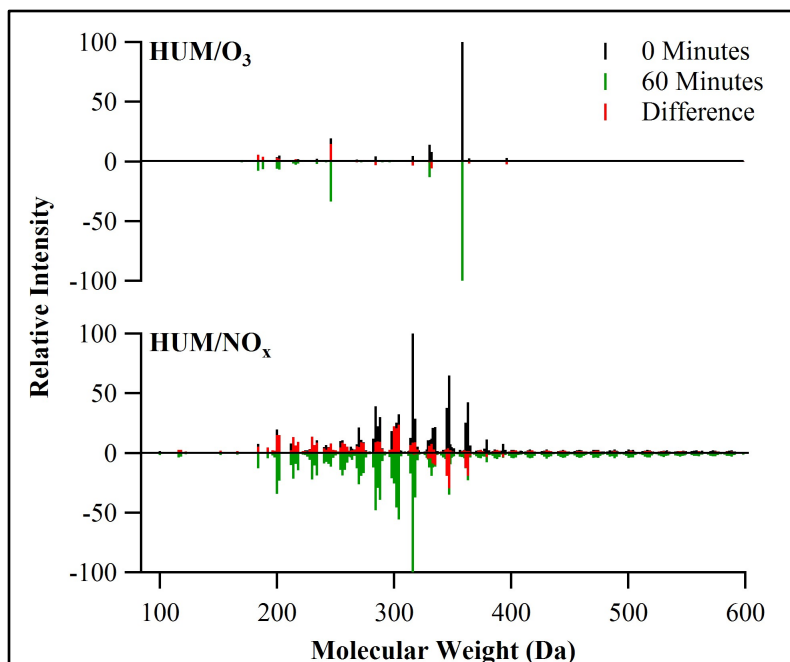


**Figure 3.6.** Mass spectra of HUM/O<sub>3</sub> and HUM/NO<sub>x</sub> SOA solutions before (black) and after (green) 1 h of photolysis. The mass spectra after photolysis are inverted for clarity. The difference (red, after - before) is representative of the change that occurred during photolysis the time.

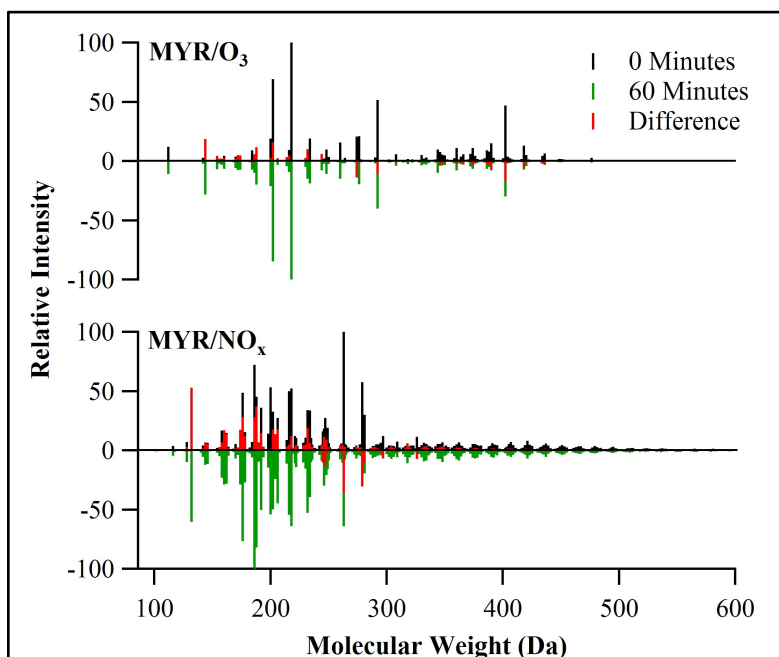


**Figure 3.7.** Mass spectra of MYR/O<sub>3</sub> and MYR/NO<sub>x</sub> SOA solutions before (black) and after (green) 1 h of photolysis. The mass spectra after photolysis are inverted for clarity. The difference (red, after - before) is representative of the change that occurred during photolysis the time.



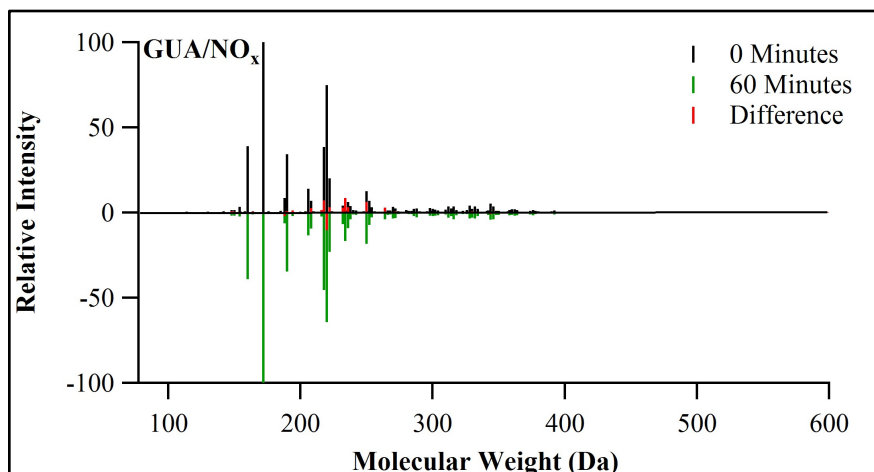


**Figure 3.8.** Mass spectra of GUA/NO<sub>x</sub> SOA solutions before (black) and after (green) 1 h of photolysis. The mass spectra after photolysis are inverted for clarity. The difference (red, after - before) is representative of the change that occurred during photolysis the time.

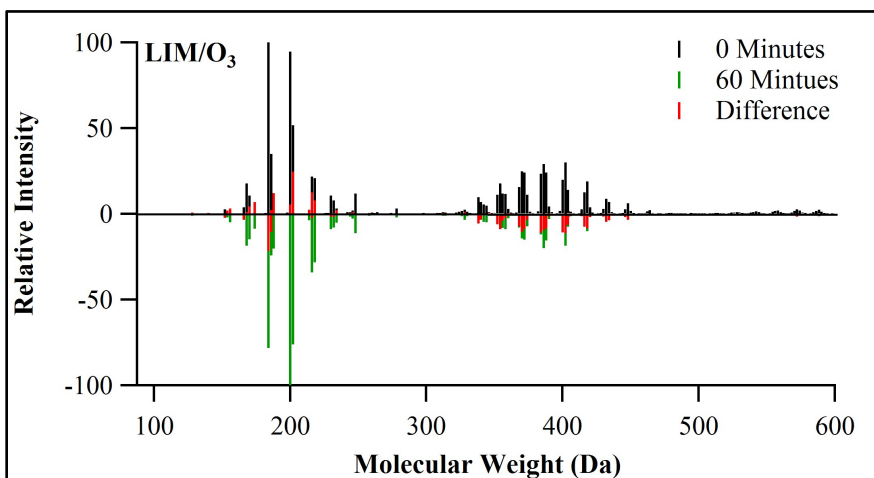


**Figure 3.9.** Mass spectra of LIM/O<sub>3</sub> SOA solutions before (black) and after (green) 1 h of photolysis. The mass spectra after photolysis are inverted for clarity. The difference (red, after - before) is representative of the change that occurred during photolysis the time.

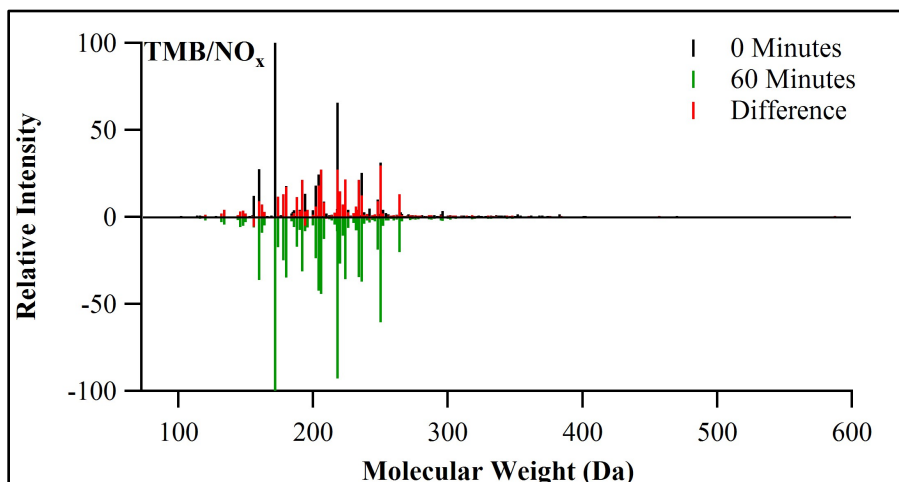


**Figure 3.10.** Mass spectra TMB/NO<sub>x</sub> SOA solutions before (black) and after (green) 1 h of photolysis. The mass spectra after photolysis are inverted for clarity. The difference (red, after - before) is representative of the change that occurred during photolysis the time.

The average atom numbers (C, H, O, N) and average elemental ratios (H/C, O/C, and N/C) can be extracted from the assigned molecular formulas C<sub>c</sub>H<sub>h</sub>O<sub>o</sub>N<sub>n</sub>. These average quantities were used to assess the extent in the photolysis-induced overall change in SOA composition. The ratio O/C indicates the degree of oxidation, while H/C is a good indicator of the degree of unsaturation in SOA molecules. All averaged quantities were weighted with respect to the relative intensity (*I*), for all assigned compounds, indexed with *i*.

$$\langle X \rangle = \frac{\sum I_i x_i}{\sum I_i} \quad (x = c, o, h, n, \text{DBE}) \quad (3.3)$$

$$\langle X/Y \rangle = \frac{\sum I_i x_i}{\sum I_i y_i} = \frac{\langle X \rangle}{\langle Y \rangle} \quad (x, y = o, h, n) \quad (3.4)$$

Table 3.5 summarizes the analysis results. The table also shows the average double bond equivalent (DBE) value, also known as degree of unsaturation to organic chemists.<sup>168</sup> Average DBE is calculated by,

$$\langle DBE_{\text{uncorrected}} \rangle = 1 - \frac{\langle h \rangle}{2} + \frac{\langle n \rangle}{2} + \langle c \rangle \quad (3.5)$$

and represents the total number of double bonds and rings in a molecule. Since most of the N-containing compounds in SOA are expected to be either nitrocompounds (-NO<sub>2</sub>) or nitric acid esters (-ONO<sub>2</sub>), the true DBE is higher than that predicted by Eq. (3.5) by the average number of nitrogen atoms:

$$\langle DBE_{corrected} \rangle = 1 - \frac{\langle h \rangle}{2} + \frac{3\langle n \rangle}{2} + \langle c \rangle = \langle DBE_{uncorrected} \rangle + \langle n \rangle \quad (3.6)$$

Some of the SOA examined in this work have higher DBE values than one would have expected based on the known oxidation mechanisms of VOCs. For example, the APIN/NO<sub>x</sub> SOA has an average formula C<sub>16.6</sub>H<sub>22.7</sub>O<sub>6.2</sub>N<sub>0.067</sub> and an uncorrected DBE of 6.3. One could potentially explain such high DBE value if all the oxygen atoms in APIN/NO<sub>x</sub> SOA compounds were tied in carbonyls groups but this scenario is unlikely. It is more reasonable to assume that a large fraction of SOA products contain intramolecular cycles that contribute to the observed high DBE values.

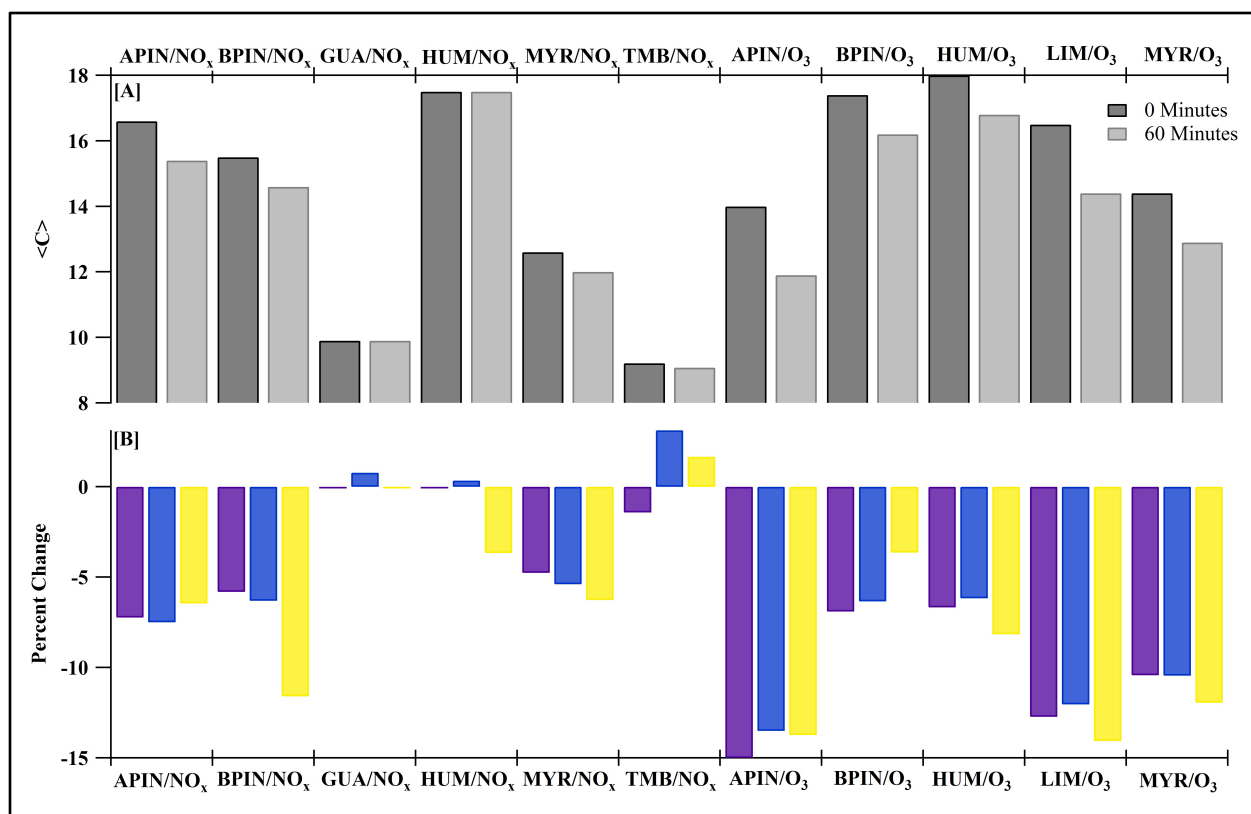


**Figure 3.11.** Panel A shows the average number of carbon atoms per molecule before (dark grey bars) and after (light grey bars) 1 h of photolysis. Panel B shows the percent change, (after-before)/before\*100, in the average number of C (purple), H (blue), and O (yellow) atoms following the 1 h of photolysis.

**Table 3.5.** The average molecular formulas and double bond equivalents (DBE) before and after 1 h of photolysis of SOA solutions.

Reaction	Average Molecular Formula		<DBE> <sup>d</sup>	
	Before Photolysis (0 min)	After Photolysis (60 min)	0 min	60 min
APIN/NO <sub>x</sub>	C <sub>16.6</sub> H <sub>22.7</sub> O <sub>6.2</sub> N <sub>0.067</sub>	C <sub>15.4</sub> H <sub>21.0</sub> O <sub>5.8</sub> N <sub>0.075</sub>	6.28	5.93
BPIN/NO <sub>x</sub>	C <sub>15.5</sub> H <sub>25.4</sub> O <sub>6.9</sub> N <sub>0.063</sub>	C <sub>14.6</sub> H <sub>23.8</sub> O <sub>6.1</sub> N <sub>0.043</sub>	3.83	3.72
GUA/NO <sub>x</sub>	C <sub>9.90</sub> H <sub>12.7</sub> O <sub>7.4</sub> N <sub>0.081</sub>	C <sub>9.90</sub> H <sub>12.8</sub> O <sub>7.4</sub> N <sub>0.075</sub>	4.59	4.54
HUM/NO <sub>x</sub>	C <sub>17.5</sub> H <sub>28.4</sub> O <sub>8.2</sub> N <sub>0.38</sub>	C <sub>17.5</sub> H <sub>28.5</sub> O <sub>7.9</sub> N <sub>0.21</sub>	4.49	4.15
MYR/NO <sub>x</sub>	C <sub>12.6</sub> H <sub>20.4</sub> O <sub>8.0</sub> N <sub>0.48</sub>	C <sub>12.0</sub> H <sub>19.3</sub> O <sub>7.5</sub> N <sub>0.28</sub>	3.64	3.49
TMB/NO <sub>x</sub>	C <sub>9.21</sub> H <sub>12.8</sub> O <sub>6.0</sub> N <sub>0.082</sub>	C <sub>9.08</sub> H <sub>13.2</sub> O <sub>6.1</sub> N <sub>0.063</sub>	3.85	3.51
APIN/O <sub>3</sub>	C <sub>14.0</sub> H <sub>23.7</sub> O <sub>5.1</sub>	C <sub>11.9</sub> H <sub>20.5</sub> O <sub>4.4</sub>	3.15	2.65
BPIN/O <sub>3</sub>	C <sub>17.4</sub> H <sub>28.4</sub> O <sub>5.5</sub>	C <sub>16.2</sub> H <sub>26.6</sub> O <sub>5.3</sub>	4.20	3.90
HUM/O <sub>3</sub>	C <sub>18.0</sub> H <sub>34.1</sub> O <sub>4.9</sub>	C <sub>16.8</sub> H <sub>32.0</sub> O <sub>4.5</sub>	1.95	1.80
LIM/O <sub>3</sub>	C <sub>16.5</sub> H <sub>27.4</sub> O <sub>6.4</sub>	C <sub>14.4</sub> H <sub>24.1</sub> O <sub>5.5</sub>	3.80	3.35
MYR/O <sub>3</sub>	C <sub>14.4</sub> H <sub>24.8</sub> O <sub>6.7</sub>	C <sub>12.9</sub> H <sub>22.2</sub> O <sub>5.9</sub>	3.00	2.80
LIM/O <sub>3</sub> <sup>a</sup>	C <sub>14</sub> H <sub>22</sub> O <sub>7.0</sub>	C <sub>12</sub> H <sub>18</sub> O <sub>6.4</sub>	4.00	4.00
ISO/NO <sub>x</sub> <sup>b</sup>	C <sub>12</sub> H <sub>19</sub> O <sub>9</sub> N <sub>0.08</sub>	C <sub>10</sub> H <sub>16</sub> O <sub>8</sub> N <sub>0.40</sub>	3.54	3.20
NAP/NO <sub>x</sub> <sup>c</sup>	C <sub>14.1</sub> H <sub>14.5</sub> O <sub>5.1</sub> N <sub>0.08</sub>	C <sub>11.8</sub> H <sub>14.9</sub> O <sub>4.5</sub> N <sub>0.02</sub>	7.89	5.36

<sup>a</sup> Bateman et al. 2001; 24 h photolysis, different light source

<sup>b</sup> Nguyen et al. 2012; 4 h photolysis, different light source

<sup>c</sup> Lee et al. 2014; 4 h photolysis, different light source

<sup>d</sup> Uncorrected DBE from Eq. (5). Corrected values can be easily calculated from Eq. 3.6.

**Table 3.6.** The average atomic ratios X/C, where X is O, H, or N, before and after 1 h of photolysis of SOA solutions.

Reaction	<O/C>		<H/C>		<N/C>	
	0 min	60 min	0 min	60 min	0 min	60 min
APIN/NO <sub>x</sub>	0.373	0.377	1.42	1.36	0.00403	0.00487
BPIN/NO <sub>x</sub>	0.445	0.418	1.64	1.63	0.00406	0.00295
GUA/NO <sub>x</sub>	0.747	0.747	1.28	1.29	0.00818	0.00758
HUM/NO <sub>x</sub>	0.469	0.451	1.62	1.63	0.0217	0.0120
MYR/NO <sub>x</sub>	0.635	0.625	1.62	1.61	0.0381	0.0233
TMB/NO <sub>x</sub>	0.651	0.672	1.39	1.45	0.00890	0.00694
APIN/O <sub>3</sub>	0.364	0.370	1.69	1.72	-	-
BPIN/O <sub>3</sub>	0.316	0.327	1.63	1.64	-	-
HUM/O <sub>3</sub>	0.272	0.268	1.89	1.90	-	-
LIM/O <sub>3</sub>	0.388	0.382	1.66	1.67	-	-
MYR/O <sub>3</sub>	0.465	0.457	1.72	1.72	-	-
LIM/O <sub>3</sub> <sup>a</sup>	0.500	0.533	1.57	1.50	-	-
ISO/NO <sub>x</sub> <sup>b</sup>	0.750	0.800	1.58	1.60	0.00667	0.0400
NAP/NO <sub>x</sub> <sup>c</sup>	0.362	0.381	1.03	1.26	0.00567	0.00169

<sup>a</sup> Bateman et al. 2001; 24 h photolysis, different light source

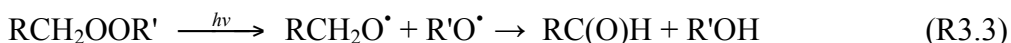
<sup>b</sup> Nguyen et al. 2012; 4 h photolysis, different light source

<sup>c</sup> Lee et al. 2014; 4 h photolysis, different light source

Degradation of oligomeric compounds seen in the mass spectra appears to be a common result for aqueous direct photolysis of the SOA, regardless of the VOC precursor and oxidation conditions leading to SOA. We note that photolysis-driven formation of lower molecular weight compounds is well known in photochemistry of dissolved organic matter (DOM), but is much less studied in the case of SOA.<sup>169–171</sup> Although the effect of photolysis on the molecular size is modest, the photolysis time used in these experiments is only 1 h, and the effect can be expected to be stronger for longer photolysis durations. For example, Nguyen et al. saw no evidence of

photodegradation stopping after 0, 1, 2, 3, and 4 hrs of the aqueous photolysis of isoprene/NO<sub>x</sub> SOA.<sup>96</sup> Using actinometry to estimate the photon flux from the lamp used in experiments, we have concluded that 1 h of photolysis under our lamp is approximately equivalent to ~4 h of photolysis under the overhead sun in the case of GUA/NO<sub>x</sub> SOA and ~8 h in the case of APIN/NO<sub>x</sub> SOA. The lifetime of droplets in cumulus clouds is typically in the range of 10 to 40 minutes, so the times probed here correspond to photolysis that may be experienced during several cloud cycles.<sup>172</sup> In this work we opted to fix the photolysis time and vary the type of SOA, assuming that the extent of photodegradation would scale with photolysis time (doing time-dependent studies for all the SOA listed in Table 3.2 would be prohibitively time-consuming).

One possible explanation for the reduction in the average number of carbon atoms during photolysis is the photochemistry that occurs with organic molecules that contain a peroxy group. Organic peroxides are known to be abundant in SOA produced by ozonolysis of alkenes. For example, Docherty et al. estimate that a large fraction of compounds in APIN/O<sub>3</sub> and BPIN/O<sub>3</sub> SOA are peroxides.<sup>173</sup> Peroxides are well-known<sup>17</sup> to undergo direct photolysis by breaking the O-O bond in the molecule:



The photolysis quantum yield is known to be high in water,<sup>174</sup> and the resulting free radicals do not recombine but rather disproportionate leading to carbonyl and alcohol products, as shown in the R3.3 example.<sup>175</sup> Even if these free radicals manage to escape from the solvent cage, secondary reactions would generally result in smaller products relative to the size of the precursor peroxide compound, which would consequentially also reduce the average C value.

Photochemistry of carbonyls also likely contributes to the reduction in the average C-number. In Norrish type-I splitting, carbonyl groups undergo  $\alpha$ -cleavage that produces peroxy radicals in the presence of dissolved oxygen.<sup>176</sup>



Secondary reactions of peroxy radicals produce carbonyls, alcohols, and carboxylic acids as stable products.<sup>177,178</sup> While Norrish type-I splitting is the predominant path for small carbonyls (C<sub>1</sub>-C<sub>5</sub>), Norrish type-II splitting is favored by the larger carbonyls. Norrish type-II splitting cleaves the molecule into a smaller alkene and a carbonyl:



The resulting carbonyl products can then be further photolyzed by the Norrish type-I and type-II mechanisms to produce even smaller products.<sup>179</sup> These processes can be efficient in water as demonstrated by Norrish type-II photoisomerization of *cis*-pinonic acid into limonic acid occurring with a quantum yield of about 0.5.<sup>114</sup>

Neither photolysis of peroxides nor photolysis of carbonyls provides an explanation for the observed reduction in the average DBE. For example, photolysis of peroxides converts a peroxide (DBE contribution = 0) into an alcohol (DBE contribution = 0) and a carbonyl (DBE contribution = 1), thus increasing the average DBE. Likewise, Norrish type-II splitting converts a carbonyl (DBE contribution = 1) into another carbonyl and alkene (DBE contribution = 1 each), leaving the average DBE unchanged. It is possible that the observed decrease in DBE is in fact an artifact of ESI, which tends to detect larger compounds with higher sensitivity.<sup>180</sup> The smaller photolysis products have suppressed intensities in the mass spectrum, and therefore contribute



less than they should to the average DBE. As DBE in SOA generally increases with molecular size,<sup>135</sup> the reduction of ESI sensitivity with molecular size would produce an artificial reduction in the apparent DBE. We note that the same effect makes the decrease in C underestimated because the precursor molecules are detected with higher sensitivity than their smaller photolysis products.

In this study, very little change is observed with regards to the average H/C and O/C ratios before and after photolysis (Table 3.6). This is an important observation as H/C and O/C are routinely measured in field studies as an indicator of SOA oxygenation or aging.<sup>181–183</sup> Results of this study indicate that tracking the average H/C and O/C ratios may miss important photochemical aging processes such as photodegradation. The changes in the molecular level composition of SOA induced by aqueous photolysis are observable; however, the average atomic ratios hardly change in the process. Furthermore, the reduction in the number of C atoms in SOA compounds with constant O/C ratio may affect the volatility of the photochemically aged aerosols. As a result, the particles are likely to lose some of their mass after exposure to solar radiation.

On the other hand, for SOA that is formed in the presence of NO<sub>x</sub>, the average N/C ratio goes down significantly with photolysis. This reduction in N/C is likely attributed to the photolysis of organonitrates



with secondary processes forming stable nitrogen-free compounds from RO radicals. This significant decrease in the N/C ratio is different from the trend observed in direct aqueous photolysis of isoprene/NO<sub>x</sub> SOA where the number of nitrogen containing compounds increased substantially during photolysis.<sup>96</sup> This suggests that nitrogen-containing molecules in isoprene

SOA may be a unique case that may require further investigation. Our results indicate that for a majority of SOA, the N/C ratio is an additional useful indicator of aerosol age, complementary to the commonly used O/C ratio.

Figure 3.13 shows the percent change in the average number of C, H, and O atoms in SOA molecules following 1 hr photolysis. This figure indicates that the extent of photolysis-driven change is generally larger for ozone-generated SOA than for OH/NO<sub>x</sub> photooxidation SOA. The ozone generated SOA was produced in the dark, and the first time these compounds encountered radiation was after they were extracted from the filter. In contrast, the OH/NO<sub>x</sub> SOA was already irradiated by the 310 nm light while it was being formed in the chamber. This gave the most photolyzable SOA compounds a chance to photolyze in the airborne particles before collection of the SOA sample and its subsequent photolysis in solution. We can extrapolate this result by predicting that SOA produced during the night, with O<sub>3</sub> and NO<sub>3</sub> serving as oxidants, should be more photolabile than SOA formed during the day, with OH serving as the oxidant. Our on-going experiments are testing this hypothesis by comparing photochemistry of SOA generated in the dark by NO<sub>3</sub> oxidation, with photochemistry of OH/NO<sub>x</sub> generated SOA.

Figure 3.13 additionally suggests that the role of direct photolysis is substantially smaller for SOA made from aromatic precursors (TMB and GUA), as evidenced by the much smaller change in C compared to SOA from non-aromatic precursors. The aromatic compounds are known to largely retain their carbon number during photolysis. For example, in the direct aqueous photolysis of 2-nitrophenol,<sup>184</sup> the major photoproducts catechol, nitrohydroquinone, 3-nitrocatechol, and 2-nitrosophenol retain the aromatic ring. It has also been previously shown that nitro-compounds photodegrade fairly slowly in aqueous solutions.<sup>185</sup> In an oxygen-depleted

environment, aromatic nitrocompounds can undergo rapid one-electron photochemical reduction. However in the presence of oxygen (under the experimental conditions of this work), this reaction is completely quenched. The photostability of these compounds is attributed to the charge-transfer character of their triplet states. Consequently, the quantum yield of direct photolysis of these compounds in water is quite low ( $\phi \sim 10^{-5}$ ).<sup>184-186</sup>

### **3.5. Conclusion**

We examined the effect of UV irradiation on the high-resolution mass spectra of water/methanol solutions of several representative types of SOA produced from biogenic and anthropogenic precursors by OH/NO<sub>x</sub> or O<sub>3</sub> oxidation. A comparison of the mass spectra taken before and after irradiation showed that SOA compounds, especially the oligomeric ones, photodegrade in solution on atmospherically relevant time scales. Peroxides, carbonyls, organonitrates, and nitroaromatic compounds likely contribute to photodegradation. The extent of the photodegradation is not correlated with the absorption coefficient; the SOA prepared from aromatic precursors appear to be more resilient to photodegradation despite being more absorbing than SOA prepared from monoterpenes. The irradiation tends to reduce the average size (carbon number) of SOA compounds. However, the average atomic ratios O/C and H/C do not change significantly suggesting that this type of photochemical aging would be missed by methods relying on measurements of the average composition instead of detailed molecular characterization. These findings have important implications for understanding the aging chemistry of atmospheric aerosols during their cloud processing cycles.

We also compared high-resolution mass spectra of unphotolyzed SOA in an effort to gauge the extent of similarity between the mass spectra. Many major peaks found in the mass spectra are not specific to their VOC precursors because they are observed in mass spectra of different types of SOA. However, a number of smaller unique peaks are also detected in the mass

spectra. Our qualitative comparison suggests that it should be possible to attribute different types of SOA to a specific VOC precursor and/or specific set of oxidation conditions based on the occurrence of sets of unique peaks in the high-resolution mass spectra. This study is a step towards building a reference library of high-resolution mass spectra for laboratory-generated SOA to aid in the assignments of field data collected by the same method. The future efforts should focus on principal component analysis of large libraries of high-resolution mass spectra collected by different groups.

**Chapter 4: Aqueous Photochemistry of Secondary Organic Aerosol of  $\alpha$ -  
Pinene and  $\alpha$ -Humulene Oxidized with Ozone, Hydroxyl Radical, and Nitrate  
Radical**

## 4.1. Abstract

Secondary organic aerosol (SOA) formation from biogenic volatile organic compounds (BVOCs) occurs via O<sub>3</sub>-initiated and OH-initiated reactions during the day and reactions with NO<sub>3</sub> during the night. We explored the effect of these three oxidation conditions on the molecular composition and aqueous photochemistry of model SOA prepared from two common BVOC. A typical monoterpene ( $\alpha$ -pinene) and sesquiterpene ( $\alpha$ -humulene) were used to form SOA in a smog chamber via: BVOC + O<sub>3</sub>, BVOC + NO<sub>3</sub>, and BVOC + OH + NO<sub>x</sub> chemistry. The resulting SOA was collected, extracted in water, and photolyzed in an aqueous solution in order to model the photochemical cloud-processing of SOA. The extent of change in the molecular level composition of SOA over 4 hours of photolysis (roughly equivalent to 64 hours of photolysis under ambient conditions) was assessed with high-resolution electrospray ionization mass spectrometry. The analysis revealed significant differences in the molecular composition between monoterpene and sesquiterpene SOA formed by the different oxidation pathways. The composition further evolved during photolysis, most notably in the depletion of nitrogen-containing compounds. Hydrolysis of nitrogen-containing compounds also occurred, but it was considerably slower than photolysis. This study highlights the potential importance of aqueous photochemistry in the aging of biogenic SOA.

## 4.2. Introduction

Secondary organic aerosol (SOA) produced by the gas-phase and aqueous-phase oxidation of biogenic volatile organic compounds (BVOCs) have both health and climate relevance.<sup>17</sup> Once in the atmosphere, SOA is known to undergo chemical aging processes from reactions with sunlight and atmospheric oxidants.<sup>47,48</sup> The mechanisms of chemical aging and the role of aging processes in determining climate and health relevant properties of SOA, such as distribution of volatilities of the SOA compounds, remain poorly explored. Part of the challenge is the high molecular complexity of SOA and the resulting complexity of the aging processes.<sup>129</sup>

Aqueous processing of atmospheric organic compounds, which may include reactions with aqueous oxidants and aqueous photolysis, is now recognized as an important mechanism of chemical aging of SOA.<sup>8,9</sup> The SOA particles produced from BVOC often get taken up by cloud and fog droplets, making the SOA compounds accessible to aqueous photochemical processes. We previously showed that exposure of dissolved SOA produced from a number of VOC precursors to actinic radiation leads to significant changes in the molecular composition of SOA.<sup>95,96,100</sup> The effect of photolysis was greater for SOA prepared by ozonolysis of VOC in darkness compared to that for SOA prepared by OH + NO<sub>x</sub> photooxidation of VOC.<sup>100</sup> This is a predictable result as the most photolabile compounds should be photolyzed already during the photooxidation in the smog chamber. Formation of SOA in the BVOC+NO<sub>3</sub> reactions is another example of a process that occurs in darkness. Our hypothesis is that this type of SOA should contain a larger fraction of photolabile molecules relative to the SOA prepared from the same VOC under OH + NO<sub>x</sub> photooxidation conditions. If this hypothesis is correct, the SOA produced by night-time chemistry would quickly change its composition after sunrise. The main goal of this chapter is to test this hypothesis.

Formation of SOA from monoterpenes, such as  $\alpha$ -pinene, has been extensively documented, especially for the OH and O<sub>3</sub> initiated oxidation pathways.<sup>187-193</sup> Several studies have examined the oxidation of monoterpenes by the nitrate radical (NO<sub>3</sub>).<sup>66,67,187,190,194-203</sup> The NO<sub>3</sub>-driven oxidation mechanism appears to be a major sink for BVOC and major source for SOA at night in regions characterized by elevated NO<sub>x</sub> (NO + NO<sub>2</sub>) and O<sub>3</sub> levels.<sup>187,204</sup>

Sesquiterpenes, such as  $\alpha$ -humulene, are less abundant in ambient air than monoterpenes.<sup>31</sup> However, their higher molecular weights make them more efficient SOA precursors compared to the monoterpenes in terms of the SOA mass yields.<sup>32,199</sup> In addition, sesquiterpenes can have up to four double bonds, making them reactive towards ozone and OH.<sup>33-35</sup> There have been limited studies on the NO<sub>3</sub> oxidation of sesquiterpenes. Canosa-Mas et al.<sup>200</sup> and Shu and Atkinson<sup>34</sup> measured the rate constants for the reactions between selected sesquiterpenes and NO<sub>3</sub> radical. Fry et al.<sup>197</sup> investigated the NO<sub>3</sub> oxidation of  $\beta$ -caryophyllene, observing high SOA yields with a low organonitrate yield in the condensed phase. Jaoui et al. found efficient formation of SOA in reactions of several sesquiterpenes with NO<sub>3</sub>.<sup>199</sup>

While numerous studies on each oxidation pathway (OH, O<sub>3</sub>, or NO<sub>3</sub>) have been done, only one study has attempted to systematically compare all three oxidations conditions for the same VOC precursor.<sup>199</sup> The authors relied on gas chromatography-mass spectrometry to analyze SOA samples, so many high-molecular-weight compounds could not be detected. The first goal of this work is to systematically compare the SOA formed in an environmental chamber from a model monoterpene ( $\alpha$ -pinene) and a model sesquiterpene ( $\alpha$ -humulene) under three different oxidation conditions. By using high-resolution electrospray ionization mass spectrometry (HR-ESI-MS), we can detect a much broader array of SOA compounds than previously possible and investigate the effect of the oxidation conditions on the molecular distribution of the SOA

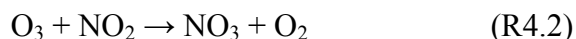
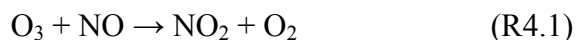


products. The second goal of this work is to examine the effect of photolysis on the molecular composition of SOA produced by NO<sub>3</sub> oxidation. Our results suggest facile photolysis of dissolved SOA compounds, especially the ones containing nitrogen.

## 4.3. Experimental

### 4.3.1. Secondary Organic Aerosol Generation

SOA was prepared in a similar manner as previously described in Section 1.3.1 for the O<sub>3</sub> and photooxidation experiments in the chamber.<sup>100,136</sup> Briefly, in a 5 m<sup>3</sup> chamber, approximately 650 ppb of ozone was added for ozonolysis experiments, while approximately 300 ppb of nitric oxide and 2 ppm of hydrogen peroxide were added for photooxidation experiments. H<sub>2</sub>O<sub>2</sub>, added to the chamber by evaporation of its 30 v/v% aqueous solution with a stream of zero air, was used to generate the hydroxyl radical. Initial mixing ratios of  $\alpha$ -pinene (APIN) and  $\alpha$ -humulene (HUM) were 500 ppb for all experiments, except for the APIN/NO<sub>3</sub> experiment, in which the concentration of APIN was 1 ppm. For OH + NO<sub>x</sub> experiments, UV-B lamps (FS40T12/UVB, Solarc Systems Inc.) with emission centered at 310 nm, were turned on and photooxidation time was 2 hours for  $\alpha$ -pinene experiments and 1 hour for  $\alpha$ -humulene experiments. To simulate the nighttime NO<sub>3</sub> radical chemistry, excess O<sub>3</sub> was first added to 300 ppb NO. The O<sub>3</sub> concentration was at least twice the concentration of NO that was introduced to ensure the following reactions:



After that, either  $\alpha$ -pinene or  $\alpha$ -humulene was added to the chamber. All experiments were performed under dry conditions at 21-25 °C and in the absence of seed particles. All chemicals mentioned above were purchased from Aldrich and used without any further purification.

SOA particles formed in the chamber were monitored by a TSI model 3936 scanning mobility particle sizer (SMPS), O<sub>3</sub> was monitored using a Thermo Scientific model 49i ozone analyzer, and a Thermo Scientific model 42i-Y NO<sub>y</sub> analyzer recorded NO/NO<sub>y</sub> data. The particles were collected through an activated carbon denuder at 17 SLM onto poly(tetrafluoroethylene) (PTFE) filters (Millipore 0.2  $\mu$ m pore size). We sampled for 3-4 hours in order to have a sufficient amount of SOA material for both photochemical and control experiments (Table 4.1). The filters were vacuum-sealed and immediately frozen at -20 °C in anticipation of offline aqueous photolysis experiments and mass spectrometry analysis.

**Table 4.1.** Experimental conditions for the SOA samples prepared from  $\alpha$ -pinene (APIN) and  $\alpha$ -humulene (HUM)

VOC Precursor	Oxidant	Initial VOC (ppb)	Initial O <sub>3</sub> (ppb)	Initial NO (ppb)	Reaction time (h)	Amount created in chamber (mg/m <sup>3</sup> )	Collection time (h)	Amount collected (mg)
APIN	O <sub>3</sub>	500	640	<5	1	1.5	3	1.8
APIN	OH/NO <sub>x</sub>	500	<5	300	2	0.18	3	0.24
APIN	NO <sub>3</sub>	1000	720	300	1	1.2	3	2.7
HUM	O <sub>3</sub>	500	660	<5	1.5	1.2	3	1.3
HUM	OH/NO <sub>x</sub>	500	<5	300	1	0.87	4	1.1
HUM	NO <sub>3</sub>	500	600	300	1	1.8	3	4.1

#### 4.3.2. High-Resolution Electrospray Ionization Mass Spectrometry (HR-ESI-MS) of Aqueous Photolysis and Control Samples

Filter SOA samples were thawed and extracted in 6 mL of water (Fluka, HPLC grade) where 3 mL of the sample was used for photolysis experiments and 3 mL was used as a dark control. This resulted in solutions containing 0.04-0.7 g/L of the dissolved SOA material. The solutions were used as soon as they were prepared. For photolysis experiments, the samples were photolyzed by a Xenon UV lamp (Newport model 66905) with a U-330 bandpass filter (Edmund optics #46-438) to reduce the visible and IR radiation. The spectrum of the resulting radiation was recorded using a portable UV-Vis spectrometer (Ocean Optics, USB4000) with most of the radiation falling in the 280-400 nm range. The sample was photolyzed from the top in a 1 cm uncapped quartz cuvette, where it was exposed to lab air during photolysis and therefore contained dissolved oxygen. An azoxybenzene actinometer was used under the same experimental conditions to determine the flux of the lamp as described by Lignell et al.<sup>114</sup> Based on the actinometry measurement, we estimate that 1 h of photolysis with our lamp was equivalent to 16 h of photolysis by the overhead sun. The control samples remained in water for the same duration of time but were not exposed to radiation.

Small aliquots (~300  $\mu$ L) were withdrawn from the sample and control cuvettes once an hour and analyzed by high-resolution electrospray ionization mass spectrometry (HR-ESI-MS) in a direct infusion mode. Immediately before the analysis, the extracted aliquot was mixed with acetonitrile in a 1:1 ratio in order to provide a more stable electrospray ionization process. A high-resolution LTQ-Orbitrap mass spectrometer (Thermo Corp.) equipped with a modified ESI source was used to analyze samples before and after photolysis.<sup>81,82,95,96,100,134-136</sup> Mass spectra of the solvent (water + acetonitrile) were also collected in order to subtract from the sample mass

spectra during data analysis. Mass spectra were acquired in the positive ion mode for all samples with a resolving power of  $10^5$  at  $m/z$  400.

The data analysis for the mass spectra was performed similarly to our previous work.<sup>100,129</sup> Decon2LS (<http://omiic.pnl.gov/software/decontools-decon2ls>) was used to generate a list of peak positions and intensities for each spectrum. The resulting peak lists for all the files in the same experimental batch (0, 1, 2, 3, and 4 hours of photolysis, 0, 1, 2, 3, and 4 hours of dark hydrolysis, and solvent blank) were clustered together. The clustered peaks were first assigned with a  $m/z$  tolerance of  $\pm 0.001$  to molecular formulas  $C_cH_hO_oN_nNa_x^+$  (small letters c,h,o,n refer to the number of corresponding atoms in the ion; the number of Na atoms, x, is restricted to 0 or 1). We limited n to 3, and allowed for the presence of N atoms in the APIN/O<sub>3</sub> and HUM/O<sub>3</sub> assignments to see whether any nitrogen-containing impurities affected our measurements. Constraints were imposed on the elemental ratios ( $0.0 < O/C < 1.3$ ,  $0.7 < H/C < 2.0$ ) to eliminate unphysical assignments.<sup>205</sup> Peaks that corresponded to molecules containing <sup>13</sup>C atoms or obvious impurities with anomalous mass defects were excluded from further analysis. The initial set of the initially assigned peaks was used to refine the calibration of the  $m/z$  axis, and the mass spectra were then reassigned with a lower  $m/z$  tolerance of  $\pm 0.00075$ . The remaining peaks that could not be assigned within these constraints and peaks with ambiguous assignments were assigned manually with help of a molecular formula calculator (<http://magnet.fsu.edu/~midas/>). Majority of the observed peaks corresponded to sodiated molecules ( $C_cH_hO_oN_nNa^+$ ); protonated molecules ( $C_cH_hO_oN_nH^+$ ) generally had small abundances. For the remainder of this paper, formulas correspond to the neutral species,  $C_cH_hO_oN_n$ , obtained by removing  $Na^+$  or  $H^+$  from the observed ion formulas.

## 4.4. Results and Discussion

### 4.4.1. Composition of SOA before photolysis

The main purpose of this section is to compare the yields and detailed molecular composition of SOA generated from the three different oxidation conditions studied (ozonolysis, OH/NO<sub>x</sub> photooxidation, NO<sub>3</sub> oxidation). Table 4.1 provides a list of the SOA samples produced for this work. Particles were observed for all experiments, although the SOA yields varied between the different samples, as judged by the peak SOA concentration and the amount of the collected SOA. The OH+NO<sub>x</sub> photooxidation resulted in the lowest relative SOA yields, whereas the NO<sub>3</sub> oxidation produced the most SOA. This is qualitatively consistent with previous reports that found the average SOA yields for the same VOC precursor to be the highest for the NO<sub>3</sub> reaction.<sup>199</sup> Despite the expected higher SOA yields from sesquiterpenes, the observed yields of APIN and HUM SOA were comparable.

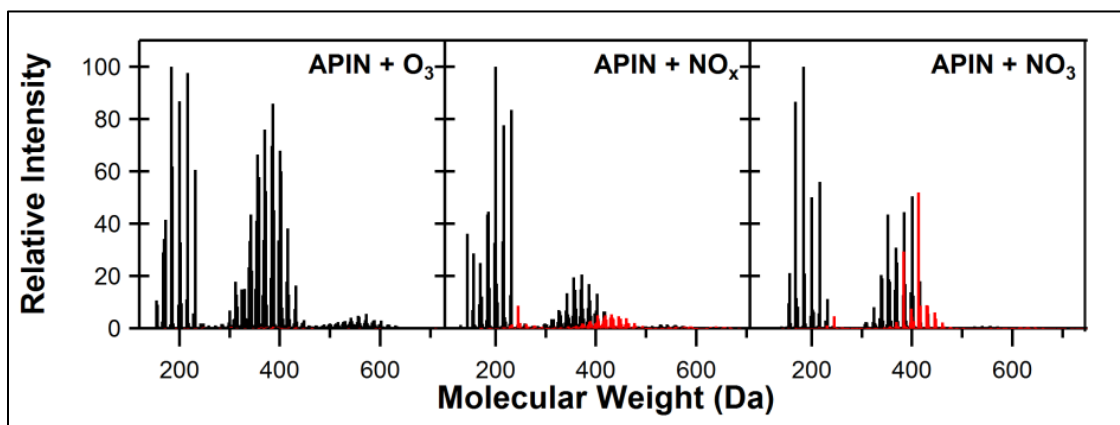
The reaction of  $\alpha$ -pinene with NO<sub>3</sub> was recently reported to produce unexpectedly low SOA yields compared to reactions of other monoterpenes with NO<sub>3</sub>.<sup>196,197</sup> Furthermore, ozonolysis was found to be much more efficient in nucleating new particles from  $\alpha$ -pinene and  $\beta$ -pinene than reaction with NO<sub>3</sub> or OH.<sup>194</sup> We were able to form particles for the APIN/NO<sub>3</sub> system using high concentrations of  $\alpha$ -pinene in our system (1 ppm), in agreement with several previous studies.<sup>68,194,195</sup> It is not clear why the APIN/NO<sub>3</sub> SOA formation should be restricted to higher concentrations because the compounds should be present in ambient particles based on equilibrium partitioning,<sup>206</sup> but they could end up being physically or chemically trapped in the particles due to kinetic limitations,<sup>207</sup> or be enhanced because of the high concentrations used in SOA preparation.

Figure 4.1 shows the high-resolution mass spectra for  $\alpha$ -pinene SOA from each oxidation condition. APIN/O<sub>3</sub> mass spectra show similarities to previous publications of monoterpene/O<sub>3</sub>

SOA in the clustering of products.<sup>100,165,208–211</sup> Clearly visible in the mass spectra are the peaks in the monomeric range (<300 Da), dimeric range (300-500 Da), and trimeric range (500-700 Da), corresponding to products containing, one, two, or three oxygenated  $\alpha$ -pinene units, respectively. The major peaks in the mass spectrum (Table 4.2) correspond to well-established products of  $\alpha$ -pinene oxidation. The famous "358 dimer"<sup>212–214</sup> corresponding to  $C_{17}H_{26}O_8$  contributed to 50% relative intensity in the sample; it was much smaller in the APIN/NO<sub>x</sub> and APIN/NO<sub>3</sub> samples. We allowed for the presence of nitrogen in the assignments but observed very few nitrogen-containing organic compounds (NOC) (Figure 4.1) confirming that nitrogen-containing impurities were absent from the chamber.

The high-resolution mass spectrum of APIN/NO<sub>x</sub> SOA is also qualitatively similar to the one we reported previously.<sup>100</sup> The key difference is intentional absence of methanol in the SOA extracting solution in this work, which converted a large number of SOA compounds in hemiacetals and esters in our previous work.<sup>100</sup> The major peaks in the spectrum (Table 4.2) retain the C<sub>10</sub> skeleton of  $\alpha$ -pinene, as expected. The fraction of oligomers is substantially smaller in the APIN/NO<sub>x</sub> SOA compared to the APIN/O<sub>3</sub> SOA. The fraction of peaks corresponding to NOC is predictably higher for APIN/NO<sub>x</sub> SOA. The NOC peaks also show clear clustering into monomers, dimers, and trimers, with the average mass each NOC cluster shifted by about 50 Da to higher molecular weight compared to the nitrogen-free peaks. This could be interpreted as a result of adding an –ONO<sub>2</sub> group instead of an –OH group to the molecule. Indeed, most of the NOC in APIN/NO<sub>x</sub> can be expected to be in the form of organonitrates. Table 4.3 shows that the fraction of peaks containing 0, 1, 2, and 3 nitrogen atoms shifts to higher N-atom values from ozonolysis to OH/NO<sub>x</sub> photooxidation to NO<sub>3</sub> oxidation.

The high-resolution mass spectrum of APIN/NO<sub>3</sub> SOA has not been reported before. The most striking difference between the APIN/NO<sub>3</sub> SOA and APIN/NO<sub>x</sub> SOA is a much higher fraction of NOC in the former. This is to be expected because NO<sub>3</sub> can react with  $\alpha$ -pinene directly by addition to the double bond resulting in NOC already at the first generation of products. It is interesting that NOC clearly prevail in the dimeric products and absent from monomeric products of  $\alpha$ -pinene oxidation. For example, one of the major peaks in the spectrum is a dimer C<sub>20</sub>H<sub>31</sub>O<sub>8</sub>N (Table 4.2). The NOC monomeric species could be too volatile to partition in to the aerosol (which could explain why little SOA is formed at lower  $\alpha$ -pinene concentrations).<sup>196,197</sup> But they could also be suppressed by the ESI source, which is not as sensitive to organonitrates as it is, for example, to carboxylic acids.



**Figure 4.1.** Mass spectra for the  $\alpha$ -pinene (APIN) SOA samples formed from three oxidation conditions (ozonolysis, OH/NO<sub>x</sub> photooxidation, and reaction with NO<sub>3</sub>). The x-axis corresponds to the molecular weight of the neutral SOA compounds. Peaks in red denote nitrogen-containing organic compounds (NOC).

**Table 4.2.** Major peaks for  $\alpha$ -pinene SOA from each set of oxidation conditions.

	<b>Chemical Formula (Molecular Weight)</b>	<b>Product</b>	<b>Relative Intensity (%)</b>
<b>APIN/O<sub>3</sub></b>	C <sub>10</sub> H <sub>16</sub> O <sub>3</sub> (184)	Pinonic Acid	100
	C <sub>10</sub> H <sub>16</sub> O <sub>5</sub> (216)	Reported by Kahnt et al., <sup>162</sup> Winterhalter et al., <sup>161</sup> Iinuma et al., <sup>215</sup> Venkatachari and Hopke, <sup>216</sup> Camredon et al., <sup>217</sup> Putman et al. <sup>218</sup>	98
	C <sub>10</sub> H <sub>16</sub> O <sub>4</sub> (200)	10-hydroxypinonic acid (Glasius et al.) <sup>219</sup>	87
	C <sub>19</sub> H <sub>30</sub> O <sub>8</sub> (386)		86
	C <sub>19</sub> H <sub>30</sub> O <sub>7</sub> (370)		76
	C <sub>17</sub> H <sub>26</sub> O <sub>8</sub> (358)	“358 Dimer” <sup>212-214</sup>	50
<b>APIN/NO<sub>x</sub></b>	C <sub>10</sub> H <sub>16</sub> O <sub>4</sub> (200)	10-hydroxypinonic acid (Glasius et al.) <sup>219</sup>	100
	C <sub>10</sub> H <sub>16</sub> O <sub>6</sub> (232)	Diaterpenylic Acid Acetate <sup>220</sup>	83
	C <sub>10</sub> H <sub>16</sub> O <sub>5</sub> (216)	Reported by Kahnt et al. <sup>162</sup>	78
	C <sub>9</sub> H <sub>14</sub> O <sub>4</sub> (186)	Pinic Acid	45
	C <sub>10</sub> H <sub>16</sub> O <sub>3</sub> (184)	Pinonic Acid	44
	C <sub>17</sub> H <sub>26</sub> O <sub>8</sub> (358)	“358 Dimer” <sup>212-214</sup>	7
<b>APIN/NO<sub>3</sub></b>	C <sub>10</sub> H <sub>16</sub> O <sub>3</sub> (184)	Pinonic Acid	100



	C <sub>10</sub> H <sub>16</sub> O <sub>2</sub> (168)	Pinonaldehyde	87
	C <sub>10</sub> H <sub>16</sub> O <sub>5</sub> (216)	Reported by Kahnt et al. <sup>162</sup>	56
	C <sub>20</sub> H <sub>31</sub> O <sub>8</sub> N (413)		52
	C <sub>20</sub> H <sub>32</sub> O <sub>8</sub> (400)		51
	C <sub>17</sub> H <sub>26</sub> O <sub>8</sub> (358)	“358 Dimer” <sup>212-214</sup>	1

**Table 4.3.** Percentage of 0N (C<sub>x</sub>H<sub>y</sub>O<sub>z</sub>), 1N (C<sub>x</sub>H<sub>y</sub>O<sub>z</sub>N), 2N (C<sub>x</sub>H<sub>y</sub>O<sub>z</sub>N<sub>2</sub>), and 3N (C<sub>x</sub>H<sub>y</sub>O<sub>z</sub>N<sub>3</sub>) compounds for APIN SOA samples.

	APIN/O <sub>3</sub>	APIN/NO <sub>x</sub>	APIN/NO <sub>3</sub>
0N	95%	64%	56%
1N	5%	36%	27%
2N	-	-	12%
3N	-	-	5%

Figure 4.2 shows the mass spectra of HUM SOA resulting from each set of oxidation conditions. Similarly to the APIN SOA, the importance of NOC in the SOA compounds increases in the series: HUM/O<sub>3</sub> (where NOC are present at the small level of impurities), HUM/NO<sub>x</sub>, HUM/NO<sub>3</sub>. The majority of the compounds in the mass spectrum are monomers retaining the C<sub>15</sub> skeleton of  $\alpha$ -humulene. Major peaks for all three sets of oxidation conditions are dominated by C<sub>15</sub>H<sub>24</sub>O<sub>x</sub> compounds with x ranging from 4 to 8. Of these compounds, only C<sub>15</sub>H<sub>24</sub>O<sub>4</sub>, attributed to  $\alpha$ -humuladionic acid, has been previously identified.<sup>221,222</sup> However, in the HUM/NO<sub>3</sub> case, a number of unexpected compounds are also detected, some of which have high relative abundance in the mass spectrum. For example, the list of major peaks (Table 4.4)

includes  $C_{11}H_{14}O_4N_2$  and  $C_{17}H_{21}O_6N_3$ , compounds that cannot be organonitrates based on their formulas (each  $-ONO_2$  group would contribute 3 oxygen atoms for each N atom in the molecule). Because of the unusual formulas, we invested a lot of effort into re-checking the mass calibration and verifying that these peaks do not correspond to impurities, but found no alternative assignments for these peaks. These compounds could potentially result from an attachment of one  $-ONO_2$  group and one  $-NO$  group across the double bond, or from an attachment of two  $-NO_2$  groups. There is no evidence for these compounds in prior literature on  $\alpha$ -humulene (a SciFinder search by these formulas constrained by "humulene" yielded zero hits). We presently do not have a good explanation for their occurrence in the ESI mass spectra of HUM/ $NO_3$  SOA.

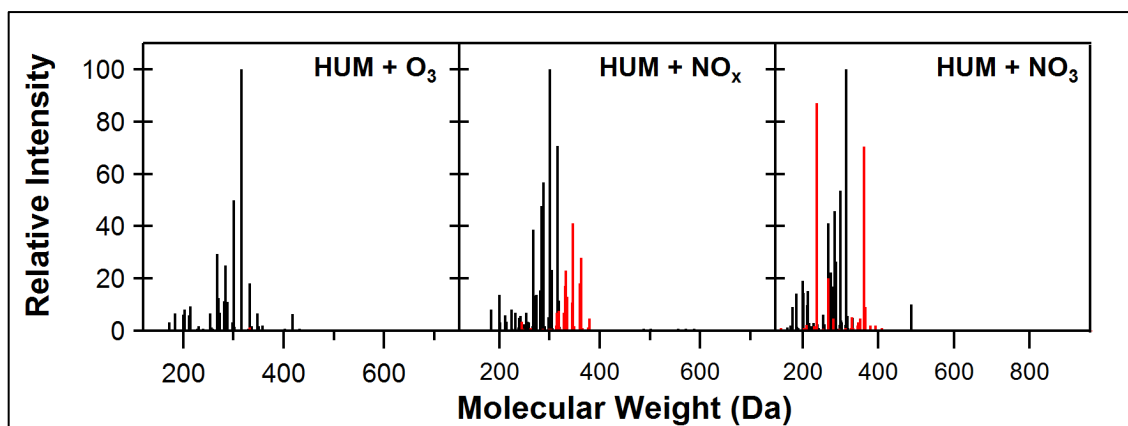


**Figure 4.2.** Mass spectra for the  $\alpha$ -humulene SOA samples formed from three oxidation conditions (ozonolysis,  $NO_x$  photooxidation, and reaction with  $NO_3$ ) before photolysis. The x-axis corresponds to the molecular weight of the neutral SOA compounds. Peaks in red denote NOC.

**Table 4.4.** Major peaks for Humulene SOA in each oxidation condition.

	<b>Chemical Formula</b>	<b>Relative Intensity (%)</b>
<b>HUM/O<sub>3</sub></b>	C <sub>15</sub> H <sub>24</sub> O <sub>7</sub>	100
	C <sub>15</sub> H <sub>24</sub> O <sub>6</sub>	50
	C <sub>15</sub> H <sub>24</sub> O <sub>4</sub>	31
	C <sub>15</sub> H <sub>24</sub> O <sub>5</sub>	26
	C <sub>15</sub> H <sub>24</sub> O <sub>8</sub>	19
<b>HUM/NO<sub>x</sub></b>	C <sub>15</sub> H <sub>24</sub> O <sub>6</sub>	100
	C <sub>15</sub> H <sub>24</sub> O <sub>7</sub>	71
	C <sub>14</sub> H <sub>24</sub> O <sub>6</sub>	57
	C <sub>15</sub> H <sub>24</sub> O <sub>5</sub>	48
	C <sub>15</sub> H <sub>24</sub> O <sub>8</sub>	41
<b>HUM/NO<sub>3</sub></b>	C <sub>15</sub> H <sub>24</sub> O <sub>7</sub>	100
	C <sub>17</sub> H <sub>21</sub> O <sub>6</sub> N <sub>3</sub>	92
	C <sub>11</sub> H <sub>14</sub> O <sub>4</sub> N <sub>2</sub>	78
	C <sub>15</sub> H <sub>24</sub> O <sub>6</sub>	49
	C <sub>15</sub> H <sub>24</sub> O <sub>5</sub>	39

**Table 4.5.** Percentage of 0N (C<sub>x</sub>H<sub>y</sub>O<sub>z</sub>), 1N (C<sub>x</sub>H<sub>y</sub>O<sub>z</sub>N), 2N (C<sub>x</sub>H<sub>y</sub>O<sub>z</sub>N<sub>2</sub>), and 3N (C<sub>x</sub>H<sub>y</sub>O<sub>z</sub>N<sub>3</sub>) compounds for HUM samples.

	HUM/O <sub>3</sub>	HUM/NO <sub>x</sub>	HUM/NO <sub>3</sub>
0N	92%	54%	63%
1N	8%	37%	19%
2N	-	6%	15%
3N	-	3%	3%

#### 4.4.2. Photolysis Induced Changes in Molecular Composition

Figure 4.3 shows the mass spectra of SOA samples during photolysis and control experiments for the 0 h and 4 h reaction time (1, 2, and 3 h mass spectra are omitted to avoid cluttering the figure). The mass spectra change significantly upon photolysis in several important

aspects. The first obvious conclusion from Figure 4.3 is that the higher molecular weight (MW) compounds are converted to lower MW compounds by photolysis. This is especially noticeable for SOA derived from  $\alpha$ -pinene: the photolysis reduced the relative intensity of the dimeric species relative to the monomeric ones and obliterates all of the trimeric species. In control samples, hydrolysis also reduced the relative intensity of the dimeric and trimeric species, however, the effect of hydrolysis was much less than that of photolysis. The effect of hydrolysis will be discussed in more detail later in this paper.

The second most obvious effect of photolysis is dramatic removal of NOC species. They were removed almost entirely for the APIN/NO<sub>x</sub> and APIN/NO<sub>3</sub> SOA. The reduction in the number of the NOC species was also obvious for the HUM/NO<sub>x</sub> and HUM/NO<sub>3</sub> SOA, although a few NOC appeared to persist. The hydrolysis in the control samples did not have the same effect; the relative amount of NOC stayed roughly the same judging from the relative peak intensity.

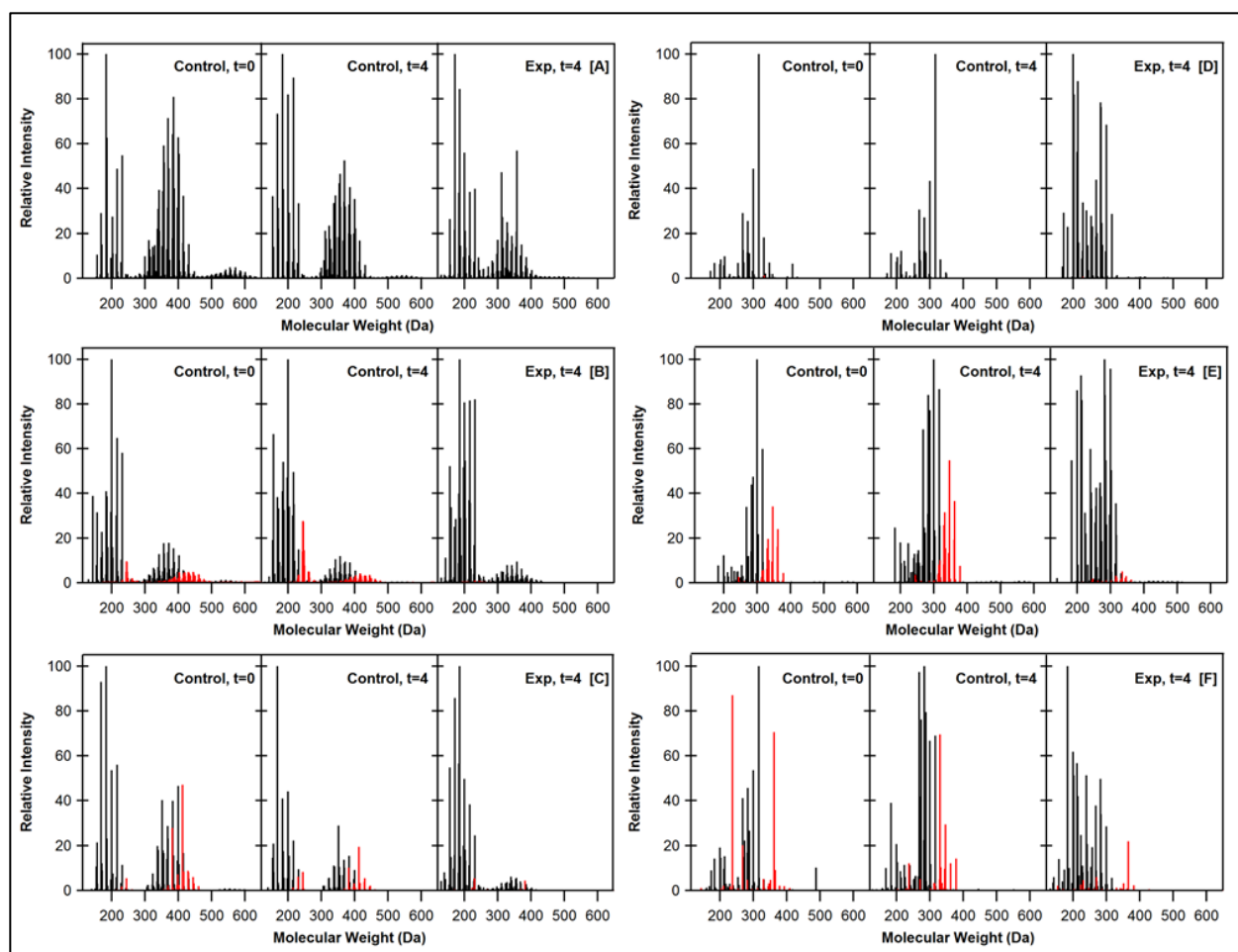


**Figure 4.3.** High-resolution mass spectra of the APIN/O<sub>3</sub> [A], APIN/NO<sub>x</sub> [B], APIN/NO<sub>3</sub> [C], HUM/O<sub>3</sub> [D], HUM/NO<sub>x</sub> [E], and HUM/NO<sub>3</sub> [F] aqueous SOA extracts at t = 0 h, the dark control after 4 hours, and the photolysis sample after 4 hours (t = 4). The X-axis corresponds to the molecular weight of the neutral compounds and the Y-axis corresponds to the intensity in the positive ion mode ESI mass spectrum. Peaks are normalized with respect to the largest peak in the sample. Peaks in red denote NOC.

Aerosol mass spectrometer (AMS) measurements of average elemental ratios (H/C, O/C, and N/C) are frequently reported in both field and lab studies.<sup>181</sup> To aid in the comparison with other experiments, we calculated the average elemental ratios, as well as the average molecular size (denoted by the number of C atoms per molecule), and average double bond equivalent (DBE) from the assigned, neutral molecular formulas. All averaged quantities were calculated with respect to peak intensities for all observed compounds as shown below:

$$\langle X \rangle = \frac{\sum I_i x_i}{\sum I_i} \quad (x = \text{c, o, h, n, DBE}) \quad (4.5)$$

$$\frac{\langle X \rangle}{\langle Y \rangle} = \frac{\sum I_i x_i}{\sum I_i y_i} \quad (x, y = \text{o, c, h, n}) \quad (4.6)$$

The results from these calculations for the control and photolysis samples are compiled in Figures 4.4 and 4.5 for APIN SOA and HUM SOA, respectively, as a function of the photolysis (or hydrolysis) time from 0 to 4 hours.

Figures 4.4 and 4.5 show a clear trend in the reduction of  $\langle C \rangle$  with photolysis, which agrees with the observation that high-MW oligomers are degraded, as reflected in the mass spectra shown in Figure 4.3. In our previous work on photolysis of SOA solutions, we also observed a reduction in the average molecular size for a broad range of SOA.<sup>95,96,100</sup> The hydrolysis in darkness also produces a reduction in  $\langle C \rangle$ , however, it is smaller than the effect of photolysis.

The  $\langle O/C \rangle$  ratio traditionally describes the degree of oxidation of a compound. For all the APIN samples, we observed an increase in  $\langle O/C \rangle$  during photolysis. This is consistent with previous aqueous photolysis studies of natural organic matter,<sup>223,224</sup> and aqueous SOA samples.<sup>95,96,100</sup>

Romonosky et al. previously reported an efficient depletion of NOC species in photolysis of a broad range of SOA prepared under high NO<sub>x</sub> conditions.<sup>100</sup> In the present study, the  $\langle N/C \rangle$  ratio for samples made in the presence of NO<sub>x</sub> and NO<sub>3</sub> also decreased dramatically with photolysis. This could be due to the photolysis of organic nitrates



with secondary processes forming stable nitrogen-free compounds from RO radicals. One potential issue with this explanation is that organic nitrates are relatively weak absorbers of near-UV radiation.<sup>225</sup> However, multifunctional compounds found in SOA are expected to be stronger absorbers and be more active in photochemistry.<sup>78</sup> NOC species appeared to be reduced in control samples as well, which is consistent with fast hydrolysis of secondary and tertiary organic nitrates.<sup>157,158,226</sup>

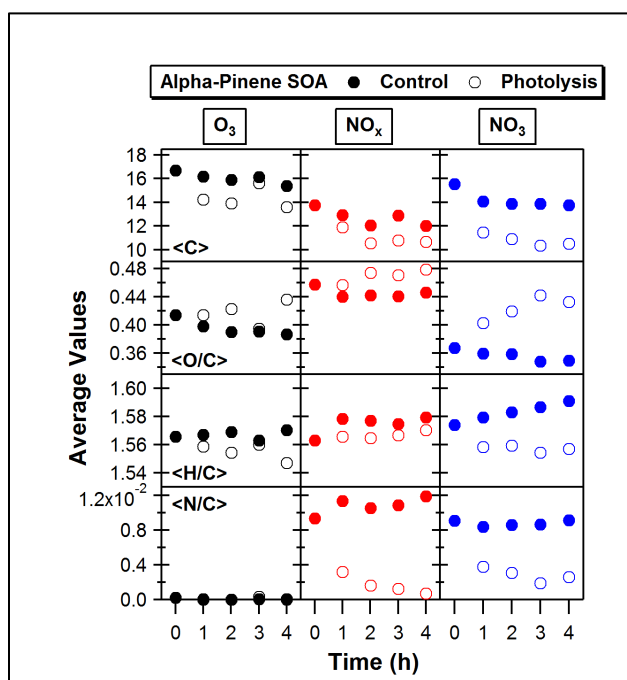


**Figure 4.4.** The time-dependent average number of carbon atoms and elemental ratios in the photolysis (open circles) and dark control samples (closed circles) for each of the  $\alpha$ -pinene oxidation conditions.

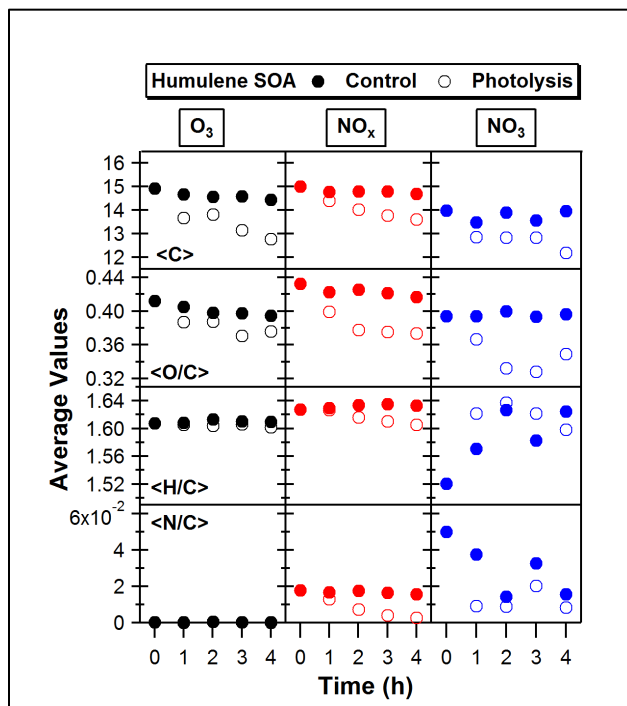


**Figure 4.5.** The time-dependent average number of carbon atoms and elemental ratios in the photolysis (open circles) and dark control samples (closed circles) for each of the  $\alpha$ -humulene oxidation conditions.

## 4.5 Conclusion

The first goal of this work was to systematically compare the SOA formed in an environmental chamber from a model monoterpene ( $\alpha$ -pinene) and a model sesquiterpene ( $\alpha$ -humulene) under three different oxidation conditions:  $O_3$ ,  $NO_x$ , and  $NO_3$ . The analysis revealed significant differences in the molecular composition between monoterpene and sesquiterpene SOA formed by the different oxidation pathways. Our APIN/ $O_3$  and APIN/ $NO_x$  mass spectra agreed with our previously published data, while the APIN/ $NO_3$  mass spectrum was reported for the first time. The most striking difference between the APIN/ $NO_3$  SOA and APIN/ $NO_x$  SOA was a much higher fraction of NOC in the former, most likely due to  $NO_3$  reacting with  $\alpha$ -pinene directly by addition to the double bond, resulting in NOC at the first generation of products. Similarly the importance of NOC in the SOA compounds increase in the series: HUM/ $O_3$  (where NOC are present at the small level of impurities), HUM/ $NO_x$ , HUM/ $NO_3$ .



The second goal of this work was to examine the effect of photolysis on the molecular composition of SOA produced by  $\text{NO}_3$  oxidation. The composition of the SOA further evolved during photolysis, most notably in the depletion of nitrogen-containing compounds. Hydrolysis of nitrogen-containing compounds also occurred, but it was considerably slower than photolysis. This study highlights the potential importance of aqueous photochemistry in the aging of biogenic SOA.

## Chapter 5: Absorption Spectra and Aqueous Photochemistry of $\beta$ - Hydroxyalkyl Nitrates

---

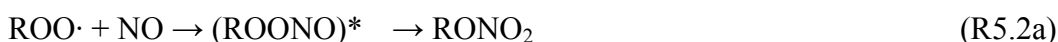
Portions of this chapter are reproduced with permission from: D.E. Romonosky, L.Q. Nguyen, D. Shemesh, T.B. Nguyen, S.A. Epstein, D.B.C. Martin, C.D. Vanderwal, R.B. Gerber, and S.A. Nizkorodov, "Absorption spectra and aqueous photochemistry of  $\beta$ -hydroxyalkyl nitrates of atmospheric interest" *Molecular Physics* 113 (2015) 2179-2190; DOI: 10.1080/00268976.2015.1017020. Copyright 2015 by **Taylor & Francis** Dorit Shemesh and R. Benny Gerber provided the theoretical data presented in Section 5.4 used in this chapter.

## 5.1. Abstract

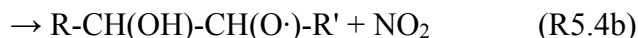
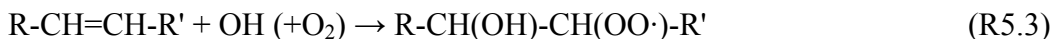
Molar extinction coefficients were measured for select alkyl nitrates and  $\beta$ -hydroxyalkyl nitrates in methanol. The presence of the  $\beta$ -hydroxyl group has a relatively minor effect on the absorption spectrum in the vicinity of the weak  $n \rightarrow \pi^*$  transition, which is responsible for photolysis of organic nitrates in the atmosphere. For both alkyl nitrates and  $\beta$ -hydroxyalkyl nitrates, there was an enhancement in the extinction coefficients in solution compared to the gas-phase values. The effect of the  $\beta$ -hydroxyl group on the spectra was modeled with molecular dynamics simulations using an OM2/GUGA-CI Hamiltonian for ethyl nitrate and  $\beta$ -hydroxyethyl nitrate. The simulation provided a qualitatively correct shape of the low energy tail of the absorption spectrum, which is important for atmospheric photochemistry. The role of direct aqueous photolysis in removal of  $\beta$ -hydroxyalkyl nitrates in cloud and fog water was modeled using a relative rate approach, and shown to be insignificant relative to gas-phase photochemical processes and aqueous OH oxidation under typical atmospheric conditions.

## 5.2 Introduction

Esters of nitric acid, better known as organic nitrates to atmospheric chemists, represent an important group of atmospheric organic compound.<sup>17</sup> Oxidation of saturated hydrocarbons in air by OH in the presence of NO<sub>x</sub> (NO + NO<sub>2</sub>) is a common pathway to unsubstituted alkyl nitrates:

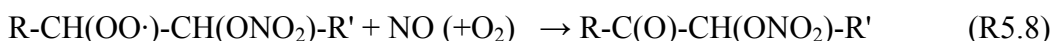
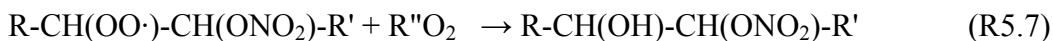
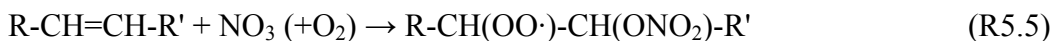


The yield of reaction (R5.2a) increases with the size of the alkyl group R and approaches ~30% for larger peroxy radicals ROO<sup>•</sup>.<sup>17</sup> Oxidation of unsaturated hydrocarbons under the same conditions commonly produces nitrates with a hydroxyl (–OH) group in the β position relative to the nitroxy (–ONO<sub>2</sub>) group.<sup>55–58</sup>



Reactions (R5.3) and (R5.4) are especially important in oxidation of biogenically emitted isoprene, monoterpenes and other unsaturated volatile organic compounds in air masses affected by urban emissions. The resulting β-hydroxyalkyl nitrates have been observed in significant concentrations in both urban and remote environments in a number of field studies.<sup>59–62</sup> Reactions of nitrate radicals with alkenes also serve as an important source of nitrates<sup>63–69</sup>

substituted by a hydroxyl, hydroperoxyl (–OOH) or carbonyl group (=O) in the  $\beta$ -position, for example through the following sequence of reactions:



Other pathways to  $\beta$ -substituted alkyl nitrates also exist; a comprehensive review of these mechanisms is beyond the scope of this dissertation.

For unsaturated nitrates, such as the ones derived from isoprene, reaction with OH serves as the most important daytime sink, while reaction with  $\text{NO}_3$  dominates at night.<sup>70</sup> For saturated nitrates, other sink mechanisms may become competitive. One of the known degradation pathways for alkyl nitrates is gas-phase photolysis by means of the weak  $n \rightarrow \pi^*$  transition.<sup>71,72</sup>



The absorption cross sections<sup>2,71–75</sup> and photolysis quantum yields<sup>76,77</sup> of gas-phase alkyl nitrates have been studied extensively making it possible to reliably predict the rate of reaction (R5.9) under all relevant atmospheric conditions. The electronic states<sup>227–231</sup> and photodissociation dynamics<sup>231–233</sup> of simple alkyl nitrates have also been investigated. Because of the low oscillator strength of the  $n \rightarrow \pi^*$  transition, the photolysis is relatively slow with typical lifetimes of days. In contrast to the simple alkyl nitrates, photochemistry of  $\beta$ -substituted nitrates is less well understood. Investigation of the neighboring group effects on photochemistry of atmospheric organic compounds is important; for example, the synergetic interaction between the carbonyl

and nitroxy groups on the neighboring carbon atoms has been shown to lead to an efficient photolysis of  $\beta$ -carbonyl nitrates that occurs at faster rates than reaction with OH.<sup>78</sup> In the case of  $\beta$ -hydroxyalkyl nitrates, absorption cross sections have been measured only for a few compounds, such as  $\beta$ -hydroxyethyl nitrate<sup>2</sup> and trans-2-hydroxycyclopentyl-1-nitrate<sup>3</sup>, and no photolysis studies have been done.

Depending on their solubility and volatility, organic nitrates can remain in the gas-phase, partition into cloud and fog droplets, or partition in aerosol particles. The presence of a hydroxyl group decreases the vapor pressure and increases the solubility of small  $\beta$ -hydroxyalkyl nitrates enough to make their wet and dry deposition a significant sink. The magnitudes of the measured Henry's solubility constants suggest that  $\beta$ -hydroxyalkyl nitrates partition into aqueous phase to a significant extent whenever cloud and fog droplets are present.<sup>79,80</sup> Larger  $\beta$ -hydroxyalkyl nitrates, such as the ones derived from oxidation of monoterpenes, may have sufficiently low vapor pressures to efficiently partition into aerosols and onto environmental surfaces, especially if they are decorated with additional functional groups. Indeed, there have been a number of observations of  $\beta$ -hydroxyalkyl nitrates in particle-phase products of oxidation of isoprene,<sup>81,82</sup> alpha-pinene,<sup>56,67,83</sup> and other terpenes.

Despite the fact that electronic excitations play a major role in the initiation of atmospheric reactions,<sup>17</sup> theoretical prediction of the accurate shapes of the absorption spectra of atmospheric compounds remains a major challenge. Significant radiation is available in the lower atmosphere only for wavelengths longer than 290 nm (photon energies below 4.3 eV) because higher energy photons are efficiently screened by stratospheric ozone. For many atmospheric molecules, the lowest electronic transition is centered deeper in the ultraviolet (UV) region, and the absorption takes place in the red tail of the spectrum, far removed from the

absorption center. Even though the absorption coefficient in the red tail of the spectrum is small, it may dominate the atmospheric photochemistry because only the near-UV photons can make it through the ozone shield. The importance of weak red tails in absorption spectra of atmospheric molecules was stressed in a study of photochemistry of methyl hydroperoxide.<sup>234</sup> This situation applies to alkyl nitrates because their  $n \rightarrow \pi^*$  transition is centered at  $\sim 260$  nm and only the tail of this transition overlaps with the tropospheric actinic wavelength region.<sup>73,227</sup> The calculation of the shape of the red tail of the spectrum requires considerable computational effort. The Franck-Condon region is greatly extended at the ambient temperatures by the internal motion of the molecule making it necessary to calculate vertical electronic transition energies and oscillator strengths at various molecules geometries. In condensed phases, the tail absorption may be affected by the shift of the electronic states due to the presence of solvent molecules. Oncak et al.,<sup>235</sup> Epstein et al.,<sup>52</sup> and Epstein et al.<sup>174</sup> provide illustrative examples of accounting for these effects in predictions of absorption spectra of atmospheric compounds. For a recent review on the applications of molecular dynamics methods to photochemical problems, the reader is referred to Gerber et al.<sup>236</sup>

The main question addressed in this dissertation is whether direct photolysis of  $\beta$ -hydroxyalkyl nitrates in aqueous phase or in organic particle phase is atmospherically relevant. With several notable exceptions, such as measurements of molar extinction coefficients of simple alkyl nitrates in hexane<sup>237</sup> and photolysis of alkyl nitrates on ice surfaces,<sup>238</sup> condensed-phase photochemistry of alkyl nitrates has not been studied enough to predict whether it can compete with gas-phase photochemistry or heterogeneous oxidation. Are solvatochromic effects significant for these types of molecules? Does the presence of the solvent affect the photolysis quantum yields? Do additional photolysis channels open up in the condensed phase? Does the  $\beta$ -

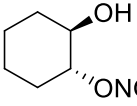
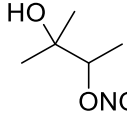
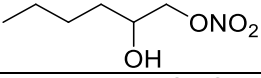
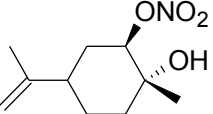
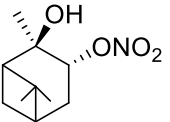
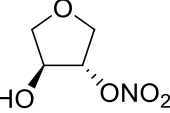
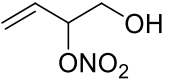
hydroxyl group play a special role in the photochemistry, e.g., by hydrogen bonding to the nitroxy group? In this study, we begin to address these important questions by examining the molar extinction coefficients of atmospherically relevant  $\beta$ -hydroxyalkyl nitrates dissolved in methanol. In addition to the experimental measurements, we explore the effect of the  $\beta$ -hydroxyl group on the shape of the  $n \rightarrow \pi^*$  band in ethyl nitrate and  $\beta$ -hydroxyethyl nitrate using on-the-fly molecular dynamics.

## 5.3. Methods

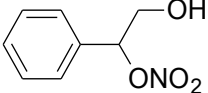
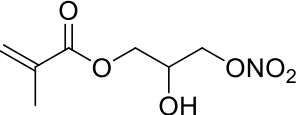
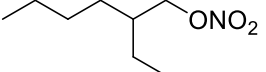
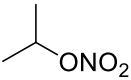
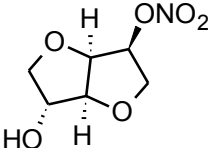
### 5.3.1. Experimental Methods

The  $\beta$ -hydroxyalkyl nitrates labeled A-I in Table 5.1 were synthesized by nucleophilic epoxide ring opening with bismuth (III) nitrate.<sup>239</sup>

**Table 5.1.** Summary of synthesized (A-I) and purchased (J-L) organic nitrates studied in this work. The first column contains letter abbreviations by which different nitrates are referred to in other tables and figures.

	Structure	Name	Notes
<b>A</b>		2-hydroxycyclohexyl nitrate	Faint yellow liquid, crystallizes
<b>B</b>		3-hydroxy-3-methylbutan-2-yl nitrate	Acquired color during storage
<b>C</b>		2-hydroxyhexyl nitrate	Faint yellow liquid
<b>D</b>		2-hydroxy-2-methyl-5-(prop-1-en-2-yl)cyclohexyl nitrate	Viscous yellow liquid, crystallizes
<b>E</b>		2-hydroxy-2,6,6-trimethylbicyclo[3.1.1]heptan-3-yl nitrate	Was not able to purify
<b>F</b>		4-hydroxytetrahydrofuran-3-yl nitrate	Viscous yellowish liquid
<b>G</b>		1-hydroxybut-3-en-2-yl nitrate	Viscous yellowish liquid



<b>H</b>		2-hydroxy-1-phenylethyl nitrate	Viscous yellowish liquid
<b>I</b>		2-hydroxy-3-(nitrooxy)propyl methacrylate	Clear, colorless "gel"; was not able to purify
<b>J</b>		2-ethylhexyl nitrate	Commercial
<b>K</b>		isopropyl nitrate	Commercial
<b>L</b>		Isosorbide mononitrate	Commercial

The procedures included addition of the nucleophile at room temperature under inert atmosphere to a solution of the selected, reagent-grade epoxide and acetonitrile. The reaction was quenched with deionized water and the resulting  $\beta$ -hydroxyalkyl nitrates were collected by extraction with ethyl acetate. All nitrates were purified using liquid chromatography with a solvent system comprised of ethyl acetate and hexanes. Solvents were removed using a rotary evaporator. Proton NMR was employed to verify the structure and purity of the resulting product. The compound obtained in the highest yield and purity was 2-hydroxycyclohexyl nitrate (A), which was obtained in crystalline form. The rest of the compounds were obtained as viscous liquids, and judging by their yellowish color, may have contained impurities from the synthesis (estimated to be under 5% based on NMR spectra). Each sample was tested for presence of nitrate and other functional groups using a Mattson GL-5030 FT-IR spectrometer. A sample FTIR spectrum of 4-hydroxytetrahydrofuran-3-yl nitrate (F) is shown in Figure 5.1.

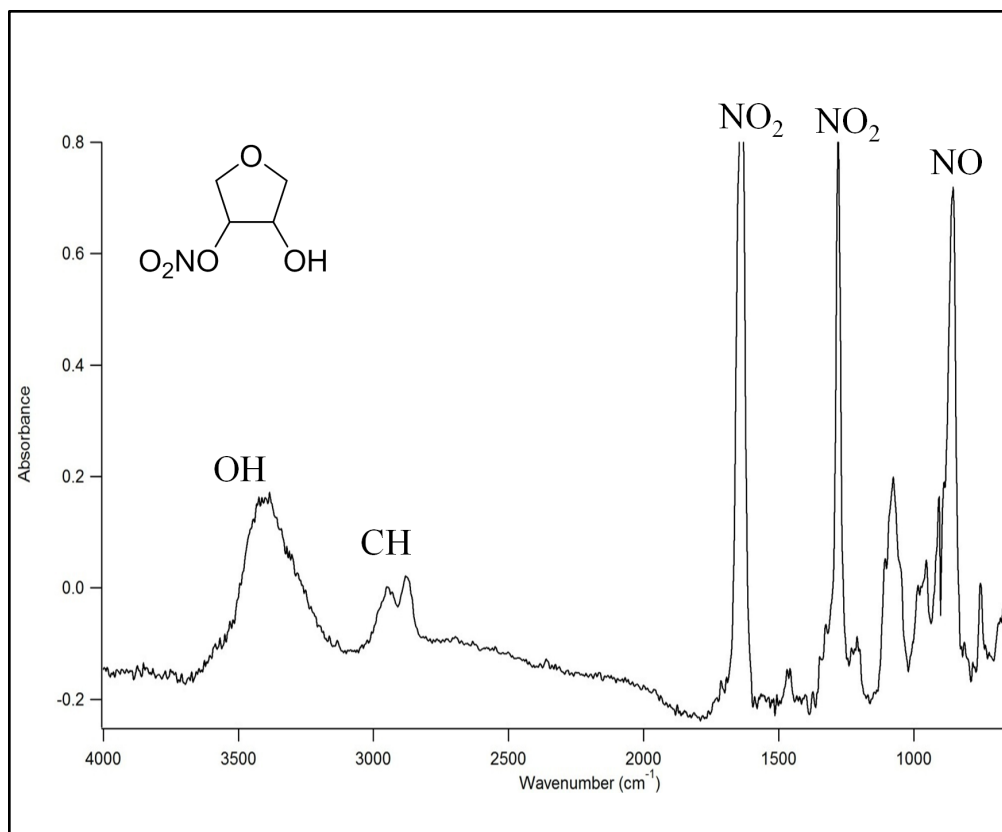


**Figure 5.1.** Sample FTIR spectrum of compound F (4-hydroxytetrahydrofuran-3-yl nitrate) with bands attributable to the  $-\text{ONO}_2$  and  $-\text{OH}$  groups labeled.

The spectra were consistent with spectra of alkyl nitrates reported by Bruns et al.,<sup>240</sup> specifically the bands attributable to nitrates were observed at 1630, 1280, and 860  $\text{cm}^{-1}$  for all compounds. For compound F, the OH stretching band associated with the hydroxyl group was also present in Fig. 5.1. Nitrates were stored in a refrigerator at 5 °C. However, some of the compounds, e.g., 3-hydroxy-3-methylbutan-2-yl nitrate (B), were unstable under standard storage conditions. Therefore, we performed all the measurements shortly after the preparation. Nitrates labeled J, K, and L in Table 5.1 were purchased and used without further purification.

The UV absorption spectra were taken by a Shimadzu UV-2450 spectrometer with an accuracy of  $\pm 0.003$  absorbance units in the base-10 absorbance range of 0 - 1. Each sample was scanned in the 200 – 700 nm wavelength range with a rate of 210 nm/min. Each experimental

run involved taking spectra for several volume dilutions of the nitrate in methanol (the only exception to that was compound L that was studied in multiple solvents). To improve baseline stability, the spectra were baseline-corrected by setting the average measured absorbance in the 500-700 nm range to zero.

### 5.3.2. Theoretical methods

The structures were built in Avogadro,<sup>241</sup> a program that includes a minimization procedure with MMFF94 force field and a conformer search option. The identified conformers were further optimized at MP2 level using the resolution of identity (RI) approximation.<sup>242</sup> The cc-pVDZ basis set was employed.<sup>243</sup> Vertical excitation energies were computed with the CC2 method<sup>244,245</sup> at the MP2 optimized structures. For some conformers, the vertical excitation energies were also computed with the orthogonalization-corrected OM2 Hamiltonian<sup>246</sup> and the GUGA-CI approach<sup>247</sup> using the MNDO program. In GUGA-CI calculations, three reference configurations were used (closed shell, single and double HOMO–LUMO excitations) and the active space was chosen to include the highest five occupied orbitals and the lowest five unoccupied orbitals with 10 electrons in 10 orbitals; in other words, a complete active space (CAS) of (10, 10) was employed. The absorption spectrum was obtained by running molecular dynamics with the OM2 Hamiltonian using a time step of 0.1 fs at 300 K for 10 ps. From each trajectory, 10,000 structures were extracted (one structure every 1 fs of the simulation), and their vertical excitation energies and oscillator strengths were calculated with the OM2/GUGA-CI Hamiltonian. For each excitation energy, the vertical transitions were convoluted with a Lorentzian line shape with width of 0.001 eV, and all of the resulting Lorentzians were added to yield the excitation spectrum. Similar OM2/MRCI-based approaches were recently used for

calculation of the absorption spectrum of methyl hydroperoxide in frozen water clusters<sup>174</sup> and for simulations of dynamics of atmospheric photochemical reactions.<sup>114,248–250</sup>

## 5.4. Results and discussion

### 5.4.1. Absorption Spectra

Figure 5.2 shows an example of determination of molar extinction coefficients for 2-hydroxycyclohexyl nitrate (A).

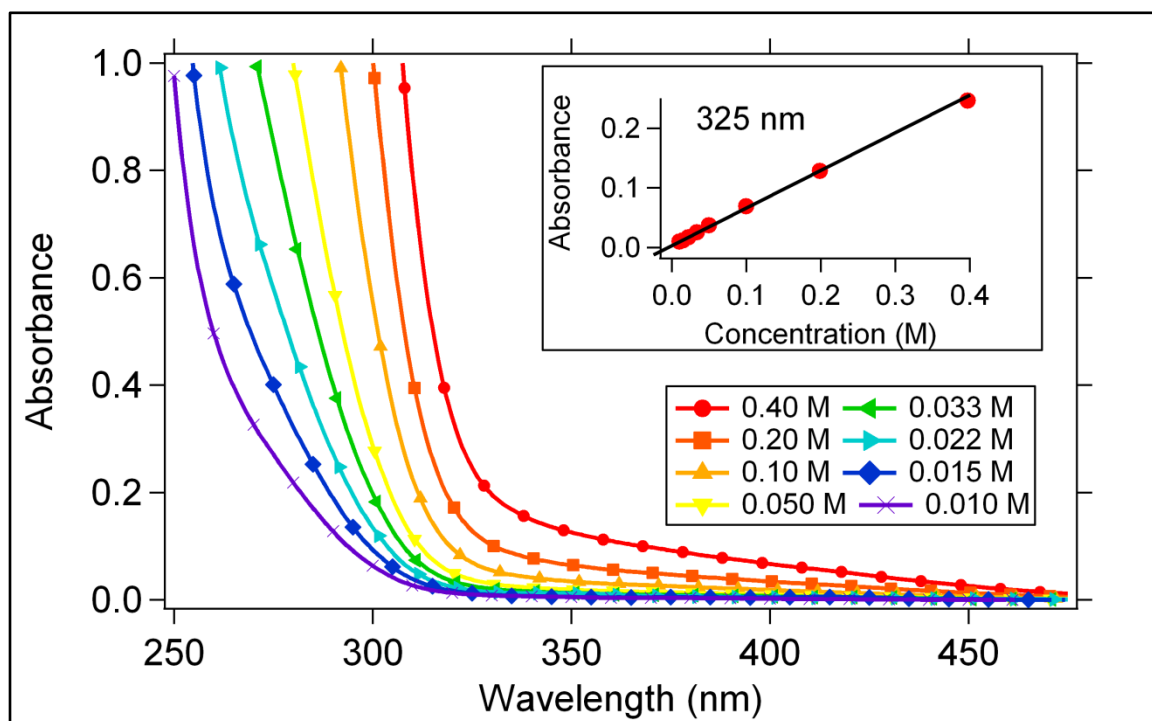


**Figure 5.2.** Representative UV-VIS spectra of 2-hydroxycyclohexyl nitrate (compound A) at different solution concentrations. The inset shows an example of calculating the molar extinction coefficient from Beer's law at 325 nm; such calculations have been done at every wavelength for every nitrate investigated in this work.

Absorption spectra were recorded at multiple dilution levels in methanol to verify linearity over the experimental range of concentrations. For each wavelength, the molar extinction coefficient was determined by a linear fit of the base-10 absorbance vs. molar concentration, as shown in the inset in Figure 5.2. The absorbance increases sharply towards the UV range; to avoid deviations from Beer's law only points with the absorbance values below  $\sim 1$

were included in the fit. Table 5.2 reports the molar extinction coefficients for the examined nitrates between 270 and 330 nm.

**Table 5.2.** Molar extinction coefficients (in  $\text{L mol}^{-1} \text{cm}^{-1}$ ) for the investigated nitrates (the labels are defined in Table 5.1). No data for compounds E and I are included because we could not purify them. The solvent is methanol, except for compound L, which was additionally investigated in water (w), acetonitrile (acn), octanol (oct), and tetrahydrofuran (thf). Each molar extinction coefficient is obtained from a fit of the available absorbance vs. concentration data as shown in Figure 5.2.

Wavelength (nm)	<b>A</b>	<b>B</b>	<b>C</b>	<b>D</b>	<b>F</b>	<b>H</b>	<b>J</b>	<b>K</b>
270	28.43	9.91	19.10	10.76	26.85		25.73	17.80
275	22.86	9.62	15.50	9.03	22.40		21.34	15.44
280	18.00	9.02	12.30	7.64	18.56		18.89	12.55
285	13.67	8.18	9.36	6.48	12.97		13.72	9.94
290	10.06	6.92	6.94	5.45	10.44	29.74	9.69	7.57
295	6.96	5.80	5.03	4.56	8.35	20.22	6.32	5.22
300	4.67	4.70	3.56	3.81	6.82	15.45	3.76	3.50
305	2.85	3.67	2.44	3.17	5.67	12.41	2.06	2.10
310	1.69	2.76	1.67	2.63	4.78	9.99	1.01	1.18
315	1.04	2.10	1.21	2.19	4.14	8.30	0.50	0.63
320	0.66	1.64	0.93	1.84	3.67	7.10	0.24	0.31
325	0.46	1.32	0.77	1.56	3.34	6.16	0.12	0.15
330	0.36	1.11	0.66	1.33	3.06	5.29	0.06	0.07

Wavelength (nm)	<b>L</b>	<b>L<sub>w</sub></b>	<b>L<sub>acn</sub></b>	<b>L<sub>oct</sub></b>	<b>L<sub>thf</sub></b>
270	23.99	23.30		22.71	
275	17.89	16.49	20.02	17.35	
280	12.49	11.48	13.85	12.45	
285	8.68	7.66	9.54	9.02	
290	5.87	5.07	6.36	6.16	6.12
295	3.75	3.15	4.03	3.96	4.44
300	2.27	1.85	2.44	2.42	2.79
305	1.28	1.01	1.40	1.37	1.62
310	0.66	0.50	0.76	0.71	0.89
315	0.31	0.24	0.40	0.34	0.49
320	0.15	0.11	0.24	0.16	0.29
325	0.07	0.05	0.16	0.08	0.20
330	0.03	0.03	0.13	0.04	0.16

We do not report values outside this range because the measured absorbance values were too small for a reliable fit above 330 nm, and there were too few measurement points with acceptably low absorbance below 270 nm. Figure 5.3a compares the molar extinction coefficient for synthesized  $\beta$ -hydroxyalkyl nitrates A, B, C, D and commercially obtained compounds J and K without the  $\beta$ -hydroxyl group. The values are comparable in the vicinity of 300 nm but diverge at 330 nm, where the extinction coefficients become small and hard to measure reliably.

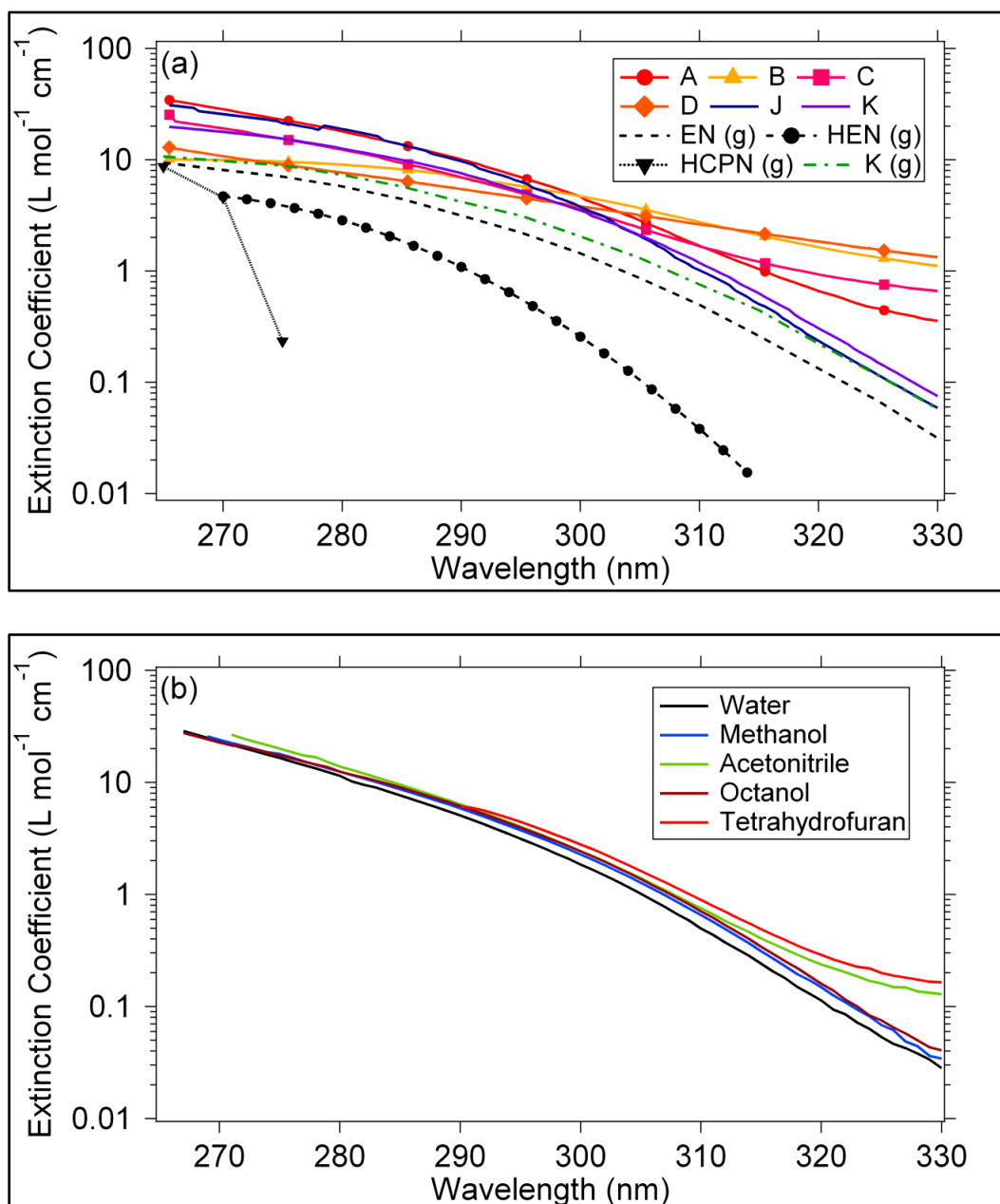


**Figure 5.3.** Panel (a): wavelength dependent molar extinction coefficients for  $\beta$ -hydroxyalkyl nitrates A, B, C, D (in various shades of red with markers) and alkyl nitrates J, K (in shades of blue without markers) measured in methanol. Gas-phase data (in black and green) for isopropyl nitrate (K),<sup>1</sup> ethyl nitrate (EN),<sup>1</sup> hydroxyethyl nitrate (HEN),<sup>2</sup> trans-2-hydroxycyclopentyl-1-nitrate (HCPN)<sup>3</sup> are provided for comparison (only a limited number of points were reported for HCPN). Panel (b) contains the measured molar extinction coefficients for compound L measured in various solvents.

Ideally, the measured molar extinction coefficients in solution should be compared to their corresponding gas-phase values. However, gas-phase absorption cross sections for any of



the synthesized compounds listed in Table 5.1 are not available. We are aware of only two gas-phase absorption cross section measurements for  $\beta$ -hydroxyalkyl nitrates, specifically for  $\beta$ -hydroxyethyl nitrate<sup>2</sup> and for trans-2-hydroxycyclopentyl-1-nitrate.<sup>3</sup> The data for both of these  $\beta$ -hydroxyalkyl nitrates are included in Figure 5.3a for comparison. In addition, we include the IUPAC recommended data<sup>1</sup> for ethyl nitrate and for isopropyl nitrate (K). In all cases, we converted the base-e gas-phase absorption cross sections ( $\sigma$ , in  $\text{cm}^2 \text{ molec}^{-1}$ ) to base-10 molar extinction coefficients ( $\epsilon$ , in  $\text{L mol}^{-1} \text{ cm}^{-1}$ ),

$$\epsilon(\lambda) = \sigma(\lambda) \times \frac{N_A}{1000 \times \ln(10)} \quad (5.10)$$

where  $N_A$  is Avogadro's number.

The direct comparison can only be done for isopropyl nitrate (K), for which the gas-phase molar extinction coefficients are smaller than the ones in methanol by a factor of  $\sim 1.6$  (Figure 5.3a). The comparison is less straightforward for other compounds because the absorption coefficients of alkyl nitrates tend to increase with the size of the substituent chain,<sup>2,73,74</sup> and have an unknown dependence on the solvent. However, based on Figure 5.3a, the solution phase extinction coefficients in methanol appear to be larger on average than the gas-phase values. According to the existing gas-phase measurements for  $\beta$ -hydroxyethyl nitrate and ethyl nitrate, the  $\beta$ -hydroxyl group could be expected to have a suppressing effect on the extinction coefficients. However, our measurements indicate that the  $\beta$ -hydroxyl group has a relatively minor effect on the absorption spectrum in solution. Roberts and Ravishankara<sup>2</sup> noted the difficulties of measuring absorption cross sections for  $\beta$ -hydroxy nitrates arising from their low vapor pressure. Indeed, examination of Figure 5.3 suggests that the existing absorption cross sections for  $\beta$ -hydroxy nitrates may be underestimated; for example, the low value of the

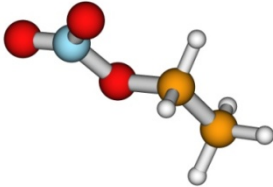
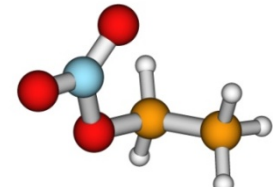

reported 275 nm cross section for trans-2-hydroxycyclopentyl-1-nitrate<sup>3</sup> seems to fall out of the general trend. Therefore, additional measurements of gas-phase absorption cross sections for  $\beta$ -hydroxy nitrates are desirable.

To further investigate the solution effects, we examined absorption spectra of isosorbide mononitrate (L) in various solutions. This compound has two ether groups in  $\beta$  positions, which should have similar electron withdrawing effect on the photochemistry of the nitroxy group as the  $\beta$ -hydroxyl group. Figure 5.3b shows that the absorption spectrum of L does not strongly depend on the type of the solvent across the range of solvent polarities (water, methanol, acetonitrile, octanol, tetrahydrofuran). The absorption coefficient appears to be systematically smaller in water compared to the less polar solvents in this group suggesting a reduction in the excited state dipole moment (confirmed by calculations, see below). However, on the whole, the solvent effect on the absorption spectrum appears to be minimal.

#### **5.4.2. Computed Structures and Absorption Spectra**

All calculations described in this section were done by Dorit Shemesh and R. Benny Gerber. The geometries, dihedral angles, relative ground state energies calculated at the MP2/cc-pVDZ level, and dipole moments of the lowest energy conformers of ethyl nitrate are summarized in Table 5.3.

**Table 5.3.** Optimized geometries, relative energies, and dipole moments of ethyl nitrate conformers as calculated with MP2/cc-pVDZ.

Conformer	Structure	N-O-C-C dihedral angle	Energy [eV]	Dipole moment [Debye]	Nomenclature
1		-180.0°	0	2.86	anti
2		78.5°	0.005	2.75	gauche+
3		-78.5°	0.005	2.75	gauche-

The  $\text{-ONO}_2$  group of all the three conformers is planar; the primary difference between them lies in the N-O-C-C dihedral angle. The conformer 2 (gauche+) and conformer 3 (gauche-) are stereoisomers, therefore their energies are the same. The conformer 1 is a global minimum at this level of theory, but it is within a fraction of a few meV from conformers 2 and 3. The vertical excitation energies for conformer 1 calculated at the coupled cluster CC2 level are provided in Table 5.4, and those for conformer 3 are given in Table 5.5.

**Table 5.4.** The lowest electronic excited states of conformer 1 of ethyl nitrate. All parameters are calculated at CC2 level, but the OM2 energies are also provided for comparison.

State	CC2 energy [eV]	OM2 energy [eV]	Transitions involved	Oscillator strength	Dipole moment [Debye]
Ground	0	0	-	-	2.86
1	5.07	4.60	HOMO-2 → LUMO 64% HOMO-3 → LUMO 31 %	$4 \times 10^{-8}$	2.34
2	6.10	4.87	HOMO-3 → LUMO 62 % HOMO-2 → LUMO 23% HOMO-6 → LUMO 11%	0.0003	3.44
3	6.58	5.36	HOMO-1 → LUMO 46% HOMO-5 → LUMO 26% HOMO → LUMO 16%	0.080	7.19
4	7.69	5.39	HOMO → LUMO 48% HOMO-1 → LUMO 12% HOMO-2 → LUMO+5 11%	0.087	1.62
5	8.19	5.99	HOMO-2 → LUMO+5 22% HOMO → LUMO 16% HOMO-3 → LUMO+5 11% HOMO-2 → LUMO+1 10%	0.14	0.88

**Table 5.5.** The lowest electronic excited states of conformer 3 of ethyl nitrate. All parameters are calculated at CC2 level, but the OM2 energies are also provided for comparison.

State	CC2 energy [eV]	OM2 energy [eV]	Transitions involved	Oscillator strength	Dipole moment [Debye]
Ground	0	0	-	-	2.75
1	5.05	4.41	HOMO-3 → LUMO 65% HOMO-2 → LUMO 32%	$3 \times 10^{-6}$	2.19
2	6.08	4.69	HOMO-4 → LUMO 26% HOMO-2 → LUMO 24% HOMO-1 → LUMO 24 % HOMO-3 → LUMO 12 %	0.0016	3.31
3	6.49	5.17	HOMO-1 → LUMO 44%	0.076	6.98
4	7.64	5.38	HOMO → LUMO 58%	0.10	1.75
5	8.20	5.78	HOMO-3 → LUMO+5 20% HOMO → LUMO 14%	0.13	1.10

The molecular orbitals involved in these transitions are shown in Figure 5.4 and Figure 5.5, respectively. The orbitals have similar features but there are subtle differences as well. For example, the first excited state for conformer 3 corresponds mainly to an excitation from

HOMO-3 to LUMO, whereas for conformer 1, the main excitation involves HOMO-2 and the LUMO orbital. The lowest electronic excited state of conformer 3 is predicted around 5.07 eV at the CC2 level. For comparison, the first excitation energy is 4.60 eV at the OM2 level.

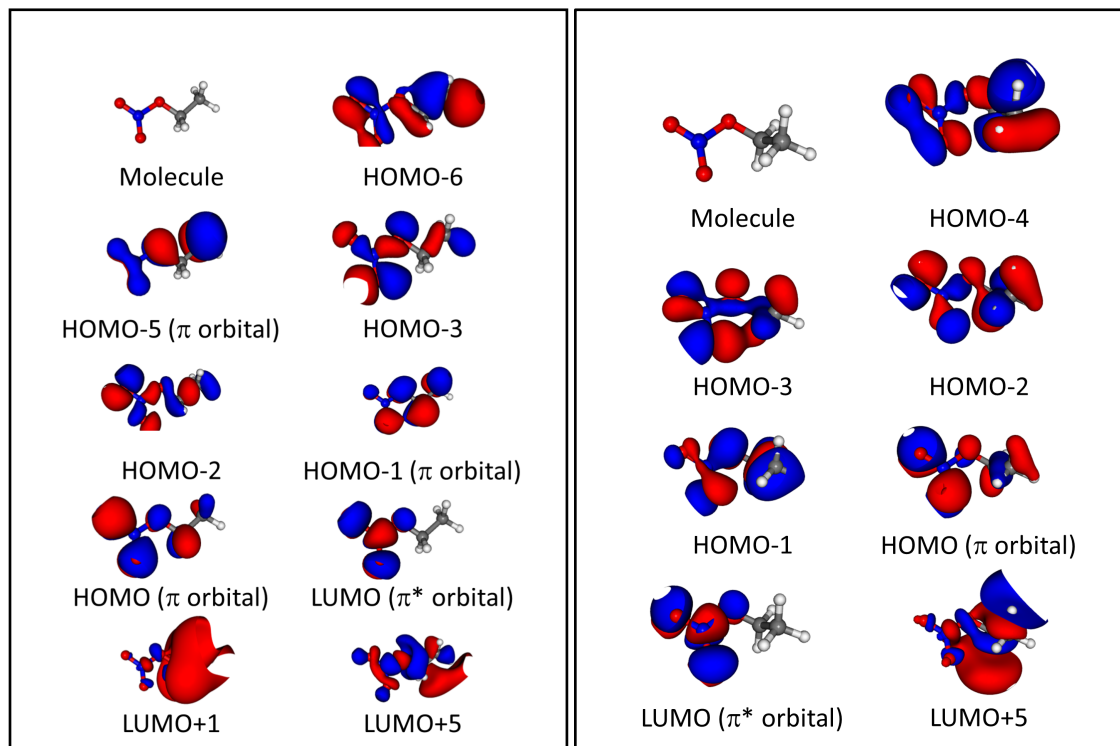


**Figure 5.4.** Molecular orbitals (obtained by MP2) involved in electronic transitions of conformer 1 (right panel) and conformer 3 (left panel) of ethyl nitrate listed in Table 5.4. and Table 5.5.

A comparison of the theoretically predicted excitation spectrum to the experimental one shows that the OM2/MRCI method reasonably describes the actual excitation energies (Figure 5.7). Normally, the *ab initio* CC2 method is supposed to be more reliable than the OM2/MRCI method. However, in the present case, we suspect that the CC2 states are not covering the relevant orbitals of the different states involved. As a result, we believe that the CC2 calculation is less accurate. An alternative explanation is that this is a case where the multireference description is essential; the semiempirical MRCI has the advantage of more fully covering the active space.

As many as 13 minima were found for  $\beta$ -hydroxyethyl nitrate. Their geometries are shown in Figure 5.5, and their relative energies and the Boltzmann populations at 300 K are listed in Table 5.6. The vertical excitation energies at the CC2 level for the lowest energy conformer are provided in Table 5.7, and Figure 5.6 shows the corresponding molecular orbitals.

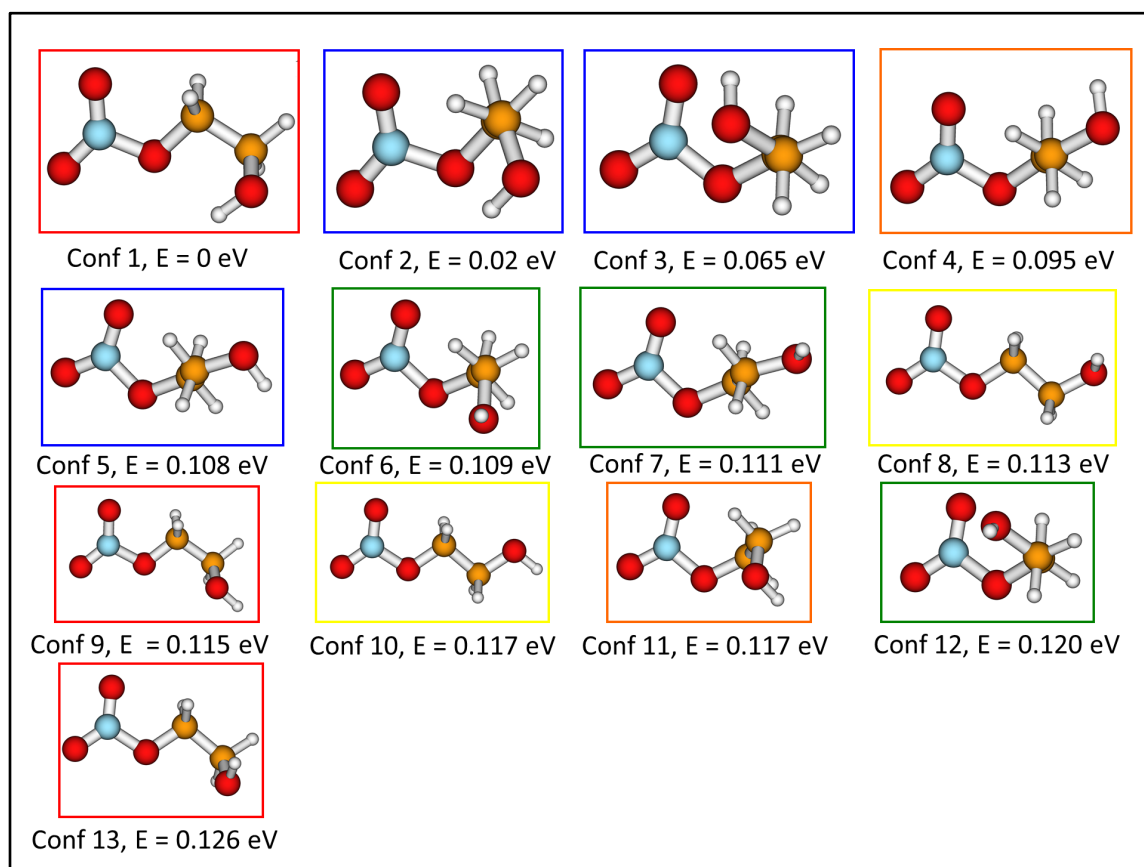


**Figure 5.5.** Structures of the conformers of  $\beta$ -hydroxyethyl nitrate as calculated by MP2 listed in Table 5.6. Same colors around the frame correspond to different rotamers around one bond.

**Table 5.6.** Relative energies (as calculated with MP2) and relative Boltzmann populations of  $\beta$ -hydroxyethyl nitrate conformers at 300 K.

Conformer	Energy [eV]	Boltzmann distribution at 300 K [%]
1	0.000	59.5
2	0.020	27.9
3	0.065	4.73
4	0.095	1.53
5	0.108	0.92
6	0.109	0.86
7	0.111	0.80
8	0.113	0.76
9	0.115	0.69
10	0.117	0.64
11	0.117	0.64
12	0.120	0.56
13	0.126	0.46

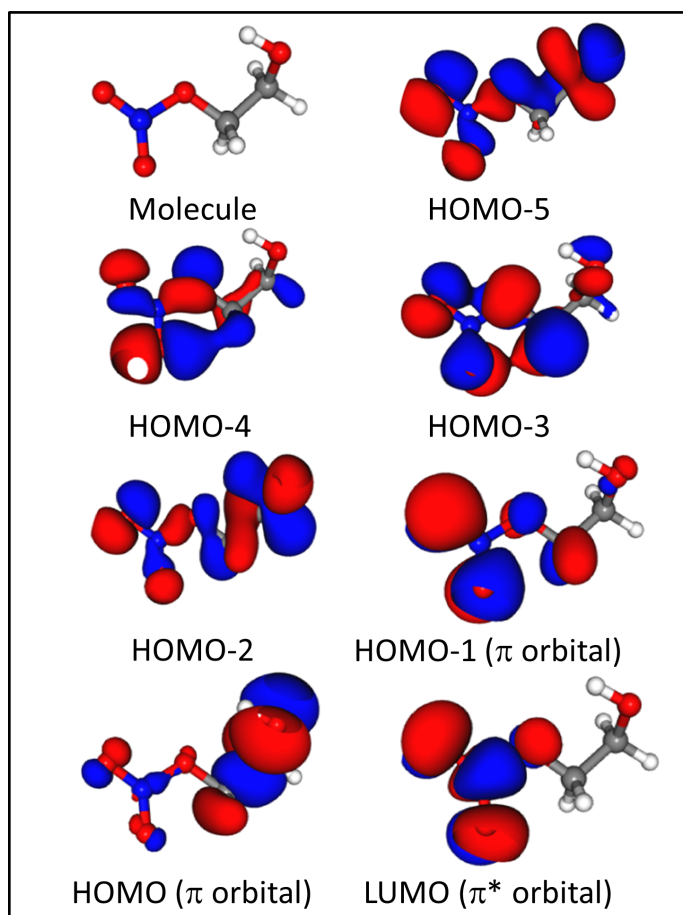


**Figure 5.6.** Molecular orbitals as obtained by MP2 involved in electronic transitions of the lowest energy conformer of  $\beta$ -hydroxyethyl nitrate listed in Table 5.7.

**Table 5.7.** The electronic excited states of the lowest energy conformer of  $\beta$ -hydroxyethyl nitrate as calculated by CC2. All parameters are calculated at CC2 level, but the OM2 energies are also provided for comparison.

State	CC2 energy [eV]	OM2 energy [eV]	Main Transitions Involved	Oscillator strength	Dipole moment [Debye]
Ground	0	0	-	-	1.69
1	5.09	4.59	HOMO-4 $\rightarrow$ LUMO 50 % HOMO-3 $\rightarrow$ LUMO 23 % HOMO-2 $\rightarrow$ LUMO 13 %	0.000050	1.35
2	6.12	5.30	HOMO-4 $\rightarrow$ LUMO 37 % HOMO-5 $\rightarrow$ LUMO 35 % HOMO-2 $\rightarrow$ LUMO 19 %	0.000311	2.29
3	6.61	5.59	HOMO-3 $\rightarrow$ LUMO 47 % HOMO-1 $\rightarrow$ LUMO 11 % HOMO-5 $\rightarrow$ LUMO 11 %	0.0721	5.85
4	7.59	5.84	HOMO-1 $\rightarrow$ LUMO 30 %	0.0263	1.81
5	7.96	6.48	HOMO $\rightarrow$ LUMO 74 %	0.0117	13.00

The lowest electronic excited state is predicted at around 5.09 eV at the CC2 level, which is very similar to the corresponding value for ethyl nitrate. The first excitation energy at the OM2 level (4.59 eV) is also essentially identical to that of ethyl nitrate. However, there are also differences between the two systems at higher excitations energies; for example, transition 5 in Table 5.7 is unique to  $\beta$ -hydroxyethyl nitrate, and is not present in ethyl nitrate. The correspondence between the molecular orbitals of ethyl and  $\beta$ -hydroxyethyl nitrates is shown in Table 5.8.

**Table 5.8.** Cross-comparison of orbitals of ethyl nitrate and  $\beta$ -hydroxyethyl nitrate.

$\beta$ -hydroxyethyl nitrate	ethyl nitrate
HOMO-5	HOMO-6
HOMO-4	HOMO-3
HOMO-3	HOMO-1
HOMO-2	HOMO-2
HOMO-1	HOMO
HOMO	---
LUMO	LUMO



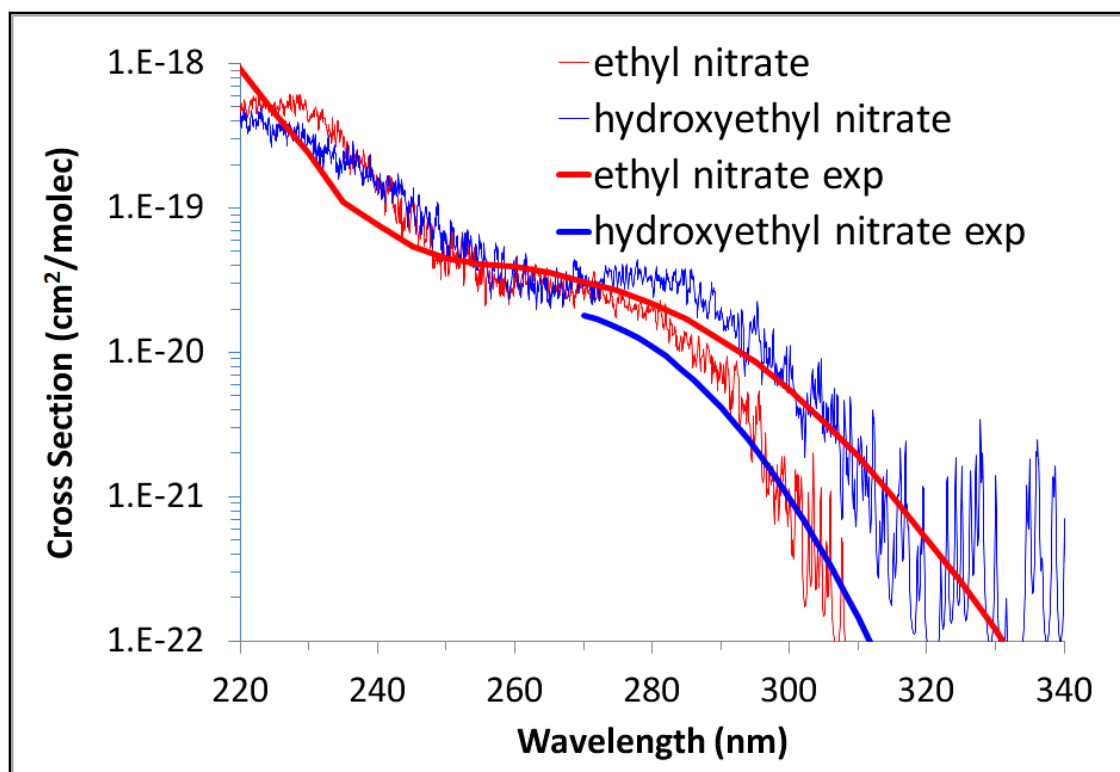


**Figure 5.7.** Comparison of theoretically predicted absorption cross sections of ethyl nitrate (red noisy trace) and  $\beta$ -hydroxyethyl nitrate (blue noisy trace). The absorption cross sections for ethyl nitrate (red solid line)<sup>1</sup> and hydroxyethyl nitrate<sup>2</sup> (blue solid line) are shown for comparison. The two theoretical results have been arbitrarily scaled by the same factor. Note that the experiments and simulations predict spectral shifts in the opposite direction for the two compounds.

The absorption spectra of ethyl nitrate and  $\beta$ -hydroxyethyl nitrate from the MD simulations using the OM2 semiempirical Hamiltonian are shown in Figure 5.7. The most important wavelength range for photochemistry in the lower atmosphere is the low energy tail of the absorption spectrum. The oscillator strength for the lowest  $n \rightarrow \pi^*$  electronic transition responsible for this tail in nitrates is quite low, which is responsible for the increased noise in the predicted spectrum. The calculations predict a small red shift of the spectrum upon addition of the  $\beta$ -hydroxyl group, whereas the available experiments suggest that the spectrum of  $\beta$ -hydroxyethyl nitrate is slightly blue shifted from the spectrum of ethyl nitrate. However, there is

reasonable agreement in the overall shape of the spectra across the entire range over which measurements are available.

We should note that the absorption spectra represent a convolution of different overlapping transitions. Figure 5.8 shows a decomposition of the predicted absorption spectra of ethyl nitrate and  $\beta$ -hydroxyethyl into contribution from the four lowest electronic states.

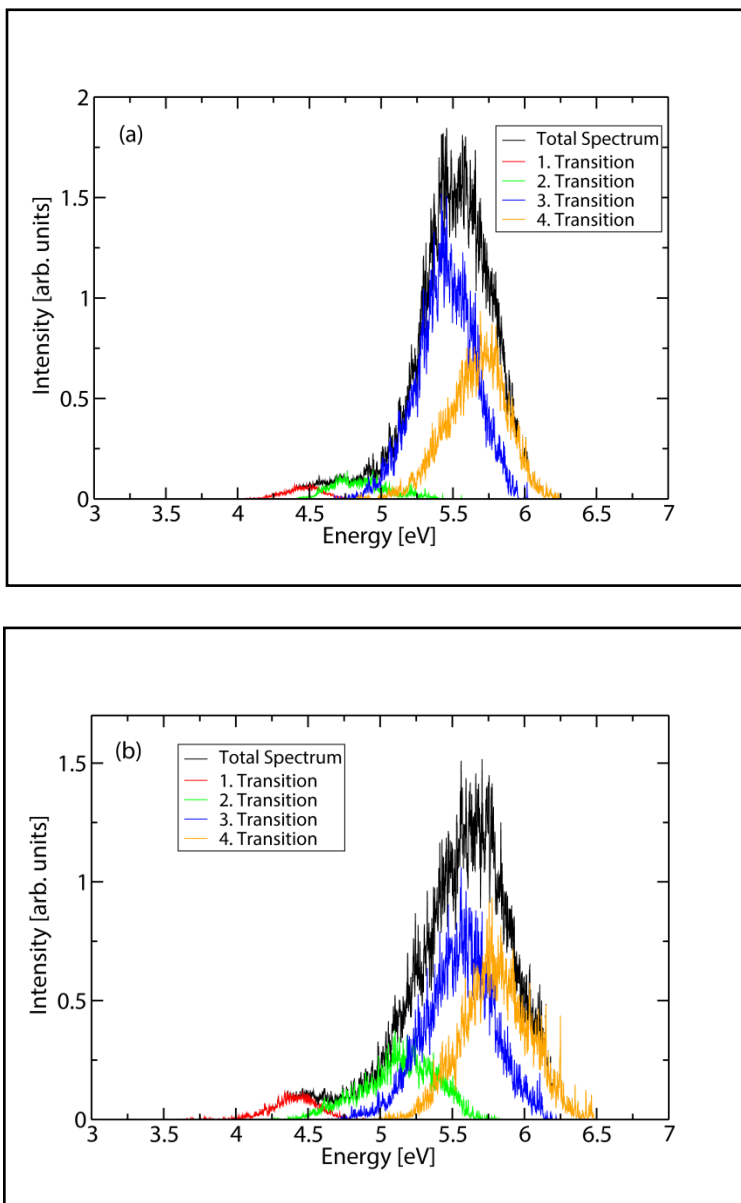


**Figure 5.8.** Decomposition of the predicted absorption spectra of ethyl nitrate (a) and  $\beta$ -hydroxyethyl nitrate (b) into contribution from the four lowest electronic states.

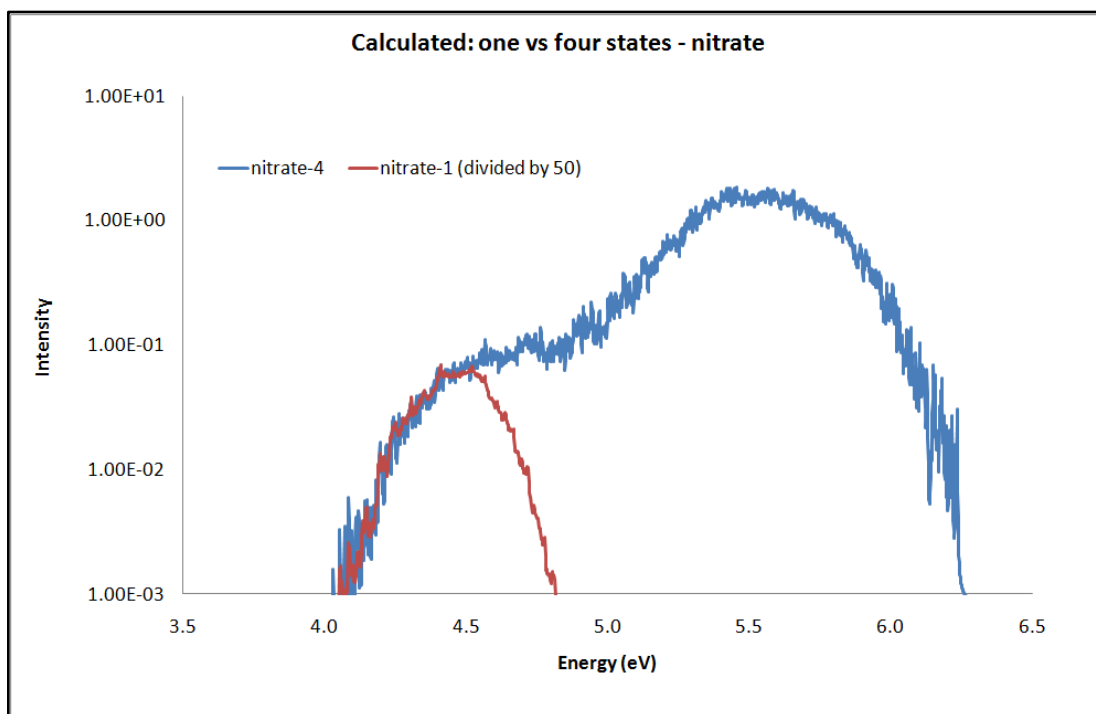


**Figure 5.9.** Predicted absorption spectrum of ethyl nitrate calculated by inclusion of one (red trace – labeled nitrate-1) and four (blue trace – labeled nitrate-4) states in the MD simulations. The one-state calculation was scaled down by 50 (to account for the difference in sampling). The shape of the low-energy tail of the spectrum is nearly identical in both cases.

The low energy tail of the spectrum is dominated by the lowest electronic state. These results (e.g., Figures 5.8 and 5.9) demonstrate that the shape of the low energy tail in the spectrum can be adequately predicted by using only one state, which greatly cuts down on the computational expenses.

## 5.5. Photochemical Fates of $\beta$ -Hydroxyalkyl Nitrates

As discussed in the introduction, the OH reaction is the most important removal mechanism for unsaturated nitrates,<sup>78</sup> but photolysis may become competitive for certain types of saturated nitrate compounds. To examine potential fates of the compounds listed in Table 5.1, we performed a scaling analysis to determine their most significant atmospheric sinks. This method was previously developed in Epstein et al.<sup>52</sup> and Epstein et al.;<sup>54</sup> therefore, we will only provide a summary of the assumptions used for this particular analysis. Oxidation by OH radicals is

typically the most dominant chemical sink for most atmospheric organics in both the aqueous and gaseous phases,<sup>251</sup> suggesting that OH oxidation is a reasonable benchmark to determine the significance of direct aqueous photolysis. We chose to compare the rates of chemical reaction via gas-phase photolysis, aqueous-phase photolysis, gas-phase oxidation by OH, and aqueous phase oxidation by OH. Note that we are not considering loss by dry deposition, which may be an important loss mechanism in the boundary layer. We are also ignoring hydrolysis of hydroxyalkyl nitrate isomers with the nitrate group in the tertiary position, which has been shown to occur with atmospherically relevant rates in both aqueous solutions<sup>157,158</sup> and water-containing aerosols.<sup>226</sup>

Henry's Law constant is used to determine the equilibrium partitioning between each phase in an air mass with a specific liquid water content. We define the parameter "Z" as the ratio between the gas-phase photolysis rate and the aqueous-phase photolysis rate:

$$Z = \frac{\frac{dn_{hv}^{gas}}{dt}}{\frac{dn_{hv}^{aq}}{dt}} = \frac{J_{gas}}{J_{aq}} (R \cdot T \cdot LWC_v \cdot K_H)^{-1} \quad (5.11)$$

where  $n$  represents the moles of the compound of interest,  $t$  represents time,  $J$  is the computed photolysis rate constant using the measured absorption coefficients (see below),  $R$  is the gas constant,  $T$  is the temperature,  $LWC_v$  is the liquid water content in volume of liquid water per volume of air, and  $K_H$  is the Henry's Law constant. The Henry's law constant for isopropyl nitrate was obtained from the experimental measurements of Hauff et al.<sup>252</sup> Henry's law constants of the remaining nitrates were unavailable and thus were predicted from HENRYWIN<sup>253</sup> using bond contribution methods (Table 5.9).

**Table 5.9.** Henry's constants used for predicting aqueous partitioning of nitrates examined in this work.

NAME	SMILES	H [atm×m <sup>3</sup> /mol]	H [M/atm]	Method
2-hydroxycyclohexyl nitrate (A)	<chem>C1(O)C(ON(=O)=O)CCCC1</chem>	1.32E-08	7.58E+04	Bond
3-hydroxy-3-methylbutan-2-yl nitrate (B)	<chem>C(C)(C)(O)C(C)ON(=O)=O</chem>	2.25E-08	4.44E+04	Bond
2-hydroxyhexyl nitrate (C)	<chem>C(O)(CCCC)CON(=O)=O</chem>	2.99E-08	3.34E+04	Bond
2-hydroxy-2-methyl-5-(prop_1-en-2-yl)cyclohexyl nitrate (D)	<chem>C(=C)(C)C1CC(ON(=O)=O)C(C)(O)CC1</chem>	3.60E-08	2.78E+04	Bond
2-hydroxy-2,6,6-trimethylbicyclo[3.1.1]heptan-2-yl nitrate (E)	<chem>C1(C)(C)C2C(C)(O)C(ON(=O)=O)CC1C2</chem>	1.81E-08	5.52E+04	Bond
4-hydroxytetrahydrofuran-3-yl nitrate (F)	<chem>C1(O)C(ON(=O)=O)COC1</chem>	8.31E-12	1.20E+08	Bond
1-hydroxybut-3-en-2-yl nitrate (G)	<chem>C(=C)C(CO)ON(=O)=O</chem>	1.26E-08	7.94E+04	Bond
2-hydroxy-1-phenylethyl nitrate (H)	<chem>c1(C(CO)ON(=O)=O)cccc1</chem>	7.77E-10	1.29E+06	Bond
2-hydroxy-3-(nitrooxy)propyl methacrylate (I)	<chem>C(=O)(C(=C)C)OCC(O)CON(=O)=O</chem>	2.52E-11	3.97E+07	Bond
2-ethylhexyl nitrate (J)	<chem>O(N(=O)=O)CC(CCCC)CC</chem>	1.44E-03	6.94E-01	Bond
isopropyl nitrate (K)	<chem>O=N(=O)OC(C)C</chem>	1.61E-03	6.21E-01	Hauff, K et al. (1998) <sup>252</sup>

The experimentally measured<sup>79,80</sup> Henry's constants for C2-C5 β-hydroxyalkyl nitrates without other functional groups range from 6×10<sup>3</sup> to 4×10<sup>4</sup> M/atm, which compares reasonably well to the range of HENRYWIN predictions of 3×10<sup>4</sup> to 8×10<sup>4</sup> M/atm for compounds A, B, C, D, E, and G which have no polar functional groups other than hydroxyl and nitroxy. We should note

that HENRYWIN Henry's constant predictions of a series of  $\beta$ -hydroxyalkyl nitrates from Shepson et al.<sup>79</sup> overestimated the measured values by factors ranging from 2.6 to 17, so the treatment presented here should be viewed as approximate. The method predicts higher solubility for the compound H with an aromatic substituent, which may be an artifact of the bond contribution method. The highest solubility ( $1.7 \times 10^{10}$  M/atm) is predicted for compound L, which has the largest O/C ratio. To investigate the significance of aqueous photochemistry during ideal conditions, we used a cloud liquid water content of  $0.5 \text{ g m}^{-3}$ , typically the largest value experienced in the troposphere.<sup>254</sup>

The aqueous- and gas-phase photolysis rate constants are a function of the actinic flux, the absorption cross section,  $\sigma$ , and the photolysis quantum yield,  $\Phi$ :

$$\frac{J_{gas}}{J_{aq}} = \frac{\int F_A(\lambda) \cdot \Phi_{gas}(\lambda) \cdot \sigma_{gas}(\lambda) \cdot d\lambda}{\int F_A(\lambda) \cdot \Phi_{aq}(\lambda) \cdot \sigma_{aq}(\lambda) \cdot d\lambda} \quad (5.12)$$

where  $\lambda$  represents wavelength. Due to the absence of gas-phase absorption cross sections, we initially assumed that the gas-phase absorption cross sections were identical to the aqueous-phase values. To test the bounds of this framework, we repeated the calculations with aqueous absorption cross sections obtained from experimental extinction coefficient measurements. In this variation, gas-phase absorption cross sections were estimated by applying a 10 nm blue shift to the measured cross sections in methanol (Table 5.2). The application of this 10 nm blue shift did not significantly affect the conclusions of this analysis. The actinic flux was calculated with the Tropospheric Ultraviolet and Visible (TUV) radiation model<sup>255</sup> at a 24-hr average solar zenith angle (SZA) of  $65^\circ$  representative of Los Angeles, CA at the summer solstice using a similar procedure described in Epstein et al.<sup>89</sup> Both aqueous- and gas-phase quantum yields are unknown, but after making the simplification that they are independent of photon energy over

the relevant wavelengths (segment of wavelengths where the actinic flux and the absorption cross section are non-zero), we can treat the quantum yields as a ratio. If gas- and aqueous-phase photolysis occur with the same chemical mechanism, we expect that the aqueous-phase quantum yields should be less than or equal to the gas-phase values<sup>52,54</sup>. In certain cases, gas- and aqueous-phase photolysis mechanisms may differ significantly, leading to a break-down in this assumption.<sup>53</sup> If the gas-phase and aqueous-phase quantum yields are of the same magnitude, the simplified factor  $Z$  reveals the significance of aqueous phase photolysis relative to gas phase photolysis.

We can also compare the rate of aqueous photolysis with the rate of aqueous oxidation by OH by defining a factor  $Q$ :

$$Q = \frac{\frac{dn_{OH}^{aq}}{dt}}{\frac{dn_{hv}^{aq}}{dt}} = \frac{k_{OH}[OH]}{J_{aq}} \quad (5.13)$$

where  $k_{OH}$  is the rate constant for aqueous oxidation by OH. The values of  $k_{OH}$  are not available experimentally in the literature, so we used group contribution structure activity relationship (SAR) that were equipped to predict values for alkyl nitrates.<sup>256</sup> We tested these SARs using experimental data from Lee et al.<sup>70</sup> of two hydroxyl nitrates: E-2-methyl-4-nitrooxybut-2-ene-1-ol and 3-methyl-2-nitroxybut-3-ene-1-ol. The SARs over-predicted aqueous oxidation by OH rate constants by a factor of 23 and 57, respectively. Therefore the behavior of this SAR is satisfactory for the purposes of examining the relative influence of aqueous photolysis. Aqueous OH concentrations were set to  $10^{-13}$  M, the daytime cloud-water value estimated in Ervens et al.<sup>8</sup> To understand the maximum contribution of aqueous photolysis, the unknown aqueous photolysis quantum yields were set to unity. Comparison of  $Z$  and  $Q$  on the same axis can illustrate the potential significance of aqueous photolysis. Figure 5.10 reveals that for the nine

compounds with measured extinction coefficients, aqueous oxidation by OH is significantly faster than aqueous photolysis even under conditions that will lead to an enhancement in aqueous photolysis rates (wet clouds, strong actinic radiation, large aqueous photolysis quantum yield).

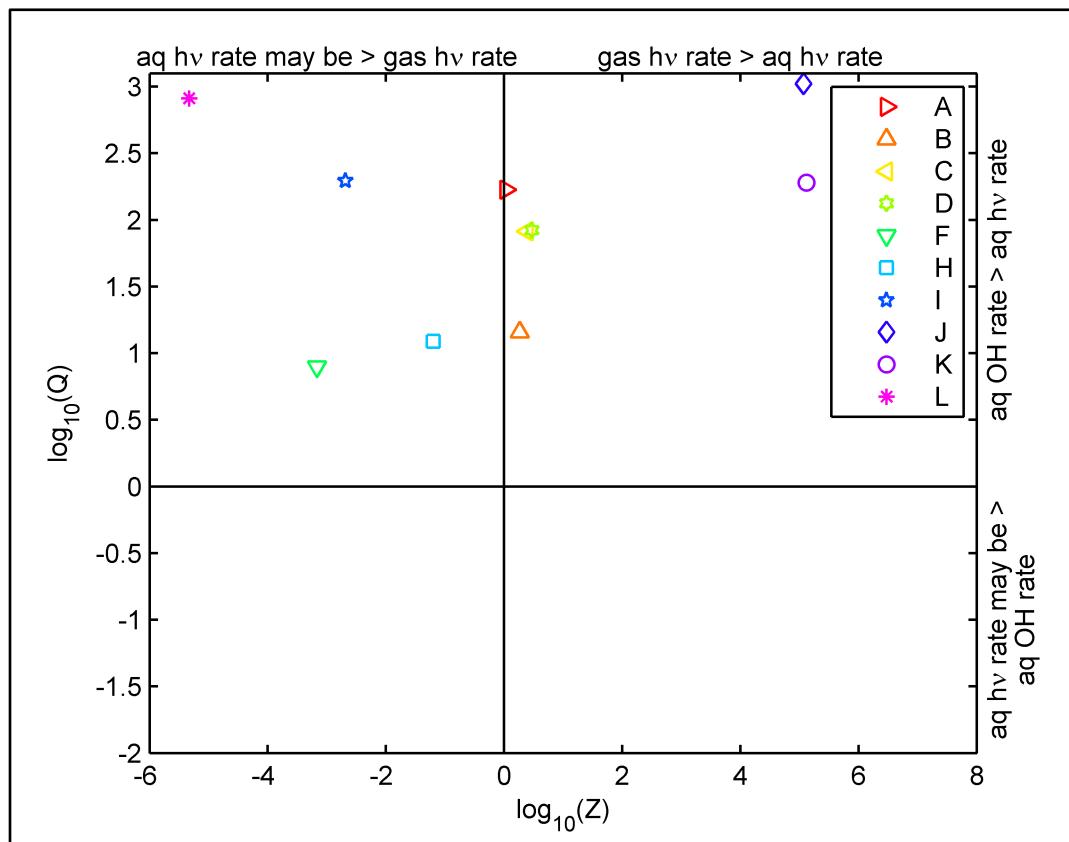


**Figure 5.10.** Likely photoinduced atmospheric sinks of studied compounds at a solar zenith angle of  $65^\circ$ .  $Q$  is defined as the ratio of the aqueous oxidation by OH rate and the aqueous photolysis rate.  $Z$  is defined as the ratio of the gas photolysis rate and aqueous photolysis rate. The lack of points with  $Q < 1$  and  $Z < 1$  indicates that liquid phase photolysis of nitrate compounds considered in this work is too slow relative other sink processes under typical atmospheric conditions.

Depending on the compound and the ratio in quantum yields, aqueous photolysis may be faster than gaseous photolysis, but in all cases, oxidation by OH appears to be the dominant photo-induced sink. Comparison of predicted and measured Henry's law constants and  $k_{OH}$  values of a few similar compounds indicates that there is the potential that each of these values may be overestimated by the predictive methods we employed. A potential overestimation in the Henry's law constant does not affect the overall conclusions as the studied compounds could be less



soluble than predicted. However, an overestimation in  $k_{OH}$  values would suppress the significance of aqueous photolysis and could potentially modify the conclusion that aqueous photolysis is not a significant sink.

## 5.6. Conclusion

The main question posed by this chapter was whether the direct photolysis of  $\beta$ -hydroxyalkyl nitrates in aqueous phase or in organic particles phase is atmospherically relevant. Results of this work suggest that the answer to this question is “no”. Unlike the  $\beta$ -carbonyl group,<sup>78</sup> the  $\beta$ -hydroxyl group appears to have a relatively minor effect on the absorption coefficients of organic nitrates in methanol, and by extension, in an aqueous solution. Therefore it is unlikely that the photochemical loss of  $\beta$ -hydroxyalkyl nitrates will accelerate once they partition in cloud droplets or aerosol particles. A more quantitative analysis of the relative rates of loss of nitrates by gas-phase and aqueous phase oxidation confirms that direct aqueous photolysis is not likely to compete with gas phase oxidation and photolysis, and with aqueous phase oxidation by OH.

The absorption coefficients of organic nitrates appear to increase slightly in solutions relative to the gas-phase. However, the effect is not dramatic. Therefore, it should be reasonable to approximate gas-phase absorption coefficients by solution-based measurements, and vice versa. This should simplify measurements for nitrates that have low volatility (and hence cannot be studied by gas-phase techniques) or low solubility (cannot be studied by solution-based methods).

The OM2/GUGA-CI computational approach utilized in this work provides reasonable predictions for the wavelength dependence of the absorption spectra of organic nitrates. The qualitative agreement for the shape of the red tail of the absorption spectrum, which plays an

important role in photochemistry of nitrates in the lower atmosphere, is especially noteworthy. The utility of this method needs to be investigated further for predicting the shapes of absorption tails of other atmospherically relevant organic molecules, such as peroxides, carbonyls, and multifunctional compounds.

## References

- (1) Atkinson, R.; Baulch, D. L.; Cox, R. A.; Crowley, J. N.; Hampson, R. F.; Hynes, R. G.; Jenkin, M. E.; Rossi, M. J.; Troe, J. Evaluated Kinetic and Photochemical Data for Atmospheric Chemistry: Volume II - Gas Phase Reactions of Organic Species. *Atmos. Chem. Phys.* **2006**, *6*, 3625–4055.
- (2) Roberts, J. M.; Fajer, R. W. UV Absorption Cross Sections of Organic Nitrates of Potential Atmospheric Importance and Estimation of Atmospheric Lifetimes. *Environ. Sci. Technol.* **1989**, *23* (8), 945–951.
- (3) Wängberg, I.; Barnes, I.; Becker, K. H. Atmospheric Chemistry of Bifunctional Cycloalkyl Nitrates. *Chem. Phys. Lett.* **1996**, *261* (1), 138–144.
- (4) Went, F. W. Blue Hazes in the Atmosphere. *Nature* **1960**, *187*, 641–643.
- (5) Liousse, C.; Penner, J. E.; Chuang, C.; Walton, J. J.; Eddleman, H.; Cachier, H. A Global Three-Dimensional Model Study of Carbonaceous Aerosols. *J. Geophys. Res. Atmos.* **1996**, *101* (D14), 19411–19432.
- (6) Koppmann, R. *Volatile Organic Compounds in the Atmosphere*; Blackwell: Oxford, 2008.
- (7) Atkinson, R. Gas-Phase Tropospheric Chemistry of Volatile Organic Compounds .1. Alkanes and Alkenes. *J. Phys. Chem. Ref. Data* **1997**, *26* (2), 215–290.
- (8) Ervens, B.; Turpin, B. J.; Weber, R. J. Secondary Organic Aerosol Formation in Cloud Droplets and Aqueous Particles (aqSOA): A Review of Laboratory, Field and Model Studies. *Atmos. Chem. Phys.* **2011**, *11* (21), 11069–11102.
- (9) Herrmann, H.; Schaefer, T.; Tilgner, A.; Styler, S. A.; Weller, C.; Teich, M.; Otto, T. Tropospheric Aqueous-Phase Chemistry: Kinetics, Mechanisms, and Its Coupling to a Changing Gas Phase. *Chem. Rev.* **2015**, *115* (10), 4259–4334.

- (10) Sisler, J. F.; Malm, W. C. The Relative Importance of Soluble Aerosols to Spatial and Seasonal Trends of Impaired Visibility in the United States. *Atmos. Environ.* **1994**, *28* (5), 851–862.
- (11) Charlson, R. J.; Schwartz, S. E. Climate Forcing by Anthropogenic Aerosols. *Science*. **1992**, *255* (5043), 423.
- (12) Stocker, T. F.; Qin, D.; Plattner, G. K.; Tignor, M.; Allen, S. K.; Boschung, J.; Nauels, A.; Xia, Y.; Bex, B.; Midgley, B. M. IPCC, 2013: Climate Change 2013: The Physical Science Basis. Contribution of Working Group I to the Fifth Assessment Report of the Intergovernmental Panel on Climate Change. **2013**.
- (13) Pope III, C. A.; Ezzati, M.; Dockery, D. W. Fine-Particulate Air Pollution and Life Expectancy in the United States. *N. Engl. J. Med.* **2009**, *360* (4), 376–386.
- (14) Hines, P. J. The Invisible Bouquet. *Science*. **2006**, *311* (5762), 803.
- (15) Guenther, C. C. Estimates of Global Terrestrial Isoprene Emissions Using MEGAN (Model of Emissions of Gases and Aerosols from Nature). *Atmos. Chem. Phys.* **2006**, *6*.
- (16) Geron, C.; Rasmussen, R.; Arnts, R. R.; Guenther, A. A Review and Synthesis of Monoterpene Speciation from Forests in the United States. *Atmos. Environ.* **2000**, *34*, 1761–1781.
- (17) Finlayson-Pitts, B. J.; Pitts, J. N. *Chemistry of the Upper and Lower Atmosphere: Theory, Experiments, and Applications*; Academic Press: San Diego, 2000.
- (18) Street, R. A.; Owen, S.; Duckham, S. C.; Boissard, C.; Hewitt, C. N. Effect of Habitat and Age on Variations in Volatile Organic Compound (VOC) Emissions from *Quercus Ilex* and *Pinus Pinea*. *Atmos. Environ.* **1997**, *31*, 89–100.
- (19) Benjamin, M. T.; Sudol, M.; Bloch, L.; Winer, A. M. Low-Emitting Urban Forests: A

- Taxonomic Methodology for Assigning Isoprene and Monoterpene Emission Rates. *Atmos. Environ.* **1996**, *30* (9), 1437–1452.
- (20) Guenther, A.; Zimmerman, P.; Wildermuth, M. Natural Volatile Organic Compound Emission Rate Estimates for US Woodland Landscapes. *Atmos. Environ.* **1994**, *28* (6), 1197–1210.
- (21) Guenther, A.; Geron, C.; Pierce, T.; Lamb, B.; Harley, P.; Fall, R. Natural Emissions of Non-Methane Volatile Organic Compounds, Carbon Monoxide, and Oxides of Nitrogen from North America. *Atmos. Environ.* **2000**, *34* (12), 2205–2230.
- (22) Singh, H. B.; Salas, L.; Viezee, W.; Sitton, B.; Ferek, R. Measurement of Volatile Organic Chemicals at Selected Sites in California. *Atmos. Environ. Part A. Gen. Top.* **1992**, *26* (16), 2929–2946.
- (23) Helmig, D.; Ortega, J.; Duhl, T.; Tanner, D.; Guenther, A.; Harley, P.; Wiedinmyer, C.; Milford, J.; Sakulyanontvittaya, T. Sesquiterpene Emissions from Pine Trees—Identifications, Emission Rates and Flux Estimates for the Contiguous United States. *Environ. Sci. Technol.* **2007**, *41* (5), 1545–1553.
- (24) Duhl, A. B. Sesquiterpene Emissions from Vegetation: A Review. *Biogeosciences* **2008**, *5*.
- (25) Chen, F.; Tholl, D.; D’Auria, J. C.; Farooq, A.; Pichersky, E.; Gershenzon, J. Biosynthesis and Emission of Terpenoid Volatiles from Arabidopsis Flowers. *Plant Cell* **2003**, *15* (2), 481–494.
- (26) Ciccioli, P.; Brancaleoni, E.; Frattoni, M.; Di Palo, V.; Valentini, R.; Tirone, G.; Seufert, G.; Bertin, N.; Hansen, U.; Csiky, O.; et al. Emission of Reactive Terpene Compounds from Orange Orchards and Their Removal by within-Canopy Processes. *J. Geophys. Res.*

- 1999**, *104* (D7), 8077–8094.
- (27) Degenhardt, D. C.; Lincoln, D. E. Volatile Emissions from an Odorous Plant in Response to Herbivory and Methyl Jasmonate Exposure. *J. Chem. Ecol.* **2006**, *32* (4), 725–743.
- (28) De Moraes, C. M.; Mescher, M. C.; Tumlinson, J. H. Caterpillar-Induced Nocturnal Plant Volatiles Repel Conspecific Females. *Nature* **2001**, *410* (6828), 577–580.
- (29) Schuh, G.; Heiden, A. C.; Hoffmann, T.; Kahl, J.; Rockel, P.; Rudolph, J.; Wildt, J. Emissions of Volatile Organic Compounds from Sunflower and Beech: Dependence on Temperature and Light Intensity. *J. Atmos. Chem.* **1997**, *27* (3), 291–318.
- (30) Katsiotis, S. T.; Langezaal, C. R.; Scheffer, J. J. C.; Verpoorte, R. Comparative Study of the Essential Oils from Hops of Various *Humulus Lupulus* L. Cultivars. *Flavour Fragr. J.* **1989**, *4* (4), 187–191.
- (31) Sindelarova, K.; Granier, C.; Bouarar, I.; Guenther, A.; Tilmes, S.; Stavrakou, T.; Müller, J.-F.; Kuhn, U.; Stefani, P.; Knorr, W. Global Data Set of Biogenic VOC Emissions Calculated by the MEGAN Model over the Last 30 Years. *Atmos. Chem. Phys.* **2014**, *14* (17), 9317–9341.
- (32) Griffin, R. J.; Cocker, D. R.; Flagan, R. C.; Seinfeld, J. H. Organic Aerosol Formation from the Oxidation of Biogenic Hydrocarbons. *J. Geophys. Res.* **1999**, *104* (D3), 3555–3567.
- (33) Shu, Y.; Atkinson, R. Atmospheric Lifetimes and Fates of a Series of Sesquiterpenes. *J. Geophys. Res. Atmos.* **1995**, *100* (D4), 7275–7281.
- (34) Shu, Y.; Atkinson, R. Rate Constants for the Gas-phase Reactions of O<sub>3</sub> with a Series of Terpenes and OH Radical Formation from the O<sub>3</sub> Reactions with Sesquiterpenes at 296 ± 2 K. *Int. J. Chem. Kinet.* **1994**, *26* (12), 1193–1205.

- (35) Atkinson, R.; Arey, J. Atmospheric Degradation of Volatile Organic Compounds. *Chem. Rev.* **2003**, *103* (12), 4605–4638.
- (36) Kim, Y. M.; Harrad, S.; Harrison, R. M. Concentrations and Sources of VOCs in Urban Domestic and Public Microenvironments. *Environ. Sci. Technol.* **2001**, *35* (6), 997–1004.
- (37) Cocker Iii, D. R.; Mader, B. T.; Kalberer, M.; Flagan, R. C.; Seinfeld, J. H. The Effect of Water on Gas–particle Partitioning of Secondary Organic Aerosol: II. M-Xylene and 1, 3, 5-Trimethylbenzene Photooxidation Systems. *Atmos. Environ.* **2001**, *35* (35), 6073–6085.
- (38) Healy, R. M.; Wenger, J. C.; Metzger, A.; Duplissy, J.; Kalberer, M.; Dommen, J. Gas/particle Partitioning of Carbonyls in the Photooxidation of Isoprene and 1, 3, 5-Trimethylbenzene. *Atmos. Chem. Phys.* **2008**, *8* (12), 3215–3230.
- (39) Paulsen, D.; Dommen, J.; Kalberer, M.; Prévôt, A. S. H.; Richter, R.; Sax, M.; Steinbacher, M.; Weingartner, E.; Baltensperger, U. Secondary Organic Aerosol Formation by Irradiation of 1, 3, 5-Trimethylbenzene-NO<sub>x</sub>-H<sub>2</sub>O in a New Reaction Chamber for Atmospheric Chemistry and Physics. *Environ. Sci. Technol.* **2005**, *39* (8), 2668–2678.
- (40) Sax, M.; Zenobi, R.; Baltensperger, U.; Kalberer, M. Time Resolved Infrared Spectroscopic Analysis of Aerosol Formed by Photo-Oxidation of 1,3,5-Trimethylbenzene and  $\alpha$ -Pinene. *Aerosol Sci. Technol.* **2005**, *39* (9), 822–830.
- (41) Sato, K.; Takami, A.; Kato, Y.; Seta, T.; Fujitani, Y.; Hikida, T.; Shimono, A.; Imamura, T. AMS and LC/MS Analyses of SOA from the Photooxidation of Benzene and 1, 3, 5-Trimethylbenzene in the Presence of NO<sub>x</sub>: Effects of Chemical Structure on SOA Aging. *Atmos. Chem. Phys.* **2012**, *12* (10), 4667–4682.
- (42) Laskin, A.; Laskin, J.; Nizkorodov, S. A. Chemistry of Atmospheric Brown Carbon.

- Chem. Rev.* **2015**, *115* (10), 4335–4382.
- (43) McDonald, J. D.; Zielinska, B.; Fujita, E. M.; Sagebiel, J. C.; Chow, J. C.; Watson, J. G. Fine Particle and Gaseous Emission Rates from Residential Wood Combustion. *Environ. Sci. Technol.* **2000**, *34* (11), 2080–2091.
- (44) Tatàno, F.; Barbadoro, L.; Mangani, G.; Pretelli, S.; Tombari, L.; Mangani, F. Furniture Wood Wastes: Experimental Property Characterisation and Burning Tests. *Waste Manag.* **2009**, *29* (10), 2656–2665.
- (45) Kibet, J. K.; Khachatryan, L.; Dellinger, B. Molecular Products from the Thermal Degradation of Glutamic Acid. *J. Agric. Food Chem.* **2013**, *61* (32), 7696–7704.
- (46) Ofner, J.; Krüger, H.-U.; Grothe, H.; Schmitt-Kopplin, P.; Whitmore, K.; Zetzsch, C. Physico-Chemical Characterization of SOA Derived from Catechol and Guaiacol—a Model Substance for the Aromatic Fraction of Atmospheric HULIS. *Atmos. Chem. Phys.* **2011**, *11* (1), 1–15.
- (47) George, C.; Ammann, M.; D’Anna, B.; Donaldson, D. J.; Nizkorodov, S. A. Heterogeneous Photochemistry in the Atmosphere. *Chem. Rev.* **2015**, *115* (10), 4218–4258.
- (48) Rudich, Y.; Donahue, N. M.; Mentel, T. F. Aging of Organic Aerosol: Bridging the Gap between Laboratory and Field Studies. *Annu. Rev. Phys. Chem.* **2007**, *58*, 321–352.
- (49) Shiraiwa, M.; Pöschl, U.; Knopf, D. A. Multiphase Chemical Kinetics of NO<sub>3</sub> Radicals Reacting with Organic Aerosol Components from Biomass Burning. *Environ. Sci. Technol.* **2012**, *46* (12), 6630–6636.
- (50) Zepp, R. G.; Hoigne, J.; Bader, H. Nitrate-Induced Photooxidation of Trace Organic Chemicals in Water. *Environ. Sci. Technol.* **1987**, *21* (5), 443–450.



- (51) Torrents, A.; Anderson, B. G.; Bilbouljian, S.; Johnson, W. E.; Hapeman, C. J. Atrazine Photolysis: Mechanistic Investigations of Direct and Nitrate-Mediated Hydroxy Radical Processes and the Influence of Dissolved Organic Carbon from the Chesapeake Bay. *Environ. Sci. Technol.* **1997**, *31* (5), 1476–1482.
- (52) Epstein, S. A.; Tapavicza, E.; Furche, F.; Nizkorodov, S. A. Direct Photolysis of Carbonyl Compounds Dissolved in Cloud and Fog-Droplets. *Atmos. Chem. Phys.* **2013**, *13* (18), 9461–9477.
- (53) Reed Harris, A. E.; Ervens, B.; Shoemaker, R. K.; Kroll, J. A.; Rapf, R. J.; Griffith, E. C.; Monod, A.; Vaida, V. Photochemical Kinetics of Pyruvic Acid in Aqueous Solution. *J. Phys. Chem. A* **2014**, *118* (37), 8505–8516.
- (54) Epstein, S. A.; Nizkorodov, S. A. A Comparison of the Chemical Sinks of Atmospheric Organics in the Gas and Aqueous Phase. *Atmos. Chem. Phys.* **2012**, *12* (17), 8205–8222.
- (55) O'Brien, J. M.; Czuba, E.; Hastie, D. R.; Francisco, J. S.; Shepson, P. B. Determination of the Hydroxy Nitrate Yields from the Reaction of C2-C6 Alkenes with OH in the Presence of NO. *J. Phys. Chem. A* **1998**, *102* (45), 8903–8908.
- (56) Ma, S. X.; Rindelaub, J. D.; McAvey, K. M.; Gagare, P. D.; Nault, B. A.; Ramachandran, P. V.; Shepson, P. B.  $\alpha$ -Pinene Nitrates: Synthesis, Yields and Atmospheric Chemistry. *Atmos. Chem. Phys.* **2011**, *11* (13), 6337–6347.
- (57) Werner, G.; Kastler, J.; Looser, R.; Ballschmiter, K. Organic Nitrates of Isoprene as Atmospheric Trace Compounds. *Angew. Chemie Int. Ed.* **1999**, *38* (11), 1634–1637.
- (58) Matsunaga, A.; Ziemann, P. J. Yields of  $\beta$ -Hydroxynitrates, Dihydroxynitrates, and Trihydroxynitrates Formed from OH Radical-Initiated Reactions of 2-Methyl-1-Alkenes. *Proc. Natl. Acad. Sci.* **2010**, *107* (15), 6664–6669.

- (59) O'Brien, J. M.; Shepson, P. B.; Wu, Q.; Biesenthal, T.; Bottenheim, J. W.; Wiebe, H. A.; Anlauf, K. G.; Brickell, P. Production and Distribution of Organic Nitrates, and Their Relationship to Carbonyl Compounds in an Urban Environment. *Atmos. Environ.* **1997**, *31* (14), 2059–2069.
- (60) Beaver, M. R.; St Clair, J. M.; Paulot, F.; Spencer, K. M.; Crouse, J. D.; LaFranchi, B. W.; Min, K. E.; Pusede, S. E.; Wooldridge, P. J.; Schade, G. W. Importance of Biogenic Precursors to the Budget of Organic Nitrates: Observations of Multifunctional Organic Nitrates by CIMS and TD-LIF during BEARPEX 2009. *Atmos. Chem. Phys.* **2012**, *12* (13), 5773–5785.
- (61) Fischer, R. G.; Kastler, J.; Ballschmiter, K. Levels and Pattern of Alkyl Nitrates, Multifunctional Alkyl Nitrates, and Halocarbons in the Air over the Atlantic Ocean. *J. Geophys. Res. Atmos.* **2000**, *105* (D11), 14473–14494.
- (62) Perring, A. E.; Bertram, T. H.; Wooldridge, P. J.; Fried, A.; Heikes, B. G.; Dibb, J.; Crouse, J. D.; Wennberg, P. O.; Blake, N. J.; Blake, D. R. Airborne Observations of Total RONO<sub>2</sub>: New Constraints on the Yield and Lifetime of Isoprene Nitrates. *Atmos. Chem. Phys.* **2009**, *9* (4), 1451–1463.
- (63) Pratt, K. A.; Mielke, L. H.; Shepson, P. B.; Bryan, A. M.; Steiner, A. L.; Ortega, J.; Daly, R.; Helmig, D.; Vogel, C. S.; Griffith, S. Contributions of Individual Reactive Biogenic Volatile Organic Compounds to Organic Nitrates above a Mixed Forest. *Atmos. Chem. Phys.* **2012**, *12* (21), 10–125.
- (64) Rollins, A. W.; Kiendler-Scharr, A.; Fry, J. L.; Brauers, T.; Brown, S. S.; Dorn, H.-P.; Dubé, W. P.; Fuchs, H.; Mensah, A.; Mentel, T. F. Isoprene Oxidation by Nitrate Radical: Alkyl Nitrate and Secondary Organic Aerosol Yields. *Atmos. Chem. Phys.* **2009**, *9* (18),

- 6685–6703.
- (65) Perring, A. E.; Wisthaler, A.; Graus, M.; Wooldridge, P. J.; Lockwood, A. L.; Mielke, L. H.; Shepson, P. B.; Hansel, A.; Cohen, R. C. A Product Study of the Isoprene + NO<sub>3</sub> Reaction. *Atmos. Chem. Phys.* **2009**, *9* (14), 4945–4956.
- (66) Spittler, M.; Barnes, I.; Bejan, I.; Brockmann, K. J.; Benter, T.; Wirtz, K. Reactions of NO<sub>3</sub> Radicals with Limonene and  $\alpha$ -Pinene: Product and SOA Formation. *Atmos. Environ.* **2006**, *40*, 116–127.
- (67) Fry, J. L.; Kiendler-Scharr, A.; Rollins, A. W.; Wooldridge, P. J.; Brown, S. S.; Fuchs, H.; Dubé, W.; Mensah, A.; Maso, M. dal; Tillmann, R. Organic Nitrate and Secondary Organic Aerosol Yield from NO<sub>3</sub> Oxidation of  $\beta$ -Pinene Evaluated Using a Gas-Phase Kinetics/Aerosol Partitioning Model. *Atmos. Chem. Phys.* **2009**, *9* (4), 1431–1449.
- (68) Wängberg, I.; Barnes, I.; Becker, K. H. Product and Mechanistic Study of the Reaction of NO<sub>3</sub> Radicals with  $\alpha$ -Pinene. *Environ. Sci. Technol.* **1997**, *31* (7), 2130–2135.
- (69) Hallquist, M.; Wängberg, I.; Ljungström, E.; Barnes, I.; Becker, K.-H. Aerosol and Product Yields from NO<sub>3</sub> Radical-Initiated Oxidation of Selected Monoterpenes. *Environ. Sci. Technol.* **1999**, *33* (4), 553–559.
- (70) Lee, L.; Teng, A. P.; Wennberg, P. O.; Crouse, J. D.; Cohen, R. C. On Rates and Mechanisms of OH and O<sub>3</sub> Reactions with Isoprene-Derived Hydroxy Nitrates. *J. Phys. Chem. A* **2014**, *118* (9), 1622–1637.
- (71) Zhu, L.; Kellis, D. Temperature Dependence of the UV Absorption Cross Sections and Photodissociation Products of C<sub>3</sub> - C<sub>5</sub> Nitrates. *Chem. Phys. Lett.* **1997**, *278* (1), 41–48.
- (72) Talukdar, R.; Burkholder, J.; Gilles, M.; Roberts, J. Atmospheric Fate of Several Alkyl Nitrates Part 2 UV Absorption Cross-Sections and Photodissociation Quantum Yields. *J.*

- Chem. Soc. Faraday Trans.* **1997**, *93* (16), 2797–2805.
- (73) Turberg, M. P.; Giolando, D. M.; Tilt, C.; Soper, T.; Mason, S.; Davies, M.; Klingensmith, P.; Takacs, G. A. Atmospheric Photochemistry of Alkyl Nitrates. *J. Photochem. Photobiol. A Chem.* **1990**, *51* (3), 281–292.
- (74) Clemitshaw, K. C.; Williams, J.; Rattigan, O. V.; Shallcross, D. E.; Law, K. S.; Cox, R. A. Gas-Phase Ultraviolet Absorption Cross-Sections and Atmospheric Lifetimes of Several C2 - C5 Alkyl Nitrates. *J. Photochem. Photobiol. A Chem.* **1997**, *102* (2), 117–126.
- (75) Barnes, I.; Becker, K. H.; Zhu, T. Near UV Absorption Spectra and Photolysis Products of Difunctional Organic Nitrates: Possible Importance as NO<sub>x</sub> Reservoirs. *J. Atmos. Chem.* **1993**, *17* (4), 353–373.
- (76) Luke, W. T.; Dickerson, R. R.; Nunnermacker, L. J. Direct Measurements of the Photolysis Rate Coefficients and Henry's Law Constants of Several Alkyl Nitrates. *J. Geophys. Res. Atmos.* **1989**, *94* (D12), 14905–14921.
- (77) Carbajo, P. G.; Orr-Ewing, A. J. NO<sub>2</sub> Quantum Yields from Ultraviolet Photodissociation of Methyl and Isopropyl Nitrate. *Phys. Chem. Chem. Phys.* **2010**, *12* (23), 6084–6091.
- (78) Müller, J.-F.; Peeters, J.; Stavrou, T. Fast Photolysis of Carbonyl Nitrates from Isoprene. *Atmos. Chem. Phys.* **2014**, *14* (5), 2497–2508.
- (79) Shepson, P. B.; Mackay, E.; Muthuramu, K. Henry's Law Constants and Removal Processes for Several Atmospheric  $\beta$ -Hydroxy Alkyl Nitrates. *Environ. Sci. Technol.* **1996**, *30* (12), 3618–3623.
- (80) Treves, K.; Shragina, L.; Rudich, Y. Henry's Law Constants of Some  $\beta$ -,  $\gamma$ -, and  $\delta$ -Hydroxy Alkyl Nitrates of Atmospheric Interest. *Environ. Sci. Technol.* **2000**, *34* (7), 1197–1203.

- (81) Nguyen, T. B.; Roach, P. J.; Laskin, J.; Laskin, A.; Nizkorodov, S. A. Effect of Humidity on the Composition of Isoprene Photooxidation Secondary Organic Aerosol. *Atmos. Chem. Phys.* **2011**, *11* (14), 6931–6944.
- (82) Nguyen, T. B.; Laskin, J.; Laskin, A.; Nizkorodov, S. A. Nitrogen-Containing Organic Compounds and Oligomers in Secondary Organic Aerosol Formed by Photooxidation of Isoprene. *Environ. Sci. Technol.* **2011**, *45* (16), 6908–6918.
- (83) Yu, Y.; Ezell, M. J.; Zelenyuk, A.; Imre, D.; Alexander, L.; Ortega, J.; D’Anna, B.; Harmon, C. W.; Johnson, S. N.; Finlayson-Pitts, B. J. Photooxidation of  $\alpha$ -Pinene at High Relative Humidity in the Presence of Increasing Concentrations of NO<sub>x</sub>. *Atmos. Environ.* **2008**, *42* (20), 5044–5060.
- (84) Fenn, J. B.; Mann, M.; Meng, C. K.; Wong, S. F.; Whitehouse, C. M. Electrospray Ionization—principles and Practice. *Mass Spectrom. Rev.* **1990**, *9* (1), 37–70.
- (85) Koch, B. P.; Witt, M. R.; Engbrodt, R.; Dittmar, T.; Kattner, G. Molecular Formulae of Marine and Terrestrial Dissolved Organic Matter Detected by Electrospray Ionization Fourier Transform Ion Cyclotron Resonance Mass Spectrometry. *Geochim. Cosmochim. Acta* **2005**, *69* (13), 3299–3308.
- (86) Presto, A. A.; Huff Hartz, K. E.; Donahue, N. M. Secondary Organic Aerosol Production from Terpene Ozonolysis. 1. Effect of UV Radiation. *Environ. Sci. Technol.* **2005**, *39* (18), 7036–7045.
- (87) Kroll, J. H.; Ng, N. L.; Murphy, S. M.; Flagan, R. C.; Seinfeld, J. H. Secondary Organic Aerosol Formation from Isoprene Photooxidation. *Environ. Sci. Technol.* **2006**, *40* (6), 1869–1877.
- (88) Surratt, J. D.; Murphy, S. M.; Kroll, J. H.; Ng, N. L.; Hildebrandt, L.; Sorooshian, A.;

- Szmigielski, R.; Vermeylen, R.; Maenhaut, W.; Claeys, M.; et al. Chemical Composition of Secondary Organic Aerosol Formed from the Photooxidation of Isoprene. *J. Phys. Chem. A* **2006**, *110* (31), 9665–9690.
- (89) Epstein, S. A.; Blair, S. L.; Nizkorodov, S. A. Direct Photolysis of  $\alpha$ -Pinene Ozonolysis Secondary Organic Aerosol: Effect on Particle Mass and Peroxide Content. *Environ. Sci. Technol.* **2014**, *48* (19), 11251–11258.
- (90) Wong, J. P. S.; Zhou, S.; Abbatt, J. P. D. Changes in Secondary Organic Aerosol Composition and Mass due to Photolysis: Relative Humidity Dependence. *J. Phys. Chem. A* **2014**, *119* (19), 4309–4316.
- (91) Kourtchev, I.; Doussin, J. F.; Giorio, C.; Mahon, B.; Wilson, E. M.; Maurin, N.; Pangui, E.; Venables, D. S.; Wenger, J. C.; Kalberer, M. Molecular Composition of Aged Secondary Organic Aerosol Generated from a Mixture of Biogenic Volatile Compounds Using Ultrahigh Resolution Mass Spectrometry. *Atmos. Chem. Phys. Discuss.* **2015**, *15* (4), 5359–5389.
- (92) Walser, M. L.; Park, J.; Gomez, A. L.; Russell, A. R.; Nizkorodov, S. A. Photochemical Aging of Secondary Organic Aerosol Particles Generated from the Oxidation of D-Limonene. *J. Phys. Chem. A* **2007**, *111* (10), 1907–1913.
- (93) Mang, S. A.; Henricksen, D. K.; Bateman, A. P.; Andersen, M. P. S.; Blake, D. R.; Nizkorodov, S. A. Contribution of Carbonyl Photochemistry to Aging of Atmospheric Secondary Organic Aerosol. *J. Phys. Chem. A* **2008**, *112* (36), 8337–8344.
- (94) Pan, X.; Underwood, J. S.; Xing, J. H.; Mang, S. A.; Nizkorodov, S. A. Photodegradation of Secondary Organic Aerosol Generated from Limonene Oxidation by Ozone Studied with Chemical Ionization Mass Spectrometry. *Atmos. Chem. Phys.* **2009**, *9* (12), 3851–

- 3865.
- (95) Bateman, A. P.; Nizkorodov, S. A.; Laskin, J.; Laskin, A. Photochemical Processing of Secondary Organic Aerosols Dissolved in Cloud Droplets. *Phys. Chem. Chem. Phys.* **2011**, *13* (26), 12199–12212.
- (96) Nguyen, T. B.; Laskin, A.; Laskin, J.; Nizkorodov, S. A. Direct Aqueous Photochemistry of Isoprene High-NO<sub>x</sub> Secondary Organic Aerosol. *Phys. Chem. Chem. Phys.* **2012**, *14* (27), 9702–9714.
- (97) Lee, H. J.; Aiona, P. K.; Laskin, A.; Laskin, J.; Nizkorodov, S. A. Effect of Solar Radiation on the Optical Properties and Molecular Composition of Laboratory Proxies of Atmospheric Brown Carbon. *Environ. Sci. Technol.* **2014**, *48* (17), 10217–10226.
- (98) Sareen, N.; Schwier, A. N.; Shapiro, E. L.; Mitroo, D.; McNeill, V. F. Secondary Organic Material Formed by Methylglyoxal in Aqueous Aerosol Mimics. *Atmos. Chem. Phys.* **2010**, *10* (3), 997–1016.
- (99) Zhao, R.; Lee, A. K. Y.; Huang, L.; Li, X.; Yang, F.; Abbatt, J. P. D. Photochemical Processing of Aqueous Atmospheric Brown Carbon. *Atmos. Chem. Phys. Discuss.* **2015**, *15* (2), 2957–2996.
- (100) Romonosky, D. E.; Laskin, A.; Laskin, J.; Nizkorodov, S. A. High-Resolution Mass Spectrometry and Molecular Characterization of Aqueous Photochemistry Products of Common Types of Secondary Organic Aerosols. *J. Phys. Chem. A* **2015**, *119* (11), 2594–2606.
- (101) Sioutas, C. Sioutas Cascade Impactor, **2004**. Patent US 6786105 B1.
- (102) Hallquist, M.; Wenger, J. C.; Baltensperger, U.; Rudich, Y.; Simpson, D.; Claeys, M.; Dommen, J.; Donahue, N. M.; George, C.; Goldstein, A. H.; et al. The Formation,

- Properties and Impact of Secondary Organic Aerosol: Current and Emerging Issues. *Atmos. Chem. Phys.* **2009**, *9* (14), 5155–5236.
- (103) Mutzel, A.; Rodigast, M.; Iinuma, Y.; Böge, O.; Herrmann, H. An Improved Method for the Quantification of SOA Bound Peroxides. *Atmos. Environ.* **2013**, *67* (0), 365–369.
- (104) Updyke, K. M.; Nguyen, T. B.; Nizkorodov, S. A. Formation of Brown Carbon via Reactions of Ammonia with Secondary Organic Aerosols from Biogenic and Anthropogenic Precursors. *Atmos. Environ.* **2012**, *63*, 22–31.
- (105) Liu, P. F.; Abdelmalki, N.; Hung, H.-M.; Wang, Y.; Brune, W. H.; Martin, S. T. Ultraviolet and Visible Complex Refractive Indices of Secondary Organic Material Produced by Photooxidation of the Aromatic Compounds Toluene and m-Xylene. *Atmos. Chem. Phys.* **2015**, *15* (3), 1435–1446.
- (106) Sander, S. P.; Abbatt, J. P. D.; Barker, J. R.; Burkholder, J. B.; Friedl, R. R.; Golden, D. M.; Huie, R. E.; Kolb, C. E.; Kurylo, M. J.; Moortgat, G. K.; et al. *Chemical Kinetics and Photochemical Data for Use in Atmospheric Studies, Evaluation No. 17*; JPL Publication 10-6: Jet Propulsion Laboratory, Pasadena, 2011.
- (107) Lignell, H.; Hinks, M. L.; Nizkorodov, S. A. Exploring Matrix Effects on Photochemistry of Organic Aerosols. *Proc. Natl. Acad. Sci.* **2014**, *111* (38), 13780–13785.
- (108) Czoschke, N. M.; Jang, M.; Kamens, R. M. Effect of Acidic Seed on Biogenic Secondary Organic Aerosol Growth. *Atmos. Environ.* **2003**, *37* (30), 4287–4299.
- (109) Nozière, B.; Esteve, W. Light-Absorbing Aldol Condensation Products in Acidic Aerosols: Spectra, Kinetics, and Contribution to the Absorption Index. *Atmos. Environ.* **2007**, *41* (6), 1150–1163.
- (110) Song, C.; Gyawali, M.; Zaveri, R. A.; Shilling, J. E.; Arnott, W. P. Light Absorption by



- Secondary Organic Aerosol from  $\alpha$ -pinene: Effects of Oxidants, Seed Aerosol Acidity, and Relative Humidity. *J. Geophys. Res. Atmos.* **2013**, *118* (20), 11,711–741,749.
- (111) Van Wyngarden, A. L.; Pérez-Montaño, S.; Bui, J. V. H.; Li, E. S. W.; Nelson, T. E.; Ha, K. T.; Leong, L.; Iraci, L. T. Complex Chemical Composition of Colored Surface Films Formed from Reactions of Propanal in Sulfuric Acid at Upper Troposphere/lower Stratosphere Aerosol Acidities. *Atmos. Chem. Phys.* **2015**, *15* (8), 4225–4239.
- (112) Lin, Y.-H.; Budisulistiorini, S. H.; Chu, K.; Siejack, R. A.; Zhang, H.; Riva, M.; Zhang, Z.; Gold, A.; Kautzman, K. E.; Surratt, J. D. Light-Absorbing Oligomer Formation in Secondary Organic Aerosol from Reactive Uptake of Isoprene Epoxydiols. *Environ. Sci. Technol.* **2014**, *48* (20), 12012–12021.
- (113) Hung, H.-M.; Chen, Y.-Q.; Martin, S. T. Reactive Aging of Films of Secondary Organic Material Studied by Infrared Spectroscopy. *J. Phys. Chem. A* **2013**, *117* (1), 108–116.
- (114) Lignell, H.; Epstein, S. A.; Marvin, M. R.; Shemesh, D.; Gerber, B.; Nizkorodov, S. Experimental and Theoretical Study of Aqueous Cis-Pinonic Acid Photolysis. *J. Phys. Chem. A* **2013**, *117* (48), 12930–12945.
- (115) Aregahegn, K. Z.; Nozière, B.; George, C. Organic Aerosol Formation Photo-Enhanced by the Formation of Secondary Photosensitizers in Aerosols. *Faraday Discuss.* **2013**, *165*, 123–134.
- (116) Monge, M. E.; Rosenørn, T.; Favez, O.; Müller, M.; Adler, G.; Riziq, A. A.; Rudich, Y.; Herrmann, H.; George, C.; D'Anna, B. Alternative Pathway for Atmospheric Particles Growth. *Proc. Natl. Acad. Sci.* **2012**, *109* (18), 6840–6844.
- (117) Rincón, A. G.; Guzmán, M. I.; Hoffmann, M. R.; Colussi, A. J. Thermo-chromism of Model Organic Aerosol Matter. *J. Phys. Chem. Lett.* **2010**, *1* (1), 368–373.

- (118) Zhong, M.; Jang, M. Dynamic Light Absorption of Biomass-Burning Organic Carbon Photochemically Aged under Natural Sunlight. *Atmos. Chem. Phys.* **2014**, *14* (3), 1517–1525.
- (119) Solomon, S.; Qin, D.; Manning, M.; Chen, Z.; Marquis, M.; Averyt, K. B.; Tignor, M.; Miller, H. L. Climate Change 2007: The Physical Science Basis. Contribution of Working Group I to the Fourth Assessment Report of the Intergovernmental Panel on Climate Change. *IPPC:2007* **2007**.
- (120) Pankow, J. F. An Absorption-Model of Gas-Particle Partitioning of Organic-Compounds in the Atmosphere. *Atmos. Environ.* **1994**, *28* (2), 185–188.
- (121) Odum, J. R.; Hoffmann, T.; Bowman, F.; Collins, D.; Flagan, R. C.; Seinfeld, J. H. Gas/particle Partitioning and Secondary Organic Aerosol Yields. *Environ. Sci. Technol.* **1996**, *30* (8), 2580–2585.
- (122) Atkinson, R.; Baulch, D. L.; Cox, R. A.; Hampson Jr, R. F.; Kerr, J. A.; Troe, J. Evaluated Kinetic and Photochemical Data for Atmospheric Chemistry: Supplement IV: IUPAC Subcommittee on Gas Kinetic Data Evaluation for Atmospheric Chemistry. *Atmos. Environ. Part A. Gen. Top.* **1992**, *26* (7), 1187–1230.
- (123) Albinet, A.; Minero, C.; Vione, D. Photochemical Generation of Reactive Species upon Irradiation of Rainwater: Negligible Photoactivity of Dissolved Organic Matter. *Sci. Total Environ.* **2010**, *408* (16), 3367–3373.
- (124) Wang, Y.; Arellanes, C.; Curtis, D. B.; Paulson, S. E. Probing the Source of Hydrogen Peroxide Associated with Coarse Mode Aerosol Particles in Southern California. *Environ. Sci. Technol.* **2010**, *44* (11), 4070–4075.
- (125) Lim, Y. B.; Tan, Y.; Perri, M. J.; Seitzinger, S. P.; Turpin, B. J. Aqueous Chemistry and

- Its Role in Secondary Organic Aerosol (SOA) Formation. *Atmos. Chem. Phys.* **2010**, *10* (21), 10521–10539.
- (126) Perri, M. J.; Seitzinger, S.; Turpin, B. J. Secondary Organic Aerosol Production from Aqueous Photooxidation of Glycolaldehyde: Laboratory Experiments. *Atmos. Environ.* **2009**, *43* (8), 1487–1497.
- (127) Tan, Y.; Carlton, A. G.; Seitzinger, S. P.; Turpin, B. J. SOA from Methylglyoxal in Clouds and Wet Aerosols: Measurement and Prediction of Key Products. *Atmos. Environ.* **2010**, *44* (39), 5218–5226.
- (128) Guzman, M. I.; Colussi, A. J.; Hoffmann, M. R. Photoinduced Oligomerization of Aqueous Pyruvic Acid. *J. Phys. Chem. A* **2006**, *110* (10), 3619–3626.
- (129) Nizkorodov, S. A.; Laskin, J.; Laskin, A. Molecular Chemistry of Organic Aerosols through the Application of High Resolution Mass Spectrometry. *Phys. Chem. Chem. Phys.* **2011**, *13* (9), 3612–3629.
- (130) Matsumoto, K.; Kawai, S.; Igawa, M. Dominant Factors Controlling Concentrations of Aldehydes in Rain, Fog, Dew Water, and in the Gas Phase. *Atmos. Environ.* **2005**, *39* (38), 7321–7329.
- (131) Munger, J. W.; Collett, J.; Daube, B.; Hoffmann, M. R. Fogwater Chemistry at Riverside, California. *Atmos. Environ. Part B-Urban Atmos.* **1990**, *24* (2), 185–205.
- (132) Volkamer, R.; Ziemann, P. J.; Molina, M. J. Secondary Organic Aerosol Formation from Acetylene (C<sub>2</sub>H<sub>2</sub>): Seed Effect on SOA Yields due to Organic Photochemistry in the Aerosol Aqueous Phase. *Atmos. Chem. Phys.* **2009**, *9* (6), 1907–1928.
- (133) Bateman, A. P.; Walser, M. L.; Desyaterik, Y.; Laskin, J.; Laskin, A.; Nizkorodov, S. A. The Effect of Solvent on the Analysis of Secondary Organic Aerosol Using Electrospray

- Ionization Mass Spectrometry. *Environ. Sci. Technol.* **2008**, *42*, 7341–7346.
- (134) Bateman, A. P.; Laskin, J.; Laskin, A.; Nizkorodov, S. A. Applications of High-Resolution Electrospray Ionization Mass Spectrometry to Measurements of Average Oxygen to Carbon Ratios in Secondary Organic Aerosols. *Environ. Sci. Technol.* **2012**, *46* (15), 8315–8324.
- (135) Bateman, A. P.; Nizkorodov, S. A.; Laskin, J.; Laskin, A. Time-Resolved Molecular Characterization of Limonene/ozone Aerosol Using High-Resolution Electrospray Ionization Mass Spectrometry. *Phys. Chem. Chem. Phys.* **2009**, *11*, 7931–7942.
- (136) Nguyen, T. B.; Bateman, A. P.; Bones, D. L.; Nizkorodov, S. A.; Laskin, J.; Laskin, A. High-Resolution Mass Spectrometry Analysis of Secondary Organic Aerosol Generated by Ozonolysis of Isoprene. *Atmos. Environ.* **2010**, *44* (8), 1032–1042.
- (137) Reemtsma, T.; These, A.; Springer, A.; Linscheid, M. Fulvic Acids as Transition State of Organic Matter: Indications from High Resolution Mass Spectrometry. *Environ. Sci. Technol.* **2006**, *40* (19), 5839–5845.
- (138) Wozniak, A. S.; Bauer, J. E.; Sleighter, R. L.; Dickhut, R. M.; Hatcher, P. G. Technical Note: Molecular Characterization of Aerosol-Derived Water Soluble Organic Carbon Using Ultrahigh Resolution Electrospray Ionization Fourier Transform Ion Cyclotron Resonance Mass Spectrometry. *Atmos. Chem. Phys.* **2008**, *8*, 5099–5111.
- (139) Gómez-González, Y.; Surratt, J. D.; Cuyckens, F.; Szmigielski, R.; Vermeylen, R.; Jaoui, M.; Lewandowski, M.; Offenberg, J. H.; Kleindienst, T. E.; Edney, E. O. Characterization of Organosulfates from the Photooxidation of Isoprene and Unsaturated Fatty Acids in Ambient Aerosol Using Liquid Chromatography/(–) Electrospray Ionization Mass Spectrometry. *J. Mass Spectrom.* **2008**, *43* (3), 371–382.

- (140) Altieri, K. E.; Turpin, B. J.; Seitzinger, S. P. Oligomers, Organosulfates, and Nitrooxy Organosulfates in Rainwater Identified by Ultra-High Resolution Electrospray Ionization FT-ICR Mass Spectrometry. *Atmos. Chem. Phys.* **2009**, *9* (7), 2533–2542.
- (141) Altieri, K. E.; Turpin, B. J.; Seitzinger, S. P. Composition of Dissolved Organic Nitrogen in Continental Precipitation Investigated by Ultra-High Resolution FT-ICR Mass Spectrometry. *Environ. Sci. Technol.* **2009**, *43* (18), 6950–6955.
- (142) Smith, J. S.; Laskin, A.; Laskin, J. Molecular Characterization of Biomass Burning Aerosols Using High-Resolution Mass Spectrometry. *Anal. Chem.* **2009**, *81*, 1512–1521.
- (143) Laskin, A.; Smith, J. S.; Laskin, J. Molecular Characterization of Nitrogen-Containing Compounds in Biomass Burning Aerosols Using High-Resolution Mass Spectrometry. *Environ. Sci. Technol.* **2009**, *43*, 3764–3771.
- (144) Mazzoleni, L. R.; Ehrmann, B. M.; Shen, X. H.; Marshall, A. G.; Collett, J. L. Water-Soluble Atmospheric Organic Matter in Fog: Exact Masses and Chemical Formula Identification by Ultrahigh-Resolution Fourier Transform Ion Cyclotron Resonance Mass Spectrometry. *Environ. Sci. Technol.* **2010**, *44* (10), 3690–3697.
- (145) Schmitt-Kopplin, P.; Gelencser, A.; Dabek-Zlotorzynska, E.; Kiss, G.; Hertkorn, N.; Harir, M.; Hong, Y.; Gebefugi, I. Analysis of the Unresolved Organic Fraction in Atmospheric Aerosols with Ultrahigh-Resolution Mass Spectrometry and Nuclear Magnetic Resonance Spectroscopy: Organosulfates As Photochemical Smog Constituents. *Anal. Chem.* **2010**, *82* (19), 8017–8026.
- (146) Mazzoleni, L. R.; Saranjampour, P.; Dalbec, M. M.; Samburova, V.; Hallar, A. G.; Zielinska, B.; Lowenthal, D. H.; Kohl, S. Identification of Water-Soluble Organic Carbon in Non-Urban Aerosols Using Ultrahigh-Resolution FT-ICR Mass Spectrometry: Organic

- Anions. *Environmental Chemistry*. 2012, pp 285–297.
- (147) Roach, P. J.; Laskin, J.; Laskin, A. Molecular Characterization of Organic Aerosols Using Nanospray-Desorption/Electrospray Ionization-Mass Spectrometry †. *Anal. Chem.* **2010**, *82* (19), 7979–7986.
- (148) Chang-Graham, A. L.; Profeta, L. T. M.; Johnson, T. J.; Yokelson, R. J.; Laskin, A.; Laskin, J. Case Study of Water-Soluble Metal Containing Organic Constituents of Biomass Burning Aerosol. *Environ. Sci. Technol.* **2011**, *45* (4), 1257–1263.
- (149) Rincón, A. G.; Calvo, A. I.; Dietzel, M.; Kalberer, M. Seasonal Differences of Urban Organic Aerosol Composition – an Ultra-High Resolution Mass Spectrometry Study. *Environmental Chemistry*. 2012, pp 298–319.
- (150) Lin, P.; Yu, J. Z.; Engling, G.; Kalberer, M. Organosulfates in Humic-like Substance Fraction Isolated from Aerosols at Seven Locations in East Asia: A Study by Ultra-High-Resolution Mass Spectrometry. *Environ. Sci. Technol.* **2012**, *46* (24), 13118–13127.
- (151) O’Brien, R. E.; Laskin, A.; Laskin, J.; Liu, S.; Weber, R.; Russell, L. M.; Goldstein, A. H. Molecular Characterization of Organic Aerosol Using Nanospray Desorption/electrospray Ionization Mass Spectrometry: CalNex 2010 Field Study. *Atmos. Environ.* **2013**, *68*, 265–272.
- (152) O’Brien, R. E.; Nguyen, T. B.; Laskin, A.; Laskin, J.; Hayes, P. L.; Liu, S.; Jimenez, J. L.; Russell, L. M.; Nizkorodov, S. A.; Goldstein, A. H. Probing Molecular Associations of Field-collected and Laboratory-generated SOA with nano-DESI High-resolution Mass Spectrometry. *J. Geophys. Res. Atmos.* **2013**, *118* (2), 1042–1051.
- (153) Kourtchev, I.; Fuller, S.; Aalto, J.; Ruuskanen, T. M.; McLeod, M. W.; Maenhaut, W.; Jones, R.; Kulmala, M.; Kalberer, M. Molecular Composition of Boreal Forest Aerosol

- from Hyytiälä, Finland, Using Ultrahigh Resolution Mass Spectrometry. *Environ. Sci. Technol.* **2013**, *47* (9), 4069–4079.
- (154) Kourtchev, I.; Fuller, S. J.; Giorio, C.; Healy, R. M.; Wilson, E.; O'Connor, I.; Wenger, J. C.; McLeod, M.; Aalto, J.; Ruuskanen, T. M. Molecular Composition of Biogenic Secondary Organic Aerosols Using Ultrahigh-Resolution Mass Spectrometry: Comparing Laboratory and Field Studies. *Atmos. Chem. Phys.* **2014**, *14* (4), 2155–2167.
- (155) Kourtchev, I.; O'Connor, I. P.; Giorio, C.; Fuller, S. J.; Kristensen, K.; Maenhaut, W.; Wenger, J. C.; Sodeau, J. R.; Glasius, M.; Kalberer, M. Effects of Anthropogenic Emissions on the Molecular Composition of Urban Organic Aerosols: An Ultrahigh Resolution Mass Spectrometry Study. *Atmos. Environ.* **2014**, *89*, 525–532.
- (156) Tao, S.; Lu, X.; Levac, N.; Bateman, A. P.; Nguyen, T. B.; Bones, D. L.; Nizkorodov, S. A.; Laskin, J.; Laskin, A.; Yang, X. Molecular Characterization of Organosulfates in Organic Aerosols from Shanghai and Los Angeles Urban Areas by Nanospray-Desorption Electrospray Ionization High-Resolution Mass Spectrometry. *Environ. Sci. Technol.* **2014**, *48* (18), 10993–11001.
- (157) Hu, K. S.; Darer, A. I.; Elrod, M. J. Thermodynamics and Kinetics of the Hydrolysis of Atmospherically Relevant Organonitrates and Organosulfates. *Atmos. Chem. Phys.* **2011**, *11* (16), 8307–8320.
- (158) Darer, A. I.; Cole-Filipiak, N. C.; O'Connor, A. E.; Elrod, M. J. Formation and Stability of Atmospherically Relevant Isoprene-Derived Organosulfates and Organonitrates. *Environ. Sci. Technol.* **2011**, *45* (5), 1895–1902.
- (159) Glasius, M.; Lahaniati, M.; Calogirou, A.; Di Bella, D.; Jensen, N. R.; Hjorth, J.; Kotzias, D.; Larsen, B. R. Carboxylic Acids in Secondary Aerosols from Oxidation of Cyclic

- Monoterpenes by Ozone. *Environ. Sci. Technol.* **2000**, *34* (6), 1001–1010.
- (160) Nguyen, T. B.; Laskin, A.; Laskin, J.; Nizkorodov, S. A. Brown Carbon Formation from Ketoaldehydes of Biogenic Monoterpenes. *Faraday Discuss.* **2013**, *165*, 473–494.
- (161) Winterhalter, R.; Dingenen, R. Van; Larsen, B. R.; Jensen, N. R.; Hjorth, J. LC-MS Analysis of Aerosol Particles from the Oxidation of  $\alpha$ -Pinene by Ozone and OH-Radicals. *Atmos. Chem. Phys. Discuss.* **2003**, *3* (1), 1–39.
- (162) Kahnt, A.; Iinuma, Y.; Mutzel, A.; Böge, O.; Claeys, M.; Herrmann, H. Campholenic Aldehyde Ozonolysis: A Mechanism Leading to Specific Biogenic Secondary Organic Aerosol Constituents. *Atmos. Chem. Phys.* **2014**, *14* (2), 719–736.
- (163) Hamilton, J. F.; Lewis, A. C.; Reynolds, J. C.; Carpenter, L. J.; Lubben, A. Investigating the Composition of Organic Aerosol Resulting from Cyclohexene Ozonolysis: Low Molecular Weight and Heterogeneous Reaction Products. *Atmos. Chem. Phys.* **2006**, *6* (12), 4973–4984.
- (164) Warscheid, B.; Hoffmann, T. Direct Analysis of Highly Oxidised Organic Aerosol Constituents by On-Line Ion Trap Mass Spectrometry in the Negative-Ion Mode. *Rapid Commun. Mass Spectrom.* **2002**, *16* (6), 496–504.
- (165) Reinhardt, A.; Emmenegger, C.; Gerrits, B.; Panse, C.; Dommen, J.; Baltensperger, U.; Zenobi, R.; Kalberer, M. Ultrahigh Mass Resolution and Accurate Mass Measurements as a Tool to Characterize Oligomers in Secondary Organic Aerosols. *Anal. Chem.* **2007**, *79* (11), 4074–4082.
- (166) Kundu, S.; Fisseha, R.; Putman, A. L.; Rahn, T. A.; Mazzoleni, L. R. High Molecular Weight SOA Formation during Limonene Ozonolysis: Insights from Ultrahigh-Resolution FT-ICR Mass Spectrometry Characterization. *Atmos. Chem. Phys.* **2012**, *12* (12), 5523–



5536.

- (167) Walser, M. L.; Desyaterik, Y.; Laskin, J.; Laskin, A.; Nizkorodov, S. A. High-Resolution Mass Spectrometric Analysis of Secondary Organic Aerosol Produced by Ozonation of Limonene. *Phys. Chem. Chem. Phys.* **2008**, *10*, 1009–1022.
- (168) Koch, B. P.; Dittmar, T. From Mass to Structure: An Aromaticity Index for High-Resolution Mass Data of Natural Organic Matter. *Rapid Commun. Mass Spectrom.* **2006**, *20* (5), 926–932.
- (169) Zanardi-Lamardo, E.; Moore, C. A.; Zika, R. G. Seasonal Variation in Molecular Mass and Optical Properties of Chromophoric Dissolved Organic Material in Coastal Waters of Southwest Florida. *Mar. Chem.* **2004**, *89* (1), 37–54.
- (170) Mopper, K.; Zhou, X.; Kieber, R. J.; Kieber, D. J.; Sikorski, R. J.; Jones, R. D. Photochemical Degradation of Dissolved Organic Carbon and Its Impact on the Oceanic Carbon Cycle. *Nature* **1991**, *353*, 60–62.
- (171) Schmitt-Kopplin, P.; Hertkorn, N.; Schulten, H.-R.; Kettrup, A. Structural Changes in a Dissolved Soil Humic Acid during Photochemical Degredation Process under O<sub>2</sub> and N<sub>2</sub> Atmosphere. *Environ. Sci. Technol.* **1998**, *32*, 2531–2541.
- (172) Jiang, H.; Xue, H.; Teller, A.; Feingold, G.; Levin, Z. Aerosol Effects on the Lifetime of Shallow Cumulus. *Geophys. Res. Lett.* **2006**, *33* (14).
- (173) Docherty, K. S.; Wu, W.; Lim, Y. B.; Ziemann, P. J. Contributions of Organic Peroxides to Secondary Aerosol Formed from Reactions of Monoterpenes with O<sub>3</sub>. *Environ. Sci. Technol.* **2005**, *39* (11), 4049–4059.
- (174) Epstein, S. A.; Shemesh, D.; Tran, V. T.; Nizkorodov, S. A.; Gerber, R. B. Absorption Spectra and Photolysis of Methyl Peroxide in Liquid and Frozen Water. *J. Phys. Chem. A*

- 2012**, *116* (24), 6068–6077.
- (175) Kamboures, M. A.; Nizkorodov, S. A.; Gerber, R. B. Ultrafast Photochemistry of Methyl Hydroperoxide on Ice Particles. *Proc. Natl. Acad. Sci. U. S. A.* **2010**, *107* (15), 6600–6604.
- (176) Norrish, R. G. W.; Bamford, C. H. Photodecomposition of Aldehydes and Ketones. *Nature* **1936**, *138*, 1016.
- (177) von Sonntag, C.; Schuchmann, H. The Elucidation of Peroxyl Radical Reactions in Aqueous Solution with the Help of Radiation-Chemical Methods. *Angew. Chemie Int. Ed. English* **1991**, *30* (10), 1229–1253.
- (178) Ingold, K. U. Peroxy Radicals. *Acc. Chem. Res.* **1969**, *2* (1), 1–9.
- (179) Noyes, W. A. The Contribution to R G W Norrish to Photochemistry. In *Photochemistry and Reaction Kinetics*; Ashmore, P. G., Dainton, F. S., Sugden, T. M., Eds.; Cambridge University Press: Cambridge, 1967; pp 1–21.
- (180) Nguyen, T. B.; Nizkorodov, S. A.; Laskin, A.; Laskin, J. An Approach toward Quantification of Organic Compounds in Complex Environmental Samples Using High-Resolution Electrospray Ionization Mass Spectrometry. *Anal. Methods* **2013**, *5* (1), 72–80.
- (181) Aiken, A. C.; Decarlo, P. F.; Kroll, J. H.; Worsnop, D. R.; Huffman, J. A.; Docherty, K. S.; Ulbrich, I. M.; Mohr, C.; Kimmel, J. R.; Sueper, D.; et al. O/C and OM/OC Ratios of Primary, Secondary, and Ambient Organic Aerosols with High-Resolution Time-of-Flight Aerosol Mass Spectrometry. *Environ. Sci. Technol.* **2008**, *42* (12), 4478–4485.
- (182) Aiken, A. C.; DeCarlo, P. F.; Jimenez, J. L. Elemental Analysis of Organic Species with Electron Ionization High-Resolution Mass Spectrometry. *Anal. Chem.* **2007**, *79* (21), 8350–8358.

- (183) DeCarlo, P. F.; Kimmel, J. R.; Trimborn, A.; Northway, M. J.; Jayne, J. T.; Aiken, A. C.; Gonin, M.; Fuhrer, K.; Horvath, T.; Docherty, K. S. Field-Deployable, High-Resolution, Time-of-Flight Aerosol Mass Spectrometer. *Anal. Chem.* **2006**, *78* (24), 8281–8289.
- (184) Alif, A.; Pilichowski, J.-F.; Boule, P. Photochemistry and Environment XIII: Phototransformation of 2-Nitrophenol in Aqueous Solution. *J. Photochem. Photobiol. A Chem.* **1991**, *59* (2), 209–219.
- (185) Lipczynska-Kochany, E. Degradation of Nitrobenzene and Nitrophenols by Means of Advanced Oxidation Processes in a Homogeneous Phase: Photolysis in the Presence of Hydrogen Peroxide versus the Fenton Reaction. *Chemosphere* **1992**, *24* (9), 1369–1380.
- (186) Albinet, A.; Minero, C.; Vione, D. Phototransformation Processes of 2, 4-Dinitrophenol, Relevant to Atmospheric Water Droplets. *Chemosphere* **2010**, *80* (7), 753–758.
- (187) Atkinson, R.; Arey, J. Gas-Phase Tropospheric Chemistry of Biogenic Volatile Organic Compounds: A Review. *Atmos. Environ.* **2003**, *37*, S197–S219.
- (188) Lee, A.; Goldstein, A. H.; Keywood, M. D.; Gao, S.; Varutbangkul, V.; Bahreini, R.; Ng, N. L.; Flagan, R. C.; Seinfeld, J. H. Gas-Phase Products and Secondary Aerosol Yields from the Ozonolysis of Ten Different Terpenes. *J. Geophys. Res.* **2006**, *111* (D7), 18.
- (189) Calogirou, A.; Larsen, B. R.; Kotzias, D. Gas-Phase Terpene Oxidation Products: A Review. *Atmos. Environ.* **1999**, *33*, 1423–1439.
- (190) Hoffmann, T.; Odum, J. R.; Bowman, F.; Collins, D.; Klockow, D.; Flagan, R. C.; Seinfeld, J. H. Formation of Organic Aerosols from the Oxidation of Biogenic Hydrocarbons. *J. Atmos. Chem.* **1997**, *26*, 189–222.
- (191) Johnson, D.; Marston, G. The Gas-Phase Ozonolysis of Unsaturated Volatile Organic Compounds in the Troposphere. *Chem. Soc. Rev.* **2008**, *37* (4), 699–716.

- (192) Kroll, J. H.; Seinfeld, J. H. Chemistry of Secondary Organic Aerosol: Formation and Evolution of Low-Volatility Organics in the Atmosphere. *Atmos. Environ.* **2008**, *42* (16), 3593–3624.
- (193) Yu, J.; Cocker III, D. R.; Griffin, R. J.; Flagan, R. C.; Seinfeld, J. H. Gas-Phase Ozone Oxidation of Monoterpenes: Gaseous and Particulate Products. *J. Atmos. Chem.* **1999**, *34* (2), 207–258.
- (194) Bonn, B.; Moorgat, G. K. New Particle Formation during  $\alpha$ - and  $\beta$ -Pinene Oxidation by  $O_3$ , OH and  $NO_3$ , and the Influence of Water Vapour: Particle Size Distribution Studies. *Atmos. Chem. Phys.* **2002**, *2* (3), 183–196.
- (195) Perraud, V.; Bruns, E. A.; Ezell, M. J.; Johnson, S. N.; Greaves, J.; Finlayson-Pitts, B. J. Identification of Organic Nitrates in the  $NO_3$  Radical Initiated Oxidation of  $\alpha$ -Pinene by Atmospheric Pressure Chemical Ionization Mass Spectrometry. *Environ. Sci. Technol.* **2010**, *44* (15), 5887–5893.
- (196) Draper, D. C.; Farmer, D. K.; Desyaterik, Y.; Fry, J. L. A Qualitative Comparison of Secondary Organic Aerosol Yields and Composition from Ozonolysis of Monoterpenes at Varying Concentrations of  $NO_2$ . *Atmos. Chem. Phys.* **2015**, *15* (21), 12267–12281.
- (197) Fry, J. L.; Draper, D. C.; Barsanti, K. C.; Smith, J. N.; Ortega, J.; Winkler, P. M.; Lawler, M. J.; Brown, S. S.; Edwards, P. M.; Cohen, R. C. Secondary Organic Aerosol Formation and Organic Nitrate Yield from  $NO_3$  Oxidation of Biogenic Hydrocarbons. *Environ. Sci. Technol.* **2014**, *48* (20), 11944–11953.
- (198) Fry, J. L.; Kiendler-Scharr, A.; Rollins, A. W.; Brauers, T.; Brown, S. S.; Dorn, H.-P.; Dubé, W. P.; Fuchs, H.; Mensah, A.; Rohrer, F. SOA from Limonene: Role of  $NO_3$  in Its Generation and Degradation. *Atmos. Chem. Phys.* **2011**, *11* (8), 3879–3894.

- (199) Jaoui, M.; Kleindienst, T. E.; Docherty, K. S.; Lewandowski, M.; Offenberg, J. H. Secondary Organic Aerosol Formation from the Oxidation of a Series of Sesquiterpenes:  $\alpha$ -Cedrene,  $\beta$ -Caryophyllene,  $\alpha$ -Humulene and  $\alpha$ -Farnesene with  $O_3$ , OH and  $NO_3$  Radicals. *Environ. Chem.* **2013**, *10* (3), 178–193.
- (200) Canosa-Mas, C. E.; King, M. D.; Scarr, P. J.; Thompson, K. C.; Wayne, R. P. An Experimental Study of the Gas-Phase Reactions of the  $NO_3$  Radical with Three Sesquiterpenes: Isolongifolene, Alloisolongifolene, and  $\alpha$ -Neoclovene. *Phys. Chem. Chem. Phys.* **1999**, *1* (12), 2929–2933.
- (201) Boyd, C. M.; Sanchez, J.; Xu, L.; Eugene, A. J.; Nah, T.; Tuet, W. Y.; Guzman, M. I.; Ng, N. L. Secondary Organic Aerosol Formation from the  $\beta$ -Pinene +  $NO_3$  System: Effect of Humidity and Peroxy Radical Fate. *Atmos. Chem. Phys.* **2015**, *15* (13), 7497–7522.
- (202) Nah, T.; Sanchez, J.; Boyd, C. M.; Ng, N. L. Photochemical Aging of  $\alpha$ -Pinene and  $\beta$ -Pinene Secondary Organic Aerosol Formed from Nitrate Radical Oxidation. *Environ. Sci. Technol.* **2015**, *50* (1), 222–231.
- (203) Ayres, B. R.; Allen, H. M.; Draper, D. C.; Brown, S. S.; Wild, R. J.; Jimenez, J. L.; Day, D. A.; Campuzano-Jost, P.; Hu, W.; Gouw, J. de. Organic Nitrate Aerosol Formation via  $NO_3$  + Biogenic Volatile Organic Compounds in the Southeastern United States. *Atmos. Chem. Phys.* **2015**, *15* (23), 13377–13392.
- (204) Wayne, R. P.; Barnes, I.; Biggs, P.; Burrows, J. P.; Canosa-Mas, C. E.; Hjorth, J.; Le Bras, G.; Moortgat, G. K.; Perner, D.; Poulet, G. The Nitrate Radical: Physics, Chemistry, and the Atmosphere. *Atmos. Environ. Part A. Gen. Top.* **1991**, *25* (1), 1–203.
- (205) Kind, T.; Fiehn, O. Seven Golden Rules for Heuristic Filtering of Molecular Formulas Obtained by Accurate Mass Spectrometry. *BMC Bioinformatics* **2007**, *8* (1), 1.

- (206) Li, Y.; Pöschl, U.; Shiraiwa, M. Molecular Corridors and Parameterizations of Volatility in the Chemical Evolution of Organic Aerosols. *Atmos. Chem. Phys.* **2016**, *16* (5), 3327–3344.
- (207) Perraud, V.; Bruns, E. A.; Ezell, M. J.; Johnson, S. N.; Yu, Y.; Alexander, M. L.; Zelenyuk, A.; Imre, D.; Chang, W. L.; Dabdub, D. Nonequilibrium Atmospheric Secondary Organic Aerosol Formation and Growth. *Proc. Natl. Acad. Sci.* **2012**, *109* (8), 2836–2841.
- (208) Heaton, K. J.; Dreyfus, M. A.; Wang, S.; Johnston, M. V. Oligomers in the Early Stage of Biogenic Secondary Organic Aerosol Formation and Growth. *Environ. Sci. Technol.* **2007**, *41* (17), 6129–6136.
- (209) Baltensperger, U.; Kalberer, M.; Dommen, J.; Paulsen, D.; Alfarra, M. R.; Coe, H.; Fisseha, R.; Gascho, A.; Gysel, M.; Nyeki, S.; et al. Secondary Organic Aerosols from Anthropogenic and Biogenic Precursors. *Faraday Discuss.* **2005**, *130* (Atmospheric Chemistry), 265–278.
- (210) Tolocka, M. P.; Jang, M.; Ginter, J. M.; Cox, F. J.; Kamens, R. M.; Johnston, M. V. Formation of Oligomers in Secondary Organic Aerosol. *Environ. Sci. Technol.* **2004**, *38* (5), 1428–1434.
- (211) Gao, Y. Q.; Hall, W. A.; Johnston, M. V. Molecular Composition of Monoterpene Secondary Organic Aerosol at Low Mass Loading. *Environ. Sci. Technol.* **2010**, *44* (20), 7897–7902.
- (212) Beck, M.; Hoffmann, T. A Detailed MS N Study for the Molecular Identification of a Dimer Formed from Oxidation of Pinene. *Atmos. Environ.* **2016**, *130*, 120–126.
- (213) Kristensen, K.; Cui, T.; Zhang, H.; Gold, A.; Glasius, M.; Surratt, J. D. Dimers in  $\alpha$ -

- Pinene Secondary Organic Aerosol: Effect of Hydroxyl Radical, Ozone, Relative Humidity and Aerosol Acidity. *Atmos. Chem. Phys.* **2014**, *14* (8), 4201–4218.
- (214) Yasmeen, F.; Vermeulen, R.; Szmigielski, R.; Iinuma, Y.; Böge, O.; Herrmann, H.; Maenhaut, W.; Claeys, M. Terpenylic Acid and Related Compounds: Precursors for Dimers in Secondary Organic Aerosol from the Ozonolysis of  $\alpha$ - and  $\beta$ -Pinene. *Atmos. Chem. Phys.* **2010**, *10* (19), 9383–9392.
- (215) Iinuma, Y.; Böge, O.; Miao, Y.; Sierau, B.; Gnauk, T.; Herrmann, H. Laboratory Studies on Secondary Organic Aerosol Formation from Terpenes. *Faraday Discuss.* **2005**, *130*, 279–294.
- (216) Venkatachari, P.; Hopke, P. K. Characterization of Products Formed in the Reaction of Ozone with  $\alpha$ -Pinene: Case for Organic Peroxides. *J. Environ. Monit.* **2008**, *10* (8), 966–974.
- (217) Camredon, M.; Hamilton, J. F.; Alam, M. S.; Wyche, K. P.; Carr, T.; White, I. R.; Monks, P. S.; Rickard, A. R.; Bloss, W. J. Distribution of Gaseous and Particulate Organic Composition during Dark  $\alpha$ -Pinene Ozonolysis. *Atmos. Chem. Phys.* **2010**, *10* (6), 2893–2917.
- (218) Putman, A. L.; Offenberg, J. H.; Fisseha, R.; Kundu, S.; Rahn, T. A.; Mazzoleni, L. R. Ultrahigh-Resolution FT-ICR Mass Spectrometry Characterization of  $\alpha$ -Pinene Ozonolysis SOA. *Atmos. Environ.* **2012**, *46*, 164–172.
- (219) Glasius, M.; Duane, M.; Larsen, B. R. Determination of Polar Terpene Oxidation Products in Aerosols by Liquid Chromatography-Ion Trap Mass Spectrometry. *J. Chromatogr. A* **1999**, *833* (2), 121–135.
- (220) Nozière, B.; Kalberer, M.; Claeys, M.; Allan, J.; D’Anna, B.; Decesari, S.; Finessi, E.;

- Glasius, M.; Grgic, I.; Hamilton, J. F. The Molecular Identification of Organic Compounds in the Atmosphere: State of the Art and Challenges. *Chem. Rev.* **2015**, *115* (10), 3919–3983.
- (221) Beck, M.; Winterhalter, R.; Herrmann, F.; Moortgat, G. K. The Gas-Phase Ozonolysis of  $\alpha$ -Humulene. *Phys. Chem. Chem. Phys.* **2011**, *13* (23), 10970–11001.
- (222) Jaoui, M.; Kamens, R. M. Gas and Particulate Products Distribution from the Photooxidation of  $\alpha$ -Humulene in the Presence of NO<sub>x</sub>, Natural Atmospheric Air and Sunlight. *J. Atmos. Chem.* **2003**, *46* (1), 29–54.
- (223) Brinkmann, T.; Horsch, P.; Sartorius, D.; Frimmel, F. H. Photoformation of Low-Molecular-Weight Organic Acids from Brown Water Dissolved Organic Matter. *Environ. Sci. Technol.* **2003**, *37*, 4190–4198.
- (224) Kujawinski, E. B.; Del Vecchio, R.; Blough, N. V.; Klein, G. C.; Marshall, A. G. Probing Molecular-Level Transformations of Dissolved Organic Matter: Insights on Photochemical Degradation and Protozoan Modification of DOM from Electrospray Ionization Fourier Transform Ion Cyclotron Resonance Mass Spectrometry. *Mar. Chem.* **2004**, *92*, 23–37.
- (225) Romonosky, D. E.; Nguyen, L. Q.; Shemesh, D.; Nguyen, T. B.; Epstein, S. A.; Martin, D. B. C.; Vanderwal, C. D.; Gerber, R. B.; Nizkorodov, S. A. Absorption Spectra and Aqueous Photochemistry of  $\beta$ -Hydroxyalkyl Nitrates of Atmospheric Interest. *Mol. Phys.* **2015**, *113* (15-16), 2179–2190.
- (226) Liu, S.; Shilling, J. E.; Song, C.; Hiranuma, N.; Zaveri, R. A.; Russell, L. M. Hydrolysis of Organonitrate Functional Groups in Aerosol Particles. *Aerosol Sci. Technol.* **2012**, *46* (12), 1359–1369.



- (227) Harris, L. E. The Lower Electronic States of Nitrite and Nitrate Ion, Nitromethane, Nitramide, Nitric Acid, and Nitrate Esters. *J. Chem. Phys.* **1973**, *58* (12), 5615–5626.
- (228) Harris, L. E. Lower Electronic States of Nitric Acid and Esters. *Nature* **1973**, *243* (128), 103–104.
- (229) Shamsutdinov, T. F.; Chachkov, D. V.; Shamov, A. G.; Khrapkovskii, G. M. Studies into the Structure of Molecules and the Gas-Phase Radical Decomposition of Aliphatic Alcohol Nitroesters by Quantum-Chemical Methods. *Izvestiya Vysshikh Uchebnykh Zavedenii, Khimiya i Khimicheskaya Tekhnologiya* **2006**, *49* (38).
- (230) Khrapkovskii, G. M.; Shamsutdinov, T. F.; Chachkov, D. V.; Shamov, A. G. Energy of the O–NO<sub>2</sub> Bond Dissociation and the Mechanism of the Gas-Phase Monomolecular Decomposition of Aliphatic Alcohol Nitroesters. *J. Mol. Struct. THEOCHEM* **2004**, *686* (1), 185–192.
- (231) Schweigert, I. V.; Dunlap, B. I. Electronic Structure and Molecular Dynamics of Breaking the RO–NO<sub>2</sub> Bond. *J. Chem. Phys.* **2009**, *130* (24), 244110.
- (232) Derro, E. L.; Murray, C.; Lester, M. I.; Marshall, M. D. Photodissociation Dynamics of Methyl Nitrate at 193 Nm: Energy Disposal in Methoxy and Nitrogen Dioxide Products. *Phys. Chem. Chem. Phys.* **2007**, *9* (2), 262–271.
- (233) Soto, J.; Peláez, D.; Otero, J. C.; Avila, F. J.; Arenas, J. F. Photodissociation Mechanism of Methyl Nitrate. A Study with the Multistate Second-Order Multiconfigurational Perturbation Theory. *Phys. Chem. Chem. Phys.* **2009**, *11* (15), 2631–2639.
- (234) Matthews, J.; Sinha, A.; Francisco, J. S. The Importance of Weak Absorption Features in Promoting Tropospheric Radical Production. *Proc. Natl. Acad. Sci. U. S. A.* **2005**, *102* (21), 7449–7452.

- (235) Oncák, M.; Slavíček, P.; Fárník, M.; Buck, U. Photochemistry of Hydrogen Halides on Water Clusters: Simulations of Electronic Spectra and Photodynamics, and Comparison with Photodissociation Experiments. *J. Phys. Chem. A* **2011**, *115* (23), 6155–6168.
- (236) Gerber, R. B.; Shemesh, D.; Varner, M. E.; Kalinowski, J.; Hirshberg, B. Ab Initio and Semi-Empirical Molecular Dynamics Simulations of Chemical Reactions in Isolated Molecules and in Clusters. *Phys. Chem. Chem. Phys.* **2014**, *16* (21), 9760–9775.
- (237) Csizmadia, V. M.; Houlden, S. A.; Koves, G. J.; Boggs, J. M.; Csizmadia, I. G. Stereochemistry and Ultraviolet Spectra of Simple Nitrate Esters. *J. Org. Chem.* **1973**, *38* (13), 2281–2287.
- (238) O’Sullivan, D.; McLaughlin, R. P.; Clemitshaw, K. C.; Sodeau, J. R. Cold-Surface Photochemistry of Selected Organic Nitrates. *J. Phys. Chem. A* **2014**, *118* (42), 9890–9900.
- (239) Das, B.; Krishnaiah, M.; Venkateswarlu, K.; Reddy, V. S. Efficient Regio- and Stereoselective Conversions of Oxiranes and Aziridines into  $\beta$ -(Nitrooxy)-Substituted Alcohols and Amines by Using Bismuth Nitrate. *Helv. Chim. Acta* **2007**, *90* (1), 110–113.
- (240) Bruns, E. A.; Perraud, V.; Zelenyuk, A.; Ezell, M. J.; Johnson, S. N.; Yu, Y.; Imre, D.; Finlayson-Pitts, B. J.; Alexander, M. L. Comparison of FTIR and Particle Mass Spectrometry for the Measurement of Particulate Organic Nitrates. *Environ. Sci. Technol.* **2010**, *44* (3), 1056–1061.
- (241) Hanwell, M. D.; Curtis, D. E.; Lonie, D. C.; Vandermeersch, T.; Zurek, E.; Hutchison, G. R. Avogadro: An Advanced Semantic Chemical Editor, Visualization, and Analysis Platform. *J. Cheminformatics* **2012**, *4* (1), 17.
- (242) Weigend, F.; Häser, M. RI-MP2: First Derivatives and Global Consistency. *Theor. Chem.*

- Acc.* **1997**, *97* (1-4), 331–340.
- (243) Dunning Jr, T. H. Gaussian Basis Sets for Use in Correlated Molecular Calculations. I. The Atoms Boron through Neon and Hydrogen. *J. Chem. Phys.* **1989**, *90* (2), 1007–1023.
- (244) Christiansen, O.; Koch, H.; Jørgensen, P. The Second-Order Approximate Coupled Cluster Singles and Doubles Model CC2. *Chem. Phys. Lett.* **1995**, *243* (5), 409–418.
- (245) Hättig, C.; Weigend, F. CC2 Excitation Energy Calculations on Large Molecules Using the Resolution of the Identity Approximation. *J. Chem. Phys.* **2000**, *113* (13), 5154–5161.
- (246) Weber, W.; Thiel, W. Orthogonalization Corrections for Semiempirical Methods. *Theor. Chem. Accounts Theory, Comput. Model. (Theoretica Chim. Acta)* **2000**, *103* (6), 495–506.
- (247) Koslowski, A.; Beck, M. E.; Thiel, W. Implementation of a General Multireference Configuration Interaction Procedure with Analytic Gradients in a Semiempirical Context Using the Graphical Unitary Group Approach. *J. Comput. Chem.* **2003**, *24* (6), 714–726.
- (248) Shemesh, D.; Blair, S. L.; Nizkorodov, S. A.; Gerber, R. B. Photochemistry of Aldehyde Clusters: Cross-Molecular versus Unimolecular Reaction Dynamics. *Phys. Chem. Chem. Phys.* **2014**, *16* (43), 23861–23868.
- (249) Shemesh, D.; Lan, Z.; Gerber, R. B. Dynamics of Triplet-State Photochemistry of Pentanal: Mechanisms of Norrish I, Norrish II, and H Abstraction Reactions. *J. Phys. Chem. A* **2013**, *117* (46), 11711–11724.
- (250) Shemesh, D.; Gerber, R. B. Femtosecond Timescale Deactivation of Electronically Excited Peroxides at Ice Surfaces. *Mol. Phys.* **2012**, *110* (9-10), 605–617.
- (251) Ervens, B.; Gligorovski, S.; Herrmann, H. Temperature-Dependent Rate Constants for Hydroxyl Radical Reactions with Organic Compounds in Aqueous Solutions. *Phys. Chem.*

- Chem. Phys.* **2003**, 5 (9), 1811–1824.
- (252) Hauff, K.; Fischer, R. G.; Ballschmiter, K. Determination of C1-C5 Alkyl Nitrates in Rain, Snow, White Frost, Lake, and Tap Water by a Combined Codistillation Head-Space Gas Chromatography Technique. Determination of Henry's Law Constants by Head-Space GC. *Chemosphere* **1998**, 37 (13), 2599–2615.
- (253) HENRYWIN. US EPA. *Estimation Programs Interface (EPI) Suite*. (United States Environmental Protection Agency). **2012**.  
<<http://www.epa.gov/opptintr/exposure/pubs/episuite.htm>>.
- (254) Hobbs, P. V. *Aerosol-Cloud-Climate Interactions*; Academic Press, 1993; Vol. 54.
- (255) Madronich, S.; Flocke, S.; Zeng, J.; Petropavlovskikh, I.; Lee-Taylor, J. Tropospheric Ultraviolet and Visible (TUV) Radiation Model. *National Center for Atmospheric Research* **2014**. <[http://cprm.acd.ucar.edu/Models/TUV/Interactive\\_TUV/](http://cprm.acd.ucar.edu/Models/TUV/Interactive_TUV/)>.
- (256) Minakata, D.; Li, K.; Westerhoff, P.; Crittenden, J. Development of a Group Contribution Method To Predict Aqueous Phase Hydroxyl Radical (HO•) Reaction Rate Constants. *Environ. Sci. Technol.* **2009**, 43 (16), 6220–6227.